IAEA-TECDOC-1277

Advanced post-irradiation examination techniques for water reactor fuel

Proceedings of a Technical Committee meeting held in Dimitrovgrad, Russian Federation, 14–18 May 2001

INTERNATIONAL ATOMIC ENERGY AGENCY IAEA

March 2002

The originating Section of this publication in the IAEA was:

Nuclear Fuel Cycle and Materials Section
International Atomic Energy Agency
Wagramer Strasse 5
P.O. Box 100
A-1400 Vienna, Austria

ADVANCED POST-IRRIDIATION EXAMINATION TECHNIQUES FOR WATER REACTOR FUEL
IAEA, VIENNA, 2002
IAEA-TECDOC-1277
ISSN 1011–4289

Printed by the IAEA in Austria
March 2002

FOREWORD

Under economic pressure, nuclear utilities strive for fuel operation under more demanding duties which include; higher burnup, longer fuel cycles, and higher temperatures. Regulatory authorities, when issuing a permit to a utility to operate the core under higher duties, should have sufficient information on nuclear fuel behaviour under normal, transient and accident conditions. This is necessary to prove that fuel safety margins have not been affected. The status of development of destructive and non-destructive fuel examination methods has always guaranteed the quality and volume of required information. International co-operation and information exchange in this area are important activities of the IAEA. Status and development trends in the examination techniques of LWR fuel in different countries were discussed at the IAEA Technical Co-operation meeting held from 14 to 18 May 2001 in Dimitrovgrad by invitation of the Ministry of the Russian Federation for Atomic Energy and SSC RF Research Institute of Atomic Reactors (RIAR).

This meeting was the fifth in a series of IAEA meetings held in 1981 and 1984 (Tokyo, Japan), 1990 (Workington, United Kingdom) and 1994 (Cadarache, France) on the recommendation of the International Working Group on Water Reactor Fuel Performance and Technology (IWGFPT). Co-ordinated Research Programmes on Examination and Documentation Methodology for Water Reactor Fuel (1994–1989 — Part 1 and 1992–1995 — Part 2) resulted in the publication of Guidebooks on Non-Destructive (Technical Reports Series No. 322, 1991) and Destructive (Technical Reports Series No. 385, 1997) Examination of Water Reactor Fuel, respectively. All of these activities were found to be of value in advancing the understanding of fuel behaviour.

As mentioned above, in the six years since the last meeting on this topic the demands on fuel have increased. Accordingly, the demands on PIE techniques and respective results have also increased and their tasks have been changed. New materials and designs, including mixed oxide fuel, burnable absorber fuel and other additive fuels, together with corrosion resistant claddings, have become more prominent. PIE of lead test assemblies is complemented with high burnup test reactor experiments including refabricated (from irradiated commercial rods) fuel rods. Changes in composition, structure and properties of fuel and structural materials are to be investigated and understood to calculate, validate and forecast fuel operational margins and safety limits. Further development of advanced PIE techniques is requested by justification and licensing of the above mentioned advanced fuels. Common approaches of PIE techniques allow comparing results obtained in different countries and different laboratories thus improving the trustworthiness of the results to be used for fuel performance evaluation and licensing.

The IAEA wishes to thank all participants for their contributions to this publication. V. Onoufriev of the Division of Nuclear Fuel Cycle and Waste Technology was the IAEA officer responsible for the organization of the meeting and the compilation of this publication.

EDITORIAL NOTE

This publication has been prepared from the original material as submitted by the authors. The views expressed do not necessarily reflect those of the IAEA, the governments of the nominating Member States or the nominating organizations.

The use of particular designations of countries or territories does not imply any judgement by the publisher, the IAEA, as to the legal status of such countries or territories, of their authorities and institutions or of the delimitation of their boundaries.

The mention of names of specific companies or products (whether or not indicated as registered) does not imply any intention to infringe proprietary rights, nor should it be construed as an endorsement or recommendation on the part of the IAEA.

The authors are responsible for having obtained the necessary permission for the IAEA to reproduce, translate or use material from sources already protected by copyrights.

CONTENTS

SPECIAL METHODS AND TECHNIQUES FOR FUEL AND CLADDING MATERIAL EXAMINATION (Session 5)

MEASUREMENT OF MECHANICAL PROPERETIES (Session 6)

SUMMARY

INTRODUCTION

The purpose of the meeting was to provide an overview of the status of post-irradiation examination (PIE) techniques for water reactor fuel assemblies and their components with emphasis given to advanced PIE techniques applied to high burnup fuel. Papers presented at the meeting described progress obtained in non-destructive (e.g. dimensional measurements, oxide layer thickness measurements, gamma scanning and tomography, neutron and X ray radiography, etc.) and destructive PIE techniques (e.g. microstructural studies, elemental and isotopic analysis, measurement of physical and mechanical properties, etc.) used for investigation of water reactor fuel. Recent practice in high burnup fuel investigation revealed the importance of advanced PIE techniques, such as 3-D tomography, secondary ion mass spectrometry, laser flash, high resolution transmission and scanning electron microscopy, image analysis in microstructural studies, for understanding mechanisms of fuel behaviour under irradiation. Importance and needs for in-pile irradiation of samples and rodlets in instrumented rigs were also discussed.

SESSION I: METHODS FOR FUEL EXAMINATION — REVIEW

The papers of this session and following discussion dealt with the improvements of existing PIE methods to comply with current day nuclear fuel rod materials and designs and with current high duty irradiation conditions. It was an interesting symbiosis of utility (EDF, France) requirements on volume and types of PIE of high burnup LWR fuel to be performed by hot-cell laboratory for providing necessary data and "response" of hot-cell laboratory (RIAR, in this specific case). Major requirements on examination of nuclear fuel to ensure fuel reliability and safety were discussed. The list of presently used and perspective examination methods was defined.

The EDF requirements on hot-cell examinations on irradiated fuels include:

- accurate burnup determination by quantitative g-spectrometry;
- qualification of EC oxide thickness measurements by developing appropriate standards;
- improvement of rod internal gas measurement, to cope with gas communication problems in high burnup rods;
- application of a nuclear microprobe for more in-depth analysis of the microscopic distribution of elements (e.g. Li and H in Zry);
- refabrication of short rodlets from industrial rods for analytical irradiations in MTReactors;
- Zry tubing pressurization for creep experiments and improved metrological control.

These validated methods are necessary for proper fuel modelling, hence to comply with safety authority requirements.

Methods applied at RIAR (Russian Federation) for the mechanical testing of specimens made of WWER zirconium fuel rod claddings include:

- machining and conditioning, i.e. corrosion by overheating in water steam and quenching into water as representative for emergency conditions, of appropriate samples;

- improvement of biaxial loading tests by dynamic both internal and external pressure control, allowing representative hoop and axial stresses to be applied during testing;
- corrosive iodine attack and additional axial laoding such as to allow simulation of actual fuel rod in-service loading and low cycle fatigue testing.

All these methods provide the results required for calculation of WWER fuel element reliability operated in nominal, transient and emergency conditions.

Issues

- The interface between hot laboratories and nuclear reactors suffers from the lack of the availability of appropriate rod extraction and transport systems.

Recommendations for future work

- Mechanical testing should be extended both to longer — intermediate storage relevant — and shorter — RIA relevant — time scales;
- Validation of both already existing and new PIE methods should comply with the changing materials and operating conditions;
- Transfer of non-destructive examination methods towards on-site is encouraged in order to enhance flexibility in fuel rod performance monitoring and to strenghten fuel rod selection for hot cell examinations.

SESSION II: FUEL INSPECTION METHODS

Session two was devoted to on-site fuel inspection methods. Very important task in this area is localization of leaky fuel rods and evaluation of the size and type of leakage. Knowledge of these characteristics is needed to repair fuel assemblies with extraction of defective rod and its replacement by the dummy.

Experience gained in Ukraine in cladding tightness inspection and its methodology is reviewed. It is observed that cladding failure criteria need to be improved based on the operation experience. It is recognized that in order to reduce refuelling work, sipping equipment could be a good alternative.

SICOM is a state of the art fuel assembly inspection system developed and introduced in Spain with extended field experience providing high resolution visual inspection, fuel assembly dimensional characterization and accurate fuel rod oxide thickness measurements. Detailed capabilities and techniques used to perform these types of measurements are described in the paper.

SICOM system consists of two types of equipment:

(1) Stand-alone system, capabilities includes fuel rod corrosion and fuel assembly dimensional characterization handling safely the fuel assembly.
(2) Two simplified equipment, same capabilities, considerable reduction of the inspection time but requires the use of the loading crane.

Conclusions and recommendations for future work

- On-site inspection campaigns objective is to obtain the maximum amount of fuel performance data after the irradiation in commercial power plants in order to satisfy the needed surveillance programs established by the utilities, regulators or fuel vendors.

- In this field over the past, several fuel vendors or utilities have shown capabilities with extensive experience on fuel leakage detection, fuel repair, fuel assembly dimensional characterization and fuel rod oxide thickness measurements. However, certain techniques need to be explored in order to increase or improve the present capabilities. Thus, a list of the type of measurements were efforts to develop the current equipment or create new ones are considered necessary is presented below:

- corrosion:
  - reduce sensitivity to crud interference in EC signal,
  - localized corrosion (welds),
  - measurements on fuel assembly structural material,
- crud sampling and characterization;
- hydrogen concentration in fuel rod cladding and fuel assembly structural material;
- guide thimbles distortion;
- measurements of wear in fuel rod cladding and guide thimbles;
- fuel rod internal pressure and fission gas release;
- fuel rod gamma-scanning.

SESSION 3: NON-DESTRUCTIVE AND DESTRUCTIVE EXAMINATION METHODS — PART I

Modern approaches to the use of neutron radiography and emission tomography for investigation of inner structure and fission product distribution in irradiated rods, respectively, are considered at the session. The session included 5 papers, 4 describing non-destructive techniques and 1 relating a destructive method.

The techniques reported in this session were:

- A method to improve both the quality and the resolution of neutron radiographs in which the dysprosium foil/X ray film technique is supplemented by a track-etch recorder consisting of a cellulose nitrate film.
- The traditional uniaxial profilometry was upgraded by using a new steering control and data acquisition system to provide 3D results.
- A method to depict, elaborate and report on PIE data in the form of a so-called image data file that can be produced by a personal computer operated by Photoshop software.
- A compression method for the determination of the remaining fuel/cladding gap after irradiation.
- The determination of the fission power in terms of burnup and linear fission power by gamma spectrometry of selected fission products.
- An emission tomography method, which allows reducing the scanning time for cylindrical fuel rods. The method uses the reconstruction algorithms based on the approximation of the radionuclide activity distribution in harmonic series.

- A Secondary Ion Mass Spectrometer (SIMS) was adapted for the remote handling in a hot cell.

Conclusions and recommendations for future work

- The improved neutron radiography method can help to reveal fuel rod degradation or failures initiated by hydrogen pick-up, pellet/cladding interaction or fuel relocation and cracking. It is a mature technique but has the drawback of needing for its implementation an adequate neutron source (a reactor with experimental beam channels) and, therefore, cannot be implemented in a normal hot cell laboratory.
- The advanced profilometry method is based on the use of two LVDTs and has been applied up to now only for short rodlets. The extension of this technique for water reactor fuel rods appears difficult but, nevertheless, possible.
- The method to show, elaborate and report PIE-data through an image file seems to be a very useful tool also in view of an increasing commitment of many hot laboratories towards work for third parties: the method could improve and streamline the report of results to the customers.
- The compression method to determine the remaining pellet/cladding gap after irradiation is a well developed and established technique but it seems to have achieved its limit of applicability at burnups of about 50 GWd/t HM. Considering the trend towards increased burnup its future concerning applicability and usefulness seems to be very limited.
- The determination of the fission power in terms of burnup and linear fission power appears as a very valuable technique. With the proper calibration procedure, the results presented demonstrate the possibility to replace the more costly and time consuming radiochemical methods by this non-destructive method.
- The tomography method described can be used for on-line (fast) emission tomography of fuel rods in hot cells, shortening the time of fuel rod scanning and improving the tomography efficiency. It can be considered a mature technique having been successfully applied to fuel rods operated under standard as well as transient conditions.
- The SIMS installation in Cadarache reflects the general trend towards the utilisation of more sophisticated techniques for a better understanding of several important new phenomena arising from the more challenging operating conditions and increased average burnup of fuel elements. Processes such as the influence of the water chemistry on cladding corrosion (B, Li-content), the content and distribution of trace elements as sulphur in UO_2, and the determination of gaseous fission products (Xe) can be advantageously studied through this technique.

SESSION IV: NON-DESTRUCTIVE AND DESTRUCTIVE EXAMINATION METHODS — PART II

In this session important characterisation methods used from the early exit of the reactor to the last microanalysis in hot cells are presented. These methods allow measuring of the burnup, fission gas release and rod diameter with high degree of accuracy. Achieved level of development of these methods provides fuel performance modellers with necessary information on processes in UO_2 and MOX fuel rods under normal, transient and accident conditions. Further development is noticed for SIMS, TEM and STEM, i.e. methods providing fuel designers and modellers with understanding mechanisms of fission gas release, fuel fragmentation and swelling, especially under high burnups.

The measure of the energy injected in a fuel rod during a fast transient is very important for calculating the thermal level achieved during the test and for understanding the fuel behaviour. The estimations based on the neutron flux integration suffer some uncertainties due to the neutron flux variation during the short time pulse used in RIAR. The measure of short time pulse energy deposit in the fuel rod slice was successfully carried out at RIAR. The energy released during such irradiation is calculated by measuring the ^{140} Ba isotope content. This method requires fuel dissolution, three stages of filtration and gamma measurement released in less than one day to obtain 5% accuracy.

This method is certainly the best but cannot be applied in any test reactor because of the little time needed for the measurement. It would be of interest to compare it with neutron calculations in order to calibrate this calculation where the RIAR method is not available.

In order to renew the apparatus for diameter measurements in the hot cell, a new profilometer was developed at RIAR. The method of mechanical profilometry remains the most informative one for analysing changes for large scale fuel rod diameters. Microprofilometer-2 facility was installed at RIAR. The test performed on unirradiated fuel proved a high accuracy in the measurement of WWER fuel rodlet of 45 cm with a precision of 2μm in diameter.

Discussion showed that profilometers in other facilities also provide a high level of accuracy. Precise description of the apparatus itself is needed for the comparison between these apparatus. Specific tests should be defined to check these performances.

In the frame of Pu recycling, India has developed a programme in which several types of MOX fuel are tested. Test fuels are fabricated, then irradiated in research reactors and examined in hot cells. The results are interpreted to define the best MOX fuel for the Indian-type power reactor. A rod piercing device was produced to measure the gas release of irradiated MOX fuels. Gas composition can be measured by mass spectrometry and gas chromatography, the free void volume is measured by two calibrated volumes. The obtained results show different fission gas releases as a function of linear power consistent with optical microscopic observations. MOX fuels with controlled porosity and annular design seem to lead to the lower gas release.

Discussion showed that there is a great dispersion of geometric characteristics of pellet in the same fuel rod which makes the comparison with code calculation difficult.

IPPE has got a pool of complementary techniques to characterise either defective or long stored material. The analysis of defective fuel evidenced chlorine induced cracks which led to corrosion product migration and fuel modification. Insignificant (less than 10 μm) corrosion induced damage of steel cladding of irradiated fuel rods stored at IPPE in the air for 38 years was detected by SEM and X ray microanalysis.

Recommendation for future work

- As a general trend there is less money for destructive examination, which implies to optimise them. In the session we have several examples of how to do it: by adapting existing method to new problems, by improving the data accuracy, by using experimental methods in the frame of a well constructed programme, or by the use of several methods to solve a given problem. In all cases, it is clear that the experiment is

not only needed for experimental results. The experiment must provide more (additional) value to their results in order to assist the needs of their clients. Doing so they will also be more persuasive in convincing their clients in using this very sophisticated method that may sometimes be more expensive.

SESSION V: SPECIAL METHODS AND TECNIQUES FOR FUEL AND CLADDING MATERIAL EXAMINATION

Status of some methods of investigation of in-pile creep and corrosion characteristics of Zr-based alloys as well as technology and practices of fuel assembly repair were presented at this session. Further development of in-pile test methods depends on requirements claimed by current fuel R & D programmes and progress in Zr-based alloy modelling with taking into account creep anisotropy.

In-pile irradiation enhanced creep phenomena of reactor materials are investigated with specific in-pile test techniques named “tensometric method” at the Institute of Physics & Power Engineering, Russian Federation. One of the essential applications is detailed investigation of in-reactor creep behaviour of zirconium alloys. The tensometric method is applied only during stable periods of power reactor operations, e.g. such suitable condition occurs in the BR-10 about 20 hours after the reactor reaches full power after a shutdown period. This limits the availability of effective test runs.

In-pile cladding corrosion tests are performed at Nuclear Research Institute, Czech Republic. Cladding corrosion project on Zr-4 compatibility with WWER water chemistry is in progress. Also, different industrial Zr-based alloys are under investigation to compare their behaviour in LWR-type reactor conditions. In addition, in-pile testing of cladding material samples is also carried out with subsequent PIE. Implementation of refabrication technique to investigate high burnup rods was recommended during panel discussion.

The experience obtained by Ignalina NPP in Lithuania in inspection and repair of damaged irradiated RBMK-1500 fuel assemblies presents significant interest for NPP operators.

Recommendation for future work:

- In-pile creep and corrosion tests should be envisaged for high burnup fuel and high fluence irradiated cladding materials.

SESSION VI: MEASUREMENT OF MECHANICAL PROPERTIES

Significant progress in development of methods of measurement of mechanical properties of irradiated cladding materials has been reached. It allows receiving mutually agreed results of mechanical tests in different laboratories and countries. Comprehensive database containing description of PIE and in-pile test methods available in Russian Federation was presented.

The session deals with special and advanced techniques for mechanical testing of irradiated cladding. Extended burnup and greater operation flexibility require better knowledge of the cladding mechanical properties. The techniques presented can provide materials data for design and model verification and can prove the mechanical integrity of highly irradiated fuel rod claddings under steady state and transient conditions.

Studsvik Nuclear AB (Sweden) has recently developed and set up a number of hot cell techniques. The techniques can be applied to fuel rod cladding to provide supplementary data in order to model load following and power ramping of fuel rods. One test technique is designed to support RIA tests. Two other test techniques address the development of long axial splits in BWR liner cladding by determining fracture toughness and improving the understanding of delayed hydrogen embrittlement.

RIAR (Russian Federation) addressed the mechanical tests that allow to study the mechanical properties of Zr-based cladding tubes in transverse and longitudinal directions. Test parameters have been derived for WWER cladding tubes that allow to investigate the effect of irradiation on the anisotropic property changes.

Sample preparation techniques not only for highly sophisticated techniques such as Transmission Electron Microscopy (TEM) and Glow Discharge Mass Spectrometry (GDMS) but also for mechanical tests such as creep/burst and long time creep test have been developed and introduced in the European Institute for Transuranium Elements. Whilst TEM and GDMS are applied to better understand corrosion mechanism of high burnup cladding materials, creep/burst and creep tests are used to provide data for interim dry storage, an area gaining more and more interest world wide.

As mentioned above, a computerized data bank system of PIE techniques available in research centers in the Russian Federation RIAR has been developed and is maintained by RIAR. Apart from the pure technique it does also contain data and information on accuracy and applicability as well as on sample requirements. The system can be used to select the most appropriate technique for a selected task.

Conclusions and recommendations on future work:

- Significant attention was paid to mechanical test techniques. This indicates the importance of mechanical properties of cladding tubes and structural components for high burnup. In order to allow for comparison of the results obtained at various laboratories a common standard on specimen shape, dimensions and test procedures would be recommended.
- Data on the mechanical behavior of high burnup fuel rods under dry interim storage are scarce and mechanical testing of highly irradiated fuel rod cladding under realistic storage conditions should be extended.
- The computerized data bank system on PIE-Techniques extends the information given in the "Catalogue of PIE Facilities which can examine LWR Fuel and Structural Components" published by the IAEA in 1996 significantly. It might be considered to extend the data base to research organisations outside the Russian Federation.

SUMMARY OF THE PANEL DISCUSSION

Technical Committee considered the most important directions of destructive and non-destructive PIE techniques as applied to water reactor fuel. Current nomenclature and development level of PIE techniques used in different countries and organizations for fuel rod control and investigation are adequate to the requirements aid down by regulatory and licensing bodies. Sufficient information can be obtained on geometrical changes of fuel and

structural components of fuel assemblies, fuel failure causes, fission product distribution, structure and property of cladding and fuel materials, etc.

Significant progress has been reached in development and use of such comprehensive non-destructive methods as of neutronography and tomography. They have recently been complemented by new methods for fuel-clad gap control and for precise measurement of fuel rod cladding diameter. Significant attention is paid to further development of non-destructive methods including control of defects, if any, in fuel rods under irradiation. It is of special importance for fuel assembly repair.

Destructive methods are widely used in hot laboratories in many countries directed on obtaining information on composition, structure and properties of fuel and structural materials. Further development has been noticed in the use of Secondary Ion Mass Spectrometry (SIMS) for irradiated fuel. This will allow receiving a new knowledge on structure and composition of irradiated fuel necessary for understanding fuel behaviour at high burnup.

In-pile methods are very effective to receive the most complex information on irradiation impact on fuel and structural materials. Their further development is expedient.

On the request of the IAEA Technical Working Group on Water Reactor Fuel Performance and Technology the issue of the revision of "Catalogue of PIE Facilities" (published by the Agency in 1996) was raised and discussed during Panel Discussion. The revision was supported by the TCM participants with further transformation of the Catalogue into database. Database developed and maintained by RIAR (Russian Federation) was evaluated as good model for this purpose.

METHODS FOR FUEL EXAMINATION — REVIEW
(Session 1)

Chairpersons

V. SMIRNOV
Russian Federation

L. SANNEN
Belgium

Review of methods used at SSC RF RIAR for mechanical testing of specimens made of WWER zirconium fuel rod claddings

I.M. Golovtchenko, S.G. Yeremin, Yu.Yu. Kosvintsev, I.A. Kungurtsev

State Scientific Center of Russian Federation, Research Institute of Atomic Reactors, Dimitrovgrad, Uljanovsk Region, Russian Federation

Abstract SSC RF RIAR uses and develops continuously the methods for investigating the different properties of fuel elements (FE) as well as their components irradiated in the WWER reactors. The methods for investigating the mechanical properties of zirconium claddings before irradiation, in irradiation and after it are of particular interest. Considering the objectives of meeting, the given report reviews the methods of mechanical testing as well methods of corrosion and thermal treatment of samples made from irradiated fuel elements and their claddings. Presented here are the procedures and some results of their application.

1. INTRODUCTION

WWER fuel elements claddings are exposed to compound thermal, mechanical effects and corrosion attack. These effects continue for a long time in nominal operation condition. Their results are studied adequately and they can be allowed correctly for calculation of fuel element reliability and life time. As for transient and emergency conditions the effects are of short duration but their consequences are studied to a lesser degree. To calculate fuel element reliability under such kind effects and the remaining lifetime of fuel elements after the affecting, it is necessary to know the mechanical properties of zirconium claddings on their long-term exposure to the combined mechanical loadings, after rather short-term and high-temperature corrosion attacks and after high-speed thermal shock.

2. METHODS OF MECHANICAL TESTING

2.1 Uniaxial loading

Test devices provided with mechanical drive are used for uniaxial loading testing. Fig. l demonstrates the most generally used shapes of the experimental samples.

These are ring samples (Fig. 1a) that are cladding cut-offs designed for tensile testing in the transverse direction with the use of semicircular supports. The cutting-off is performed using the high-speed diamond cutting wheel.

These are longitudinal samples (Fig. 1b) that are made with the use of electro-erosion cutting and designed for tensile testing in the axial direction.

These are tubular samples (Fig. 1c). They are cladding cutoffs provided with terminal parts that are welded on each end face and intended for axial tensile testing.

2.2. Biaxial loading

For a long period of time the mechanical testing of claddings under biaxial loading was performed using samples (Fig. 2a) sealed under the excess gas pressure. Sealing is followed

by the sample exposure at high temperatures. The method is the simplest one but it makes the variation of tangential stresses in the cladding impossible at constant temperature.
Such variations are possible when the external source of the controlled gas pressure in sample is used that is exposed to heat (Fig. 2b).

Fig. 3 presents the schematic drawing of the in-cell test rig that is used for such kind of tests. The engineering properties of the test rig:

Test temperature- up to 1200°C;
Internal pressure of the sample- up to 16Mpa;
Sample length- 275mm.

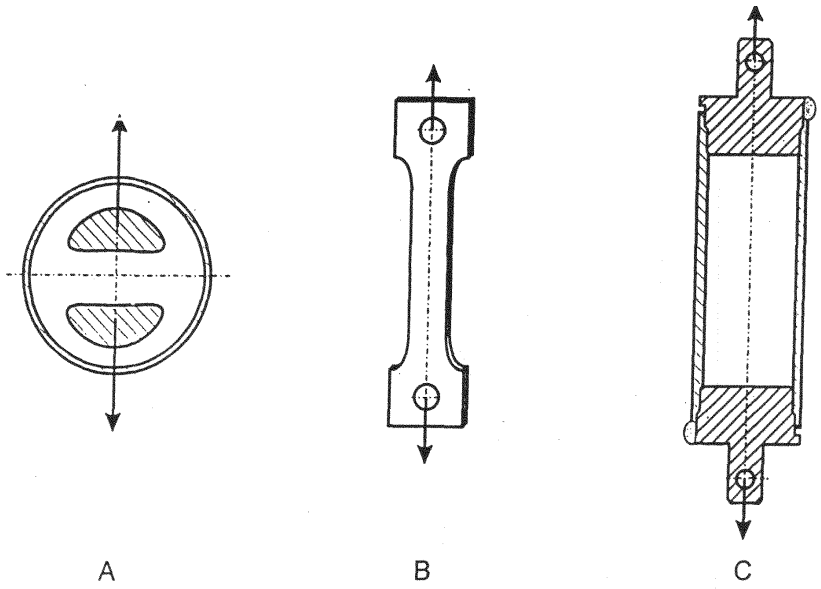

FIG. 1. Samples for uniaxial tension.

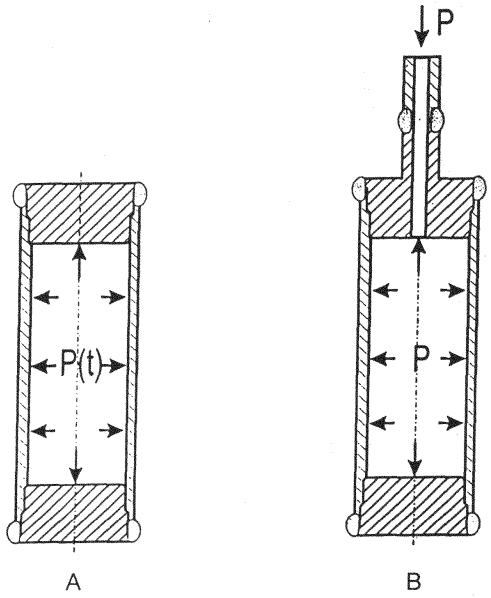

FIG. 2. Samples for biaxial tension $\sigma_\theta / \sigma_z = 2$.

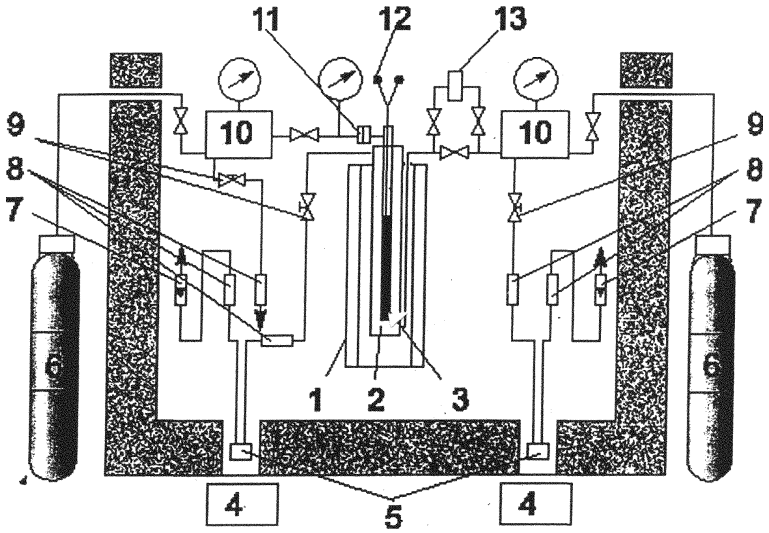

1 –electric furnace
2 - sulacapr
3 - sample
4 - detector
5 –accumulative chamber
6 - gas-cylinder
7 -rotameter
8 - filter
9 -reducer
10 -container
11 –demountable conntctor
12 -thermocouple
13 –ateam generator

FIG. 3. In-cell test rig for gas loading.

The biaxial stress-strained state forming the different relation of hoop-axial stresses σ_θ/σ_Z occurs in cladding as a result of thermomechanical UO_2 pellet-cladding interaction. This relation depends on the factor of UO_2 pellet-cladding friction. And in the general case it can change in the range from 2 (without contact) to 1 (full engagement and isotropic fuel extension). The test rig was developed to determine the failure parameters of tubular samples in conditions of biaxial stress-strained stress with the hoop-axial loading relation of σ_θ/σ_z=l...2.. The facility is illustrated in Fig.4. The cutoff sample of WWER and RBMK fuel element becomes free of UO_2 pellets and it is sealed mechanically on each end face using the metal sealing bushings. The internal sample pressure is created by the external source of the controlled hydraulic pressure. The independent external source creates the controlled axial loads on the sample. The cladding diameter of central section, internal sample pressure and axial load are measured in testing.

The engineering properties of the test rig:

Test temperature- up to 500°C;
Rate of pressure increase inside the sample -0.01... 1,0MPa/s;
Internal sample pressure - up to 150MPa;
Additional axial load- up to 10kN;
Sample length- 275mm.

Results of mechanical tests conducted with non-irradiated and irradiated claddings of WWER fuel elements are given on Fig. 5 [1] to show the significant effect of the additional axial loading.

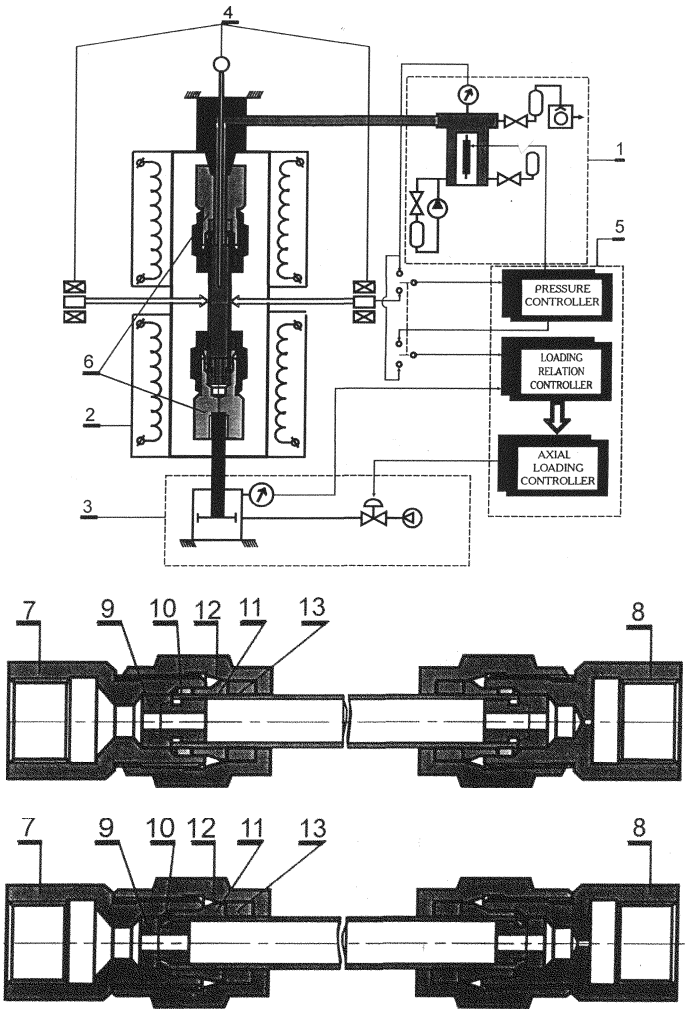

FIG. 4. Rig for tubular sample testing when $\sigma_\theta/\sigma_z=1...2$.

A test rig pictured in Fig. 6 is used for studying the effects of corrosion attack of fission iodine on the cladding. The source provided with coarse control of gas pressure creates the internal pressure in the sample that is the FE cladding cutoff. Another source of gas pressure is used for fine control of external pressure. As a result, the preset pressure is maintained inside the sample to high accuracy. The sample dimensions vary in the course of long-run testing.

The required quantity of iodine is in the glass capsule that breaks at a right time. The iodine is placed inside the sample being tested.
As this takes place, the corrosion damage of zirconium claddings is simulated when fuel element is operated in steady- state or power ramping conditions. The engineering properties of the test rig:

Test temperature- up to 500°C;
Internal sample pressure - up to 100 MPa;
External sample pressure- up to 1 MPa;
Sample length- 275mm.

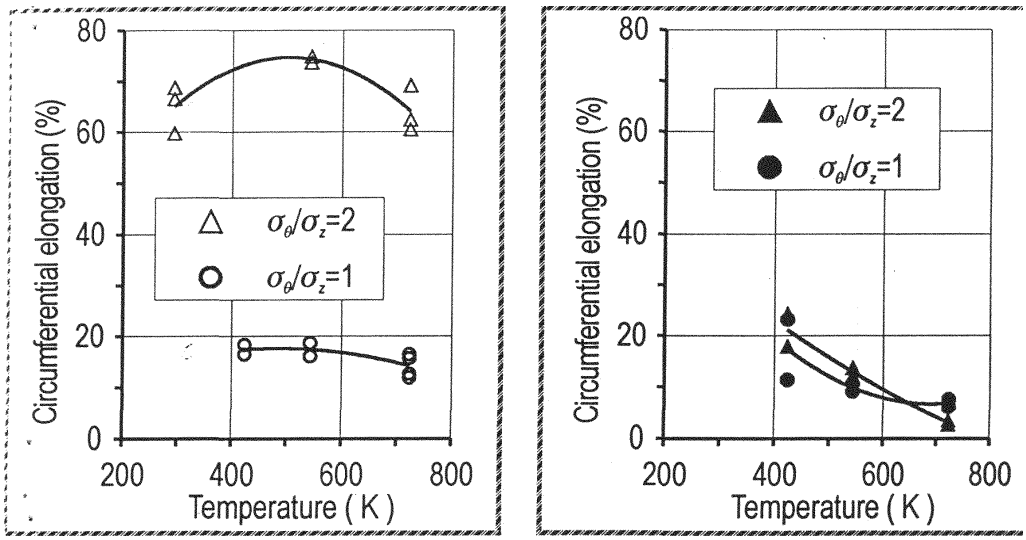

Fig. 5. The influence of σ_θ/σ_z relation on hoop strain of non-irradiated and irradiated for WWER FE claddings.

The results of irradiated cladding testing exposed for a long time to the internal gas pressure at 350°C are presented in Fig. 7 to demonstrate the significant effect of iodine as a corrosive agent.

A test rig demonstrated in Fig. 8 is designed for biaxial loading of claddings with internal gas pressure. Claddings can be loaded with hydraulic pressure on the outside that is capable of cycling with time. As an alternative to possible ways of testing the examples are plotted. This is the external hydraulic pressure cycling against constant internal gas pressure. Such kind of loading allows us to simulate the mechanical loading of FE claddings having high burnups and to study low-cycle cladding fatigue. The simulation is performed under power ramping conditions.

The engineering properties of the test rig:

Test temperature- up to 500°C;
Internal sample pressure - up to 100 Mpa;
External sample pressure- up to 200 Mpa;
Possibility of external hydraulic pressure cycling on a frequency of<l cycle/min;
Sample length- 275mm.

3. METHODS OF CORROSION AND THERMAL TREATMENT.

3.1. Overheating of claddings and samples in water steam

The in- reactor superheating of FE claddings under emergency conditions was simulated with the help of local overheating stand [2] using muffle furnace (Fig. 9). The sealed or unsealed fuel element cutoff (or FE cladding cutoff) is exposed to different temperatures (up to 1000°C) at different points as shown in the Figure. As a result of this, corrosion and thermal effects in the cladding material are distinguished by height. The differences are revealed in the course of mechanical testing of ring samples that are cut-offs of different cladding sections to be distinguished by height when the cladding is tested using the test rig.

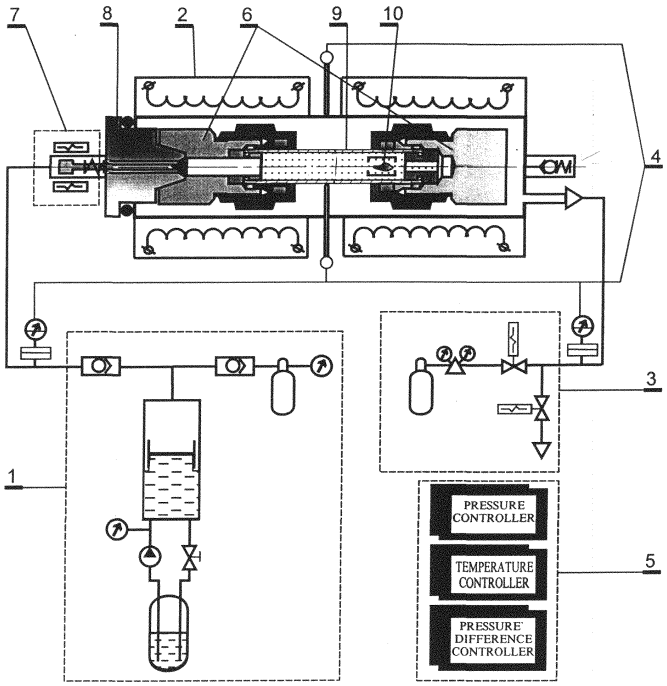

1 - high gas pressure generator
2 -electric furnace
3 - system for pressure difference keeping
4 - instrumentation sensor
5 - controlling system
6 - final elements
7 -electromagnetc valae
8 - sealing unit
9 -sample 10-corrosive agent

FIG. 6. Rig for tubular testing under iodine corrosion.

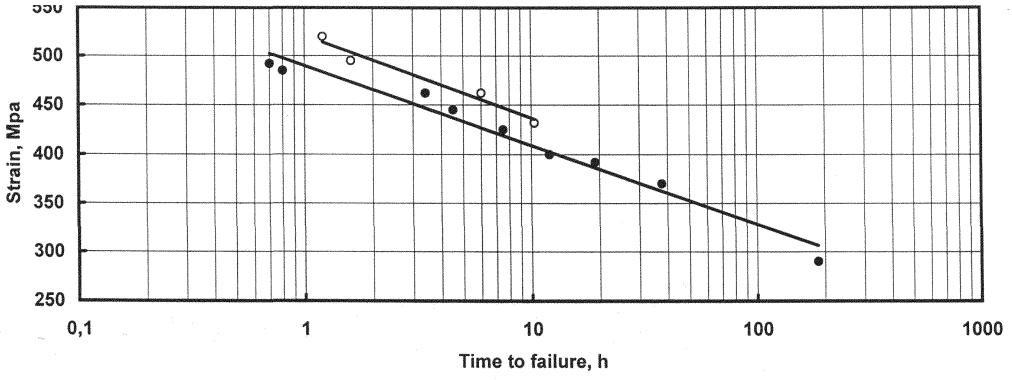

FIG. 7. Iodine effect on long-term strength of irradiated WWER FE clading samples at 350°C.

o *Iodine-free samples*

• *Samples whith iodine*

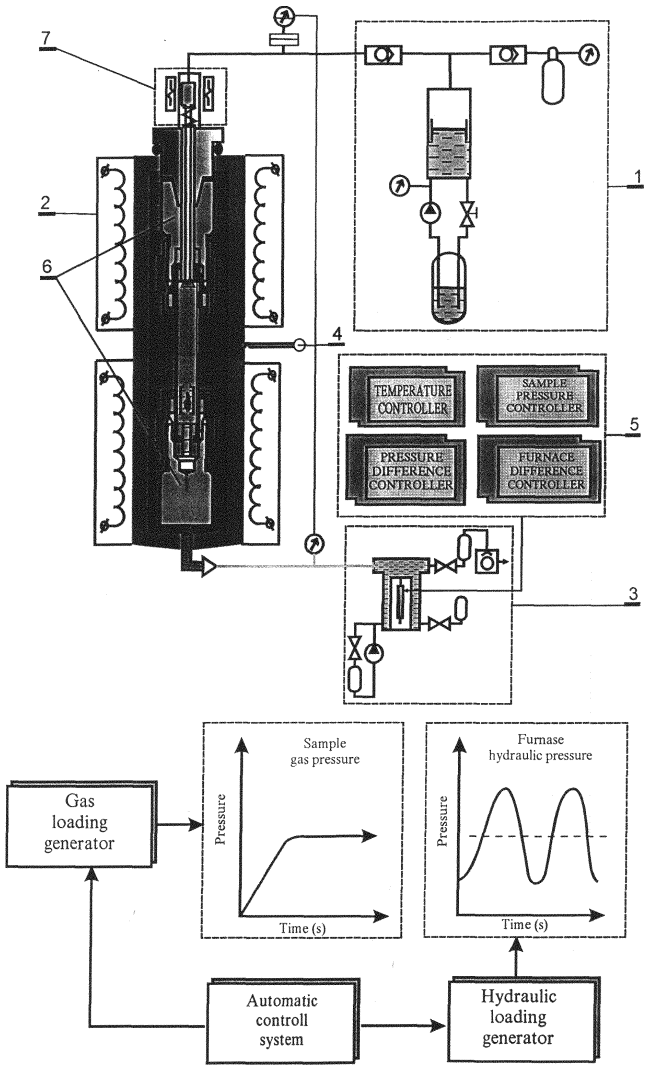

FIG. 8. Rig for low-cycle fatique testing of tubular samples under iodine corrosive effect.

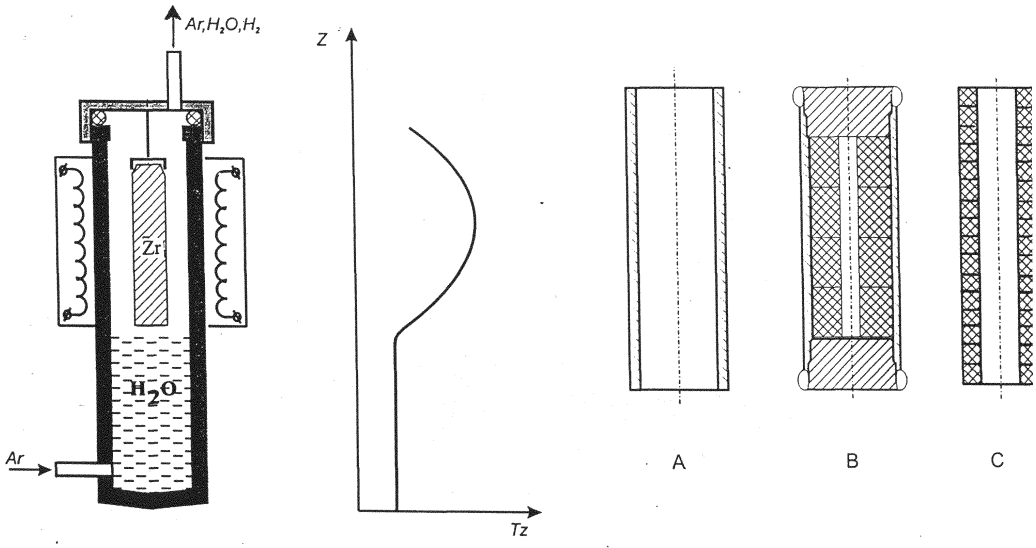

Fig.9 Facility provided with muffle furnace for corrosion and thermal treatment of zirconium samples
A- cladding cutoffs
B- sealed FE cutoffs
C- annular samples for mechanical testing

The ring sample cut-off for mechanical testing of claddings exposed to active oxidation in heating may involve difficulties due to considerable reduction of zirconium plasticity. In such a situation, the sequence of operations was as follows.

At first the ring samples were cut out from the FE cladding cut-off. These samples were stringed using suspension rod. The suspension rod was placed at the specified section of the furnace. By this means the ring samples made in advance were exposed to overheating in water steam at produced temperature gradient inside the furnace. The specific mode of corrosion and thermal treatment is assigned to each ring specimen when the mechanical test data of these samples are analyzed.

The similar facility is illustrated in Fig. 10. A smaller sample is exposed to uniform heating up to higher temperatures using this facility. The engineering properties of the facility:

Test temperature- up to 2000°C;
Heating rate of sample in inert atmosphere- up to 100°C/s;
Heating rate of sample in water steam and gas environment- up to 10°C/s;
Sample length- 45mm.

3.2. Quenching of claddings and samples into water

The quenching of fuel elements after their emergency overheating in the nonuniform temperature field was simulated using the same facility (Fig. 9). But some additional devices were used for this purpose. These devices made sample falloff into the water at the predetermined time period possible. The samples were after the corrosion and thermal treatment that was performed at the top end of the stand. Cutoffs of fuel elements, claddings as well as ring samples made beforehand were under mechanical testing (Fig. 9a, 9b).

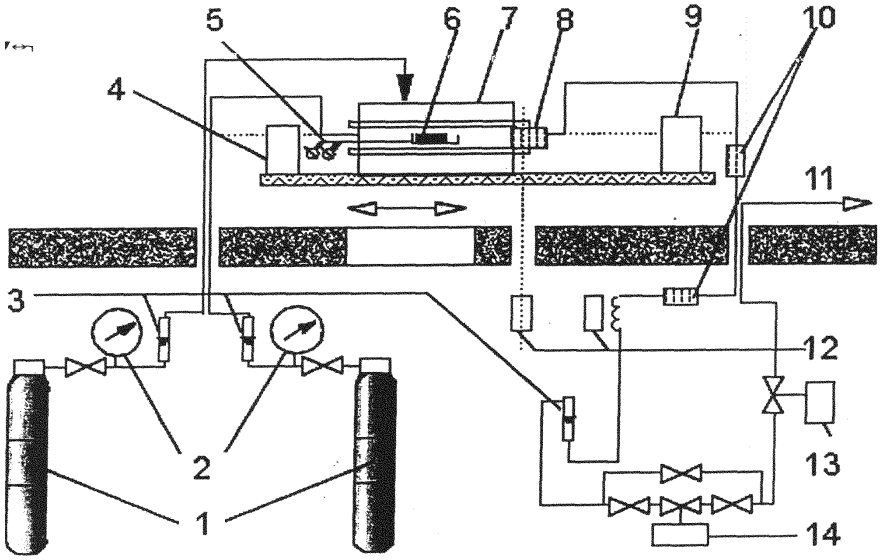

1 - argon cylinder
2 - pressure gauge
3 - rotameter
4 - steam generator
5 - micro-thermocouple
6 - sample
7 - heater
8 - base filter
9 - condenser
10 - additional filter
11 - discharge to special ventilation system
12 - gamma detector
13- gas-analyzer
14 - mass spectrometer

FIG. 10. Experimental setup for sample oxidation study.

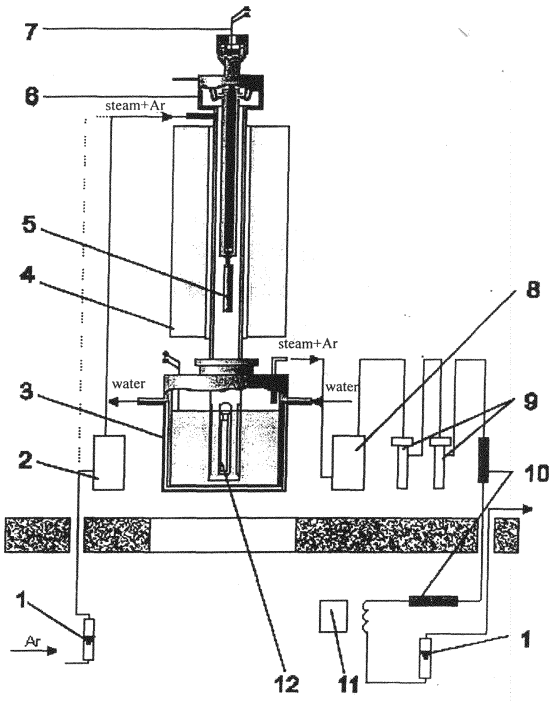

1-Rotameter
2-Steam generator
3-Water tank
4-Heater
5-Sample
6- Device for sample falloff
7-Micro thermocouple
8-Condenser
9-Bubbler
10-Filter
11- Semi-conducting detector
12-Sample after falling off

Fig.11. Experimental setup for cladding thermal stability study.

The similar facility is presented in Fig. 11. The samples are exposed to uniform heating up to higher temperatures using it. The engineering properties of the facility:

Test temperature-up to 1300°C;
Water temperature- up to 100°C;
Sample length- up to 200mm.

4. CONCLUSION

The methods of corrosion and thermal treatment as well as methods for mechanical testing of samples made of claddings irradiated in the WWER reactors that have been developed and used in SSC RF RIAR provide the results required for calculation of WWER FE reliability operated in nominal, transient and emergency conditions.

REFERENCES

[1] L. YEGOROVA, V. SMIRNOV, S. YEREMIN et al, "Mechanical Properties of Unirradiated and Irradiated Zr-l%Nb Cladding under Accident Conditions". Report presented on twenty-seventh Water Reactor Safety Information Meeting, Washington, USA, October 25–27, 1999.

[2] I. GOLOVCHENKO, "Research Methodology and Equipment to Study Properties of Irradiated Fuel upon In-cell Local heating". Report presented on European Working Group "Hot Laboratories and Remote Handling", Petten, Netherlands, May 14–15, 1996.

EDF requirements for hot cells examinations on irradiated fuel

J. C. Segura[a], G. Ducros[b]

[a]EDF/SEPTEN/T/CN, Villeurbanne, Cedex, France
[b]CEA/DEN/DEC, Saint-Paul-lez-Durance, Cedex, France

Abstract The objectives of increasing French Nuclear Power Plants (NPP) availability while lengthening the fuel irradiation cycle and reaching higher burnups lead EDF to carry out on site and hot cell examinations. The data issued from such fuel behaviour monitoring programmes will be used to ascertain that the design criteria are met. Data are also needed for modelling, development and validation. The paper deals quickly with the logistics linked to the selection and transport of fuel rods from NPP to hot cell laboratory. Hot cell PIEs remain a valuable method to obtain data in such fields as PCI (Pellet-Cladding Interaction), internal pressure, FGR (Fission Gas Release), oxide thickness, metallurgical aspects. The paper introduces burnup determination methods, inner pressure evaluation, preparation of samples for further irradiation such as power ramps for PCI and RIA (Reactivity Initiated Accident) testing. The nuclear microprobe of Perre Süe laboratory is also presented.

1. SUMMARY

The objectives of increasing French Nuclear Power Plants (NPP) availability while lengthening the fuel irradiation cycle and reaching higher burnups lead EDF to carry out on site and hot cell examinations. Although there is a trend towards replacing hot cell examinations by more up-to-date and cheaper on site PIEs, in many ways hot cell PIEs remain the only available method: they will be used in such fields as PCI (Pellet-Cladding Interaction), internal pressure, FGR (Fission Gas Release), oxide thickness, metallurgical aspects. Particular hot cell techniques may also be valuable to prepare further experimental irradiations. These items will be investigated both for UO_2 and MOX fuel. The data issued from the monitoring programmes will be used to ascertain that the design criteria are met. Data are also needed for modelling, development and validation.

In France the R&D programmes started with 900 MW(e) plants and are now being extended to the 1300 MW(e) and 1450 MW(e) plants. Three categories of cooperative programmes meet the above objectives:

- *R&D programmes*, with the aim of determining fuel behaviour under irradiation and the associated modelling programmes
- *Monitoring programmes,* with the aim of verifying design compliance of current fuel and validating new designs
- *''Specific programmes'',* for detailed investigation in hot cells.

Only a general outline will be given about the operations to be performed to select and transfer a fuel rod from the NPP to the laboratory; in this purpose related on site servicing on fuel assemblies includes PIEs on rods and structures, and fuel rod extractions with R&D objectives.

On site PIEs are done in the spent fuel pool. These interventions are carried out under water with a specific chemistry. The spent fuel pool is cooled to about 60°C and servicing tools can be in contact with fuel assemblies (FAs). Specific Safety rules must apply.

For example, handling FAs and servicing tools must comply with seismic qualification. As some tools need to be transported from one NPP to another, radiological cleansing must be done in compliance with exit and admission regulations.

This paper will therefore mainly deal with current hot cell PIEs, new PIEs trends and how they comply with the objectives of EDF. To sum up, current on site PIEs include oxide thickness, length and diameter of the rods and structural measurements. On site measurements allow better sampling. Hot cell PIEs are becoming more and more specific, focusing on the irradiated pellet and metallurgical characterisation. The main points examined in the rod itself by destructive testing are internal pressure and FGR.

While examining current hot cell PIE, it appeared necessary to update and develop new non-destructive or destructive analysis. A comprehensive programme has been carried on by the French Atomic Energy Commission (CEA), Electricité de France (EDF) and Framatome. The following techniques have been developed or are under development:

- Gamma spectrometry to measure the burn up of a given fuel rodlet
- Oxide layer measurement on Zircaloy, to develop up-to-date EC methods
- Lithium contents, hydride measurement in Zircaloy and more generally light elements contents of cladding as well as of pellets
- Internal pressure measurement by destructive or non destructive methods
- Techniques allowing manufacturing, pressurisation and instrumentation of irradiated rodlets or tubes
- Metrology improvements to monitor mechanical testing.

2. SELECTION, EXTRACTION AND TRANSFER OF IRRADIATED FUEL RODS

Prior to hot cell examination the fuel rods need to be selected at the NPP. For this purpose the following on site examinations may be of interest:

- Measurement of fuel rod diameter, length, fissile stack length on peripheral rods,
- Measurement of oxide thickness using EC technique,
- An EDF Service is able to provide the average burnup of every rod of the fuel assembly at the end of the related cycle.

The rods chosen for hot cell PIE are extracted from the fuel assemblies using the RSA device, this is a simplified repair device for FAs with removable upper nozzles. RSA is a simple, easy to use set of tools, designed for the extraction and replacement of fuel rods after removal of the top nozzle. This process takes place in the fuel building pool. The fresh fuel elevator is needed to support and to move the FA. During the insertion and extraction process the fuel assembly is moved up and down while the device holding the fuel rod remains in a fixed position. The equipment includes a set of tools to control the operations and to inspect the rods.

Only three people are needed to operate the RSA equipment in less than 60 hours including set up, removal and decontamination of the equipment. FRAMATOME has acquired an R&D experience base of more than 300 fuel rod extractions. Almost all of these rods were taken to hot cells.
In EDF plants, this tool is either used for cost effective R & D purposes or for repair purposes. In the R&D field about 250 fuel rods have been extracted. Regarding repairs, the tool allowed significant additional F/A x Cycles further irradiation. The extracted fuel rods are then placed in the "guide tubes" of a special structure derived from a F/A skeleton. The structure is inserted under water in a fuel transfer cask.

The licensing agreement of the fuel cask has to be respected, concerning load type, burnup, residual activity and heat. The rods are then transported from the NPP hot cells laboratories.

3. AGREED SHARING OF RESPONSIBILITIES

The PIE on fuel rods is generally described in a specific agreement between the laboratory, EDF and the fuel supplier. This agreement sets down the objective of the examinations and related share of costs and schedule data. The performance of a monitoring programme encompasses ten elementary items shared between the above partners according to each one's field of activity:

- **Task 1:** *The manufacturing file*
  The fuel vendor must provide a document describing the related fuel rods manufacturing data.
- **Task 2**: *Additional characterisation*
  When partners find it necessary the fuel supplier will give additional information.
- **Task 3**: *The irradiation file*.
  EDF has to provide data about the fuel power history of the rods to be examined.
- **Task 4**: *To provide a storage and transfer cask*
  The partners must provide such a structure. It can be necessary for the vendor to manufacture a new one. Specific fabrication can be required.
- **Task 5**: *FA and rods on site PIE (nuclear power plant fuel pond)*
  These examinations may be useful to select the rods to be extracted. For a given irradiation several vendors can carry out this examination.
  EDF will publish the synthesis of the results for the attention of the others.
- **Task 6**: *Fuel rods extraction*
  The fuel supplier will extract the selected fuel rods (cf. 2). The accurate number of rods needed for the downstream hot cell programme will be extracted. The concern is to limit the source term of the laboratory.
- **Task 7**: *Fuel rods transfer*
  Within the NPP, the transfer cask is loaded, transferred by road and unloaded at the laboratory. EDF works out the data needed by the sender, the carrier and the consignee in terms of fissile material balance, residual activity and heat of the load.
- **Task 8**: *Hot cell examinations*
  The CEA has the responsibility of carrying out hot cell non destructive and destructive testing. They forward their results to the two other partners as they obtain these results. The results are then collected in a specific report by the CEA and sent to the partners.

- **Task 9**: *Conclusion report*

The agreement assesses the respective contributions of the partners to this task. Generally speaking a partner is responsible for publishing of the papers concerning his part.

- **Task 10**: *Waste management*

  The CEA is responsible for managing, packaging, and storing or reprocessing the resulting nuclear waste. These actions require an agreement of the partners determining there is no further use for the material.

  To be allowed to any further experiment, the CEA needs EDF agreement, as the latter retains ownership of the material along the whole fuel cycle.

3.1. Irradiation file, burnup evaluation

According to tasks 3 and 6, EDF owes an irradiation file to their partners. EDF publishes a paper called fuel power history. These papers will collect all the information on the irradiation of the fuel rods to be tested in hot cells and the FA they come from. Such papers are published at each cycle of the irradiation programme when fuel rods to be tested in hot cells are extracted. Beyond giving the official fuel rod average burnup, these papers group together the main manufacturing and characterisation values from tasks 1 and 2.

A quick comparison of the various burnup values as a function of their method of acquisition will be given later on. The average burnup, leading to local values along a fuel rod remains a fundamental parameter for any R&D development.

3.2. Hot cell experimentation description

The following encompasses the most complete programme currently carried out on fuel rods:

3.2.1. Fuel rods hot cell testing

This experimentation divides into two main families:

- Non Destructive Examination (NDE), the fuel rods remain intact,
- Destructive examination, needing working out on the material eliminating any return to integrity.

Non Destructive Examinations

- Accurate visual examination of the fuel rod

  This examination consists in a video recording and photographing the noticeable areas such as metallurgical defects, welding failures, peeling hints, wear areas...

- Continuous diameter profile along the rod

  It is required to measure the diameter creep of the cladding and possibly to characterise, assess and measure wear scars[1] on the cladding.

- Search of cladding defects using Eddy Current technique
- Fuel rod radiography

[1] Wear scar or fretting.

This examination will be carried out to obtain the lengths of the rod, the fissile stack, the vacuum and the spring, it will also give the number of fuel pellets composing the fissile stack.

- Fuel rod diameters measurements (several diameters along the rod)
- Oxide thickness measurement along the whole length
- Axial gamma activity. The aim is:
  - To obtain an axial relative curve of burnup (BU). To obtain the effective BU values along the rods, the official value of 2.1 will be allocated as the average value to this curve,
  - To know the distribution of fission products axially.

Destructive testing

- Fuel rod hold spring length
- Puncturing of the rod, to measure inner pressure and free volume of the fuel rod fission gases contents and calculation of the released fraction
- Analysis of the gases allowing to know the contents of the free gaseous part and the fraction of fission gases released from the pellets

3.2.2. Pellet examinations

- Axial and radial cuttings ceramographies, allowing estimation of space between pellet and cladding
- Density measurement
- Porosity measurement
- Chemical analysis
- Radio chemical analysis
- Microprobe analysis with the aim of estimating fission products distribution.

3.2.3. Cladding examinations

- Microprobe or MEB examinations, fractographies. The aim is to point out the damaging mechanisms of the cladding
- Mechanical testing (tensile, uniaxial and biaxial creep…)
- Metallographic examination (oxide thickness, local hydriding)
- Hydrogen contents analysis

3.2.4. Other F/A components examinations

Guide tubes, mixing grids and control rods are the items to be considered

- Visual
- Dimensional

- Metallography
- Mechanical testing.

4. COOPERATIVE WORK TO IMPROVE HOT CELL EXAMINATIONS

Since 1994, EDF, Framatome and CEA signed four R&D collaboration agreements. They tend to install in hot cell new measurements methods proven in non active environment. These agreements led essentially to the development of the following techniques:

- Quantitative gamma spectrometry,
- EC oxide thickness measurements,
- Internal pressure destructive evaluation,
- Use of nuclear microprobe,
- Irradiated samples pressurising,
- To improve geometric measurements on mechanical testing samples,
- Internal pressure non destructive evaluation.

These items will be reviewed later in this paper.

4.1. Quantitative gamma spectrometry, fuel rod burnup evaluation

Quantitative gamma spectrometry on an irradiated fuel rod makes it possible to obtain the value of the local burnup with an equivalent accuracy to that obtained by dissolving a pellet and looking for the neodym contents.

For this purpose the rod is scanned axially in front of the measurement device holder according to joint spectra equalling the width of the collimator slot, along the whole length of the fissile stack. Two methods are used to obtain the burnup: the standard method and the simplified one.

The standard method is the more accurate but it is more complicated to operate; it consists in:

- A local measurement of gamma emission along the fuel rod,
- Calibration of the measuring channel allowing the obtaining of fission product concentration in the examined region using ^{152}Eu source,
- Calculation of fission nuclei production using an appropriate calculation code. Such a code uses **in a relative way** the rod power history and the neutronic characteristics of the fuel.
- An adjustment of calculation versus measurement is carried out by fitting in an absolute way the fuel power history in order to make converge calculation and main fission products measurements. Among fission products ^{137}Cs will be usefully used, given its half life of 30 years it will be the best integrator for burnup. It will be significant not to have operated at a power higher than nominal conditions: cesium migrates easily out of hot points.
- Such an adjusted calculation provides the value of the burnup for every measured area.

The simplified method consists in comparing measurements, carried out using the same collimating conditions and an identical setting up of the electronic acquisition equipment: both the standard rodlet (the burnup of which is known) and the rod with an unknown burnup will be measured. A simplified formula, using fuel characteristics as well as the irradiation history in the PWR makes it possible to obtain directly the burnup. Four standard rodlets were shared between four EDF and CEA high activity laboratories. It was shown that this simplified method only deteriorates the result by a few % versus the standard measurement.

4.2. Oxide thickness measurement using Eddy Current (EC)

This measurement is carried out using an EC probe. Two significant improvements were brought about during the recent years: qualifying a standard easing the measurement along the rod and studying of a more open measurement device (FAST EDDY) enabling the knowledge of calibration characteristics and accelerating the measurement.

Up to now, the thickness measurement standard is made from a zirconium tube with MYLAR pads fixed on it. The thickness of the insulator was certified by the manufacturer. Such a calibration standard allowed only punctual measurements because of the risk of pulling out the MYLAR film. FRAMATOME manufactured three new types of calibration standards: they are made from a coating of plasma vaporised aluminium on rectified Zy-4 tubes. These standards are used on the measurement device MEGAFOX. The measurements which have been carried out for two years show no evolution of the calibration standard under irradiation. They indicate that the aluminium pads remain sufficiently homogeneous in order to guarantee the correct calibration along the standard rodlet.

The FAST EDDDY was already used for integrity checking, it allows also thickness measurement. Operating frequency can be chosen between 10 Hz and 5 MHz. The information provided is impedance variation between measurement probe and a standard one. The probe is a FISHER one with diamond head. When comparing the measure performed with this new device minor uncertainties of about 2 μm are noticed. This method offers the following advantages:

- Shorter time of measurement, reading through an analogical card is immediate, a factor 4 bonus might be reached versus the current,
- Axial calibration along the standard, similar to the measurement along the fuel rod, precise knowledge of the calibration curve,
- The same apparatus can be used for integrity control of the cladding and oxide thickness measurement.

4.3. Destructive measurement of the internal pressure

Fission Gas Release (FGR) from the fuel matrix during irradiation and gathering of these gases in the upper plenum of the rod results in increasing the internal pressure of the fuel rods. This factor reduces the possibility of using fuel at high burnups. In order to assess this physical parameter, CEA developed an accurate device for puncturing the cladding and installed it in a hot cell. Internal pressure and free volume of the rod can be obtained by using this tool. The device, updated in 1998, consists in a double pressure reduction into calibrated volumes, enabling not to use a Toepler pump.

The accuracy related to free volume is about 3%. The device allows the sampling of the gases into glass tubes for further analysis. Fission gas analysis is then carried out in a dedicated laboratory next to the hot cell. It allows to assess various gases contents with a better than 1% accuracy:

- Stable isotope of Xe and Kr by using chromatography in gaseous phase coupled with mass spectrometer, the device was recently installed in a glove box,
- ^{85}Kr by gamma spectrometry using a Ge(HP) high efficiency detector.

4.4. Nuclear microprobe utilisation

4.4.1. Principle

The fundamental principle of the two microprobes (electronic and nuclear) is the same: a particle beam is focused on the sample and the rays emitted in return are analysed. The electronic microprobe is able to send an electron beam, with an energy of 30 keV which can only reach 1 μm under the surface of the sample. The nuclear microprobe, on the other hand, emits protons reaching an energy of 3.8 MeV. The beam can penetrate 10 μm under the surface. The particularity of this analyser is that it can be used in three different ways.

4.4.2. Applications

The nuclear microprobe of the Pierre Süe Laboratory, located on the Nuclear Center of Saclay is operational since 1993. It can perform highly sensitive analyses based on the use of atomic and nuclear reactions induced by light charged particles (proton, deuteron, helium-3 or helium-4) in the energy range of 0.3 to 3.8 MeV. It provides a efficient means to determine the isotopes of the light elements (H to Si) by using nuclear reactions. Simultaneously, heavier elements (Na to U) are measured by X-ray emission with an accuracy of few wt ppm.

With a beam size resolution of (1x3 μm^2), it is also used for non-destructive recording of concentration profiles. It can also map the microscopic distribution of the elements within the regions of interest. Volume analysis can be performed by nuclear resonant reactions. The beam is analysed by a magnetic dipole giving two beam lines. The line at 90° is used for multi purpose studies on non radioactive samples for Material Science (oxidation processes under constraints, impurities in grain boundaries…) and Earth Science (analysis of melt and fluid inclusions in minerals or meteorites). The second beam line, at 45°, is devoted to radioactive sample studies.

Radioactive samples are embedded, cut and polished in the EPMA preparation line of Saclay hot laboratories, and sent to Pierre Süe building. The beam line for radioactive samples of this laboratory includes a reception cell, a transfer cell and the shielded hot cell for examination.

The primary goal of the radioactive beam line was the measurement of lithium concentration in the zirconia layer. Lithium was identified by the $^{7}Li(p,\alpha)^{4}He$ nuclear reaction (Nuclear Reaction Analysis technique NRA). The α emitted particles are detected by a ”telescope” consisting of two solid state silicon detectors in order to identify the nuclear reaction products of interest from the elastic scattering on zirconium and oxygen contained in the sample as well as the α particles emitted by the activation products of a residue of fuel fixed on the analysed piece of cladding. The first results show the ability to detect very low concentration, down to

25 wt ppm, with the nuclear reactions method for very active samples. The results are comparable to those obtained on a shielded SIMS in PSI.

The second goal was the determination of the hydrogen distribution across Zry cladding thickness, by using Elastic Recoil Detection Analysis technique (ERDA). In this case elastic scattering result in the ejection of light nuclei, like protons, when a specimen containing hydrogen, is bombarded by heavier ions. Using a glancing incidence angle the light nuclei can reach the specimen surface and lose energy along their trajectories in the material. A 3 MeV helium beam, 5 x 20 μm², was used. For a cladding thickness of 550 μm, the scans were achieved in the radial direction of the cross section plane. For the geometry used and the energy of the helium beam, the number of sampled zirconium atoms in the recoil process is known. The concentration of protons in zirconium, normalized to the ratio of atomic weights, was obtained in ppm for each spot in the scan. Some specimens from PWR fuel cladding were examined and are in good agreement with destructive LECO data.

The third objective is to use the nuclear microprobe in PIXE mode in order to identify the fission gases trapped in irradiated pellets and located at a depth greater than 1μm. Tests have shown that it was not easier to detect Xenon than when using the electronic microprobe. The difficulty stems from the fact that the X Ray emitted by Xenon does not have energy enough to leave the 10 μm thickness. Next efforts will be made on Krypton that seems more detectable.

4.5. Fabrication of rodlets for further irradiation (FABRICE process)

The reconditioning of irradiated PWR irradiated fuel rods is necessary to obtain rodlets of about 50 cm long. They are needed to carry out analytical experiments in research reactors. The rodlet obtained using the reconditioning process called FABRICE comprises the original cladding and fuel (UO_2 or MOX) sampled at the appropriate level. It is then repressurised with Helium to reproduce the conditions of a fuel rod at the end of its irradiation in a PWR reactor. These analytical programmes cover the whole range of current R&D on fuel such as:

- Reaching higher burnups (fission Gas Release – FGR and Pellet Cladding Interaction – PCI concerns),
- Specific behaviour of MOX fuel,
- Power ramps,
- Accident conditions testing (LOCA and RIA).

The FABRICE process was completed in CEA Saclay toward the end of the seventies and recently transferred to CEA Cadarache. In a practical way, it consists of the following steps:

- Cutting and facing the lower end
- Fuel pellet extraction to empty 10 mm at the bottom
- Insertion of insulating pellet and plug
- Lower plug welding
- Cutting and facing the upper end
- Fuel pellet extraction at the upper end to empty 40 mm at the top
- Insertion of insulation pellet, spring and upper plug
- Upper plug welding
- Pressurisation (up to 35 bar at present, 50 bar in development) and seal welding.

After reconditioning the following non destructive examinations are carried out: visual, Xray testing of the welds, metrology, Eddy currents to assess cladding thickness and status) and gamma spectrometry. The device enables the reconditioning of about 10 rodlets per year. It is foreseen to install a second device in a different cell in order to increase the production capacity.

4.6. Samples pressurisation and laser metrology

In the framework of studying creep of irradiated cladding, irradiated tubular samples, fuel free, are repressurised up to 200 bars under Helium pressure. Such samples allow to assess creep of the cladding according to successive decreasing of load as a function of test time, temperature and previous irradiation (see G.M. Decroix presentation a the same meeting). In order to measure the metrologies of the outer diameter of the samples before and after testing a new Laser device was installed in a high activity cell in CEA Saclay.

- A Z-Mike type scanner enabling to obtain global uncertainties better than ±5 μm and to be able to repeat the measurement work in a satisfactory way,
- An holder allowing a linear translation of 260 mm,
- A motorised rotative mandrel allowing measurements at accurate angles (e. g. 30°) and to check possible ovalization.

The whole device is controlled by a computer, allowing definite and programmable positioning. The device holder is multipurpose and can be used to assess deflection (studying relaxation properties under irradiation of current or Zirconium alloys under three points flexion. Such alloys being are or will be used for thimble tubes [irradiation REFLET] or tube profiles for inner parts of the PWR shell.

The device has been set up in active conditions since 2000, after adapting and nuclearising a common device. The wall thickness measurement of the samples is now carried out using a new mechanical bench. It uses an LVDT transducer and the accuracy obtained is ±10 μm versus ±40 μm formerly by calculating the difference between external and internal diameters.

5. CONCLUSION

On site and hot cell examinations answer to the needs of R and D programmes or specific examinations programmes, they enable:

- To comply with safety authority requirements related to the behaviour of a given product.
- They help validating and modelling fuel behaviour at high burnups : in this objective new cladding alloys have been developed.

Some methods presented above are already used, others are under development. There is a permanent trend to transfer some hot cell examinations towards on site examination. Another trend is to validate in high activity conditions methods already proven in cold conditions.

FUEL INSPECTION METHODS
(Session 2)

Chairpersons

J.J. SERNA
Spain

M. ZMITKO
Czech Republic

SICOM: On-site inspection systems

J.J. Serna*, M. Quecedo* J.R. Fernández**

* ENUSA, Madrid, Spain
** TECNATOM, Madrid, Spain

Abstract

As the irradiation conditions become more demanding for the fuel than in the past, there is a need for surveillance programs to gather in-reactor operating experience. The data obtained in these programs can be used to assess the performance of current fuel designs and the improvements incorporated to the fuel assembly design, the performance of the advanced cladding alloys, etc. In these regards, valuable data is obtained from on-site fuel inspections. These on-site data comprise fuel assembly dimensional data such as length and distortion (tilt, twist and bow) and fuel rod data such as length and oxide thickness.

These data have to be reliable and accurate to be useful thus, demanding a high precision inspection equipment. However, the inspection equipment has to be also robust and flexible enough to operate in the plant spent fuel pool and, sometimes, without interfering in the works carried out during a plant outage.

To meet these requirements, during the past years ENUSA and TECNATOM have developed two on-site inspection systems. While the first system can perform most of the typical measurements in a stand-alone manner thus, without interfering with the critical path of the reload, the second one reduces the inspection time but requires using the plant capabilities.

The paper describes both equipment for fuel on-site inspection, their characteristics and main features.

1. INTRODUCTION

As the irradiation conditions become more demanding for the fuel than in the past, there is a need for surveillance programs to gather in-reactor operating experience. The data obtained in these programs can be used to assess the performance of current fuel designs and the improvements incorporated to the fuel assembly design, the performance of the advanced cladding alloys, etc.

In these regards, valuable data is obtained from on-site fuel inspections. These on-site data typically comprise fuel assembly dimensional data such as length and distortion (tilt, twist and bow) and fuel rod data such as length and oxide thickness.

These data have to be reliable and accurate to be useful thus, demanding a high precision inspection equipment. However, the inspection equipment has to be also robust and flexible enough to operate in the plant spent fuel pool and, sometimes, without interfering in the works carried out during a plant outage.

To meet these requirements, during the past years ENUSA and TECNATOM have developed two on-site inspection systems. While the first system, SICOM, can perform most of the typical measurements in a stand-alone manner thus, without interfering with the critical path of the reload, the second one, SICOM-DIM & SICOM-COR, reduces the inspection time but requires using the plant capabilities.

The paper describes both equipment for fuel on-site inspection, their characteristics and main features.

2. SICOM EQUIPMENT CONFIGURATION

Figure 1 is a general representation of the SICOM equipment. The main parts of the equipment are described in the following sections.

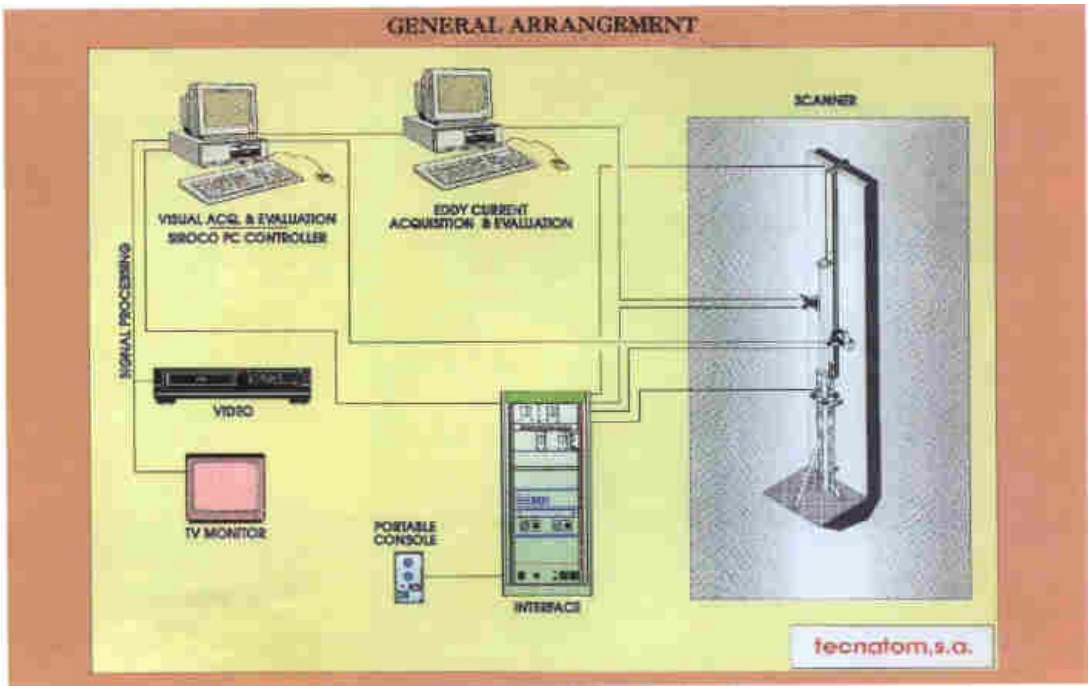

FIGURE 1. Representation of SICOM equipment

2.1. *Mechanical equipment*

Since this equipment must be installed in the spent fuel pool of different nuclear plants, it is necessary to adapt the equipment to fit in the different existing configuration.

Apart from the elements required to fit the equipment to each particular site, the mechanical equipment is designed to safely hold the fuel assembly, make it turn so each face can be inspected, and provide precise axial movement of the inspection modules.

The main sub-assemblies of the mechanical equipment are as follows:

- *Upper anti-seismic assembly:* This assembly, hanging from the rest of the mechanical equipment, is anchored outside the pool and allows the overall assembly to be leveled. It is designed such that SICOM is capable of withstand an earthquake, even in the case a fuel assembly is being inspected at the same time.

- *Mast*: Is hanging from the upper support and rests on the floor of the spent fuel pool. The inspection modules are displaced along its faces via linear guides, rack and pinions.

- *Mast support*: Provides the base to support the equipment on the floor of the pool.

- *Fuel assembly support*: Support and rotates the fuel assemblies in order to line up each face with the inspection modules.

- *Clamp*: Prevents the fuel assembly from falling, ensuring the safety of the assembly during the inspection. The clamp has no contact with the fuel assembly.

- *Displaceable modules*: The function is to transport the eddy current modules, television cameras, lights, etc. to any position along the length of the fuel assembly.

The mechanical equipment is designed and manufactured taking into account the high levels of radiation to which it will be exposed and the fact that it will operate under water.

An overview of the SICOM equipment handling a dummy assembly during the qualification test at TECNATOM is shown in figure 2.

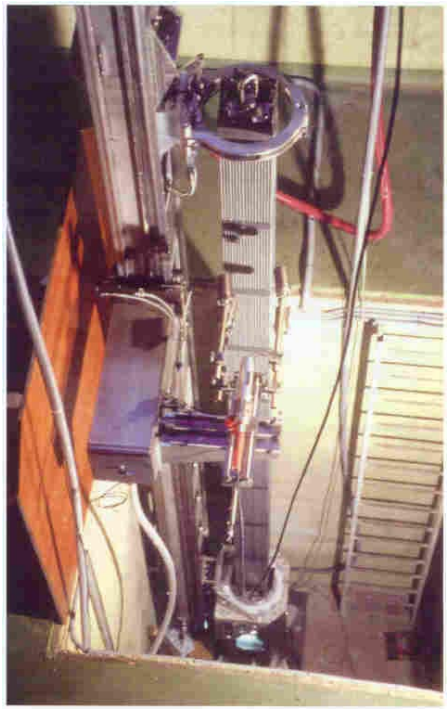

FIGURE 2. General overview of SICOM

2.2. Visual and dimensional inspection system

Dimensional measurement aims to measure variation in overall fuel assemblies geometry, namely that caused by the irradiation induced growth of the components, and the general distortion of the assembly.

The system is made up of an inspection module and the data acquisition, processing and storage equipment. The inspection module, located on the mechanical equipment, includes a radiation-resistant television camera and four spotlights. The acquisition system is made up of a personal computer including a digitizer card and software for image processing and for automatic calculation of the corresponding measurements by means of artificial vision algorithms.

The movements of the mechanical equipment for data acquisition are also automatically programmed from the visual inspection computer, along with those for the corresponding illumination. The SIROCO-PC controller executes the movements and actions generated. All the information from the visual system may be stored in the computer as well as in the video recorder.

A summary of the main characteristics SICOM measures is presented below:

a) Distance between top and bottom nozzles measured in the centre of each face.
b) Length of peripheral rods.
c) The rod-to-nozzle gap of peripheral rods on each nozzle.
d) The gap between rods at the centre of each span.

e) Assembly distortion, that is bow, tilt and twist.
f) Height of the top nozzle springs.
g) Grids width.

The basic method utilised by SICOM system to perform dimensional measurement is as follows:

The camera is positioned at the edge of the characteristics to be measured. The edge co-ordinates are obtained by a digital image processing system that has been previously calibrated using a standard length gage. Then, the camera is moved to the other edge and the co-ordinates will be obtained as above. Finally, the characteristic to be measured is calculated subtracting both co-ordinates. (This method is applied to the b), c), f) and g) measurements from above).

For type a) measurement, the length is calculated as the distance between the upper edge of the bottom nozzle and the lower edge of the upper nozzle adding the nominal bottom nozzle height.

The rod-to-rod gaps, measurement d), are obtained directly with the digital image processing system. Figure 3 is an example of the system while gathering this characteristic.

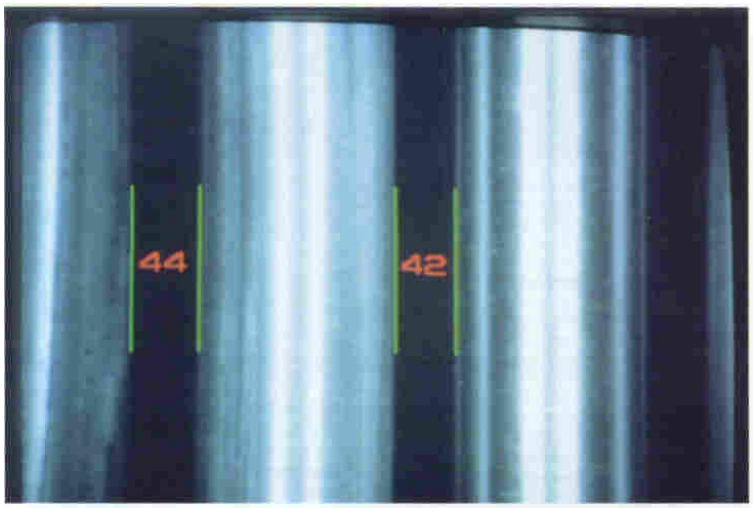

FIGURE 3. Gap between rods

For fuel assembly bow measurement two reference straight lines are drawn along the corresponding corners of the bottom and top nozzles. The horizontal distance between each grid corner edge and the reference line are measured at both corners of the grid. The bow value is determined as the average of the two measurements at each grid.

For tilt evaluation, a vertical reference straight line starting from the bottom nozzle corner edge is established. Then, the tilt would be the distance between the top nozzle edge and the reference line.

For fuel assembly twist the reference is a vertical straight line containing the bottom nozzle edge. The distance between each grid and top nozzle edges and the reference line are measured. Then, the difference between the measurements at both corners of the grid or top nozzle and the reference line gives the twist value.

In addition, the visual inspection system is used to check the general conditions of the fuel assembly (physical integrity, fuel rods, grids, nozzles and springs) and provides detailed visual examination to support, for example, oxide thickness data analysis.

2.3. *Oxide layer measuring system*

Measurement of the oxide layer on the peripheral fuel rods is performed using eddy current techniques based on measuring the separation between the probe in contact with the zirconia (not conductive) and the cladding material (conductive).

The system consists of an inspection module and a data acquisition system for data processing and storage. The inspection module includes the sensor (coil) which moves in constant contact with the fuel rod, and a television camera for observation of sensor coupling. The acquisition system is made up of a personal computer including the eddy current equipment and corresponding specific software. The results of the measurements performed may be displayed on the screen and printed out. Figure 5 shows an example of oxide layer thickness data display.

In order to ensure accurate alignment of the probe tip to the circular surface of the rod, the system counts with three degrees of freedom. Besides, grid collisions are avoided during the inspection thanks to this mechanical design.

The qualification of the equipment includes, apart from laboratory tests, hot cell metallography of irradiated rods with oxide thickness up to 100 μm. The accuracy of the measurement is estimated to be ± 6 microns.

3. SIMPLIFIED EQUIPMENT

In order to satisfy the utility generic needs such as reduced equipment size, short inspection time, adaptable to different fuel designs, low cost, etc., TECNATOM and ENUSA are developing new on-site inspection equipment.

With this objective two simplified equipment, with capabilities and accuracy comparable to SICOM, have been designed. One equipment is dedicated to the dimensional characterization of the fuel assemblies and a separate one is devoted to the measurement of the oxide thickness in peripheral rods.

As regards the dimensional equipment, SICOM-DIM, the measurements are based on LVDT

technology rather than in image analysis as is the case of SICOM. The corrosion equipment, SICOM-COR, uses essentially the same corrosion inspection module than SICOM.

The principal characteristics of these simplified equipment compared to SICOM are:

- Smaller size, lighter.
- Portable. Installation over the spent fuel rack.
- Faster assembling.
- The handling crane supports the fuel assembly during the inspection.
- Reduced inspection time (on line with the reload in the case of the dimensional equipment).

Figure 4 shows a general view of SICOM-COR equipment.

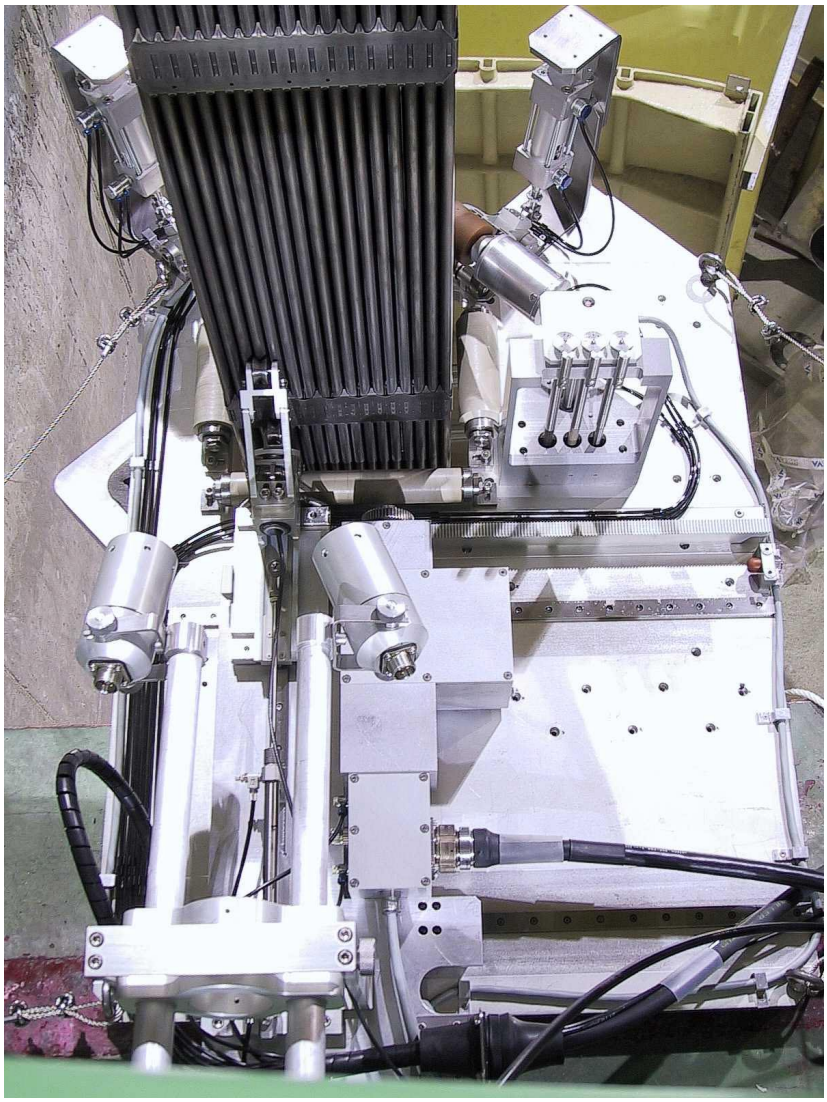

FIGURE 4. SICOM-COR equipment.

4. CONCLUSIONS

SICOM is a state of the art fuel assembly inspection system providing high resolution visual inspection, fuel assembly dimensional characterization and accurate fuel rod oxide thickness measurements.

The development of on-site inspection equipment carried out consists of two types of equipment:

- Stand-alone system, SICOM, whose capabilities includes fuel rod corrosion and fuel assembly dimensional characterization handling safely the fuel assembly.
- Two simplified equipment, SICOM-COR & SICOM-DIM, with the same capabilities show a considerable reduction of the inspection time but requires the use of the handling crane.

Field experience of these equipment includes the exam of more than 300 fuel assemblies and the measurement of the oxide thickness of more than 1500 fuel rods.

Ukrainian WWER-type NPP units. Methodological basement, results of cladding tightness inspection

O.V. Bykov

NAEC "Energoatom", Kiev, Ukraine

Abstract. In the overview report the generalized results of cladding tightness inspection are reviewed for all Ukrainian WWER-type NPP units. Brief analysis of cladding tightness inspection methodology is drawn. Approaches of Ukrainian NPPs are generalized from the viewpoint of use of widened inspection sample analysis.

1. INTRODUCTION

NAEC "Energoatom" is Ukrainian nuclear utility. We have 4 nuclear power plants in Ukraine. Today 13 units are in operation. 11 of them have WWER-1000 reactor, another 2 are WWER-440. The eldest unit has more than 20 years operation experience. Each type of reactor has Cladding Leak Tightness Inspection (CLTI) instructions that were recommended by nuclear fuel supplier JSV “TVEL”. During units operation large fuel depressurization statistics was accumulated.

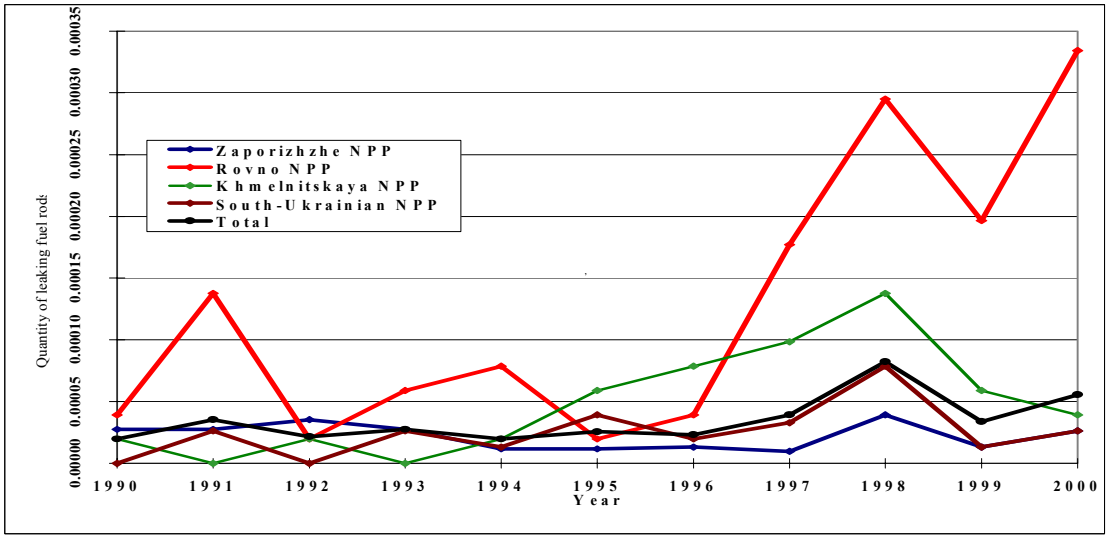

Fig. 1. Dynamics of relative quantity of leaking fuel rods (WWER-1000) from 1990 to 2000.

As you know CLTI method is based on measurements of reference isotopes activity. Results of CLTI measurements of coolant activity in operating reactor define quantity of fuel assemblies (FA) that have to be tested during refueling outage in Cask for Cladding Leak Test. So quantity of FAs tested during refueling outage can differ from 0 up to whole number of FAs loaded in reactor core. As a rule depressurized fuel assembly has 1 depressurized fuel rod. Relative quantity of FAs that have depressurized fuel rods is presented at the diagrams as illustrative material. Diagrams are given for all Ukrainian NPPs. Because of quantity of tested FAs is unstable depressurized FAs are normalized on whole number of fuel rods in reactor core.

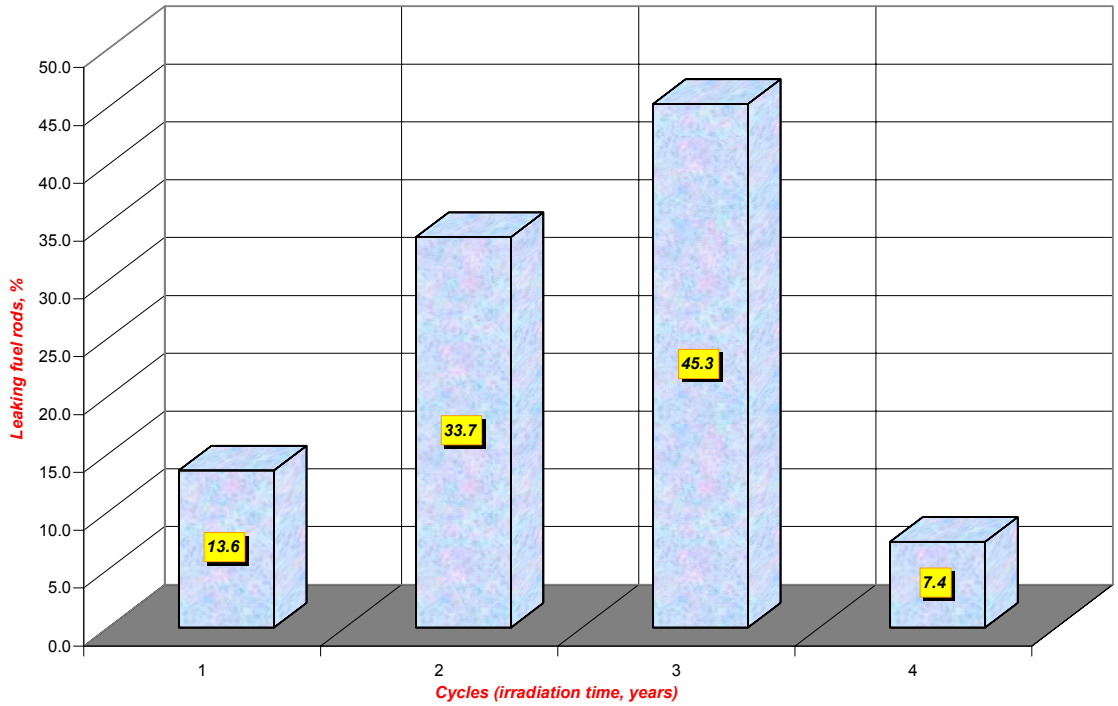

Fig. 2. Distribution of leaking FAs by spent time (1988 - 2000).

It is evident that depressurization of FAs sufficiently dropped at the period from 1995 to 1997. You can see it on histograms that have been presented. At the last 3 years fuel depressurization have been raized sufficiently on third unit of Rovno NPP. Now Rovno-3 statistics is much greater then common one for other Ukrainian WWER-1000 units. To determine the reasons of smart peak of fuel depressurization the special committee was organized. Fuel supplier, fuel fabricator, scientific and research organizations were asked by operating utility to solve that problem. Analysis was carried out. As a result correction measures were produced and putted under operation by utility to rize operation and outage quality.

The growth of first year operation FAs depressurization as it figured on histogram causes anxiety of the utility. Nowadays Ukrainian utility can analyse only operational conditions for the FAs. It is happened because of absence of scientific and technical support of fuel operation in Ukraine. Now scientific and technical support is provided by Russian organizations. In particular state scientific centre RIIAR carry out post-irradiation researches of Ukrainian FAs to find believable reasons of fuel depressurization.

2. EXISTING METHODOLOGY ANALISYS

During the analysis of fuel depressurization dynamics we have to take into consideration a number of factors that give an uncertainty in reflected values. In particular:

1. Number of tested FAs is forming as a result of analysis of reference isotopes activity in the coolant circuit and the criteria “most probable year of operation” for the leaking FAs is not used. So mostly the fourth year of operation FAs[1] (for WWER-1000) and discharging FAs are tested according to the existing methodology. In this connection leaking FA can be

[1] For WWER-440 is 4 and 5 year of operation FAs correspondingly.

detected while it is discharging at the end of operation. In some cases that one can not be detected at all if we can suppose some hypothetical mechanism of defect closure. All that reasons are correct for the small quantity of leaking fuel rods and corresponding small coolant activity in the reactor core. In this case just test of the whole number of FAs is correct. But the test of the whole number of FAs leads to the unjustified prolongation of outage.

2. Existing methodology of in cask CLTI has sufficient drawback in determination of large cladding defects. It is evident that the great part of gaseous and volatile fission products is bringing out from the fuel rod with serious defect while reactor is cooling down and pressure is dropped before outage procedures. Thus FAs that have fuel rods with serious defects may not be detected during the standard CLTI method in Cask test. That fact is very actual for the case of high coolant activity in the reactor core. That activity can be produced by huge fuel rods leaking and further contamination of cladding by uranium and fission products. So average activity becomes strong background that hides leaking FAs.

3. The existing methodology of standard CLTI is based on definite physical model. Limitations of this model may cause the unexpected results. For example the border cases of fuel rod depressurization may not be detected or tight FA can be detected as depressurized one. In particular the cases of hypothetical defect closure can be explained by overrunning the model basis. Such cases were found in Ukrainian NPPs. Some leaking FAs do not prove their depressurization after next year operation in reactor core.

3. OPERATION EXPERIENCE

Nevertheless existing equipment for in-cask CLTI allows to modify CLTI methodology on the basis of so called “expanded CLTI probe”. In that case both reference isotopes and other fission products can be used to detect FA’s leakage. The only consideration for fission products usage is the spectrum intensity of selected isotope have to be considerably higher than background one.

Rovno NPP use proportion of cesium 134/137 isotopes activities to form criteria "the most probable year of operation of leaking FA". As well known from literature [1] proportion of cesium isotopes activities strongly depends from fuel burnup. In particular that fact can be used as additional information to determine probable leaking of FA with small burnup (up to 20-25 MWt×days/kg U). Fuel burnup depends on position in FA and can substantially differ from average burnup in FA. In spite of that fact the qualitative determination of year of operation for the leaking FA is available. The most effective way to use that methodology is to determine proportion of isotopes while their output is high enough. As you know high level of coolant activity happens during sufficient changes of reactor power with registration of spike-effect, for example during cold shutdown before outage. At that time registration of coolant activity should be provided not rarely than every hour. Now operation experience of Rovno NPP is delivered to others Ukrainian NPPs.

Besides CLTI using iodine isotopes can be difficult in case of high coolant activity. That activity is conditioned by soiling of fuel rod cladding by fuel composition. In that case Cesium isotopes can be used as reference one. According to the existing methodology that isotopes are recommended to obtain additional information.

In case of high coolant activity gaseous fission products also can be used as a reference isotopes. First of all that is concerned with noble radioactive gases (NRG) for example xenon-133. Those facts are stipulated by large output of NRG from under the cladding and lighten output of them from the fuel in comparison with iodine and cesium.

Also we can use non-volatile and solid fission products such as barium-140, niobium-95, rubidium-103, cerium-141, 144 and others. Presence of them in CLTI probe indicate as a rule large fuel rod cladding defect up to direct contact between fuel and coolant. Leaking FA identifying can be carried out using those isotopes. As was said before analysis of iodine isotopes activities may show that such FA is tight. All that enumerated isotopes are preferable to identify large defects. Analysis of activity of transuranium elements such as neptunium-239 is difficult because of their small concentration and large Compton effect background.

We can use statistical criteria to identify leaking FA using NRG, non-volatile or solid fission products. Criteria "activity of reference isotope in probe greater than average activity plus 3σ" is formulated in existing methodology and used to identify leaking FA by iodine isotopes activity.

4. THE NEAREST FUTURE

CLTI in Cask demand sufficient time expenditures. So introduction of sipping method in Refueling machine working shaft is on the agenda. At the nearest future modernization of refueling machine is planned. After the introduction of sipping system whole FAs inspection is available during outage without spending additional time. Sipping method is qualitative. Necessity of CLTI in Cask tests is evident from the point of view of receiving quantitative values and identifying type of defect. In such a case CLTI in Cask is used for the FAs that have been detected as leaking one by sipping method. Introduction of sipping method allows reducing both an uncertainties in CLTI results and terms of outage.

We also have to modernize CLTI in Cask method from the viewpoint of operation experience. Now only tight FAs and FAs with defect of "Gas Leak" type are allowed for the shipping to the storage and recycling facilities. Current CLTI in Cask method do not allow determining defect type. But it can be completed using widened CLTI probe results.

The next crucial moment of existing methodology is the present value of failure criteria for leaking FA. Activity level of reference isotopes for the failed FA was selected from the experimental dissection of fuel rod. South-Ukrainian NPP case can be given as an example of lack of correspondence between CLTI probe and real defect type. FA after 2 years of operation was detected as leaking one but its activity was sufficiently less then failure criteria. According to the visual observation results fall-out of an upper fuel rod plug was detected. That means direct contact between fuel and coolant. It is evident that failure criteria have to be reduced in the basis of operation experience. Also FA is failed if it has fuel rod with direct contact. New FA failure criteria should be confirmed from the viewpoint of modern models of fission products output.

Utility is looking forward to purchase inspection facility at the nearest years. One of main requirements for such facility is ability to test all the fuel rods to find depressurized one. Now our fuel supplier has designed demountable FA. Utility is looking forward to have an ability to

change leaking fuel rods. Then rebuild FA can be used again or it can be shipped to the storage or recycling facilities.

Unfortunately there is no serious scientific and technical support of this problem in Ukraine. Now scientific and technical support is provided within the framework of fresh fuel supply contract. Corresponding Russian scientific and research organizations are involved. In current time all previously mentioned questions are at the solution stage.

REFERENCES

[1] Kolobashkhin V.M., Radiation characteristics of irradiated nuclear fuel, Energoatomizdat, Moskow (1983).

[2] 62444-03DIK Instruction. Cladding Leak Test Inspection of WWER-440 reactors (type V-230 and V-213) at the operation and after cold shutdown, OKB "Gidropress" (1979).

[3] 0401.00.00.000 DNG Instruction. Cladding Leak Test Inspection of WWER-1000 reactors at the operation and after cold shutdown, OKB "Gidropress" (1998).

[4] Results of Cladding Leak Test Inspection, Rovno NPP, Zaporizhzhe NPP, Yuzhno-Ukrainskaya NPP, Khmelnitskaya NPP (1980-2000).

[5] Reports of participants of Russian-Ukrainian workshop, Rovno NPP, (22-25.01.01).

NON-DESTRUCTIVE AND DESTRUCTIVE FUEL EXAMINATION METHODS — PART 1
(Session 3)

Chairpersons

E.H. TOSCANO
European Commission

V. ZHITELEV
Russian Federation

Improvements in PIE-techniques at the IFE hot-laboratory
"Neutron radiography, three dimensional profilometry and image compilation of PIE data for visualization in an image based user-interface"

H.K. Jenssen, B.C. Oberländer

Institutt for energiteknikk, Metallurgy Department, Nuclear Fuel Section, Kjeller, Norway

Abstract. The PIE-techniques used at IFE are continuously improved through upgrading of equipment and methods, e.g. image handling techniques and components utilized in data acquisition and editing techniques. To improve the quality or spatial resolution of neutron radiographs the normal technique was complemented with another method, i.e. the dysprosium foil/X ray film technique is supplemented with a track-etch recorder consisting of a cellulose nitrate film. For further examination of the neutron radiographs the cellulose nitrate film can be digitized to allow electronic image treatment. Promising results were obtained with this technique on neutron radiographs, namely higher spatial resolution compared to the normal technique, high contrast and sharp neutron radiography images. The traditional uniaxial profilometry of fuel rods was modified so that diameter/bow measurements are possible at several angular orientations during one acquisition sequence. This extension is very useful in several ways, for instance the built-in data symmetry of the method is used to check the correctness of the measurement results. Diameter and bow measurements give information of cladding irregularities and fuel rod profiles. Implementation of electronic image handling techniques is particularly useful in PIE when data are collected and compiled in an image file. Inspection and examination of the file contents (examination results) are possible through an ideal user-interface, i.e. Adobe Photoshop software with navigator possibilities. Examples incorporating PIE data acquired from neutron radiography, visual inspection and ceramography are utilized for illustration of the user-interface and some of its possibilities.

1. INTRODUCTION

Data from the state of the fuel and the cladding in an entire fuel rod can be obtained by non-destructive examination (NDE) in a relatively fast, environment compatible and cost efficient way compared to destructive examinations. However, to obtain satisfactory results from NDE the methods applied have to be improved steadily. Therefore, a major emphasis was put into the improvement of NDE methods for detailed post irradiation examination (PIE) of fuel rods in hot cells, such as improved spatial resolution of neutron radiographs and improved profilometry in order to give data for the diameter variation of the entire fuel rod, both in the complete axial extension and in 360 degrees angular orientation. To obtain a more complete picture of the state of an irradiated fuel rod, work was put into the electronic compilation of data obtained from various NDE methods and visualization in an image based user-interface.

2. NEUTRON RADIOGRAPHY OF IRRADIATED FUEL RODS – AN APPROACH TO IMPROVE SPATIAL RESOLUTION OF NEUTRON RADIOGRAPHS.

The main objective for neutron radiography is to reveal fuel rod degradation or possible failures initiated by for instance, intrusion of moisture, pellet-cladding interaction or fuel relocation and cracking. Neutron radiography also provides geometrical information of the fuel column for definition of cutting positions of samples for ceramography examinations.

Two neutron radiography techniques are used at Kjeller in NDE of irradiated fuel rods with UO_2 or MOX, Zircaloy cladding and instrumentation devices. Both techniques allow an unfiltered neutron beam to be used and enable neutron radiography of very active samples [2]. The traditional method uses an activation transfer technique, utilizing a dysprosium foil and X ray film. The other method uses a special solid nuclear-track detector, designed for recording ionizing particle tracks. Solid nuclear-track detectors have numerous applications [2], for example the dosimetry of neutrons and of the heavier ionizing particles such as alpha particles, protons, fission fragments, spallation fragments, heavy ions and very heavy ions such as cosmic rays etc. In every instance the thickness of the cellulose-nitrate substrate should be in accordance with the mass and energy of the particle type to be detected in order to obtain the optimum level of energy transfer. The track-etch recorder consists of a 100 μm thick plastic film of lightly rose-tinted cellulose nitrate, coated on both sides with an (n, α) energy converter material. Prior to neutron radiograph analysis the film is digitized. Illustrative examples of the two techniques are compared in the paper.

2.1 Experimental set-up in neutron radiography

Principle: The principle of image formation in neutron radiography is based on attenuation[1] of a collimated beam of neutrons transmitted through a sample. The degree of attenuation is measured by detecting the intensity I of the neutron beam passing through the sample or fuel rod with unaltered direction and it is given by

$$I = I_0 \exp(-\Sigma_t z),$$

where z is the sample thickness. I_0 is the intensity of the incoming beam and Σ_t is the total macroscopic cross section of the material, i.e. $\Sigma_t = \Sigma(n\sigma_a)/V + \Sigma(n\sigma_s)/V$. Σ is the sum of all the different atoms in the volume V, and n is the number of atoms of one kind with microscopic absorption cross section and microscopic scattering cross section given by σ_a and σ_s.

The primary source of neutrons was obtained from one of the radial channels of the JEEP II reactor[2] at the Institute for Energy Technology, Kjeller. The sample or fuel rod was irradiated by a collimated thermal neutron beam of height 220 mm and width 30 mm[3]. The thermal neutron flux in the beam channel is $\sim 10^7$ n/cm^{2}s, and the length between graphite collimator and activation screen is 390 cm.

2.2 Methods applied in neutron radiography

The dysprosium foil/X ray film technique: The method relies on the buildup of radioactivity in the foil produced by neutron absorption. In this way an activation image is formed in the foil. The neutrons captured by the dysprosium foil will generate radioactivity that subsequently decays with a convenient half-life [1],

[1] The sum of absorption and incoherent scatter.
[2] 2 MW HBWR with central thermal flux 3×10^{13} n/cm^{2}s.
[3] See Figs. 1 and 2.

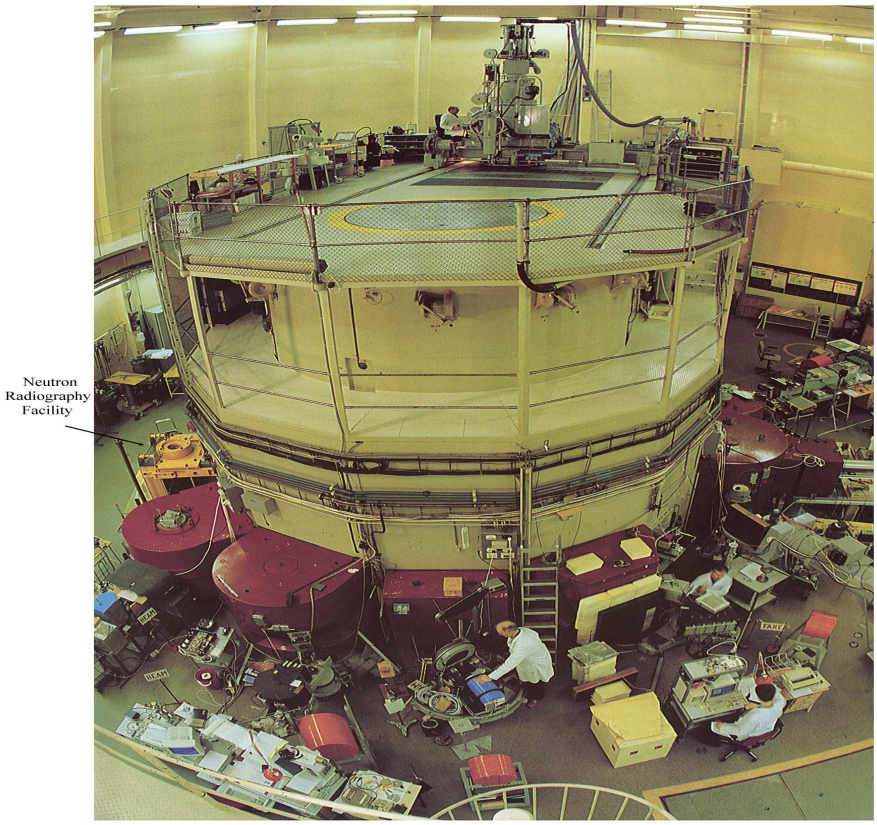

Fig. 1 JeepII reactor with experimental beam channels

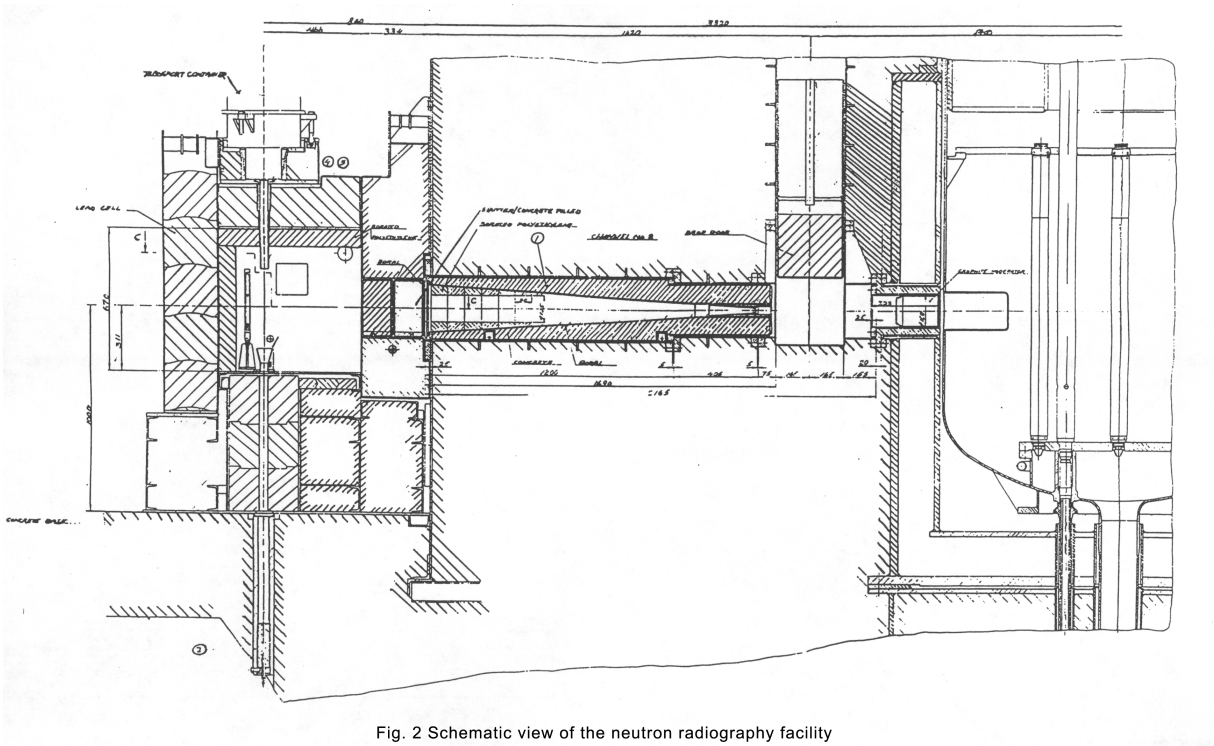

Fig. 2 Schematic view of the neutron radiography facility

$$^{164}_{66}Dy + {}^{1}_{0}n \rightarrow {}^{165}_{66}Dy \xrightarrow[2.3h]{\beta^-,\gamma} {}^{165}_{67}Ho$$

The pattern of radioactivity is transferred to the X ray film by simply placing the activated metal foil in close contact to the film. The X ray film is then irradiated for several hours and thereafter developed using a standard photographic technique.

The cellulose nitrate film technique (track-etch recorder): The film consists of a 100 μm thick plastic layer substrate of lightly rose-tinted cellulose nitrate. The film is primarily intended for recording the emission from α-particle sources (below 4 MeV) so for neutron radiography the film is therefore coated with an (n, α) energy converter material. The record thus obtained is a neutron radiographic image formed by means of the (n, α) energy converter. Transmitted neutrons will reach the vacuum deposited lithium tetra borate layer or converter screen that promptly emits ionizing α-particles, which impinge on and generating damage pits in the cellulose nitrate matrix. The α-particles take short and straight paths through the material and so give good resolution. The nuclear reactions in the (n, α) energy converter are,

$$^{10}_{5}B + {}^{1}_{0}n \rightarrow \alpha + {}^{7}_{3}Li \quad \text{and} \quad {}^{6}_{3}Li + {}^{1}_{0}n \rightarrow \alpha + {}^{3}_{1}H$$

After irradiation, the converter layer is removed by washing off in water and the cellulose nitrate film is thereafter etched in a 10 % solution of caustic soda (NaOH) at 60 °C for approximately 10 minutes. The damage produced along the particle tracks alters the chemical properties of the cellulose nitrate material in such a way that the damaged area can be removed in the etching process [2].

Electronic data treatments (digitising): After developing, the neutron radiographs (cellulose nitrate- and X ray film) are digitized with a "state of the art" photo-scanner controlled from a power Macintosh computer. By electronic data treatment, the neutron radiographs can be enlarged, stitched and combined with other PIE data of interest (e.g. fuel rod macro photos). The main purpose here is to reproduce neutron radiographs for reports and presentations with the highest achievable quality in order to visualize fuel rod details, such as pellet crack patterns, or the instrumentation of the rod.

Compilation of fuel rod neutron radiographs in an image file is ideal for further evaluation, documentation and presentations.

2.3 Qualification tests performed on neutron radiographs from an irradiated fuel rod

Quality inspection of neutron radiographs (Fig. 3, 4): The cellulose nitrate film and dysprosium foil techniques were both applied in neutron radiography of an irradiated fuel rod from a fuel assembly irradiated in the HBWR[4]. For assessment of the neutron radiography quality, it is necessary to use indicators that expose the resolution and sharpness of details of the neutron radiographs. Known features, such as the fuel rod instrumentation — in the example a bellows pressure transducer (PF), can be used as a quality indicator. Fig. 3 shows neutron radiographs (1:1) acquired with both methods from the upper end of the fuel rod. Important details marked on the figure are the plenum spring, the PF and the upper end plug . The neutron radiographs were digitized to a relatively high resolution, equal to 600 dpi, i.e. an

[4] Abbreviation for Halden Boiling Water Reactor.

approximate pixel size of 45 μm. From a first glance at Fig. 3, it can be seen that the image digitized from the cellulose nitrate film exhibits higher quality in terms of sharpness. To further check the quality of the images, it is necessary to enlarge them.

The PF shown in Fig. 4, Section B is enlarged three times. It is easy to see the PF bellows and other details on the copies from the cellulose nitrate film. On the copies taken from the X ray film the details are almost lost. This fact is even better illustrated at still higher magnifications. From Fig. 4, section C it can be seen that the X ray film contains on this scale no important information at all. The situation is quite different for the cellulose nitrate film.

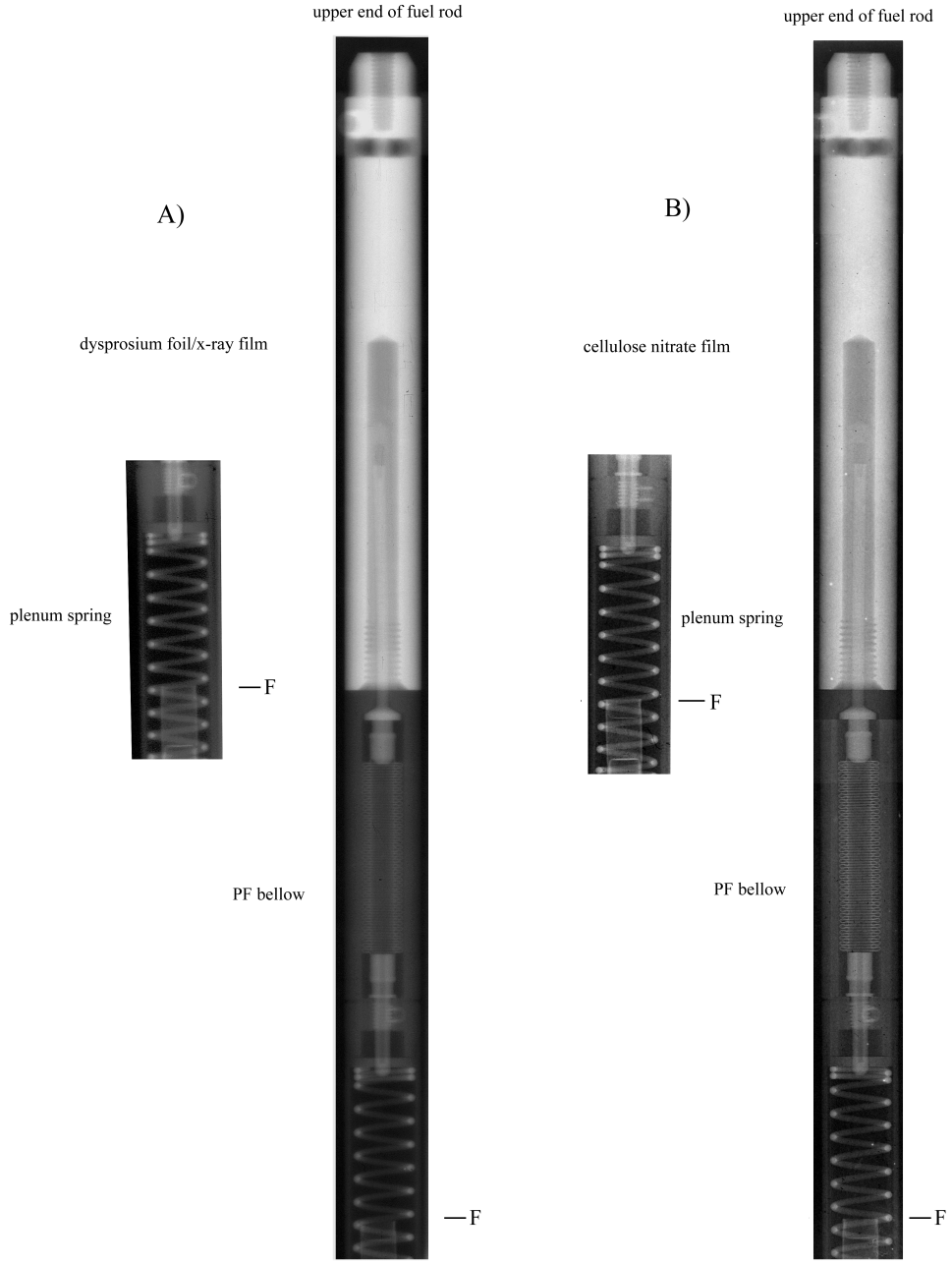

Fig. 3 Neutron radiography applied with the dysprosium foil (A) and cellulose nitrate (B) techniques.

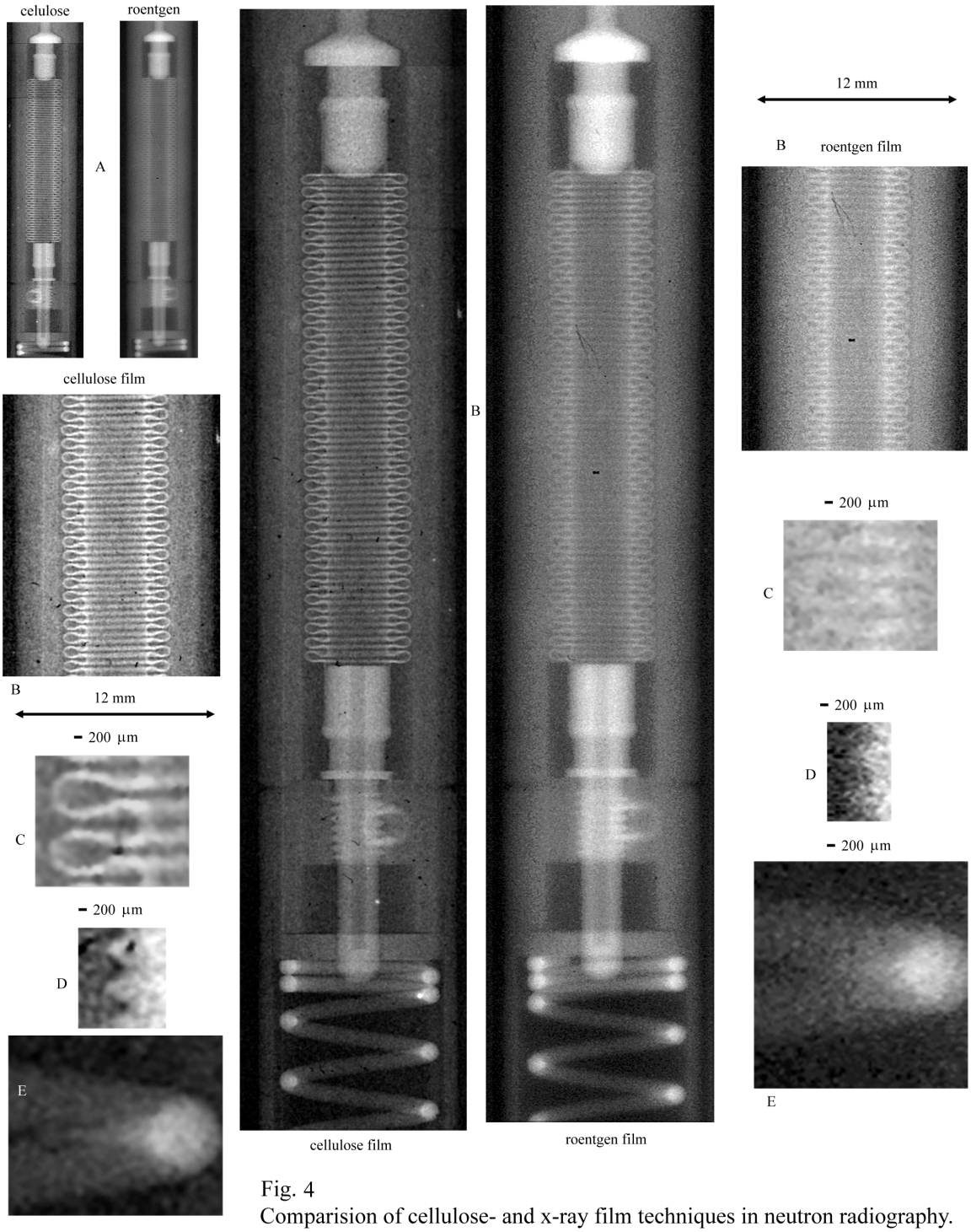

Fig. 4
Comparision of cellulose- and x-ray film techniques in neutron radiography.

Sharp details around 100 µm in size can be seen in the enlargements. For instance, the PF steel bellows is reproduced with high quality, and dimensional measurements can also be done directly on the file by utilizing suitable image handling software. Two other enlargements are given in Fig. 4, sections D and E. Again it is striking that the neutron radiographs based on the X ray film technique contain more noise than the neutron radiographs acquired from the cellulose nitrate films. The reason for the quality difference is mainly related to spreading of the gamma rays generated in the dysprosium foil under neutron radiography and spreading of the light beam through the X ray film under digitizing. With a thinner Dy-foil the gamma

radiation will spread less and thereby produce sharper film details. However, the α-particles generated in the energy converter during neutron irradiation produce sharp details in the cellulose nitrate film.

It should be said that the X ray film used in the test is double coated and during digitizing this film will spread the light beam more than a single coated film would. The main contribution to the blackening of the X ray film is β-particles emitted from the neutron activated dysprosium foil. But, the film blackening generated by the gamma radiation will superimpose and produce a less sharp image.

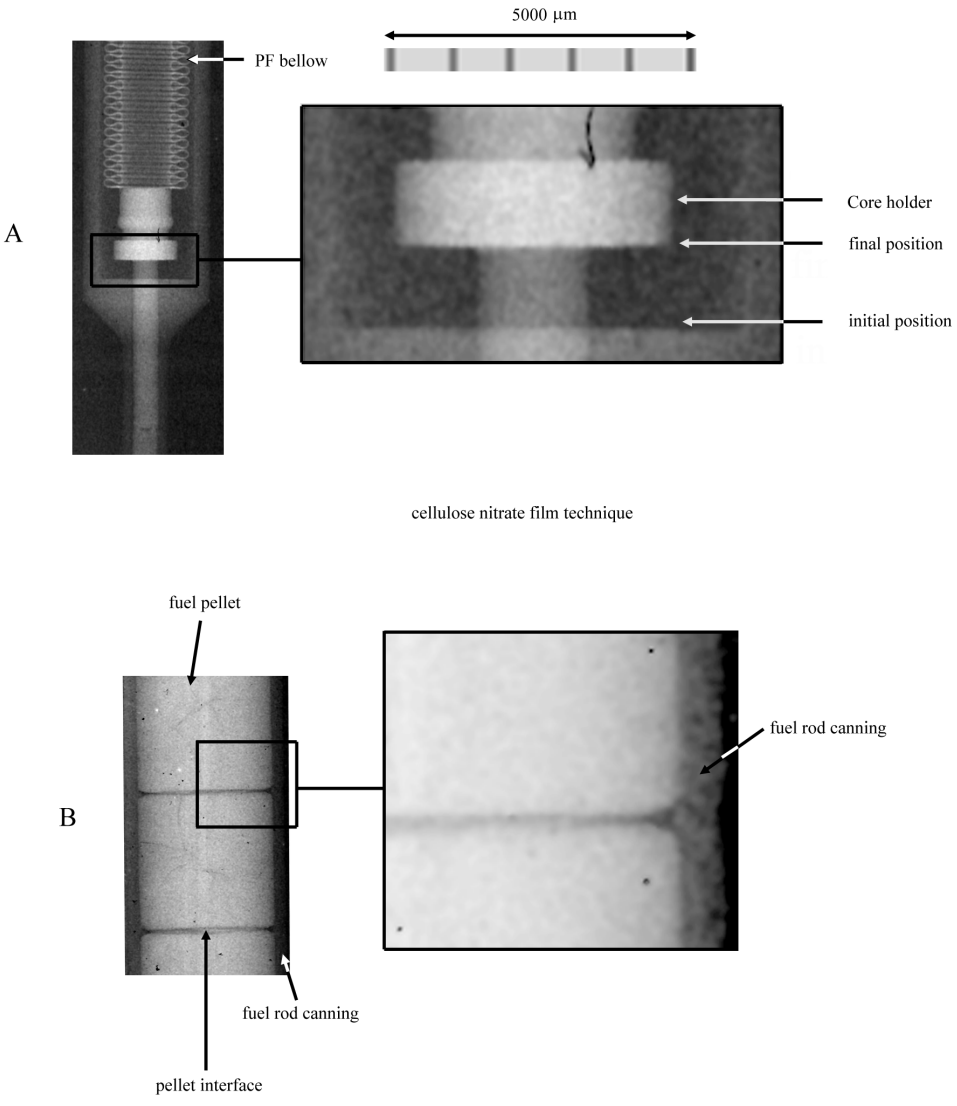

Fig. 5 Neutron radiograph of PF core holder (A) and canning (B).

Instruments readings from neutron radiographs (Fig. 5): An example taken from a sphere packed fuel rod is used to illustrate how end of life rod pressure can be estimated from the total displacement of the magnetic core holder or the extent of compression of the PF bellows after irradiation. The PF bellows is shown in Fig. 5, section A. The PF bellows and fuel rod were pre-pressurized to 21.5 and 22.5 bar respectively at room temperature. The sensitivity of the bellows is 11.14 bar per mm and an initial magnetic core holder position of 0.1 mm from the bottom or fundament is assumed. The total displacement of the magnetic core holder after irradiation is measured as 1.26 mm, i.e. total Δl due to total $\Delta P = 1.16$ mm. The gas in the fuel rod will be at elevated temperature after irradiation due to decay heat from the fuel and if we assume a gas temperature of 30°C, the temperature corrected fill gas pressure is 23.6 bar. The PF bellows is thus being compressed due to the fuel rod filler gas, which is now at higher temperature, as well as the released fission gas. The bellows compression is approximately 0.1 mm due to the filler gas temperature increase, which leaves a bellows compression of 1.06 mm due to the fission gas pressure. The fission gas pressure is therefore 12.7 bar at the actual temperature and 12.1 bar at room temperature, i.e. a final pressure of 34.6 bar for fuel rod gas composition. The fuel rod internal pressure was measured in the HBWR as 34 bar at room temperature and the two results are in good agreement. The small uncertainty of the estimate of the end of life pressure given above is because the exact position of the magnetic core holder after rod fabrication is not known. However, an acquisition of fuel rod neutron radiographs before irradiation in the reactor would remove this uncertainty.

Inspection of fuel and cladding details (Figs. 5 to 11): The neutron radiographs presented in Fig. 6 of a fuel rod[5] were taken by applying both techniques. The actual section is characterized by a relatively high degree of *fuel cracking* and it is not from the dry-out zone, but from the lower end of the fuel rod. The image given in section A is at 1:1 scale, and the images in sections B and C are enlarged 2 and 5 times, respectively. It is obvious that the reproduction of the neutron radiography image on the cellulose nitrate film is very detailed and clear.

Figure 5, section B shows an image acquired in the dry-out region of another fuel rod. It is possible to observe that the cladding has collapsed in between the pellet-pellet interface in a permanent deformation. The neutron radiograph was acquired with the high-resolution cellulose nitrate film technique.

Examples from a *fuel degradation test* are given in Figs. 7, 8, 9 and 10. The objective of the *fuel degradation test* was to study phenomena and mechanisms of severe degradation of fuel cladding caused by a small primary defect away from the location of secondary failure. For simulation of the primary defect, the interior of the rod was exposed to a controlled ingress of coolant water by opening an in-core valve. The experimental details are not described here. The intention is more to show some interesting neutron radiographs and thereby to understand the usefulness of the utilized techniques. The dysprosium foil/X ray film technique was applied at two angular orientations for neutron radiography of rods from the fuel degradation test. These radiographs were used for an overview inspection of the fuel rods. The overviews presented in Figs. 7 and 9 facilitate the selections of interesting fuel rod regions for further destructive PIE. Neutron radiography was again applied for these specific regions, see Figs. 8 and 10, but now the high-resolution cellulose nitrate film was utilized. Several conclusions could be drawn from these pictures, e.g. some pellets located near position 795 mm have

[5] The fuel rod was exposed in a dry-out experiment in the HBWR.

central voids and there is also a crack or defect in the cladding at the same location[6] generated by PCI mechanisms. At position 735 mm in Fig. 10 of another fuel rod in the test, voids in the pellet centre and additionally an axial crack in the cladding generated by the PCI mechanism are seen. A very interesting aspect is the possibility of zooming in with these high-resolution digital neutron radiographs for further qualitative image analysis on a PC screen.

A combination of neutron radiographs and vector-based images is shown in Fig. 11. The intention with this image construction was to make an overview picture of a complicated cutting plan.

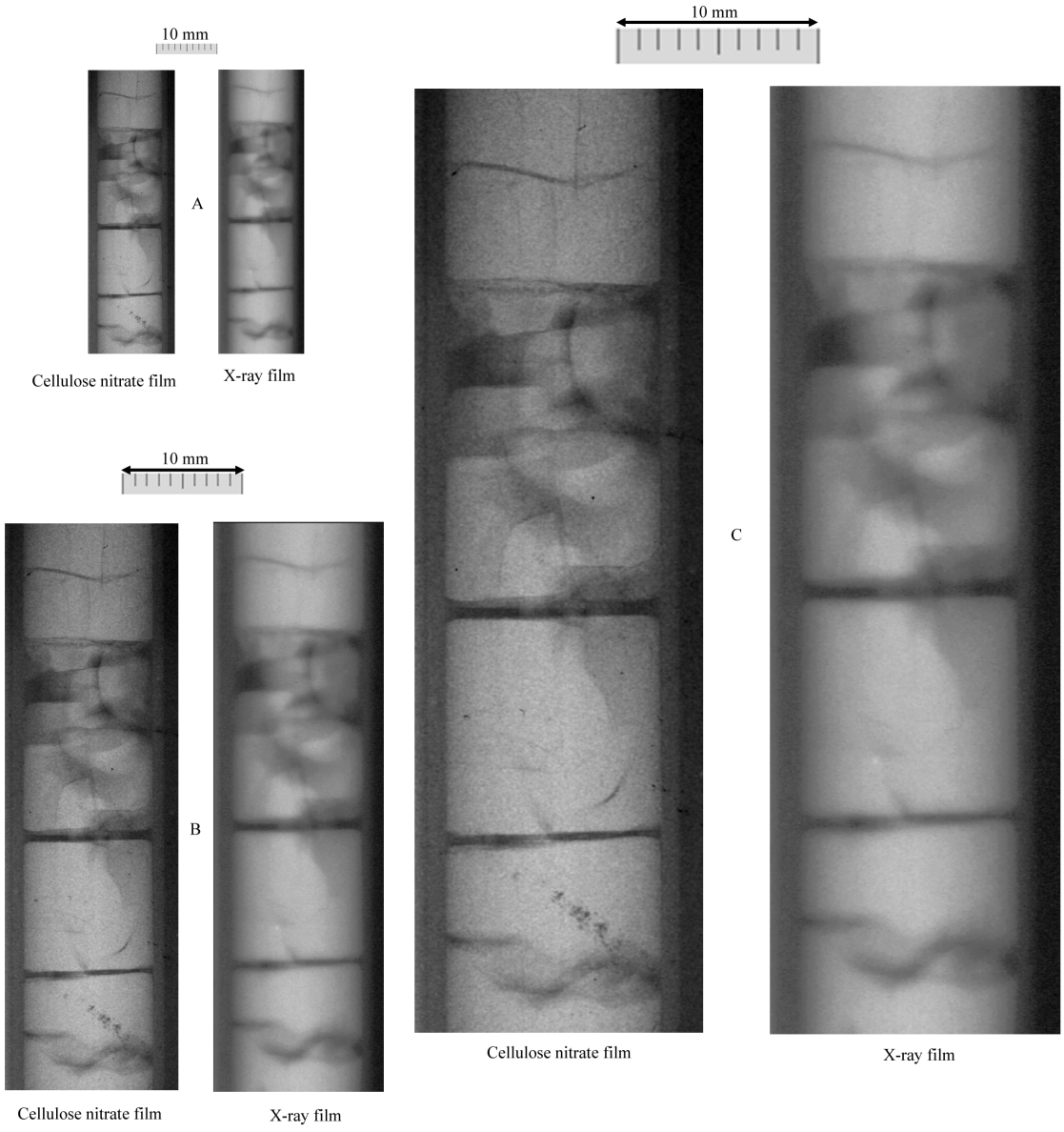

Fig. 6 Neutron radiographs of fuel column.

[6] See the 4X magnification in Fig. 8.

2.4 Concluding remarks on neutron radiography

Utilization of cellulose nitrate film[7] in neutron radiography eliminates the prolonged handling of activated dysprosium foils. A high-resolution cellulose nitrate film gives sharp and detailed radiographs compared to the dysprosium foil/X ray film technique [3, 4]. Some examples given in the paper show that it is possible to zoom-in with neutron radiographs acquired with the cellulose nitrate film technique. Fuel rod details at 10 times magnification are still sharp enough to allow dimensional measurements to be made with great precision (50 μm). Fuel rod instrumentation devices and other details can be detected with high reliability and the results can be used for example to estimate the *end of life pressure* in instrumented fuel rods.

However, it is also useful to combine the dysprosium foil/X ray film and the cellulose nitrate techniques in evaluation and examination of fuel and cladding conditions, e.g. in fuel failure degradation tests.

The last five years of upgrading and use of advanced electronic data treatment tools in PIE have improved both the inspection possibilities and documentation quality of neutron radiographs. An important issue with digital PIE information is the possibility to communicate data directly to the customers and to have an ongoing dialog during PIE.

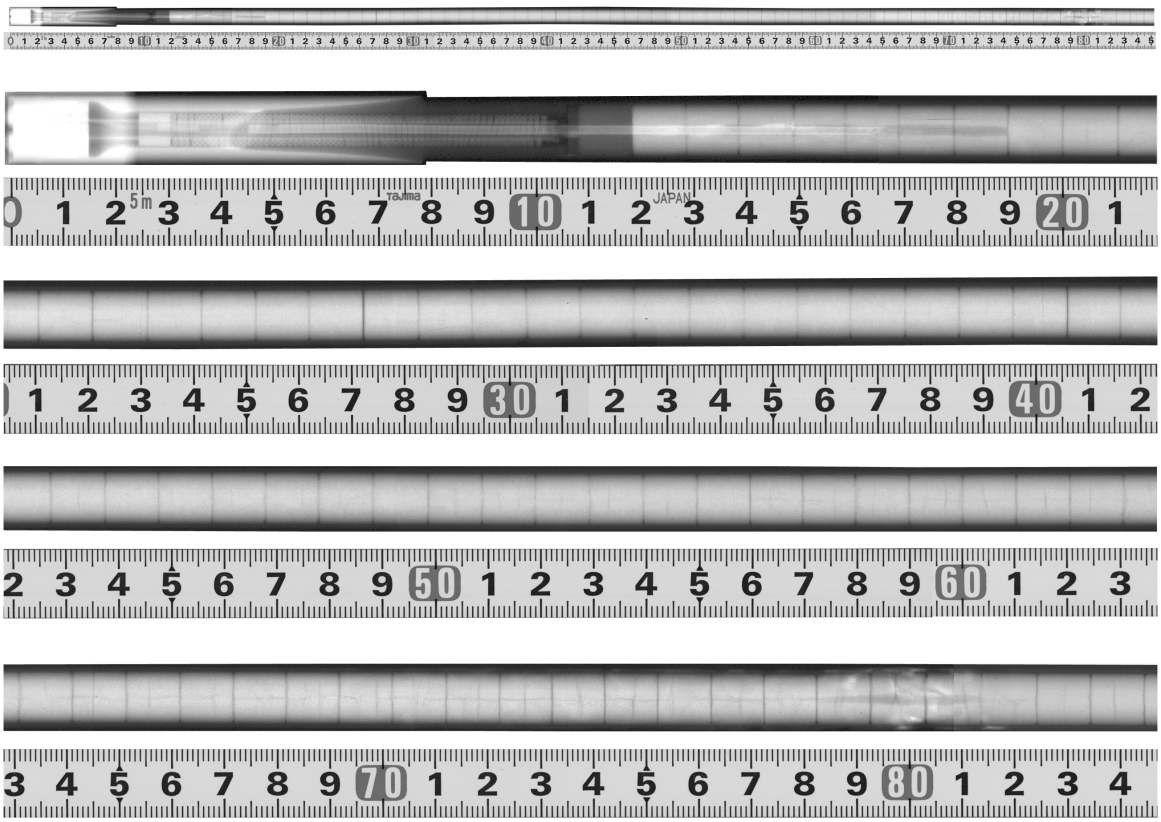

Fig. 7 Neutron radiographs of a fuel rod at 90 degrees orientation from the fuel degradation test.

[7] Kodak CA 80-15 type B film.

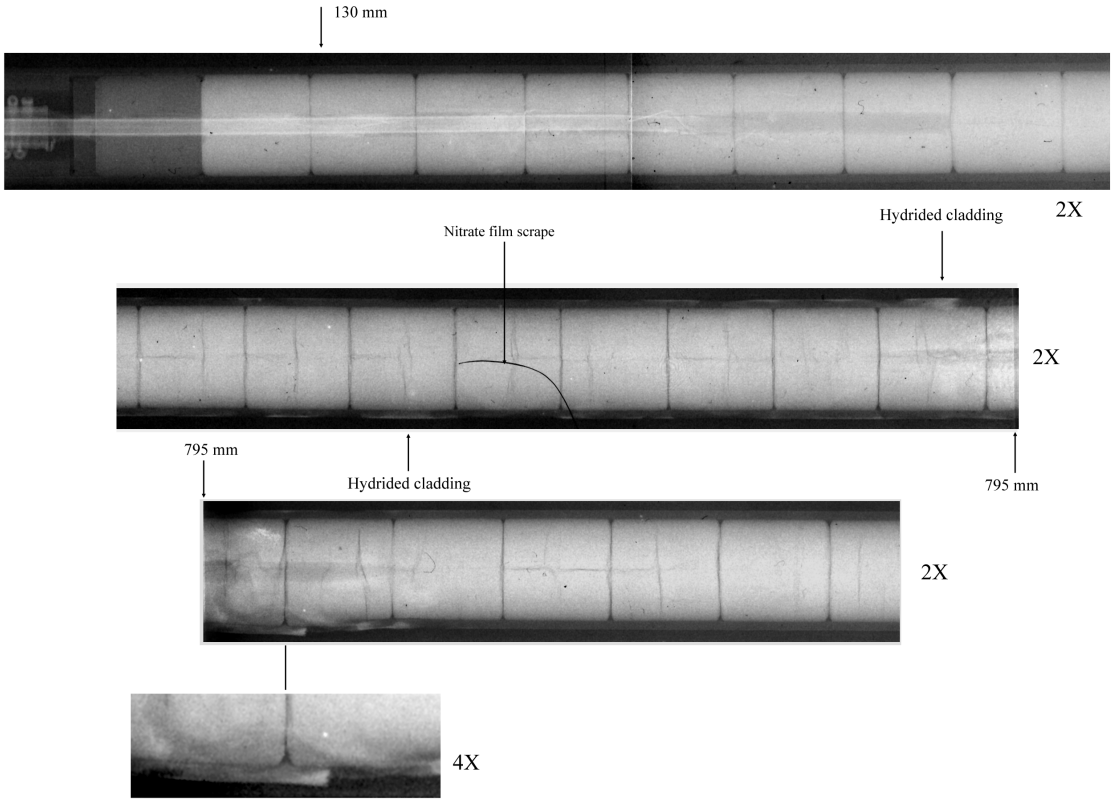

Fig. 8 Neutron radiographs (cellulose nitrate film) of a fuel rod at 90 degrees orientation from the fuel degradation test.

We are also working with neutron tomography as a tool for evaluation of PIE, so in the future, measurements of many other fuel rod features should be possible by non-destructive methods.

3. DIMENSIONAL MEASUREMENTS

Physical parameters, such as diameter and bow or profile, of experimental fuel rods are measured in profilometry. The measurements are an important experimental control of reactor induced deformations of fuel rods, e.g. pellet cladding interaction that can lead to rod degradation or failure. Some years ago results from profilometry were usually presented in two dimensional x-y graphs, showing for one given angular orientation the values for the fuel rod axial position (x-axis) versus the measured diameter/profile values (y-axis).

Recently, the laboratory carried out modifications to the profilometer bench. This includes a new steering control and data acquisition system. The acquisition system in profilometry was upgraded for three dimensional surface measurements, i.e. fuel rod outer diameter and straightness or profile. Four parameters are logged in three dimensional measurements, i.e. circumferential orientation, axial position, diameter and profile of the rod. The uni-axial profilometry of fuel rods was modified in order that it could be performed at several angular orientations during one acquisition sequence. This extension is very useful in several ways, for instance the built-in data symmetry of the method is used to check the validity of the measurement results. Profilometry gives in addition detailed information of cladding irregularities and fuel rod profiles. Profile acquisition is actually a measure of the length between the fuel rod and the bench structure. It was therefore necessary to develop further the data processing methods to “see” the real profile of the fuel rod under examination.

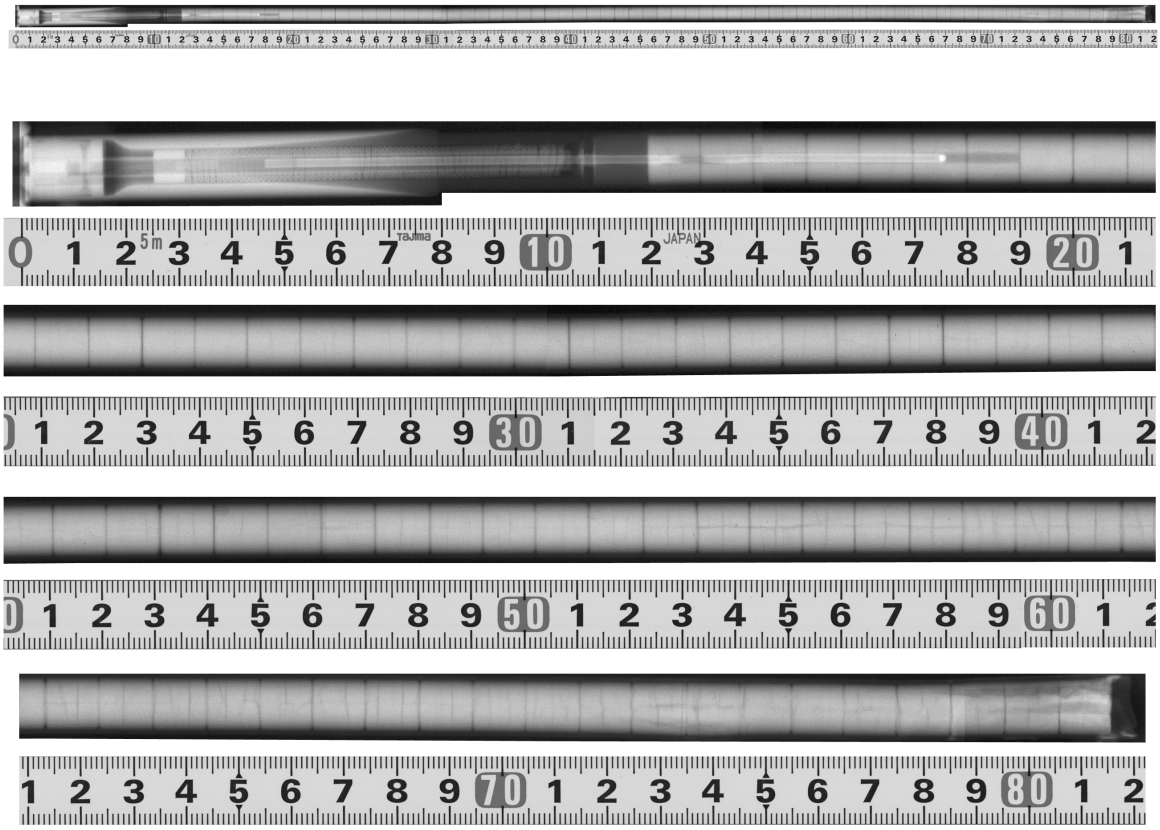

Fig. 9 Neutron radiographs of a fuel rod acquired at 90 degrees orientation from the fuel degradation test

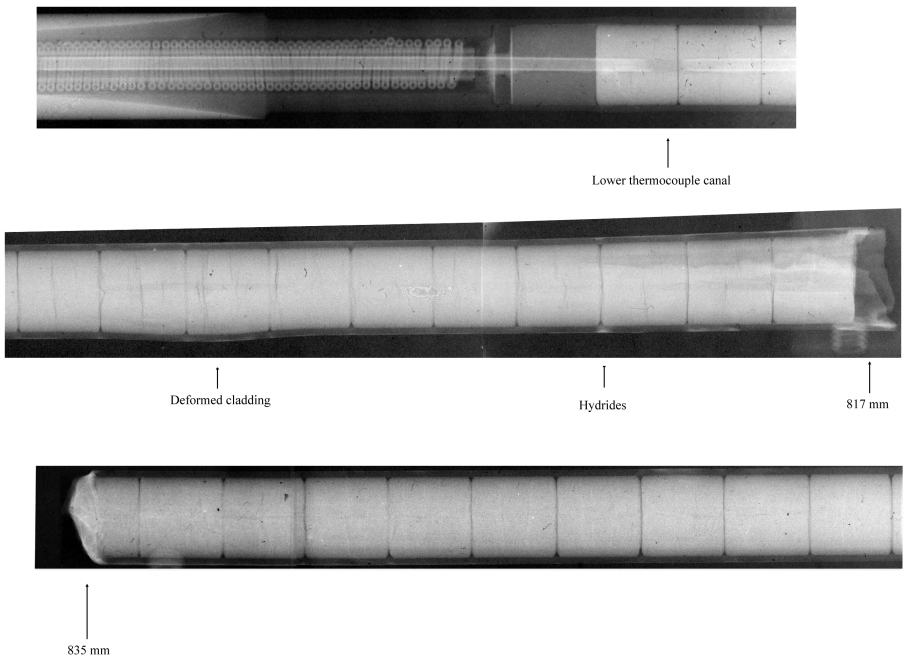

Fig. 10 Neutron radiographs (cellulose nitrate film) of a fuel rod at 90 degrees orientation from the fuel degradation test

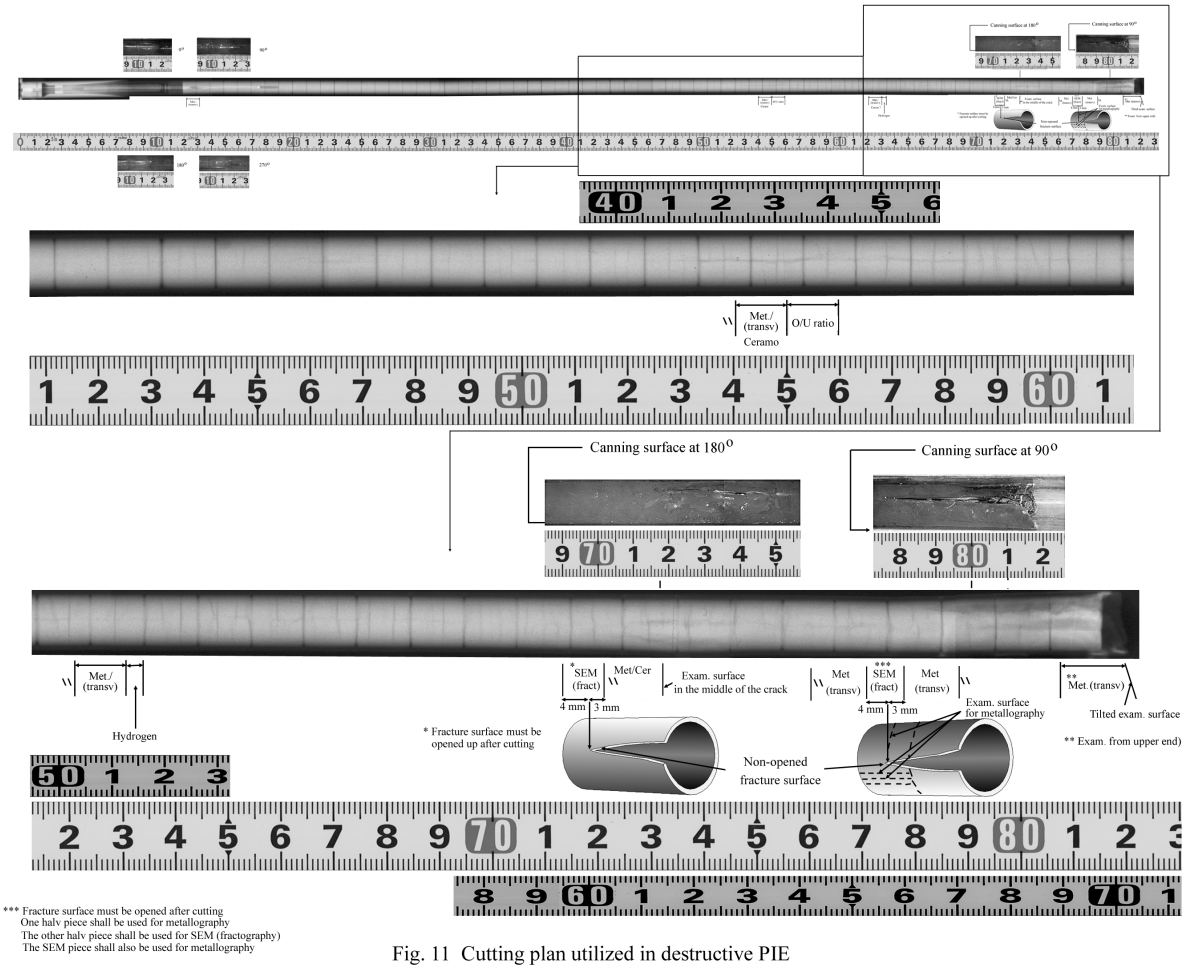

Fig. 11 Cutting plan utilized in destructive PIE

3.1 Experimental set-up for three dimensional profilometry

Description of the profilometer bench: The measurement principle of the profilometer bench is based on linear voltage displacement transducers (LVDT) connected with two measurement knives. The profilometer bench with transducer arrangement is given in Fig. 12. The knife edge (sapphire) is made of a 2 mm diameter polished sapphire rod. Both knives are connected to the diameter LVDT and one of them is also connected to the profile LVDT. One of the transducers measures the outer diameter of the fuel rod and the other one the profile or distance from the rod to the bench structure (steel axle). Programmable step motors control the movement of the measuring bridge or trolley in the vertical direction[9] and around the circumference of the rod. The trolley is moved up and down in steps. Minimum step-length variation corresponds to a displacement of 5 μm and minimum angular displacement corresponds to 0.9 degrees. This means that the measuring trolley moves upward one step and then the rod rotates up to 400 small steps until it reaches the zero degree orientation, moves another axial step and so on. The data acquisition is performed between each rotation step while the rod and trolley is completely at rest, i.e. static measurement principle.

Alignment of the knives: Prior to all dimensional measurements, correct alignment of the knives is vital to achieve high accuracy of the acquired data set. The knives have to be aligned

[9] The vertical direction is approximately parallel to the fuel rod.

parallel and horizontally tip to tip. Parallel alignment and knife wear are checked with a precise calibration bar or rod[10] that is moved (on rails) back and forth along the knife edges, while reading the LVDT sensor signals. When doing profilometry measurements on a slightly bowed fuel rod with poor alignment of the two knives, the measurement error introduced at certain angular orientations of the fuel rod can be quite large (30–50 μm). A procedure for adjusting the alignment of the knives within certain limits is implemented to assure satisfactory measurement accuracy.

Steering control, data acquisition, and data storage: The programme utilized for calibration rod and fuel rod measurements is performed by a personal computer and software developed at IFE, called ROD MASTER. The data programme with its hardware, generates the pulses to the two step-motors to obtain the correct measuring position and reads the signal values from the two transducers. The values are stored together with the generatrices (angular orientation) and axial position on a data storage disk. When the dimensional measurements are completed the acquired data set is transferred to a password protected network disk. The fuel rod axial position is usually counted relative to its lower end and is positive in the up-direction. The generatrix values are counted from 0 to 360 degrees and counter-clockwise when viewing the rod from above.

Calibration: The diameter and profile sensor is calibrated by measuring on a special calibration rod assembled with two or more accurate regions with diameter D_1 and D_2. D_1 and D_2 are close to the fuel rod diameter (D), i.e.

$$D(x,\theta) = \{\frac{\Delta D}{\Delta C}\}\{C(x,\theta) - C_2\} + D_2$$

Where $\{\frac{\Delta D}{\Delta C}\} = \{\frac{D_1 - D_2}{C_1 - C_2}\} \equiv (sensitivity)^{-1}$ and C_1 and C_2 represent the analogue to digital converter (ADC) values acquired from the two calibration steps and C (z, θ) is the ADC value for the diameter sensor at an arbitrary position. The bow or profile of the rod is given by,

$$P(x,\theta) = 0.5 \cdot \{\frac{\Delta D}{\Delta C}\} \cdot C'(x,\theta)$$

Where $C'(x,\theta)$ is the ADC value for the profile sensor at arbitrary position.

In order to deduce of the fuel rod straightness it is necessary to calculate the values of the straight line crossing two points (x_{upp}, x_{low}) near the upper and lower end plug welds.

The equation representing the ideal straight cladding at an arbitrary θ and x is then,

$$\Psi(x,\theta) = \{\frac{P(x_{upp},\theta) - P(x_{low},\theta)}{x_{upp} - x_{low}}\} \cdot x + \{\frac{P(x_{low},\theta) \cdot x_{upp} - P(x_{upp},\theta) \cdot x_{low}}{x_{upp} - z_{low}}\}$$

[10] Diameter accuracy of the calibration rod is ± 1μm.

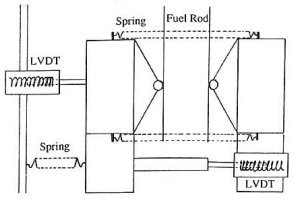

Transducer arrangement

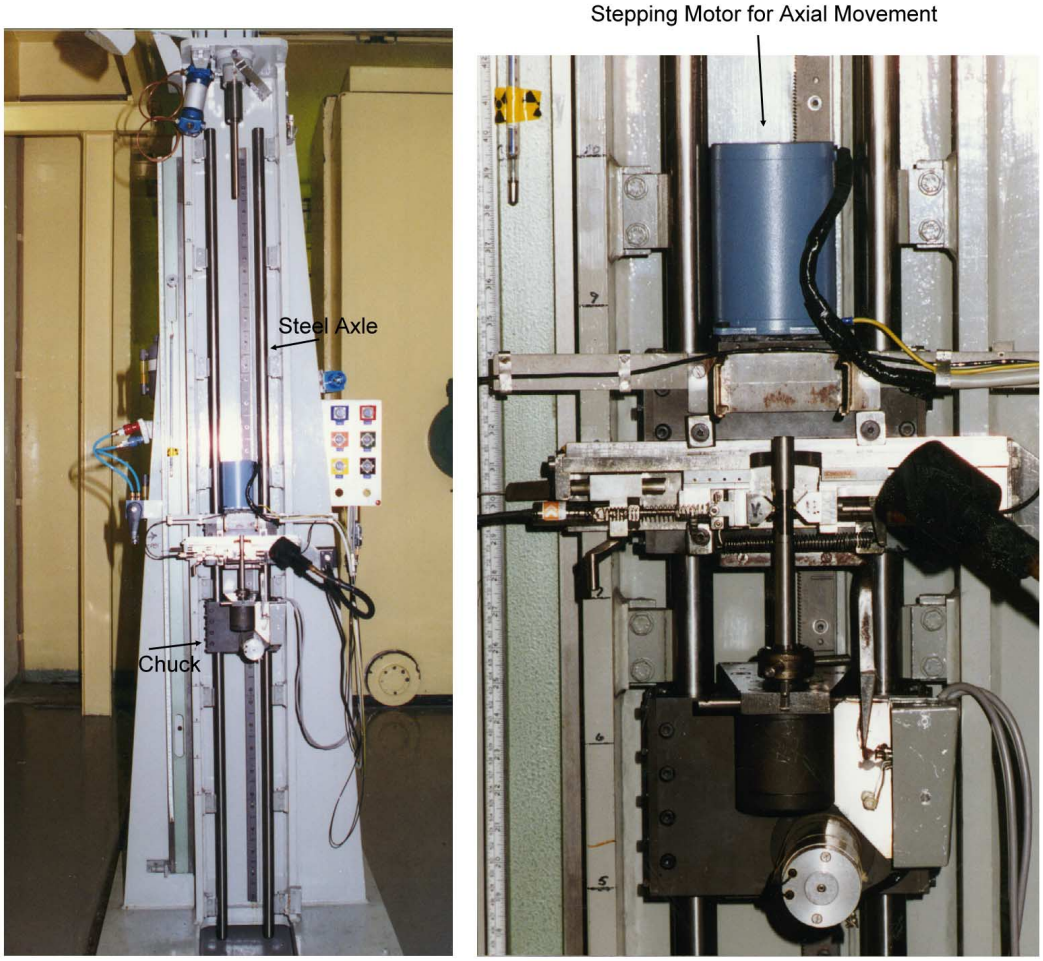

Fig. 12 Dimensional measurement bench

The expression for the fuel rod straightness or profile is $Bow(x,\theta) = P(x,\theta) - \Psi(x,\theta)$

Data treatment: The presentation software used in the visualization of measurement values in a three dimensional surface map such as shown in Fig. 13, is called 'Surfer', a standard software package from Golden Software, Inc. (USA). *Surfer* is a grid-based contouring and three dimensional surface plotting/mapping programme that runs under Microsoft Windows, Windows 95/98 and Windows NT. *Surfer* interpolates irregularly spaced XYZ data on a regular spaced grid, and places the interpolated data in a grid file. The grid files are used to produce contour maps and surface plots. Maps are enhanced with *Surfer* by adding boundary

information, posting data points, and combining several maps. Further functions can be performed with the program, such as adding drawings to a map, annotating maps with text, etc. It is also possible to operate on the grid files made from the data set. *Surfer* has commands for smoothing the surface represented by the grid, performing mathematical transformations on grids, and creating grids that represent mathematical surfaces. It is also possible to slice arbitrary traces out from the actual surface and plot it with a *Grapher* package (two dimensional).

3.2 Profilometry of an irradiated fuel rod

Example of a 3D profilometry map of an irradiated fuel rod (Fig. 13): The rod used in the example is a commercially irradiated fuel rod re-fabricated at IFE, Kjeller. After ramp testing in the HBWR the fuel rod diameter is measured in the profilometer bench. The x-axis along the fuel rod is measured from 100 to 600 mm[11] and the φ-direction[12] from 0 to 360 degrees. The measurement results are presented in a 3D map in Fig. 13. Special features, such as the start and end of the active fuel stack region, a vent hole and the weld area are indicated in the map. Further, a number of striking features can be seen in the 3D map. Firstly, and most dominant is the dark-grey area in upper end of the fuel rod. This is a ground area used for electric contact during welding operations in the hot cells. Secondly, there is a diagonal background pattern that looks like waves. The background pattern is made up of parallel and diagonal stripes, alternating dark and bright. The diagonal stripes in the background represent most probably a roller pattern generated during the fabrication process of the tube. The diameter difference of minimum and maximum in the roller pattern is estimated to be below 10 μm. Due to the 180 degrees measurement symmetry, the diameter contour map from 0 to 180 degrees must coincide with the contour map from 180 to 360 degrees. As can be seen in the actual figures, the upper image at 180 to 360 degrees is nearly a perfect duplicate of the lower one at 0 to 180 degrees.

However, a few vertical lines do not appear on the upper as well as on the lower image. These lines represent 'dust' on the cladding or knives. The overall symmetry in the lower and upper images proves that the contact knife setting (i.e. parallelism, vertical positioning) is correct and that sapphire rods with negligible wear were used. The measurement resolution is 2.3 μm. The vent hole and puncturing hole in the lower end of the fuel rods are indicated at 0 and 180 degrees in Fig. 13. The measurement was performed after the fuel rod was punctured.

Example of extracted graphs for diameter at two angular orientations from the 3D profilometry map (Fig. 14): The diameter measurements at 0 and 90 degrees orientation are extracted from the map and are given in graphs in Fig. 14. The figure shows "smoothed" curves (noise reduction). The smoothing has been done by replacing each measured value by a new value (y_n ') where y_n ' = ¼ (y_{n-1} + 2 y_n + y_{n+1}). The mean cladding diameter in the fuel stack region is approximately 10.71 mm. It is seen that the diameter trace at 0 degree is 180 degrees out of phase compared to the 90 degrees trace. It is assumed that this correlation is generated during the production of the tubes (roller pattern). No cladding ridges can be seen. Ridging would appear as vertical lines located at the pellet-pellet interface positions.

[11] Along the fuel stack region, Δx = 1 mm.
[12] Around the circumference, Δφ = 7.2 degrees.

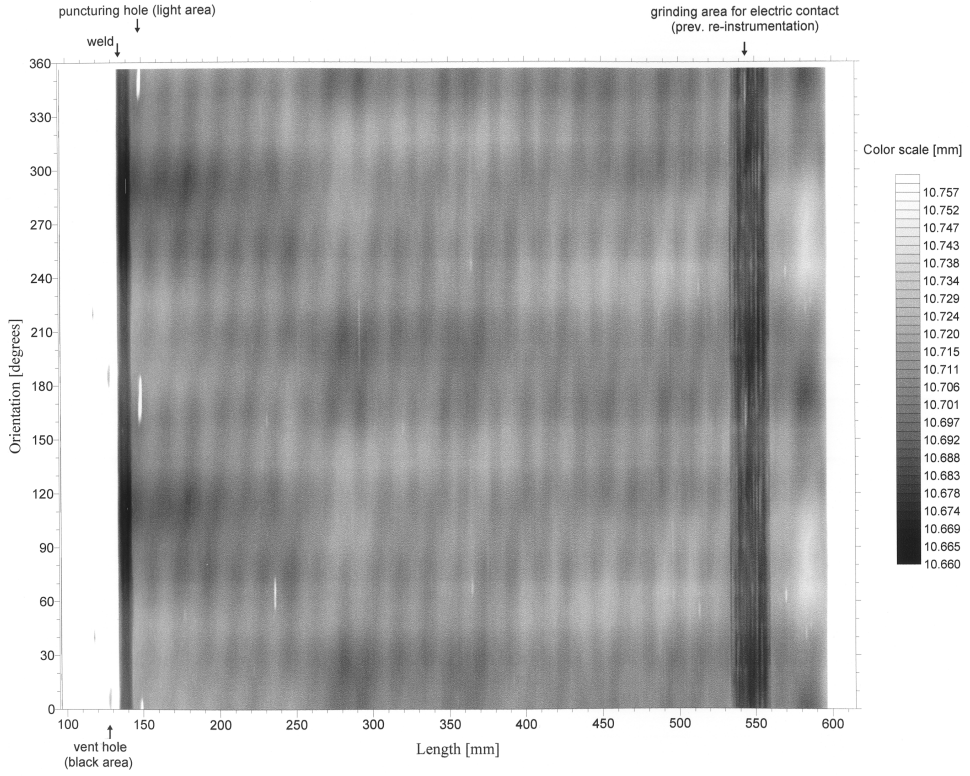

Fig. 13. Diameter contour map of a fuel rod.

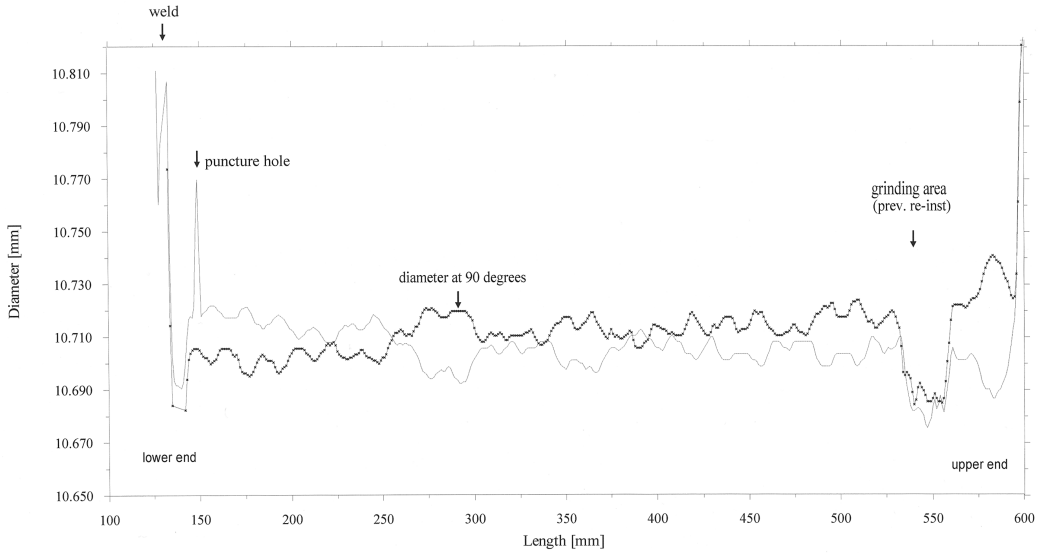

Fig. 14. Smoothed diameter scans of fuel rod at 0 and 90 degrees orientations

Example of extracted graphs for profile at two angular orientations from 3D profilometry map (Fig. 15): The profile measurements (i.e. $P(x,\theta)$) at 0 and 90 degrees orientation are extracted from the map and are given in the graphs in Fig. 15. The bow of the fuel rod is below 0.2 mm in these two orientations. The puncturing hole is seen on the profile curve at 0 degree. The two profile curves in the example are not compensated for tilting of the fuel rod in the measurement bench.

Cladding lift-off (Figs. 16 to 19): The next example is taken from a fuel rod exposed in a cladding lift-off experiment performed in the Halden reactor. Three dimensional diameter and compensated fuel rod profiles are given. The results are presented in Figs. 16 to 19. Weld locations, start and end of the fuel stack and other details are indicated in the figures. Again, a tilted pattern is observed in the diameter contour plot. This is generated during the production of the tube. The cladding ridges are seen in the contour diameter plot as parallel vertical dark lines. There are also some dark spots, which were probably generated near the spacer location during base irradiation in a commercial reactor. The acquired profile data were compensated for tilting of the rod and the result is given in Fig. 17 with a contour step of 30 μm. Here, we see that the maximum bow profile is located at 30 and 210 degrees orientations. The minimum profile is 90 degrees in-between the maximum, i.e. at 120 and 300 degrees orientations. The profile appearance of the rod is called a "banana" bow. A marked surface-area with a rather rough appearance is extracted and highlighted in the figure. This area is also observed in the diameter plot at approximately 120 and 300 degrees orientations.Two dimensional curves for the diameter and bow of the fuel rod are extracted from the 3D map and are shown in Figs. 18 and 19. It can be seen that all profile curves are zero at the anchor points, i.e. the profile data are compensated for tilting of the rod under the measurements.

3.3 Concluding remarks on 3-D profilometry

The new concept of dimension measurement and electronic data treatment results in a more complete image of the surface of interest in terms of visualizing fuel rod features. With the traditional measurement performed at two angular orientations it is furthermore difficult to find the maximum bow of the fuel rod.
Future modifications to the knives used in measurement on the profilometer bench may give access to the ability to detect fine defects in fuel rod cladding, such as thin cracks etc. But an electromagnetic interaction system (e.g. eddy current) is maybe better to utilize in detection of cladding irregularities or failures than fine tip knives implemented in the dimensional measurement system.

4. COMPILATION EXAMPLES OF RELATED PIE DATA VISUALIZED IN AN IMAGE BASED USER-INTERFACE

PIE results document the state of a fuel rod. Normally, the results are image data from visual inspection, neutron radiography, metallography, ceramography etc. Additionally there are numerical data from dimensional measurements, gamma scanning, mechanical testing, other tests and quantitative image analysis. In order to obtain a complete picture of the state of the fuel rod it is important to combine and compare all such data, possibly on overview image pages with the option to zoom for details.

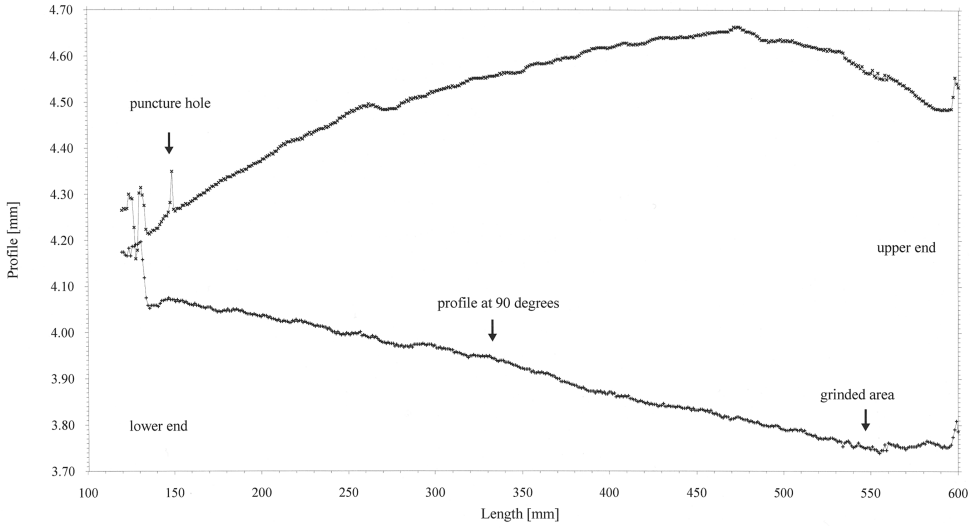

Fig. 15 Profile scan of a fuel rod at 0 and 90 degrees orientation

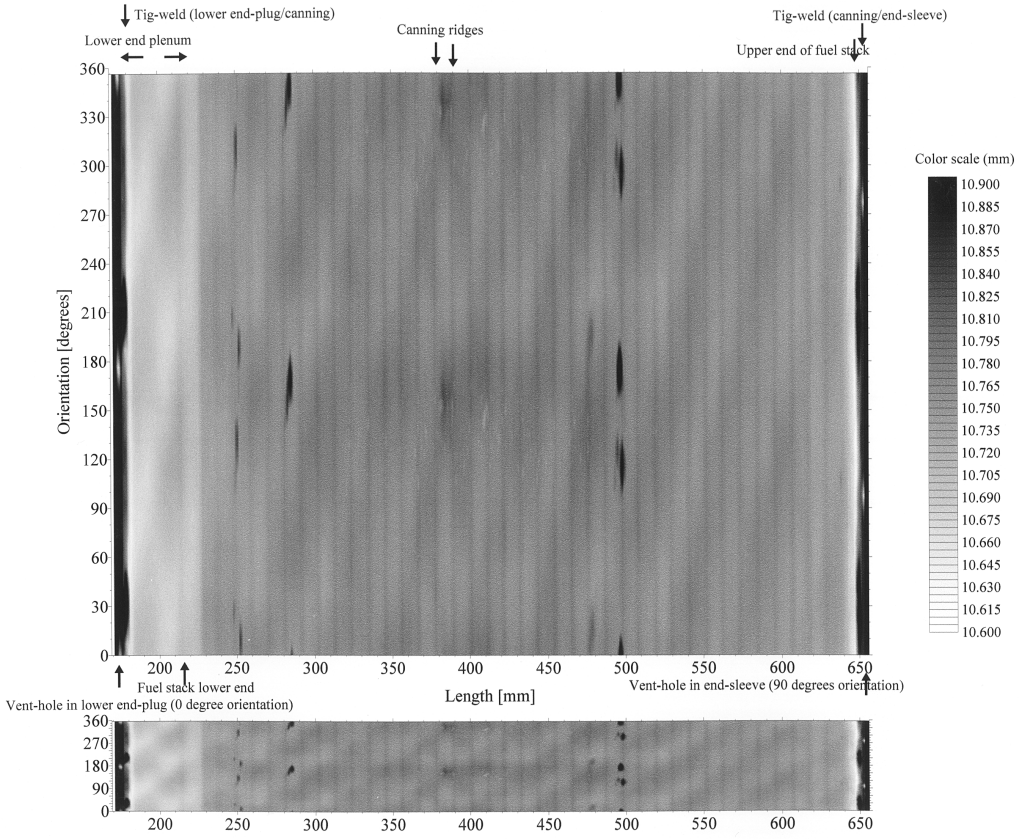

Fig. 16 Diameter contour plot of a fuel rod irradiated in a lift-off experiment

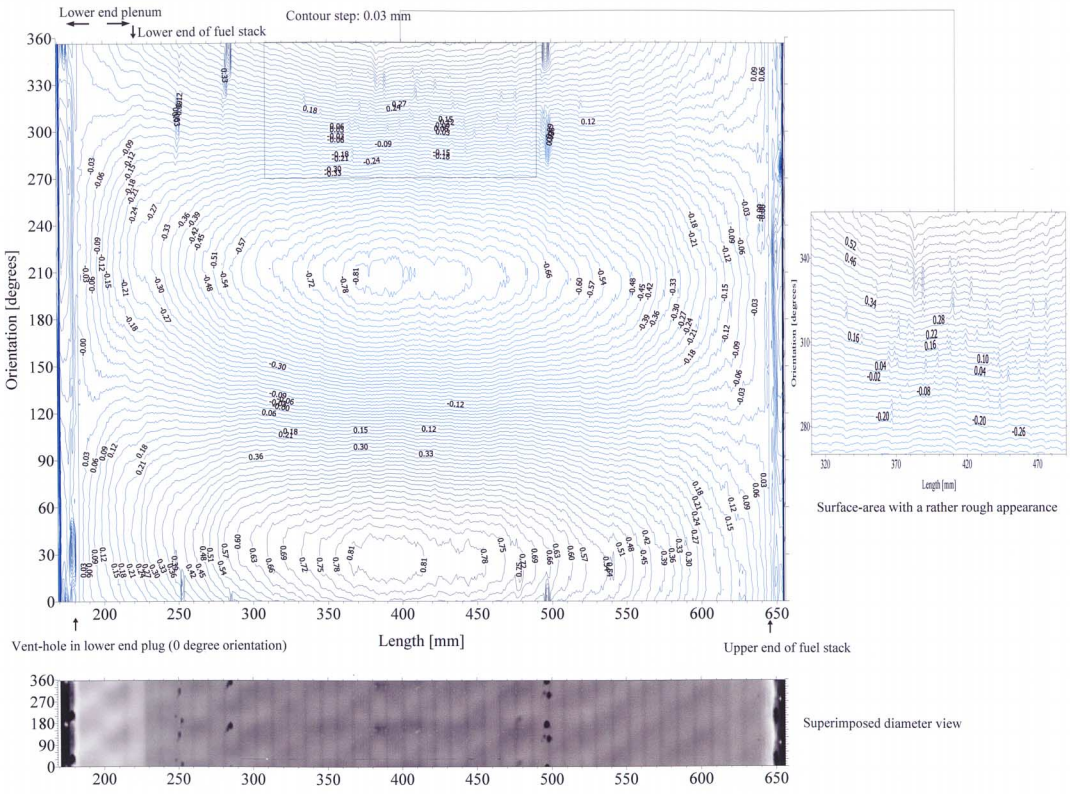

Fig. 17 Profile contour plot of a fuel rod irradiated in a lift-off experiment

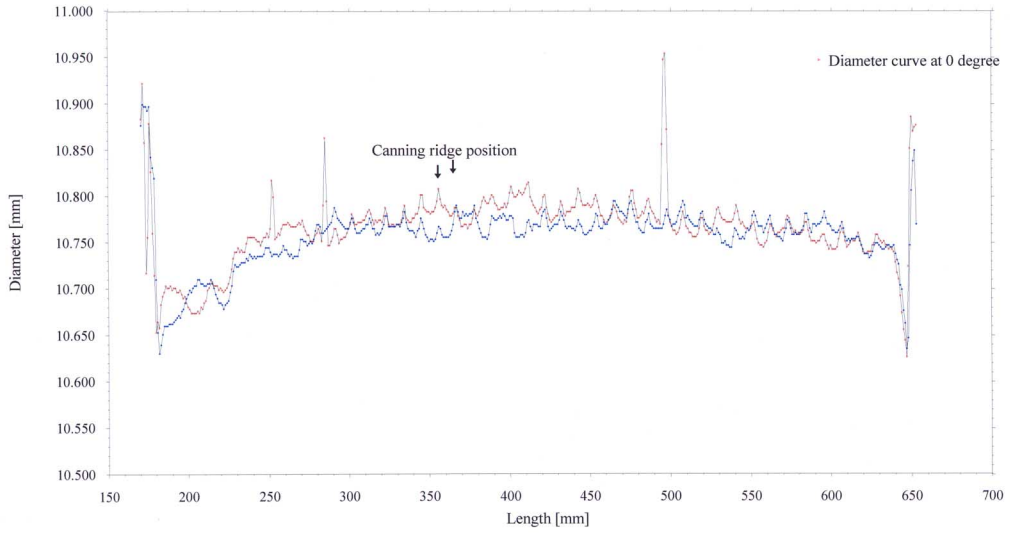

Fig. 18 Diameter of a fuel rod irradiated in a lift-off experiment at 0 and 90 degrees orientation

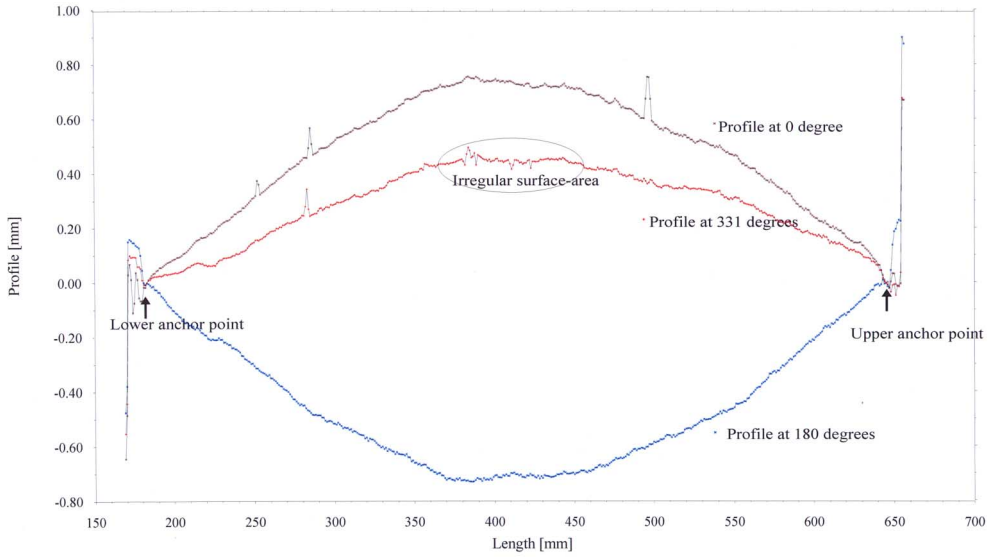

Fig. 19 Profile of a fuel rod irradiated in a lift-off experiment at 0, 180 and 331 degrees orientation

4.1 Experimental set-up

A personal computer with sufficiently high capacity and suitable software allows handling of digital images and the application of image compilation techniques. Viewing, working and reporting of PIE data in an image file can be performed with photoshop software with navigator, zooming and stitching possibilities.

Data from visual inspection and neutron radiography are first mounted and stitched to produce a complete fuel rod picture. Then length calibration is performed before execution of the documentation into an overview page facilitates fuel rod analysis. Layer effects and others specific features are supported by the photoshop software utilized at the laboratory.

4.2 Image compilation example from neutron radiography and visual examination

Example from neutron radiography — image stitching and overview page (Fig. 20): The main intension with the stitching and compilation of the neutron radiographs in this example is to produce a digital fuel rod overview and detailed pictures that make it easy to examine the results of the experiment and in addition to make flexible documentation. The digital file is produced from high resolution data acquired from all the individual neutron radiographs. This makes, for instance, zooming and navigation possible during a PC presentation or examination. The neutron radiographs in Fig. 20 are acquired from a fuel rod exposed in a fuel failure degradation test with unlimited steam ingress. The axial zero position of the rod is given relative to the lower edge of the lower end plug, and pictures from both 0 and 90 degrees orientation are shown together.

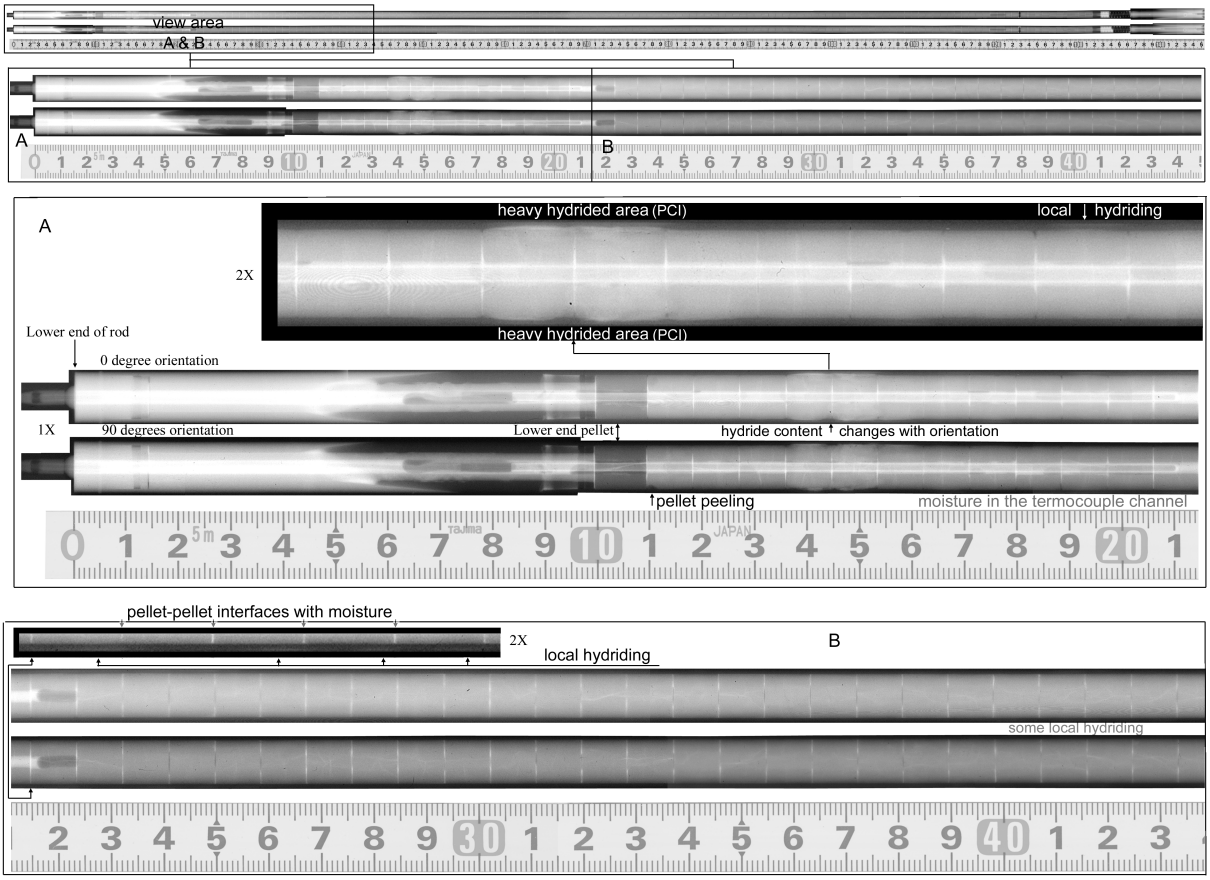

Fig. 20 Compiled neutron radiographs from a fuel failure degradation test at two azimuthal orientations.

As a general remark, it must be said that the neutron radiographs show heavy hydrided areas in regions of the cladding near the lower end of the fuel stack where the hydrogen accumulation is largest. The cladding is oxidized when the unlimited amount of water/steam ingress occurs. In the oxidising process, hydrogen is released from the water/steam and the cladding will pick up some of the hydrogen and the remaining will accumulate in the lower end of the fuel rod. It is obvious that the cladding is not intact in the heavy hydrided areas. It is seen in the enlarged neutron radiograph that the hydriding was initiated at the cladding inner surface and proceeded towards the outer surface. The most hydrided area is between position 136 – 153 mm where swelling and pellet-cladding interaction produces bulges at the surface. Also, the hydride content is very large in this region and it is actually up to 100 % zirconium hydride, i.e. a "sun burst" appearance. In addition we observe that nearly all pellet-pellet interfaces and pellet cracks contain moisture.

Example from visual inspection – image stitching (Fig. 21): The next example shown in Fig. 21 is taken from visual examination of re-fabricated guide tubes. First, the individual pictures of one guide tube are stitched together and then the result is length calibrated. The image stitching is performed automatically with special software. The image compilation in this example is used again to collect the guide tubes into various design groups.

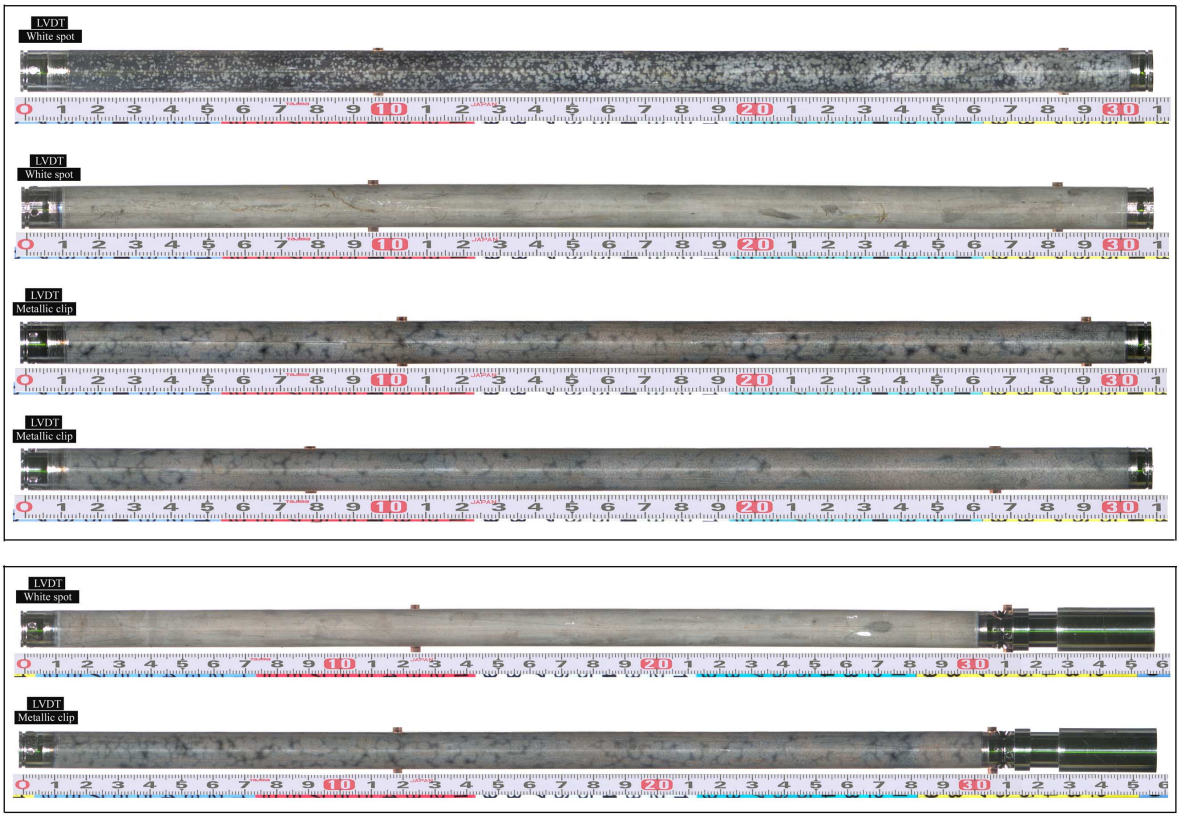

Fig. 21 Visual examination of refabricated guide tubes arranged in two design groups.

4.3 Image compilation example presenting in an overview page the state of an irradiated rod based on NDE and DE (Fig. 22)

The compilation example in Fig. 22 summarizes PIE results in an overview page. The acquired data are combined from visual inspection, neutron radiography, metallography, ceramography, ring tensile testing and dimensional measurements. The main purpose of constructing the rather large image (100 MB) page is to have all PIE data available in only one file for easy handling possibilities, i.e. zooming and inspection. Experimental details and PIE observations will not be explained in detail — this is documented elsewhere. The intention here is to demonstrate digital image compilation techniques.

The stitched images from neutron radiography and visual inspection are aligned and dimensionally calibrated so that correlation of cladding details and the interior of the fuel rod is directly visualized. The cutting positions and image details related to the destructive examination are marked on the Fig. 22. Various rulers are also incorporated and can be copied and handled in separate transparent layers. Ruler movements on top of the images are possible with this technique. Microstructures, oxide thickness and other details are possible to inspect when the images of interest are zoomed. Figures for reports are generated by copying and scaling operations. It is also possible to show the file contents and the possibilities described above on a large canvas with a modern projector and a suitable PC.

4.4 Concluding remarks on compilation of PIE data

Electronic compilation of PIE data using commercial software and personal computers provides numerous benefits for PIE. Digital data from related PIE, compiled in a high-resolution image file, can be inspected, navigated and zoomed for fuel rod details. The technique facilitates database work for PIE results and opens up new possibilities in documentation and presentation.

REFERENCES

[1] H. JUSTNES, KNUT BRYHN-INGEBRIGTSEN and G. O. ROSVOLD, " Neutron radiography: an excellent method of measuring water penetration and moisture distribution in cementitious materials", Advances in Cement Research, 1994, 6, No. 22, Apr., 67–72.

[2] PILKER et al, "Particle tracks", American Journal of Physics. Lancaster, Pa, 1972, 40, p. 679–683.

[3] J.F.W. MARKGRAF, "The practical utilization of nitrocellulose film in neutron radiography", Neutron radiography (3), Proceedings of the Third World Conference, Osaka, Japan May 14–18, 1998, p. 353–364.

[4] J. C. DOMANUS, "How good is nitrocellulose film for neutron radiography" Neutron radiography, Proceedings of the First World Conference San Diego, California, U.S.A., p. 729–736.

[5] HÅKON K. JENSSEN, "Neutron radiography-an approach to improve spatial resolution in neutron radiography", IFE/KR/F-98/159.

[6] HÅKON K. JENSSEN, SVEIN THORSHAUG, K.B. INGEBRIGTSEN, P. ARNESEN AND B.

[7] OBERLÄNDER, "Improvements of PIE methods for dimensional measurements, neutron radiography and gamma scanning", Report IFE/KR/F-98/043.

[8] HÅKON K. JENSSEN, "Recent improvements in PIE-techniques at the IFE hot-laboratory", Report IFE/KR/F-99/078.

Specific features of the determination of the pellet-cladding gap of the fuel rods by non-destructive method

S.V. Amosov, S.V. Pavlov

State Scientific Center of the Russian Federation, Research Institute of Atomic Reactors, Dimitrovgrad, Uljanovsk Region, Russian Federation

Abstract. This report describes the specific features of determining the pellet-cladding gap of the irradiated WWER-1000 fuel rods by nondestructive method. The method is based on the elastic radial deformation of the cladding up to its contact with the fuel. The value of deformation of cladding till its contacting fuel when radial force changes from F_{max} to 0 is proposed as a measuring parameter for determination of the diametrical gap. Because of the features of compression method, the obtained gap value is not analog of the gap measured on micrograph of the fuel rod cross-section. Results of metallography can provide only qualitative evaluation of its method efficiency. Comparison of the values determined by non-destructive method and metallography for WWER-1000 fuel rods with burnup from 25 to 55 MWd/kg U testified that the results of compression method can be used as a low estimate of the pellet-cladding gap value.

1. GAP MEASUREMENT SYSTEM

The principle of the gap measurement is described in the paper by R. Manzel [1]. This so-called "compression method has been known for more than 20 years and is used in many research laboratories, including RIAR [2] Fig.1 presents the scheme of the facility of the fuel-cladding gap measurement by the compression method.

The system of a loading fuel rod is pneumatic. The piezoelectric force transducer with high rigidity (~ 2000 N/μm) is used as an immovable support for the fuel rod. The length of the loading zone is 20 mm that covers two or three fuel pellets. The diametrical gap value from 0 to 110 μm is measurable. The maximum force appled to the cladding does not exceed 1200 N.

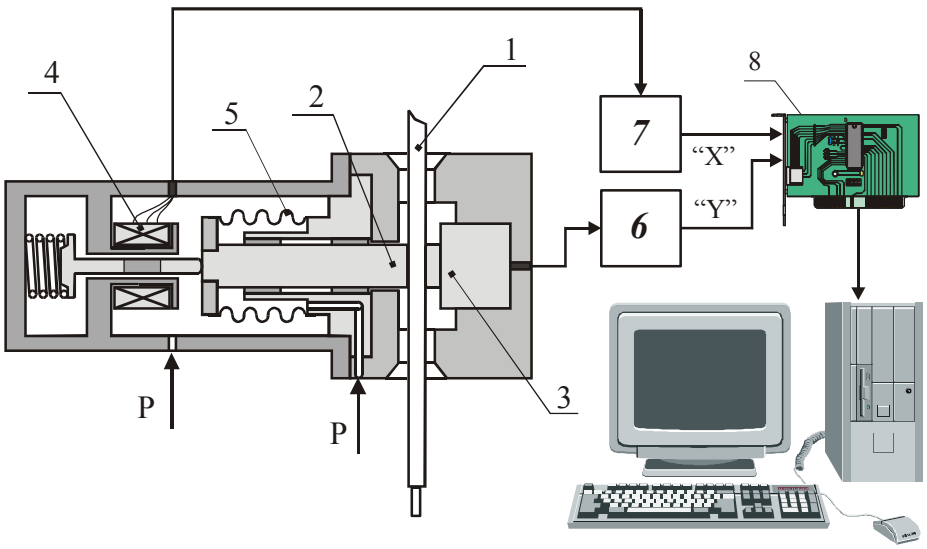

FIG.1. Schematic representation of the gap measurement facility: 1-fuel rod; 2-loader rod; 3-piezoelectric force transducer; 4-LVDT; 5-silphon; 6-charge amplifier; 7-normalizing amplifier; 8-analog/digital converter (ADC).

More than 150 fuel rods have been examined at the facility to date. Based on the gained data and the operating experience it's possible to indicate some advantages of this method:

- high efficiency (measurement of the fuel-cladding gap with step 50–100 mm along the length of the WWER-1000 fuel rod takes no more than 1.5 h);
- possibility of obtaining statistically reliable data on distribution of the gap along the fuel rod length. In this case, the number of the measurement points compensates the possibly low accuracy of the gap measurement in one point;
- possibility of performing the measurements before and after irradiation of the fuel rods in the reactor, and comparison of their results. It provides qualitatively new data on fuel behavior under various operating conditions.

But for the correct application of the results of the compression method the most important is a question of the measurement accuracy, and how these results correlate with the gap values measured by the traditional methods of optical metallography. The investigation of the facility characteristics using special rod test samples is not sufficient for the estimation of the gap determination accuracy for the irradiated fuel rods. Reasons of appearance of an additional error can be (Fig.2):

- misalignment of the fuel pellets relation to each other and to the cladding;
- nonuniform distribution of the gap both in limits of one cross-section, and on the height of the pellets;
- fragmentation of the fuel pellets;
- formation of oxides and deposits on the cladding surface, change of the fuel porosity etc., causing the rigidity change of the fuel-to-cladding system.

Because of the enumerated factors, the diagram of the loading irradiated fuel rod considerably differs from the diagrams obtained on the test samples.

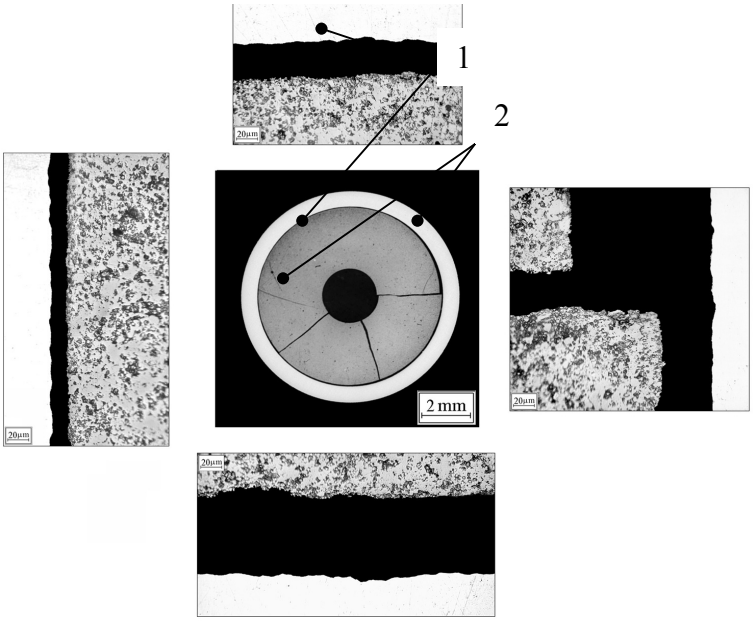

FIG. 2. Micrograph of cross-section of the WWER-1000 fuel rod: 1-cladding, 2-fuel.

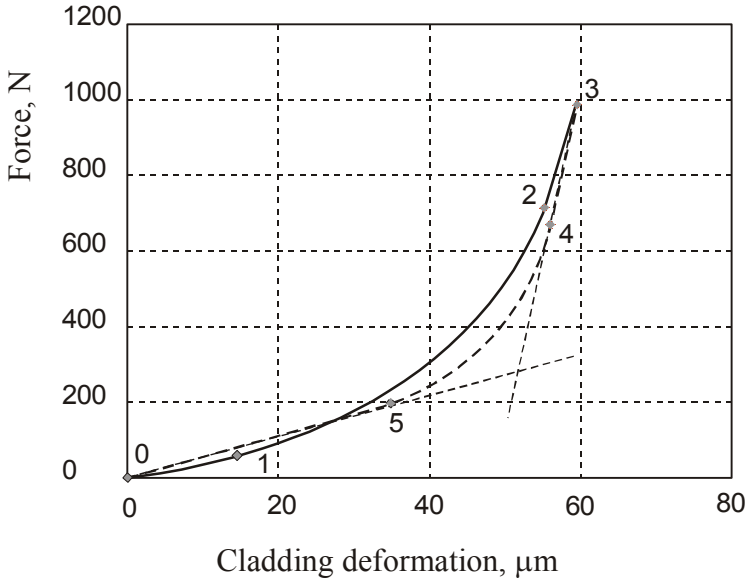

FIG .3. Typical „force-deformation" diagram of the rod loading of the WWER fuel rod: increase loading force, decrease loading force.

2. DETERMINING OF THE PELLET-CLADDING GAP ON THE „FORCE-DEFORMATION" DIAGRAM

Fig.3 presents a typical diagram of the WWER fuel rod loading pattern.

As a rule, the several linear parts can be distinguished on the loading diagram at the non-zero value of a cold gap.

The linear part 0-1 corresponds to the elastic deformation of the cladding before it's contact with the fuel. The length of the part 0-1 depends on a position of the fuel fragments relation to each other and to the cladding and can differ at one and the same diametrical gap value.

The part 2-3 corresponds to the cladding deformation when the pellet fragments are in a hard contact with the cladding.

The nonlinear cladding deformation dependence on the load for the part 1-2 is being explained by the displacement of the fuel fragments and the appearance of the local deformation of the cladding and fuel in the contact points.

As the displacement of the fuel fragments at the loading is irreversible, at decrease of load (curve 3-4-5-0) described above parts are clearly defined and width of the transient zone (part 4-5) decreases in comparison with the curve 0-1-2-3. The size of part 5-0 can be defined more exactly and the cladding rigidity, that determines the line slope on this part, can change slightly.

Therefore the deformation of cladding on the part 5-0 is used as a measuring parameter for determining of the pellet-cladding gap by compression method.

3. CORRELATION BETWEEN COMPRESSION METHOD AND METALLOGRAPHY

Let's consider the fuel rod segment *(a-b)*, which is deformed at measuring.
The diametrical gap values determined by the compression methods (δ_{ND}) and metallography (δ_{MG}) can be defined as:

$$\delta_{ND}(\varphi) = \min\{\delta_r(z,\varphi)\}_{(a,b)} + \min\{\delta_r(z,\varphi+\pi)\}_{(a,b)} \quad (1)$$

$$\delta_{MG}(z,\varphi) = \delta_r(z,\varphi) + \delta_r(z,\varphi+\pi) \; ; \quad (2)$$

$$\min\{\delta_{MG}(\varphi)\}_{(a,b)} = \min\{\delta_r(z,\varphi) + \delta_r(z,\varphi+\pi)\}_{(a,b)}; \quad (3)$$

where: $a \le z \le b$, $0 \le \varphi \le \pi$;
$\delta_r(z,\varphi)$, $\delta_r(z,\varphi+\pi)$ - radial gaps in section with the coordinate *z* in orientation φ ;
$min\{\delta_{MG}(\varphi)\}_{(a,b)}$ - minimum diametrical gap value determined by metallography for the segment *a-b* and orientation φ.

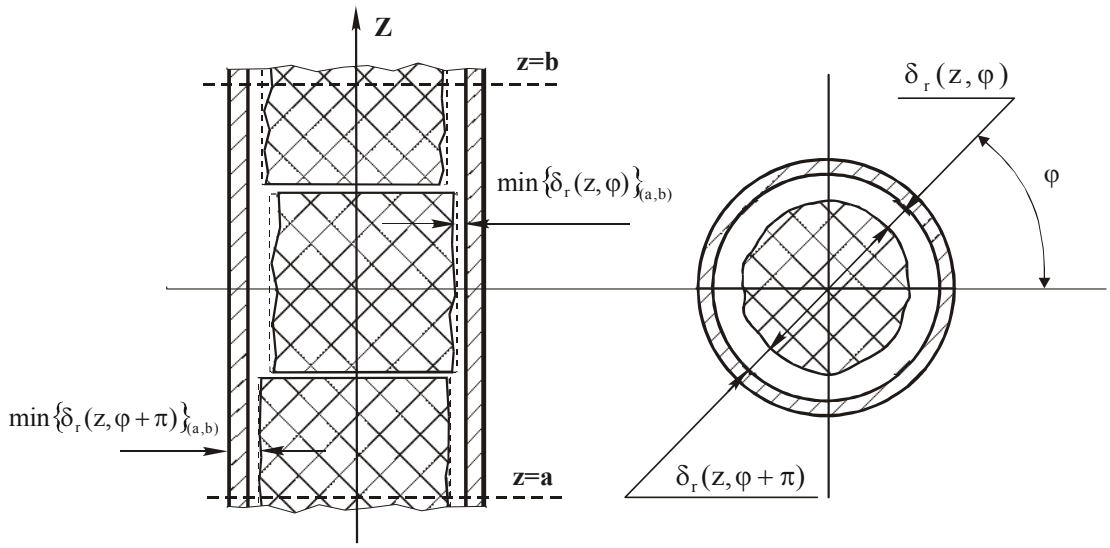

а б

FIG. 5. Schematic drawing of the fuel rod longitudinal (a) and cross-section (b): 1-cladding; 2-fuel pellets.

If the fuel fragments are immovable during the loading, the following equations should be true:

$$\delta_{ND}(\varphi) \le \min\{\delta_{MG}(\varphi)\}_{(a,b)} \le \delta_{MG}(z,\varphi), \quad (4)$$

In other words, for the orientation φ the gap value measured by the compression method should not exceed the value determined by metallography in the same orientation for any cross-section of the segment *a-b:*

$$\delta_{ND}(\varphi) \le \delta_{MG}(z,\varphi), \quad a \le z \le b \quad (5)$$

Due to the displacement of the pellets fragments during the loading, the value $\delta_{ND}(\varphi)$ should increase. In this case the equation (5) can be used for the experimental estimation of the effect of this factor on the measurement result.

Thus the compression method gives the value, which is an estimate of the minimum diametrical gap value for the segment *a-b* and orientation φ. Analysis of the accuracy of the compression method by the direct comparison with the results of the metallographic examination of one or several cross-sections, in view of different physical meaning of values, determined by these methods, is incorrect. Therefore only qualitative comparison of the metallography and the compression method results is possible. For this purpose fifteen cross-sections of the WWER-1000 fuel rods with burnup from 25 to 55 MWday/kgU were used — one for each segment of the rod, where the gap was determined by compression method in one arbitrary orientation. The diametrical gap on the micrograph was measured no less than in four orientations without considering the gaps between fuel fragments.

4. COMPARISON OF RESULTS OBTAINED BY COMPRESSION METHOD AND METALLOGRAPHY.

Fig.6 presents the comparison of the compression method results with the maximum, average and minimum gap values measured by metallography.

The comparison with the minimum gap value is most interesting (Fig. 6c). All the diagram points are split into two groups corresponding to the measured values of the gap δ_{ND} more or less than 50 μm. In spite of the fact that the compared data are not related to the azimuth coordinate, the points of the first group (δ_{ND} <50 μm) lie above the line of the equal values. For points of the second group (δ_{ND} >50 μm) the exceeding over the minimum values obtained on the cross-sections achieves 50 μm. This difference between the specimens of the first and second groups is explained by a different state of the fuel.

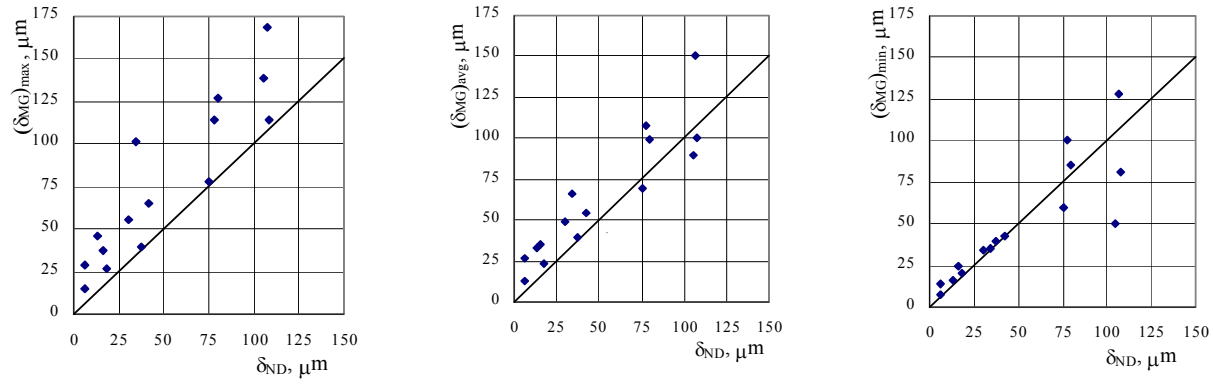

a) *b)* *c)*

FIG. 6. Comparison of the diametrical gap values determined by the compression method (δ_{ND}) with the maximum (a), average (b) and minimum (c) gap values measured by metallography: — line of equal values ($\delta_{ND}=\delta_{MG}$).

In the range of small values of the cold gap (the first group) the influence of the fuel fragmentation and initial non-uniform distribution of the gap is minimum. The difference between results of the methods does not exceed 10 μm for these specimens.

For the specimens of the second group the greater influence of fragmentation of fuel could be expected. At gap between the pellet fragments at 30–50 μm the value δ_{ND} should exceed $(\delta_{MG})_{avg}$ and should verge towards $(\delta_{MG})_{max}$. But this was not observed (Fig. 6 a,b). It seems the force of the loading (F_{max}=1200 N) was not sufficient in this case.
The described experimental data testify that the results of the compression method can be used as a low estimate of the pellet-cladding gap value at predicting the fuel rod performance.

5. APPLICATION OF THE COMPRESSION METHOD

As mentioned above, the advantages of the compression method is a high efficiency and the possibility obtaining statistically reliable data.

Fig.7 shows the cold diametrical gap values dependence on burnup. The data was obtained by the compression method on 67 WWER-1000 fuel rods with the maximum burnup from 22 to 57 MWday/kgU. The step of measurement along the fuel rod was 50–100 mm. The averaging of the diametrical gap values was performed in the range from 500 to 3000 mm. The average gap values determined by metallography for 20 cross-sections of the WWER-1000 fuel rods are presented in the same plot.

The line of least-squares trend for the compression method results crosses the vertical axis in the point $\delta_0 \approx 210$μm. This is in good agreement with the average value of the initial diametrical gap for the WWER-1000 fuel rods which equal to 225 μm [3].

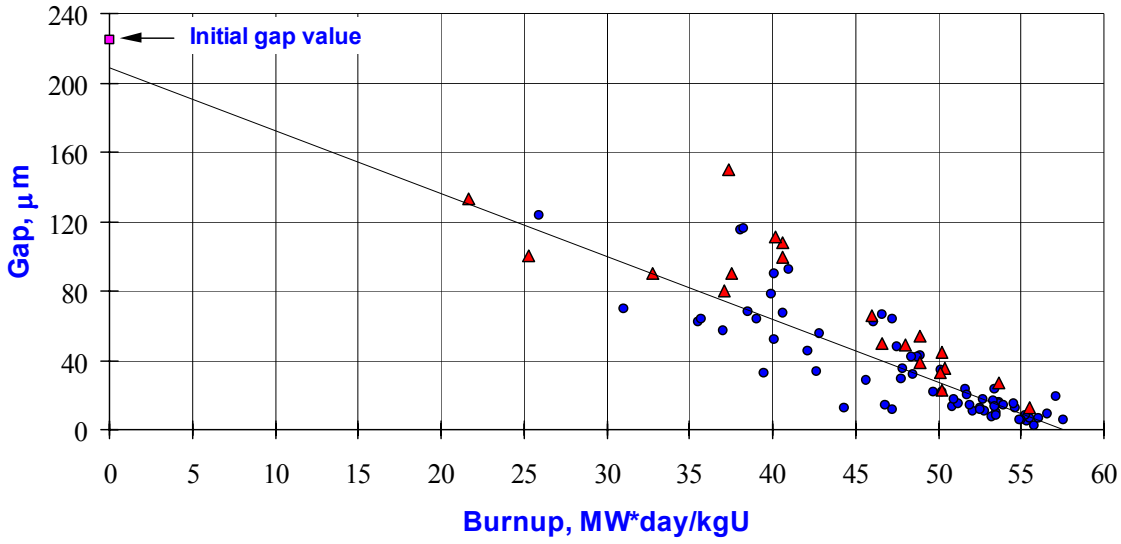

FIG. 7. The diametrical fuel-cladding gap dependence on burnup of the fuel rods:
● *gap values $(\delta_{ND})_{avg}$ determined by the compression method and averaged along the length of the WWER-1000 fuel rods;*
▲ *average values of the diametrical gap determined by metallography;*
the line of least-squares trend for the compression method results.

The gap values determined on the cross-sections, mainly, lie higher than trend line. It confirms the conclusion made before that the compression method provides a low estimate of the pellet-cladding gap value.

6. CONCLUSION

- Because of the features of the compression method, the obtained gap value is not analog of the gap measured on micrograph of the fuel rod cross-section. Therefore results of metallography can give only qualitative evaluation of the compression method efficiency.
- The comparison of the values determined by the compression method and metallography for the WWER-1000 fuel rods with burnup from 25 up to 55 MWday/kgU testifies that the results of the compression method can be used as a low estimate of the diametrical pellet-cladding gap value at predicting the fuel rod performance.

- In the range of the small gap values (<50 μm) the results of the compression method does not exceed the minimum diametrical gap values measured by metallograpfy. In the range of major gaps (> 50 μm) the compression method results approach to the average values of gap measured by metallography.

REFERENCES

[1] MANZEL, R., KNAAB, H., Performance evaluation of LWR fuel, Specialists' Meeting on Examination of Fuel Assambly For Water Cooled Power Reactors (Tokyo, Japan 9–13 November 1981) Austria: IAEA (1982) 152–159.

[2] AMOSOV, S.V., PAVLOV, S.V., "Installation of non-destructive measurement of the gap between fuel and rod cladding", Issues of Atomic Science and Techniques, Series of Material Science and New Materials **6** 40 (1990) 17–18 (In Russian).

[3] TSHEGLOV, A.S. et al, Results of Statistical Treatment of Design and Technological Parameters of WWER-1000 Fuel Rods, Preprint IAE-5334/4 (1991) (In Russian).

Gamma-spectrometric determination of the fission power of fuel rods

L. Sannen, L. Borms, Ch. de Raedt, A. Gys

SCK•CEN, Mol, Belgium

Abstract. The fission power constitutes essential information for the evaluation of the behaviour of fuel rods under irradiation. At SCK•CEN several methods are applied to determine this fission power: the in-pile thermal balance method and the out-of-pile γ-spectrometric, fluence-dosimetry and destructive-radiochemical methods. The present paper discusses the γ-spectrometric determination of both burnup and linear fission power. It relies on the determination of the concentration within the fuel of long living (^{137}Cs–burnup) or short living fission products (^{140}Ba-La–linear fission power). Their measured activities are converted into absolute concentrations by calibrating the measurement system with a reference $^{152\text{-}154}$Eu source. The measurement methodology and data processing are described — the uncertainty on the final results is estimated to amount to ±6 %. Comparison with the other fission power determination methods reveals that the γ-spectrometric method is the best out-of-pile method next to the destructive-radiochemical method, with which excellent agreement within ± 2 % is observed.

1. INTRODUCTION

The fission power which fuel rods experience during their irradiation stage(s) is a basic vital quantity both to judge on the fuel rod behaviour and their specification in terms of safeguards. Experimental post-irradiation quantitative determination of this fission power is performed at the SCK•CEN hot laboratory LHMA (Laboratory for High and Medium level Activity) by high resolution γ-spectroscopy. This measurement technique has the advantage:

- to be non-destructive, hence to be
  - reversible;
  - applicable at intermediate irradiation stages;
- to be fast;
- to generate at the same time
  - reliable quantitative data on total fuel rod fission power;
  - the fission power profile along the rod axis;
  - the axial profile of individual radionuclides, hence allowing to recognize fission product migration.

The present paper focuses on the methodology applied to determine both the rod burnup (based on ^{137}Cs activity analysis) and the linear power (based on ^{140}Ba-La activity analysis). The accuracy of the method will be assessed on the basis of error analysis and through cross comparison of results obtained with other techniques.

2. GAMMA-SPECTROMETRY METHODOLOGY

The γ-spectrometric determination of the fission power relies on the sequential measurement, within a fixed collimated geometry, of the fuel rod under examination and a calibration source. From these measurements the absolute concentration of fission products inside the fuel, and hence the fission power, can be obtained.

2.1. Measurements

The fuel rod or calibration source is positioned in a fixed geometry in front of a collimator system. Both the fuel rod and the calibration source are extended volume sources — only a very small part is visible to the detector. The information present in the measured spectrum is specific for a well-defined portion of the source, i.e. A_{ix} [counts·s^{-1}·mm^{-1}] is the net measured count rate for γ-peak i at position x within a cross section width Δx equal to the collimator system width (different collimators are available, 0.5, 1, 2 and 4 mm, in order to cope with different activity levels, which depend on fuel irradiation history and cooling time).

Multiple measurements (spectra) are required to obtain an accurate representation of the axial activity distribution along the source axis. The number of measurements and their position is chosen to yield a measured axial activity profile as close as possible to the actual activity profile. In regions where the activity gradients are low one measurement every ~ cm (each up to each third fuel pellet in case of fuel rods) is sufficient. Regions with large activity gradients are measured at intervals equal to the size of the collimator system. The presence and positions of gradients are determined by performing a gross-γ scanning prior to γ-spectroscopy. Typically ~ 20 measurements are performed on the calibration source, ~ 100 measurements on experimental fuel rods ~ 1 m in length and ~ 200 measurements on industrial rods ~ 4 m in length.

2.2. Fission indicator activity calculation

As a large number of spectra are measured, a high degree of automation of the data processing is implemented in order to take full advantage of the method.

2.2.1. Spectrum analysis

The fully automated accurate γ ray spectrum analysis program scans every spectrum for the occurrence of peaks and generates the location and net peak area of every peak. The net peak count rate is calculated as:

$$A_{ix} = \frac{N_{ix}}{t_{el}} \tag{1}$$

with N_{ix} = net peak area of peak i at axial position x [counts·mm^{-1}]
Running the spectrum analysis program on a benchmark spectrum validates the peak identification, location and net peak area determination. This benchmark spectrum contains ~ 1000 γ-peaks with exact known position, width and area. For peak to background ratios >1 the peak position is determined within ±0.1 channel width and the net peak area within ±2%.

t_{el} = elapsed life time [s]
The loss of pulse correction is determined experimentally. A ^{152}Eu source, having a reasonable number of γ-lines in the energy range 100 keV-1.4 MeV, is measured at several known distances from the detector in order to have activities ranging from very small values – typically a few 100 counts·s^{-1} – to the maximum possible – viz. ~20,000 counts·s^{-1}. The count rate errors due to loss of pulses are found to remain below 2% at the highest total incoming count rate of 20,000 counts·s^{-1} (at this count rate the measurement system dead time is approximately 60%). By using appropriate collimators, the count rate can be kept well below this value, thus giving rise to limited and accurately known loss of pulse corrections.

The elapsed lifetime is known to within ± 0.02 %.

A_{ix} = the net measured count rate for γ-peak i in the spectrum at axial position x [counts·s^{-1}·mm^{-1}]
with a global accuracy of ±2%

2.2.2. *Efficiency calibration*

The certified activity of the calibration source equals the total activity present inside the source. Hence, the efficiency of the measurement set-up is calculated from this total source activity, i.e. from the total area of the measured activity profile:

$$\varepsilon_i = \frac{1}{C_D P_\gamma TC} \times \frac{1}{2} \sum_n \left[A_{ix_{n+1}} + A_{ix_n} \right] \left[x_{n+1} - x_n \right] \qquad (2)$$

with C_D = decay correction
The decay correction corrects for isotope decay between reference date and measurement date. It depends on the half-life (known to within ±1.2% for ^{154}Eu and to within ± 0.3 % for ^{152}Eu)[1] and decay time (known very accurately). Hence the decay correction is done within ±1 %.

P_γ = γ emission probability [γ·des^{-1}]
It relates the number of γ-photons to the number of atoms responsible for it. Values of the number of γ-photons emitted per desintegration are taken from nuclear data libraries [2],[3] and are known to within ±1%.

T = transparency correction
The transparency corrects for the attenuation of γ-photons emitted inside the source travelling in the direction of the detector. It is calculated by a code ST (Source Transparency) that determines the non-interaction escape probability for mono-energetic γ- or X ray photons originating from arbitrary shaped geometric 2D objects. Total cross-sections for each compound are calculated on the basis of its composition and element cross-sections as taken from ref. [4]. Comparison of ST results with experimental measurements (by use of a calibrated source) proves the precision to be within ±2%.

C = calibration source certified value [des·s^{-1}]
For the Eu4 standard source the certified value amounts to 45.7±0.5 (±1%) GBq ^{152}Eu and 6.46±0.10(±1.5%) GBq ^{154}Eu. [5]

ε_i = measurement efficiency at energy *i* [counts·γ^{-1}]
Taking into account the precision on the individual constituents, the overall accuracy amounts to ±4.5%.

The efficiency ε_i versus energy *i* is fitted by a polynomial on a log-log scale. The obtained polynomial parameters and their covariance matrix are used to calculate the efficiency and its precision at any energy value. This precision is found to range from 2 to 5 %, corresponding very well to the one estimated above from the precision on the individual constituents (± 4.5 %).

2.2.3. *Fission indicator activity calculation*

Knowing the efficiency ε_i of the measurement system, the activity of a specific isotope (^{137}Cs as long life BU indicator or ^{140}Ba-La as a short life linear power indicator) can be calculated from the net measured count rate of its γ-peak *i* as obtained from the spectrum analysis:

$$\alpha_i = \frac{1}{C_D P_\gamma T \varepsilon_i} \times \frac{1}{2} \sum_n \left[A_{ix_{n+1}} + A_{ix_n} \right] \left[x_{n+1} - x_n \right] \quad (3)$$

with C_D = decay correction
With the half-life of ^{137}Cs known to within ±0.7% and of ^{140}Ba-La to within ±0.4% (ref. [1]), the precision of the decay correction amounts to ±1%. As reference date the end of irradiation (EOI) date is taken.

P_γ = γ emission probability [γ·des^{-1}]
As for $^{152\text{-}154}$Eu within the calibration source, the number of γ-photons emitted per desintegration for ^{137}Cs and ^{140}Ba-La is known to within±1%.

T = transparency correction
The same ST code is used to calculate the attenuation of γ-photons emitted by ^{137}Cs inside the fuel rod on their way to the detector. In addition to the intrinsic precision of the ST code (±2%), the calculation of the source transparency for fuel samples might suffer from a non-uniform radial ^{137}Cs distribution. Depending on the irradiation and especially the temperature history of the fuel rod, the radial BU is non-uniform (viz. higher burnup at pellet rim) and ^{137}Cs might have migrated (towards the pellet periphery). In order to estimate the error introduced when assuming a flat radial activity distribution, the energy dependence of the source transparency for a typical fuel rod has been calculated for different radial activity distributions. For the ^{137}Cs (daughter ^{137m}Ba) γ-peak at 661.6 keV, the difference of the transparency for a flat radial distribution and the extreme maximum transparency case with all activity concentrated in an annular ring of 0.5 mm width at the pellet surface amounts to 7 %.

ε_i = measurement efficiency at energy i [counts·γ^{-1}]
with accuracy ±4.5% - eq. (2)

$_i$ = total activity within a fuel rod of a specific isotope, measured on the basis of γ-peak i, at reference date [Bq]
accuracy ± 5.7 % in case of uniform radial activity distribution

2.3. Burnp calculation

Foregoing activity $_i$ still has to be corrected for the decay of the concerned radioactive nuclide during the irradiation period.

As the time-integrated total amount of fissions having occurred during the total irradiation period is the measure for the burnup of a fuel rod, the irradiation-history-corrected activity in case of burnup determination is calculated as:

$$A_{i_{BU}} = \alpha_i \times \frac{\lambda_i \times \sum_j P_j t_j}{\sum_j P_j \times (1 - e^{-\lambda_i t_j}) \times e^{-\lambda_i t_{r_j}}} \quad (4)$$

with P_j = relative measure of fuel rod power during irradiation time t_j
The thermal reactor power [MW_{th}] is mostly used as representative basis for relative power history assessment.

t_j = irradiation time at constant power P_j [s]

λ_i = decay constant for nuclide i [s^{-1}]

t_{r_j} = elapsed time between end of irradiation time t_j and reference date (EOI) [s]

$A_{i_{BU}}$ = total equivalent activity of a specific fission product (e.g. ^{137}Cs as long living BU indicator) within a fuel rod resulting from the time-integrated fissions within the fuel [Bq]
The correction factor is a measure of the ratio between the total amount of fission product formed (numerator = equivalent perfect integrator as if no decay had happened during the irradiation period) and the amount present at the reference date (EOI) as due to the formation/decay during the irradiation period (denominator).

The irradiation history correction is invariant with respect to absolute power scaling. In order to estimate the influence of the uncertainties in relative fuel rod power assessment, the relative range of irradiation history corrections per unit of relative power variation has been calculated. The precision on the irradiation history correction is found to range, for a ±10% variation on the relative power levels, from ±0.1% to ±5% depending on the isotope half life. By selecting appropriate isotopes accurate irradiation history corrections well below ± 1 % can be obtained, hence giving rise to an accuracy of $A_{i_{BU}}$ within ±5.8%.

In order to calculate the burnup from the above activity $A_{i_{BU}}$, still two fuel specific factors need to be calculated:

- the average yield of fission product atoms is calculated as a weighed average over all contributing fissile targets:

$$Y_i = \frac{\sum_j n_j \sigma_j Y_{i_j}}{\sum_j n_j \sigma_j} \tag{5}$$

with
n_j = fraction of atoms of fissile target j
as obtained from the initial fuel composition – mostly known with an accuracy better than ± 1 %
σ_j = thermal fission cross-section for fissile target j [b]
as obtained from ref. [2], accuracy±0.5%
Y_{i_j} = yield of fission product i for fissile target j [at/fission]
as obtained from ref. [2], accuracy±0.5%
Y_i = average yield for fission product i [at/fission]
within±1%

- the average energy release per fission is also calculated as a weighed average over all contributing fissile targets:

$$E_f = \frac{\sum_j n_j \sigma_j E_j}{\sum_j n_j \sigma_j} \tag{6}$$

with
n_j = fraction of atoms of fissile target j
as obtained from the initial fuel composition – mostly known with an accuracy better than ± 1 %
σ_j = thermal fission cross-section for fissile target j [b]
as obtained from ref. [2] , accuracy±0.5%
E_j = the total energy released per fission for fissile target j [MeV/fission]
as obtained from ref. [2] , accuracy±0.5%
E_f = average energy release per fission [MeV/fission]
within±1%

The burnup of the fuel rod ($i = {}^{137}Cs$) is then obtained as:

$$BU_r = \frac{A_{i_{BU}}}{\lambda_i} \times \frac{1.854 \times 10^{-24} \times E_f}{Y_i} \times \frac{1}{W_{HM_r}} \tag{7}$$

with $A_{i_{BU}}$ = total equivalent activity of a specific fission product (e.g. ^{137}Cs as long living BU indicator) within a fuel rod resulting from the time-integrated fissions within the fuel – eq. (4) [Bq]

λ_i = decay constant for nuclide i [s^{-1}]
known within ±0.7% (^{137}Cs)

E_f = average energy release per fission – eq. (6) [MeV/fission]
with 1.854×10^{-24} being the conversion from MeV to MWd

Y_i = average yield for fission product i – eq. (5) [at/fission]

W_{HM_r} = heavy metal weight within the fuel rod [t]
as obtained form the fuel rod specifications – mostly known with an accuracy better than ± 1 %

BU_r = fuel rod burnup [$MWd \cdot t_{HM}^{-1}$]
with a global accuracy of ±6%

2.4. Linear power calculation

As the fission rate is the measure for the linear power level of a fuel rod, the irradiation-history-corrected activity in case of linear power determination is calculated as:

$$A_{i_{LP}} = \alpha_i \times \frac{P_{ref}}{\sum_j F_d(F_a(P_j, t_j), t_{r_j})} \tag{8}$$

with P_j = relative measure of fuel rod power during irradiation time t_j
The thermal reactor power [MW_{th}] is mostly used as representative basis for relative power history assessment.

P_{ref} = reference power level
The power level P_j [MW_{th}] most prevailing during the irradiation history is mostly taken as reference

t_j = irradiation time at constant power P_j [s]

t_{r_j} = elapsed time between end of irradiation time t_j and reference date (EOI) [s]

$F_a(P_j,t_j)$ calculation of fission product activity buildup after irradiation at power P_j during a time t_j
If a precursor isotope exists that has any effect on the time evolution of the treated isotope, the more complicated mother-daughter formalism is used.

$F_d(F_a,t_{r_j})$ decay correction
If a precursor isotope exists that has any effect on the time evolution of the treated isotope, the more complicated mother-daughter formalism is used.

$A_{i_{LP}}$ = total equivalent saturation activity at the reference power of a specific fission product (e.g. ^{140}Ba-La as short-life linear power level indicator) within a fuel rod [Bq]
The correction factor converts the activity of a fission power indicator present at the reference date (EOI) taking into account the power history induced buildup/decay (denominator) to the saturation activity corresponding to the chosen reference power (numerator).

As in the case of the burnup calculation, the irradiation history correction is invariant with respect to absolute power scaling and the accuracy of $A_{i_{LP}}$ amounts to ±5.8%.

The linear power level of the fuel rod (i = ^{140}Ba-La) is then obtained as:

$$LP_r = A_{i_{LP}} \times \frac{1.602 \times 10^{-13} \times E_f}{Y_i} \times \frac{1}{L_f} \tag{9}$$

with $A_{i_{LP}}$ = total equivalent saturation activity at the reference power of a specific fission product (e.g. ^{140}Ba-La as short life linear power level indicator) within a fuel rod – eq. (8) [Bq]
E_f = average energy release per fission – eq. (6) [MeV/fission]
with 1.602×10^{-13} being the conversion from MeV to J [W·s]
Y_i = average yield for fission product i – eq. (5) [at/fission]
L_f = length of the fuel stack witching the fuel rod [cm]
as obtained form the fuel rod specifications and/or the gross-γ scan, with an accuracy < ±0.1%
LP_r = linear power level of the fuel rod at reactor power P_{ref} [W·cm^{-1}]
with a global accuracy of ±6%

3. RESULTS AND COMPARISON WITH OTHER METHODS

At the Belgian high flux materials testing reactor BR2 (Belgian Reactor 2), several methods are applied to determine the fission power: the thermal balance method, the fluence-dosimetry method, the destructive radiochemical method and the γ-spectrometry method.[6],[7] The various methods are compared for two typical irradiations in BR2:

- the irradiation of a fuel bundle of 9 rods within the CALLISTO loop (Capability of LWR Irradiation in Steady State and Transient Operation Conditions – a closed loop within BR2 in which PWR conditions of water chemistry, pressure and temperature are simulated);[8]
- the irradiation in the PWC-CCD device (Pressurized Water Capsule – Cycling and Control Device) — an instrumented irradiation rig filled with stagnant water, which can contain a single fuel rod to be tested under steady-state and transient conditions.[9]

3.1. Other methods for fission power determination

3.1.1. The thermal balance method

The thermal balance method relies on the measurement of the total heat produced during irradiation. Both irradiation devices are equipped with appropriate instrumentation:

- differential Cr-Al thermocouples to measure the temperature gradient between the outlet and the inlet of the cooling water circuit of the device;
- a diaphragm connected to an accurate differential manometer to measure the coolant flow rate in the irradiation device.

The uncertainty of fuel rod power determination by the thermal balance method at BR2 amounts to ±5%.[6]

3.1.2. The fluence-dosimetry method

In this method, the fuel rod is irradiated together with fluence dosimeters, located as close as possible to the rod. Two types of dosimeters are used: Co (with response in the thermal and epithermal neutron energy range) and Fe (with response in the fast neutron energy range). The irradiation device is modelled in a multigroup neutron calculation. The calculated dosimeter response, at the dosimeter location, is then normalized to the measured dosimeter response, which normalizes the whole calculated neutron flux chart. The calculated fission power in the fuel rod is thus obtained in absolute units.

3.1.3. The destructive radiochemical method

The radiochemical method involves fuel dissolution, chemical separation steps, and radiometric (α- and γ-spectrometry) and TIMS (Thermal Ionisation Mass Spectrometry) measurement of selected fission indicators (Nd, Ce and Cs isotopes) and U, Pu and transuranium isotopes (Am, Cm).[10] The procedure using ^{148}Nd as fission indicator is widely accepted as the reference method for burnup measurements, since it has been qualified as ASTM E321-69. The destructive radiochemical measurement method allows the determination of the fuel rod burnup (i.e. of the time-integrated fission power) to within ±2.5%.

3.2. Comparison of results from the various methods for fission power determination

The peak burnup values obtained for fuel rods irradiated in CALLISTO are compiled in Table I, while the peak linear power values obtained for fuel rods being transient tested in the PWC-CCD device are compiled in Table II.

Table I. Peak burnup values obtained for fuel rods irradiated in the CALLISTO PWR simulator in BR2, according to the various methods.

Fuel Rod	Peak burnup [GWd·t_M^{-1}]		
	Thermal Balance	γ-Spectrometry	Radiochemistry
UN1 (UO_2)	23.6 ⟨–8.4⟩[a]	25.8	25.9 ⟨+0.4⟩[a]
MN1 (MOX)	25.3 ⟨+5.3⟩	24.0	23.5 ⟨–2.1⟩
MN2 (MOX)	45.0 ⟨–1.8⟩	45.8	45.2 ⟨–1.3⟩
MN3 (MOX)	57.0 ⟨+4.4⟩	54.6	54.3 ⟨–0.5⟩

[a] The values indicated between ⟨⟩ are the percent differences with respect to the γ-spectrometry

Table II. Peak linear fission power values obtained for fuel rods transient tested in the PWC-CCD device in BR2, according to the various methods.

Fuel Rod	Peak linear fission power [W·cm^{-1}]		
	Thermal Balance	γ-Spectrometry	Fluence-dosimetry
UR1 (UO_2)	477.5 ⟨+1.1⟩[a]	472.4	479.4[b] ⟨+1.5⟩[a] 428.1[c] ⟨–9.4⟩
UR2 (UO_2)	476.1 ⟨+2.9⟩	462.9	386.7[b] ⟨–16.5⟩ 382.7[c] ⟨–17.3⟩
MR1 (MOX)	439.6 ⟨–4.2⟩	458.8	421.7[b] ⟨–8.1⟩ 385.7[c] ⟨–15.9⟩
MR2 (MOX)	468.3 ⟨+4.7⟩	447.2	- 398.5[c] ⟨–10.9⟩

[a] The values indicated between ⟨⟩ are the percent differences with respect to the γ-spectrometry

[b] These values are deduced from the Co dosimetry measurements

[c] These values are deduced from the Fe dosimetry measurements

One observes:

- for the peak burnup values:
  - an excellent agreement between the γ-spectrometry and the radiochemistry results – this is also the case for other samples, not considered in the present paper;
  - a good agreement between the γ-spectrometry results and those obtained by the thermal balance method;
- for the peak linear fission power:
  - a good agreement between the γ-spectrometry results and those obtained by the thermal balance method;
  - the agreement between the γ-spectrometry (or thermal balance) and the fluence dosimetry results lies within 20 %, the agreement being better for the Co than for the Fe dosimeters – the fluence-dosimetry seems to systematically underestimate the fission power – this method still suffers from the cumulation of calculation, modelling and measurement errors and is still under refinement.[7]

4. CONCLUSIONS

Using appropriate fission indicators and applying appropriate calibration, γ-spectrometric post-irradiation measurements allow to determine the fission power, both in terms of burnup and of linear fission power, of fuel rods within an estimated accuracy of ±6% as derived from the measurement/calculation formalism.

Application of the γ-spectrometry methodology to well characterized fuel irradiations within the BR2 materials testing reactor proves excellent agreement with the radiochemistry method (within ±2%), often considered as the reference determination, as well as a good agreement with the thermal balance method (within ±8%, which is reasonable with regard to the estimated precision of the individual methods).

REFERENCES

[1] NUCLIDES 2000, An Electronic Chart of the Nuclides on CD, ITU, 2000.

[2] BAARD, J.H., ZIJP, W.L., NOLTHONIUS, H.J., Nuclear Data Guide for Reactor Neutron Metrology, 1989.

[3] FIRESTONE, R.B., SHIRLEY, V.S., BAGLIN, C.M., CHU, S.Y.F., ZIPKIN, J., Table of Isotopes – 8th Edition, John Wiley and Sons Inc., 1996.

[4] CULLEN, D.E., CHEN, M.H., HUBBELL, J.H., PERKINS, S.T., PLECHTATY, E.F., RATHKOPF, J.A., SCOFIELD, J.H., Tables and Graphs of Photon Interaction Cross Sections from 10 eV to 100 GeV derived from the LLNL Evaluated Nuclear Data Library (ENDL), UCRL-50400, Vol. 6, Rev. 4, Part A: Z = 1 to 50 and Part B: Z = 51 to 100, Lawrence Livermore National Laboratory, 1989.

[5] REHER, D.F.G., DENECKE, B., DE ROOST, E., VAN DER MEER, K., Standardization of a 50 GBq ^{152,154}Eu Extended Volume Source, Nucl. Instr. and Meth. A 339 (1994) 334.

[6] DE RAEDT, Ch., BODART, S., WEBER, M., VANMECHELEN, P., VAN DER MEER, K., AIT ABDERRAHIM, H., DEKEYSER, J., Assessment of the Fission Power Level in Fuel Rods Irradiated in the High Flux Materials Testing Reactor BR2 at Mol – Comparison of Several Methods, ANS Radiation Protection and Shielding Division Topical Conference, "Technologies for the New Century", USA, Nashville, Tennessee, April 19–23, 1998.

[7] DE RAEDT, Ch., MALAMBU, E., BODART, S., WEBER, M., WILLEKENS, M., Assessment of the Fission Power Level in Fuel Rods Irradiated in the High Flux Materials Testing Reactor BR2 with the Aid of Fluence Dosimetry – Comparison with Other Methods, Tenth International Symposium on Reactor Dosimetry, Japan, Osaka, Sept. 12–17, 1999, Proceedings ASTM STP 1398 (2001) 252.

[8] BENOIT, Ph., DECLOEDT, C., DEKEYSER, J., DE RAEDT, Ch., JOPPEN, F., VERWIMP, A., WEBER, M., CALLISTO, a PWR in BR2: Design, Construction and Licensing, International Conference on Irradiation Technology, France, Saclay, May 20–22, 1992.

[9] SANNEN, L., BODART, S., GYS, A., VAN DER MEER, K., VERWERFT, M., Nuclear Fuel Rod Qualification by Ramp Testing and Pre- and Post-Irradiation Examination, ENS Class 1 Topical Meeting on Research Facilities for the Future of Nuclear Energy, Belgium, Brussels, June 4–6, 1996.

[10] DE REGGE, P., BODEN, R., Determination of Neodymium Isotopes as Burnup Indicator of Highly Irradiated (U,Pu)O_2 LMFBR Fuel, J. Radioanal. Chem. 35 (1) (1977) 173.

Performance of emission tomography of cylindrical fuel rods by the use of algorithms based on approximation of radionuclide activity distribution in harmonic series

V.A. Zhitelev, V.G. Dvoretsky, V.P. Smirnov, A.V. Komarov, I.A. Kungurtsev, A.N. Dorofeyev, S.V. Kuzmin

State Scientific Center of Russian Federation, Research Institute of Atomic Reactors, Dimitrovgrad, Uljanovsk Region, Russian Federation

Abstract. Considered here is the problem of applying the reconstruction algorithm that is based on approximation of radionuclide activity distribution in harmonic series in on-line emission tomography of cylindrical fuel rods. The paper presents the results of tomogram plotting with respect to ^{137}Cs distribution in VVER-1000 failed fuel rod and RBMK spent fuel rod operated in power ramping conditions at the research reactor MIR. Results of tomography are compared with the results of Electron Probe Microanalysis (EPMA) and images of metallographic sections made with the help of optical microscope.

1. INTRODUCTION

Tomography is the main mean for fuel rod studying in the course of post-irradiation examinations (PIE) and it is of particular importance for fuel rods operated in transient and emergency conditions. Distribution of radionuclide activity over the fuel rod cross-section represented with the help of emission tomography allow for estimating thermal as well as neutron-physical operating parameters. For instance, distribution of cesium on a radius of fuel pellet and along the fuel column length takes into account the final result of volatile fission product (FP) yield and FP migration in plenum. Both processes in turn depend on temperature and fuel oxidation in case of failed fuel rod.

Computer-aided tomography [1,2] is based on imaging of the internal structure of the object (image reconstruction) with due regard to the data set on projection obtained at different angles. As for emission tomography the projection is the set of measurements performed with the help of gamma ray detector in scanning of the object. Processing of projections made at different angle orientations results in definition of the bivariate function for γ-emitter activity distribution at the object cross-section.

Time required for emission tomography is determined by the scanning and depends upon the desired resolution of the tomogram, performance of equipment used for radiation monitoring and activity of radiation sources distributed in the material. The equipment allowing for parallel scanning with one detector is commonly used in hot cells intended for post-reactor examination of irradiated fuel. The total scanning time required for systems provided with one detector is rather long and doesn't allow for the desired efficiency of the applied technique.

If the emission tomography is performed for elements of nuclear reactors such as cylindrical fuel rods the image reconstruction procedure is simplified in this case. Except for severe accident resulted in the reactor core melting, density distribution for materials and radioisotopes in them is of radial-symmetric or radial-asymmetric nature generally and it can be approximated with simple bivariate functions. In this case it is necessary to execute the reconstruction algorithms so that the provision should be made for estimating the parameters of approximation functions in order to avoid estimating the function values in Cartesian coordinates (that is specific for the majority of algorithms applied in tomography). The approximation function complexity will specify the degree of detail for tomogram and the desired number of measurements. The simple approximation functions will allow for lessening the desired number of measurements and improving the efficiency of the method.

It is suggested to apply the reconstruction algorithms based on approximation of radionuclide activity distribution at the fuel rod cross section in harmonic series for on-line emission tomography of VVER and RBMK fuel rods. The paper presents the results of tomogram plotting with respect to ^{137}Cs distribution in VVER-1000 failed fuel rod and RBMK spent fuel rod operated in power ramping conditions at the research reactor MIR. Results of tomography are compared with the results of EPMA and images of optical micrographs.

2. RECONSTRUCTION ALGORITHM PRESENTATION

The type of approximation function applied in image reconstruction should primarily make allowance for the properties of objects subjected to study. As a rule cylindrical fuel rods operated under the conditions characterized by the lack of unsymmetrical mass transfer at cross sections (among these are standard operation, transient operation, all types of accidents with the exception for severe accident resulted in core melting) have symmetrical density distribution in the cross section. Thus, it is allowable to apply the bivariate function offering radial symmetry for linear attenuation factor distribution (μ) over the fuel rod cross section.

$$\mu(r,\varphi) = \mu(r) \tag{1}$$

Equation (1) is written in polar coordinate system (r,φ).

Radionuclide distribution at the fuel rod cross section can be of radial-symmetric or radial-asymmetric character. Non-uniformity of distribution can be conditioned by neutron flux tilting, characteristic properties of diffusion process, migration and adsorption of volatile products etc. Functions of different complexity can be implemented for the distribution definition. One of the simplest functions that adequately defines the radial-symmetric distribution in general with allowance for tilting in the single direction can serve the harmonic sequence of the following type:

$$Q(r,\varphi) = Q^{o}(r) + Q^{1}(r)\sin(\varphi + \varphi_{o}), \tag{2}$$

where $Q^{o}(r)$, $Q^{1}(r)$ - coefficients defining the distribution character, φ_{o}.- initial phase defining the direction of the tilting $Q(r,\varphi)$.

If distribution of γ - emitter activity at the cross section of cylindrical fuel rod is defined by function (2), the equation applied for I emission rate measured by the detector in the rectangular coordinate system will be written in the following way:

$$I(x_k,\psi)=\varpi\,\xi\int\left[Q^o(x_k,y)+Q^1(x_k,y)\sin(\psi+\varphi+\varphi_o)\right]\exp\left[-\int\mu(x_k,y)dy\right]dy, \qquad (3)$$

where ϖ -solid angle determined in accordance with the geometry of the collimator;
ξ - detection efficiency; x_k - scanning coordinates; ψ - angle of fuel rod rotation about the axis of symmetry.

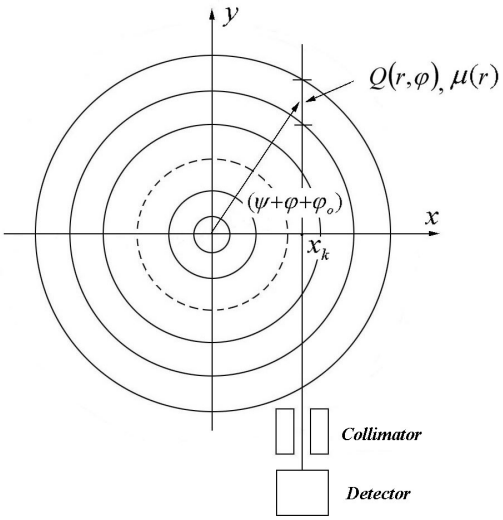

FIG. 1. Scanning scheme.

In order to calculate $Q^o(r)$, $Q^1(r)$ coefficients and initial phase φ_o defining the distribution of emitter activity at the cross section of the object it is enough to make four projections for angles ψ of 0, 90, 180 and 270°. Moreover, the integral in the right side of equation (3) has certain properties that allow the reconstruction to be simplified when the linear attenuation factor μ offers the radial-symmetric distribution. These relations bring out the following things:

$$\frac{I(x_k,\psi=0^o)-I(-x_k,\psi=180^o)}{I(x_k,\psi=90^o)-I(-x_k,\psi=270^o)}=-ctg(\varphi_o), \qquad (4)$$

$$\begin{aligned}&I(x_k,\psi=0^o)+I(x_k,\psi=180^o)=I(x_k,\psi=90^o)+I(x_k,\psi=270^o)=\\&=2\varpi\,\xi\int Q^o(x_k,y)\exp\left[-\int\mu(x_k,y)dy\right]dy\end{aligned} \qquad (5)$$

$$\begin{aligned}&I(x_k,\psi=0^o)-I(x_k,\psi=180^o)=\\&=2\varpi\,\xi\int Q^1(x_k,y)\sin(\varphi+\varphi_o)\exp\left[-\int\mu(x_k,y)dy\right]dy\end{aligned} \qquad (6)$$

$$I(x_k,\psi=90^o)-I(x_k,\psi=270^o)= \\ =2\varpi\,\xi\int Q^1(x_k,y)\sin(\varphi+\varphi_o+90^o)\exp\left[-\int\mu(x_k,y)dy\right]dy \tag{7}$$

By applying relations (4–7), the general problem in finding parameters $\varphi_o, Q^o(r),\ Q^1(r)$ can be broken up into three independent sub-problems. The initial phase φ_o is calculated from equation (4). As for $Q_o(r),\ Q_1(r)$ coefficients they are calculated from equations (5–7).

If the distribution of the linear attenuation factor and γ-emitter activity over the cross section is defined as the table function with due regard to the cylindrical object breaking up into the rings having the same thickness (Table 1), equations (5–7) become linear by applying the numerical methods:

$$z(x_k)=Q_1G^1(x_k)+Q_2G^2(x_k)+...+Q_iG^i(x_k)+...+Q_nG^n(x_k), \tag{8}$$

where $z(x_k)$ - sum or difference in detector measurements obtained relative to one coordinate x_k for two opposite projections, Q_i - coefficients of approximation function, $G^i(x_k)$ - parameters making allowance for attenuation of material radiation and change in section of $\sin(\varphi+\varphi_o)$ function.

Actually the procedure of Q_i coefficients calculation is a solution of combined equations n in m unknowns.

$$z_k=Q_1G_k^1+Q_2G_k^2+...+Q_iG_k^i+...+Q_nG_k^n, \tag{9}$$

where $i=1,...,n$ - number of elements in radial discretization of the object sections, $k=1,...,m$ - number of pairs of measurements made with the detector in opposite directions.

In order to solve equation (9), m should be equal to n. Due to the fact that every measurement result in error caused by statistical fluctuations, number of measurements m is usually in excess of n. Different methods are used for error diminishing. Among these methods are least squares technique, iterative procedures, different filters etc. [3,4,5].

Algorithms based on the method of optimal estimation [6,7,8] have good effect on reconstruction accuracy. To obtain the coefficients of approximation function we used Kalman stochastic filter [6].

3. EQUIPMENT INTENDED FOR EMISSION TOMOGRAPHY OF FUEL RODS

The equipment schematic is shown in Fig.2. The hardware incorporates the following component part:

- Scanning table;
- Programmable controller to operate stepper motor;

- Collet;
- Collimator;
- Semiconductor gamma ray detector;
- Spectrometer;
- ^{152}Eu γ -source.

Table 1. Distribution of linear attenuation factor and (-activity.

№	*Inner radius* r_o	*Outer radius* r_k	Q^o	Q^1	μ
1	0	δ	Q_1^o	Q_1^1	μ_1
2	δ	2δ	Q_2^o	Q_2^1	μ_2
...	...	...			...
i	$(i-1)\delta$	$i\delta$	Q_i^o	Q_i^1	μ_i
...	...	...			...
$n-1$	$(n-2)\delta$	$(n-1)\delta$	Q_{n-1}^o	Q_{n-1}^1	μ_{n-1}
n	$(n-1)\delta$	$n\delta$	Q_n^o	Q_n^1	μ_n

Scanning table is intended for progressive displacement of fuel rod gripped in the collet with respect to the collimator. The table is available of two controllable coordinates: here φ is the angle of fuel rod rotation about its own axis and x – displacement in the perpendicular direction to the collimator axis. The stepper motors are the electric drive mechanism for fuel rod displacement. The programmable controller provides the control over the actuating units. It provides auto control over the stepper motors of scanning mechanism in accordance with the assigned program.

The collimator is designed to generate the narrow gamma ray bundle from the fuel rod section, to dispose it through the penetration in the hot cell wall and bring it to the detector located in the operator room. ^{152}Eu γ-source is used for control over density distribution at fuel rod cross- section.

4. PERFORMANCE OF EMISSION TOMOGRAPHY FOR VVER-1000 AND RBMK FUEL RODS

The emission tomography was carried out for one failed fuel rod (VVER-1000) and one refabricated fuel rod (RBMK) that was operated in power ramping conditions at the research reactor MIR. It was carried out with the use of reconstruction algorithms based on approximation functions. The emission tomography was used to study volatile fission product behavior in fuel rods. The particular attention was given to cesium.

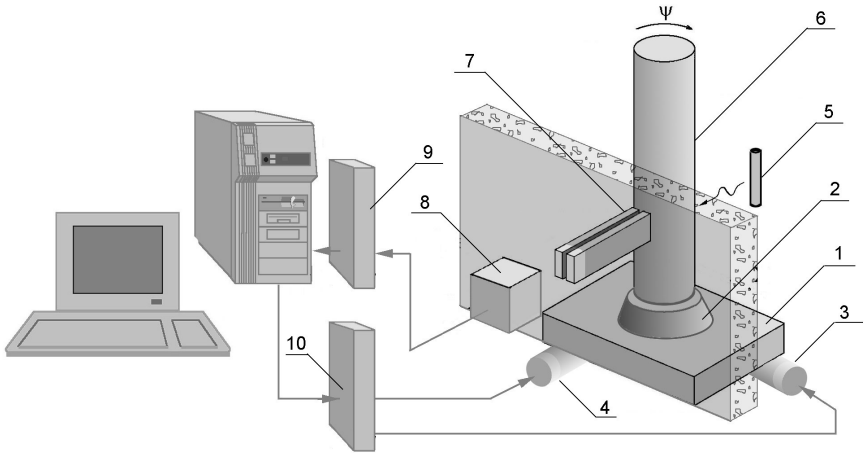

FIG. 2. The schematic diagram of equipment intended for emission tomography of fuel rods
1- Scanning table; 2- Collet chuck; 3,4- Stepper motors; 5- ^{152}Eu source; 6- Fuel rod;
7- Collimator; 8- Ge(Li) Detector; 9- Spectrometer; 10- Programmable controller.

The following works were included in emission tomography of fuel rods:

- Scanning of fuel rod in the transverse direction at different angles of orientation about the symmetry axis.
- Processing of the resulted gamma radiation spectra and projection calculation for different emission lines. The lines correspond to emission of the external radiation source and fuel rod radionuclide.
- Definition of the linear attenuation factor distribution over the fuel rod cross-section with respect to different emission lines of ^{152}Eu source by the use of algorithms of radial-symmetric transmission tomography.
- Reconstruction of radionuclide activity distribution over the fuel rod cross-section by the use of algorithms applied in emission tomography.

Fuel rods were scanned in transverse direction with respect to four azimuthal orientations (0°, 90°, 180°, 270°) by the use of collimator (with 0.4mm x 20mm aperture). Time of exposure was 300s and the job step 0.2mm. The use of collimator having a big collimation aperture was conditioned by the necessity to provide the satisfactory statistics of spectrometric measurements and to reduce the time of scanning over one fuel rod cross-section. However, the distribution picture was insignificantly blurred. This fact was conditioned by the inferior resolution of the measuring device. It should be noted that the resultant distribution pictures were average data peculiar to the fuel column area that comes into the view of collimator. When the collimation hole is 20mm, it is approximately two fuel pellets.

4. VVER-1000 FAILED FUEL ROD

The failed fuel rod involved in investigation was operated during one fuel cycle and reached a burnup of 14.8MW day/kg U. Fig.3 demonstrates the diagrams of axial γ-scanning constructed for one failed fuel rod and intact one that is available of a similar energy release and burnup level. As for the failed fuel rod, the analyzed diagrams showed that cesium released along the full length of fuel column. This fact points to fuel oxidation along the full length of fuel column. High cesium content can be noticed at the end parts of fuel rod. It results from axial migration and adsorption occurred in the "cold" parts of fuel rod.

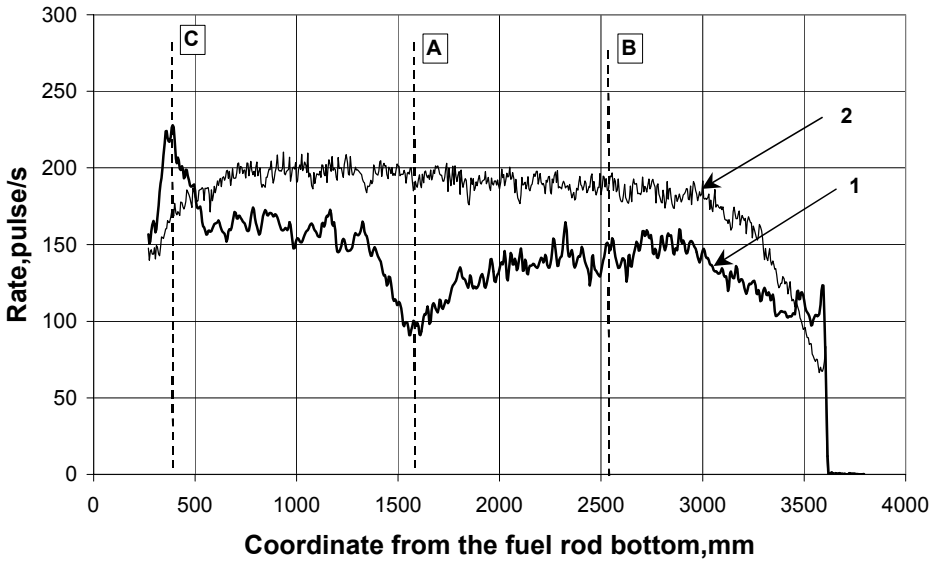

FIG. 3. Diagrams of axial ^{137}Cs distribution constructed for failed fuel rod and intact one: 1–failed fuel rod, 2-intact fuel rod.

The optical micrographs and tomograms of ^{137}Cs distribution plotted for one cross-section of intact fuel rod and three cross-sections of failed fuel rod are shown in Fig.4. Coordinates locating the cross-sections A, B, C are given in Fig.3. The cross-section A is found in the immediate vicinity to through-the-thickness crack of cladding that is characterized by the highest cesium release. Projections obtained for ^{137}Cs and averaged with respect to four angle orientations are given in Fig.5. Radial distributions of cesium obtained from the projection reprocessing are shown in Fig.6. The dot line is used for the outer boundary of the fuel pellet.

The analysis of the presented tomograms and diagrams plotted relative to ^{137}Cs distribution reveals that cesium distribution on a radius of fuel pellet is axially symmetric and uniform in its nature at the cross section of intact fuel rod. The mentioned above effect of image blurring explains the absence of well-defined boundaries in distribution of activity at the outer surface of fuel column and central hole surface. Uniform distribution of ^{137}Cs on a radius points to the lack of cesium migration in fuel of intact fuel rod.

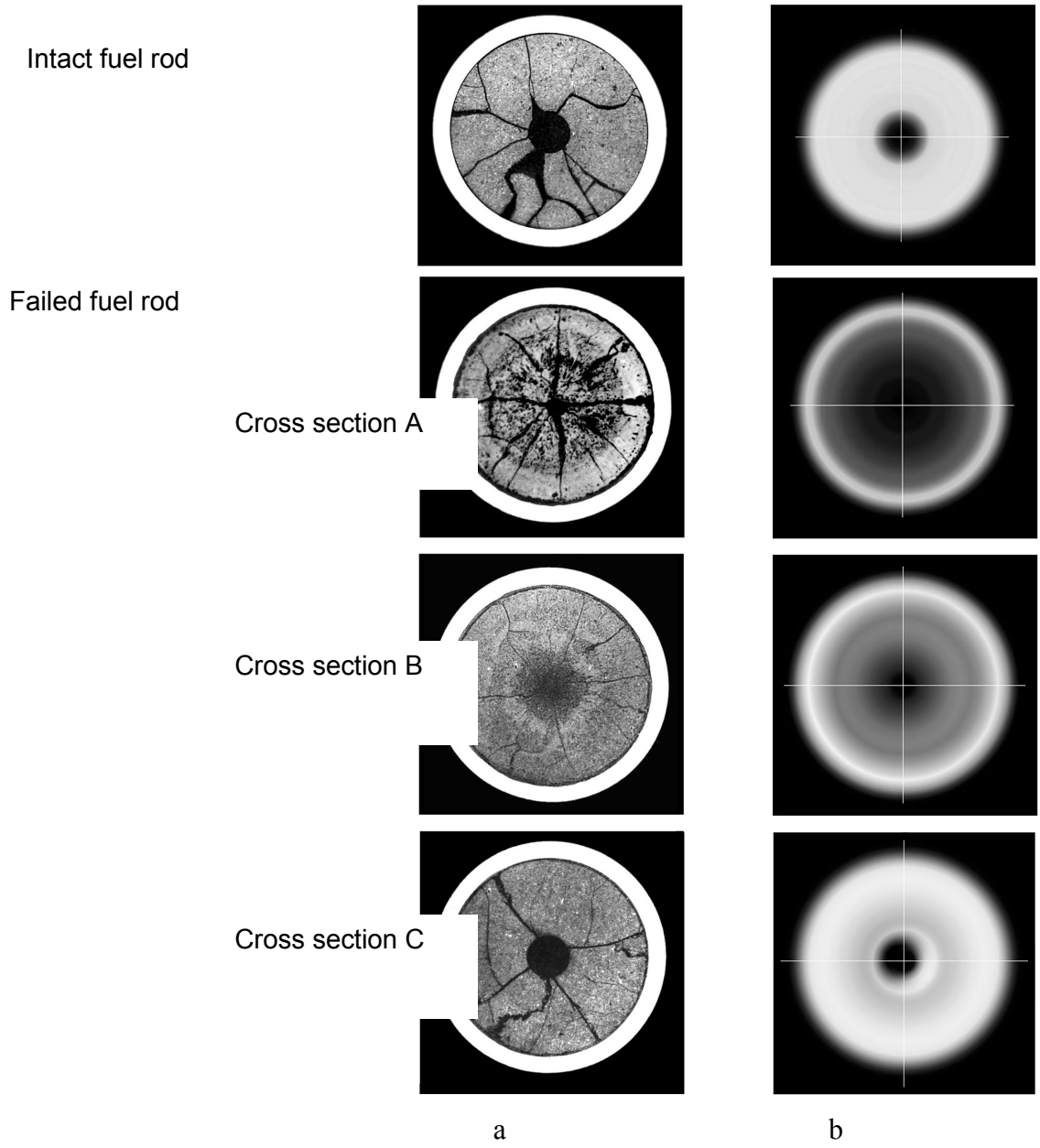

FIG. 4. Optical micrographs and tomograms of ^{137}Cs distribution: a- Optical micrographs formed by the optical microscope; b- Tomograms of ^{137}Cs distribution.

^{137}Cs distribution is nonuniform on a radius with respect to all cross sections of failed fuel rod. Moreover, cesium distribution demonstrates a distinct axial asymmetry at the cross section C. According to cesium distribution on a radius at different cross sections of failed fuel rod, it is evident that cesium released from fuel at every cross section. A decrease in cesium concentration as it approaches the central hole points to the fact that cesium releases from the hotter central parts of the fuel column in the majority of cases. The greatest cesium release was noticed at the cross section A that is found in the immediate vicinity to the defect.

As for the cross section C, a local increase in cesium concentration was noted nearby the central hole concurrent with a decrease in its concentration as it recedes from the outer surface of the fuel column**.** This effect is conditioned by the transferring of cesium released from the

fuel in the central channel and its adsorption at the inner surface of the fuel column that is the "cold" lower part of fuel rod. As mentioned above, this cross section is characterized by axial asymmetry in cesium distribution. As the asymmetry is specific for the area that is adjacent to the central hole, it results form the greater cesium adsorption at one surface of the central hole in comparison with the other one.

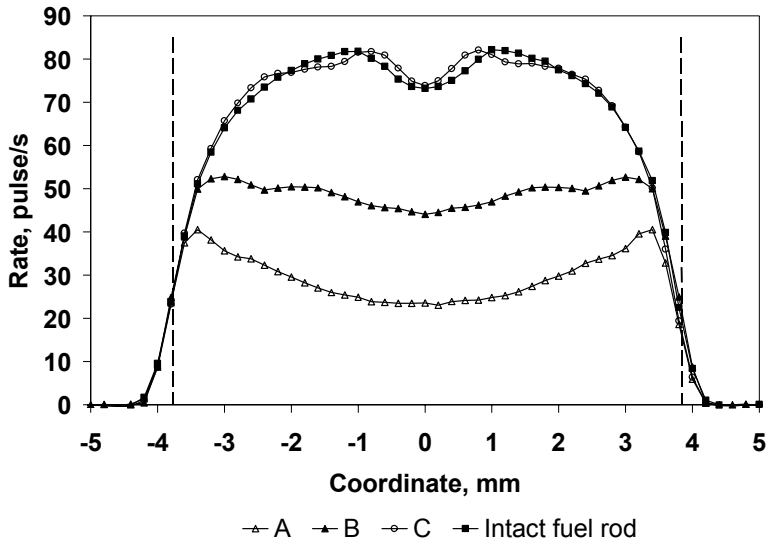

FIG. 5. ^{137}Cs projections obtained for an intact fuel rod and failed one and averaged with respect to four angle orientations.

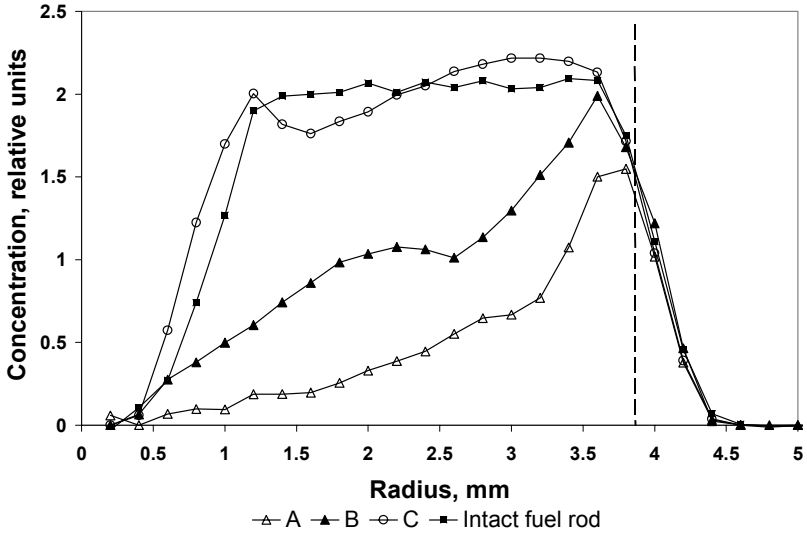

FIG. 6. Distribution of ^{137}Cs on a pellet radius at the cross sections of intact fuel rod and failed one.

Tomograms plotted with respect to cesium distribution at the cross sections of failed fuel rod are consistent with optical micrographs that make allowance for changes in micro-structural characteristics of fuel (Fig.4). It is evident that fuel microstructure was subjected to notable changes in the failed fuel rod. The coolant ingress into the fuel rod resulted in considerable oxidation of fuel and increase in its operational temperature. As a consequence, the coolant ingress stimulated the release of gaseous and volatile fission products from grains on their boundaries. The interlinkage grain-boundary porosity, grain growth and formation of zones with columnar grains gave rise to gaseous and volatile fission product release in the final analysis.

The whole cross-section of fuel column can be conventionally broken down into two zones according to the degree of volatile fission product release:

(1) The central high-temperature zone. It is characterized by considerable cesium release. Here cesium concentration is determined by the distance from the fuel pellet center and depends on the local temperature. Fuel microstructure was subjected to notable changes in this zone.

(2) Peripheral low-temperature zone. It is characterized by minor cesium release. Cesium concentration remains at the initial level or changes insignificantly.

The local energy release, temperatures and oxidation rate dictate the size of zones.

Cesium distributions on a fuel pellet radius were obtained using tomography. They are in reasonable agreement with the EPMA data. Fig.7 demonstrates the data obtained relative to the cross section A with the use of tomography (Cs) and EPMA (Cs and Xe). One plot is used for both sets of data.
Generally, cesium distributions reproduced by two techniques are the same in character. This fact is supported by xenon distributions. It is well known that [9] mechanisms of cesium and xenon releasing are similar at a temperature beyond 1200°C.

It should be noted that complete agreement between the tomography and EPMA data is impossible. Data obtained in the course of EPMA make allowance for cesium and xenon concentrations in grains due to the shallow penetration of electro beam into the material (≈2μm). But tomograms represent the concentration of all cesium found in the fuel rod i.e. in grains, gas bubbles as well as concentration of cesium adsorbed in cracks and contained in fuel-to-cladding gap.

5. RBMK REFABRICATED FUEL ROD

The refabricated fuel rod was made from fuel rod of RBMK fuel assembly. It reached a burnup of 18.9MW days/kg U. The fuel rod was tested in the research reactor MIR in power ramping conditions.

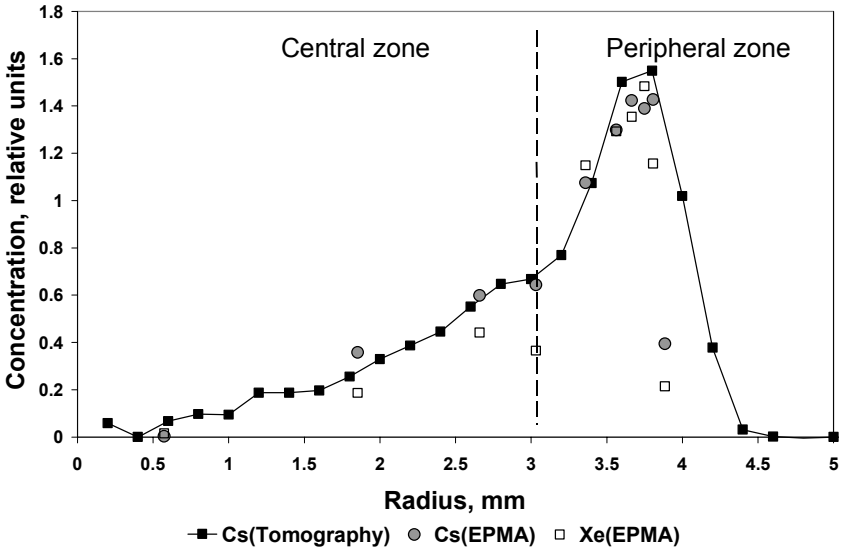

FIG. 7. Distribution of volatile and gaseous fission products at the cross -section A reproduced with the use of emission tomography and EPMA..

The maximum linear power in power ramping was about 400W/sm at the cross-section subjected to tomography. In order to carry out the comparative analysis between the obtained data and similar data obtained with respect to fuel rod that was irradiated in normal conditions we performed emission tomography of witness fuel rod.

The optical micrographs and tomograms of ^{137}Cs distribution plotted for one cross-section of witness fuel rod and one cross-section of refabricated fuel rod are shown in Fig.8. According to tomogram, cesium distribution at the cross section of witness fuel rod is asymmetric to some extent. It is conditioned by non-uniform burnup of fuel that in its turn results from neutron flux tilting.

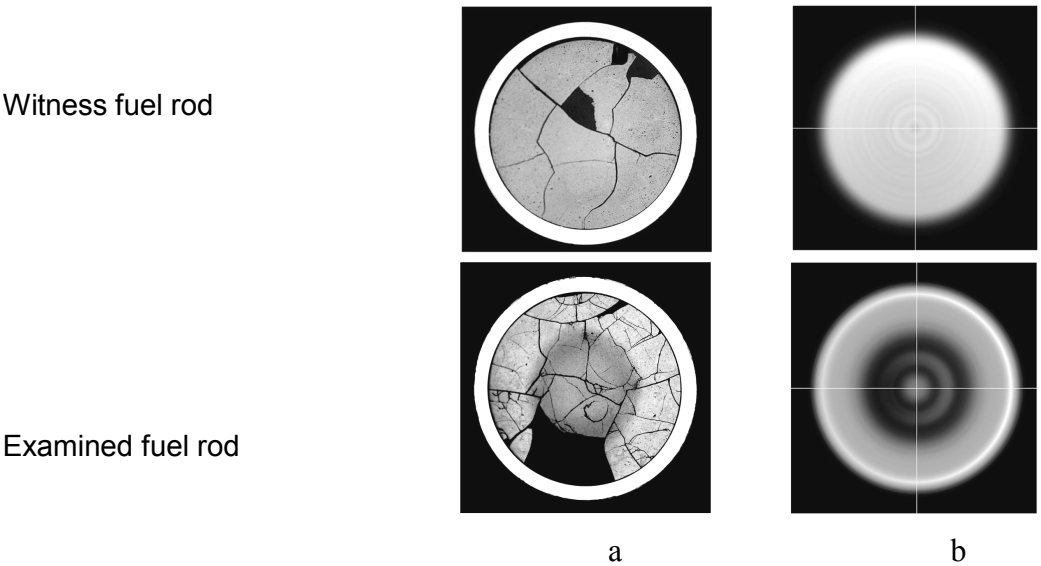

FIG. 8. Optical micrographs and tomograms of ^{137}Cs distribution: a-Optical micrographs formed by the optical microscope; b- Tomograms of ^{137}Cs distribution.

Cesium distribution at the cross section of refabricated fuel rod is significantly radial-asymmetric in nature. Projections obtained for ^{137}Cs with respect to four azimuthal orientations (0, 90,180 и 270°) and a diagram of cesium distribution in one of the directions are given in Fig.9 and 10 respectively. Fig.10 presents the data on radial distribution of cesium obtained with the help of EPMA along with the data on diametric distribution obtained by tomography technique.

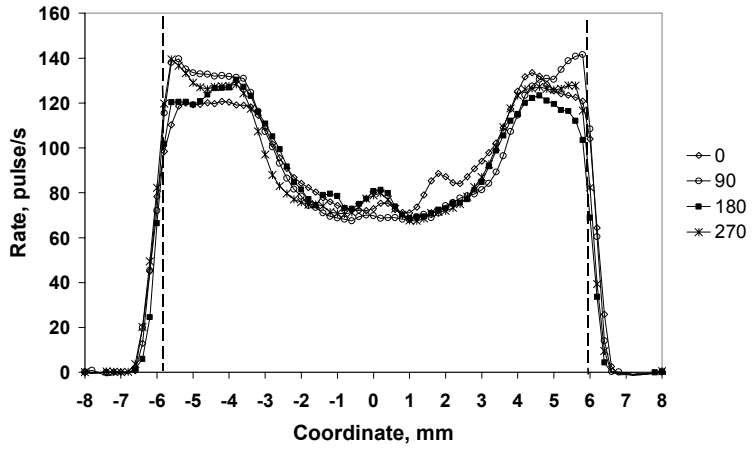

FIG. 9. Projections obtained with respect to ^{137}Cs at 0, 90, 180 and 270°.

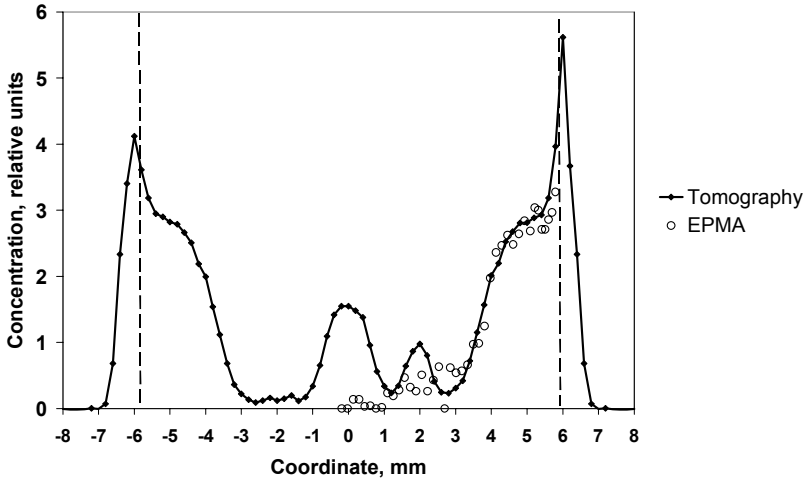

FIG. 10. Cesium distribution in diametric direction reproduced with the use of tomography technique and EPMA.

The analysis of tomography data obtained for refabricated fuel rod results in the following conclusions:

- Cesium distribution at the fuel rod cross-section is nonuniform in nature. A decrease in cesium concentration in the central parts of fuel column points to cesium release from fuel.

- Cesium distribution isn't monotonic in nature. There are local zones of high concentration in the central area and peak concentrations in the outlying regions. It is likely that they result from the accumulated cesium in "fuel-to-cladding gap".
- Cesium distribution at the cross section isn't radial-symmetric in nature. The peaks are not the same in the outlying regions. The local zones of high cesium concentration in the central area are asymmetric in their nature too.
- As a whole, EPMA data agree with the tomography data. A discrepancy between the data is noted into the fuel-to-cladding gap and in the narrow region located in the fuel pellet center. It points to the fact that cesium is present not only inside the grains in these regions.

High cesium concentration in the central part of fuel column is rather interesting exhibition of the distinguishing features of cesium migration in fuel rods where fuel is free from the central hole. Cesium behavior in power ramping conditions has been already described [9,10]. The local increase in cesium concentration in the central part of fuel column was mentioned in these papers too. This phenomenon can be supplied with different explanations. It may depend on cesium adsorbed at the face of fuel pellets. But it is highly improbable because the temperature is very high nearby the fuel pellet center even at the surfaces that are at the turn of fuel pellets and cesium should migrate in radial directions to "cold" areas. The following explanation looks more convincing. Fuel microstructure in the central part of fuel pellet presents a severe problem in cesium transferring to the open surface and that's why it is accumulated in traps (large voids, cracks etc.) or forms low-volatile compounds.

6. CONCLUSION

The reconstruction algorithms have been proposed to carry out the on-line emission tomography of cylindrical fuel rods that is based on approximation of radionuclide activity distribution in harmonic series. Such algorithms allows us to short the time of fuel rod scanning and improve the tomography efficiency in the course of post-reactor examination of irradiated fuel significantly. The technique checkout resulted in accumulation of experimental data bulk on emission tomography of fuel rods operated in standard as well as emergency and transient conditions. According to testing, the tomography data are not only in good agreement with the data obtained with the help of other examination techniques (EPMA, optical microscopy) but complement them. Specifically, the emission tomography as opposed to EPMA shows the distribution of the whole cesium contained in the fuel rod rather than contained in grain body only.

REFERENCES

[1] E.Yu. VASILIEV, L.I. KOSAREV, N.R. KUZELEV, Radiation computer-aided tomography in nuclear power engineering. Edited by A.S.Shtan. M., Energoizdat, 1998.

[2] A.S. KEK, Computer-aided tomography using X radiation, radioactive isotopes and ultrasound. TIIER, 1979, V.67, №9.

[3] I.N. TROITSKY, Statistical tomography theory. M., Radio and Communication, 1989.

[4] F. HATTERER, Mathematical aspects of computer-aided tomography. M., MIR, 1983.
[5] G.T. XERMEN, Image reconstruction according to projections. Fundamental Reconstructive Tomography. M, MIR, 1983.
[6] R.E. KALMAN, A new approach to linear filtering and prediction problems. Trans. ASME, Journ. Basic Engineering, 1960, V.79, p.33–45
[7] Guide on automatic control theory. Edited by A.A. KRASOVSKY. M., Science, 1987.
[8] V.G. DVORETSKY, V.A. ZHITELEV, V.B. IVANOV, YU.B. BARANENKOV, A.D. RABINOVICH, V.P. SMIRNOV, L.A. TSELISHCHEVA, N.S. GLUSHAK, Algorithms and hardware support of tomography carried out for spent fuel rods. Preprint. RIAR-2(829)..- Dimitrovgrad, 1992.
[9] C.T. WALKER, C. BAGGER, M. MOGENSEN, "Observation on release of cesium from UO_2 fuel", J.Nucl.Mater., 240, 32–42, 1996.
[10] Hiroshi SAKURAI, Masana SASAKI, Osamu KUBOTA, Teruo ISPGAI, "Fission Gas Release and Related Behaviours of BWR Fuel under Steady and Transient Conditions", International Seminar on Fission Gas Behaviour in Water Reactor Fuels, 26–29 September, 2000, Cadarache Guest House, France.

Installation of a shielded SIMS in CEA Cadarache

L. Desgranges[a], B. Pasquet[a], B. Rasser[b]

[a] CEA DEN/DEC/S3C/LECMI,. Cadarache, Saint-Paul-lez-Durance, France
[b] CAMECA, Courbevoie, France

Abstract. A shielded SIMS 6f has been installed in the LECA in 1999 and will examine nuclear fuels before the end of this year. Meanwhile several studies have been realised to test its technical performance for nuclear materials analysis. After a brief presentation of the design of the shielded SIMS, five examples of preliminary results will be underlined. In the nuclear field, SIMS is currently used for the analysis of Zircaloy cladding corrosion because it can detect light elements like boron or lithium. More than a quantitative measurement of isotopes, it was possible with our SIMS to produce a two dimension image of the corrosion layer focusing on the protective layer. SIMS has also the advantage to detect isotopes with a low concentration. This property will be enlightened with some results obtained on sulphur in UO_2. Because SIMS uses the erosion of the sample surface, it is possible to make depth profile. This possibility will be demonstrated on water altered glass samples on which the altered layer will be evidenced on depth profile. The last application of SIMS presented in the paper is addressed to nuclear fuel with detection of xenon. Fission gases release is indeed of first importance for nuclear fuel because it affects fuel swelling, rod internal pressure, fuel thermal conductivity via the formation of pores etc. We have demonstrated that it was possible to measure xenon on an unirradiated UO_2 sample implanted with xenon. It was also proved that xenon could be measured in gaseous state, which would make possible the measurement of xenon filling pores.

1. INTRODUCTION

The Fuel Study Department of CEA has decided to install a shielded SIMS in Cadarache centre. This apparatus is designed as a complementary tool for the characterisation of the physical and chemical state of irradiated nuclear fuels together with SEM, EMPA, ceramography and X ray diffraction. The CAMECA company was chosen to design and construct this apparatus because its IMS 6f had the best analytical performances and also because CAMECA accepted to design the shielding which interfere with the measurement device. A more comprehensive description of the IMS nuclearisation will be given elsewhere [1].

The apparatus was installed in 1999 and could work with unirradiated samples since May 99. Some modifications of the room, where it is installed, are needed in order to handle irradiated samples. This will be done this summer only because the whole facility is in a renewal process which implies that no new apparatus can be installed without a renewal of the room where it is located in. This delay was used as a training period in order to test the capabilities of the SIMS method on nuclear topics.

The IMS 6f is indeed a very versatile apparatus with the ability of doing mass spectrum, ionic images in scanning or in direct mode, three dimensions ionic images, isotopic measurements. Experimental conditions must of course be optimised to the wanted analysis. In this paper this versatility will be illustrated on samples relevant to nuclear industry. But first we will start with a brief description of the SIMS principle and of the shielded IMS 6f.

2. SIMS FOR NUCLEAR APPLICATION

2.1. SIMS physical principle

SIMS provides a local isotopic analysis of a solid sample. Figure 1 illustrates schematically the way this analysis is performed. A primary beam is focused on the sample and sputter its surface. The sputtered atoms are essentially neutral but a small fraction (of the order of the percent) is ionised and can be extracted thanks to an electrical field. The ionised atoms then go to a mass spectrometer for isotopic analysis. Based on this physical principle, all commercial SIMS can provide a mass spectrum from which isotopic measurements can be deduced, and a cartography of the sample for a given mass by scanning the primary beam.

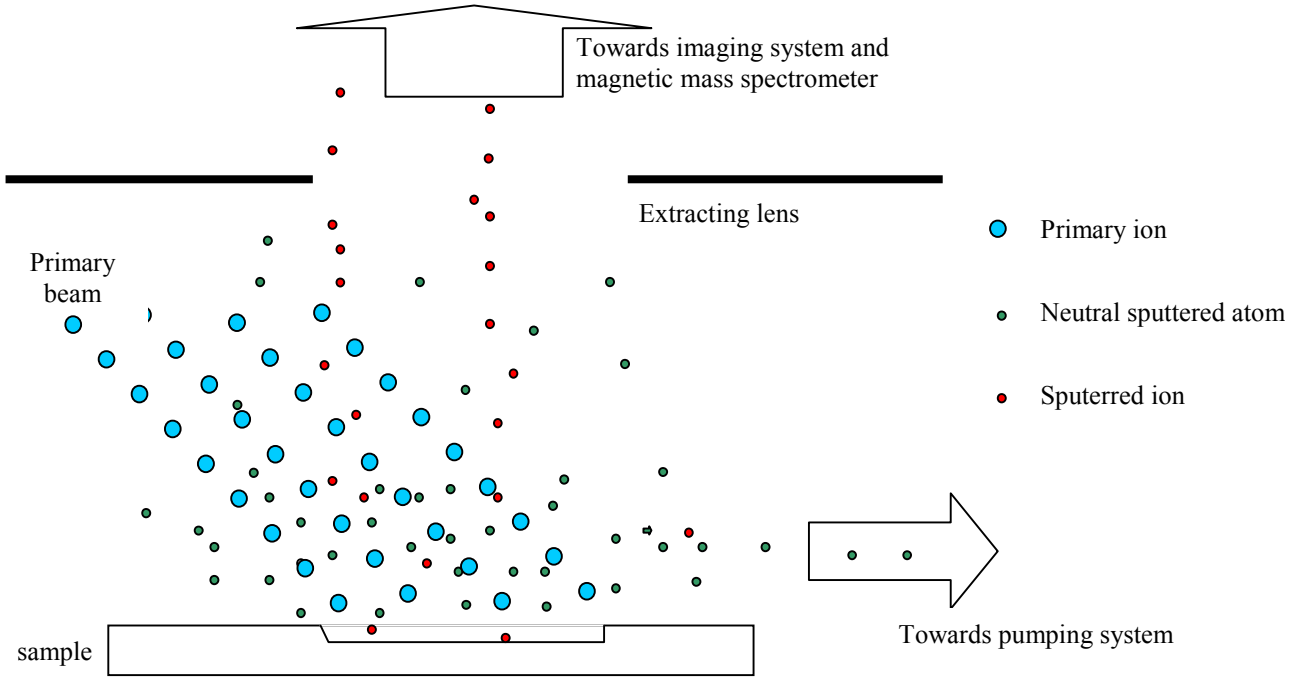

FIG. 1. Schematic description of SIMS principle In the IMS 6f configuration.

The main features of the IMS 6f include:

- Caesium microsource, producing high brightness spots down to 0.2 µm.
- the mass analysis is supplied by a spectrometer which allows high mass resolution: ultimate M/ΔM ~ 25 000 compared to M/ΔM ~ 500 for quadrupoles.
- The extracting lens is 5 mm away from the sample which allows efficient capture of secondary ions.
- The ionic optics makes possible to get direct images. Ions can be measured on a 2D detector at a location which is correlated to the location where the ion was emitted.

Other key features of the IMS 6f include: electron gun with unique self compensation mode for insulating material analysis, multiple primary ion species (O_2^+, O^-, Cs^+ and Ar^+), variable primary ions incident energy, full automation.

2.2. SIMS adaptation for irradiated samples

In order to handle radioactive material the commercial IMS 6f was modified by adding a glove box and a lead shielding. The layout of the modified apparatus is presented on Figure 2.

The glove box is limited to the space necessary for the sample transfer and for the apparatus maintenance. The shielding is design to protect the operator and the detectors from the irradiation of the sample, but it is also designed so that every part of the apparatus is reachable where some piece has to be changed. As a consequence it consists of a big lead box around the glove box and the sample chamber of the IMS 6f, keeping the back of the apparatus free. However some leak between the apparatus and this lead box needed to be closed with additional shielding in the back of the apparatus. The description of these modifications will be explained in more detail elsewhere.

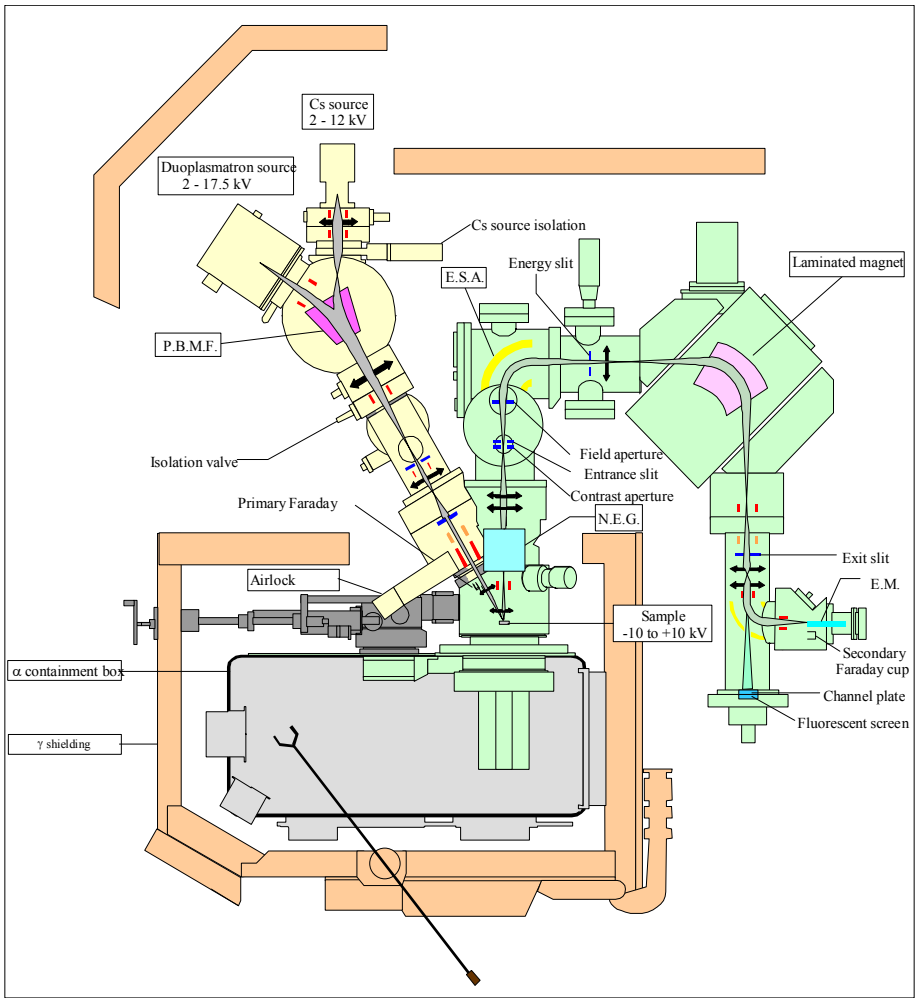

FIG. 2. General synoptic of the IMS 6fR..

Despite these modifications the performances of the IMS 6f were kept equivalent to those of a standard apparatus, and were evaluated during the testing period. The more significant performances obtained are:

- 7.10^{-7} bar vacuum in the sample chamber
- mass resolution M/ΔM better than 25 000
- detection limit of 10^{13} atoms/cm^3 of boron and 10^{14} atoms/cm^3 of phosphor in implanted silicon
- lateral resolution of 0.2 µm with a caesium beam in scanning mode

3. FIRST RESULTS

In SIMS analysis proceeds in two steps: detection of a selected mass and then fitting of the measurement parameters as a function of signal abundance and desired analysis. Several samples, representative of irradiated materials, were analysed with our SIMS. The obtained results are presented in the following showing the versatility of the apparatus and the accuracy of the method.

3.1. Slightly irradiated aerosols

The first step of an analysis is mass identification. This is not necessary an easy task because not only isotopes should be taken into consideration but also some ionised molecules. We shall illustrate that point with the analysis of some FPT0 aerosols. In the framework of the international Phebus program, aerosols produced during the core degradation in a thermal transient are released in the reactor vessels. These aerosols are characterised in order to produce modelling of the radionuclides dispersion during a nuclear accident. A specimen of such aerosols had been made for SEM examination, and we examined it with our SIMS. The aerosols were stuck on a conductive tape, being itself stuck to a metallic cylinder which was settled in the sample holder. Because the sample was old, its activity was low enough to handle it in a "green area".

The mass spectrum was first determined for positive secondary ions with an oxygen primary beam. Some uranium was detected and it was decided to determine the ratio $^{235}U/^{238}U$. Figure 3 presents the mass spectrum between masses 233 and 239 with a mass resolution of $M/\Delta M=2000$. Not one but several peaks are observable on mass 235 and 238. The peaks corresponding to the actual 235 and 238 uranium isotopes are those with higher mass. This example evidences that accurate measurement of the ratio $^{235}U/^{238}U$ requires high mass resolution, using a $M/\Delta M$ resolution of around 300 would have given a 10% false value.

In the positive secondary ions spectrum, some discrepancies appeared with previous SEM-EDS measurements: Rhenium was indeed identified as a major compound with SEM, and it was hardly detected with positive secondary ions.

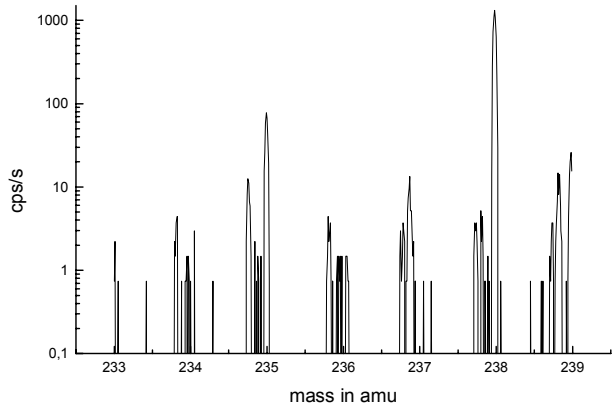

FIG. 3. Mass spectrum of FPT0 aerosols in the range 233 –239 amu.

That is why the mass spectrum of the negative secondary ions was also measured. Rhenium is clearly seen in the negative secondary ions mass spectrum as RhO, RhO_2, RhO_3 and RhO_4. From these results it was concluded that Rh was oxidised. This was confirmed by EPMA measurements showing that oxygen and rhenium were mostly collocated.

3.2. Glasses

Mass identification is not only complicated by mass interference but also by the sample itself. The examination of glass adds the difficulty of insulating samples. Glass alteration by water is a major issue for long term storage of glass matrix. This alteration involves the diffusion of oxygen and silicon through the alteration layer. To study this phenomenon isotopic marking was used: a glass with natural isotopic ratios was altered by a solution enriched with ^{18}O and ^{29}Si.

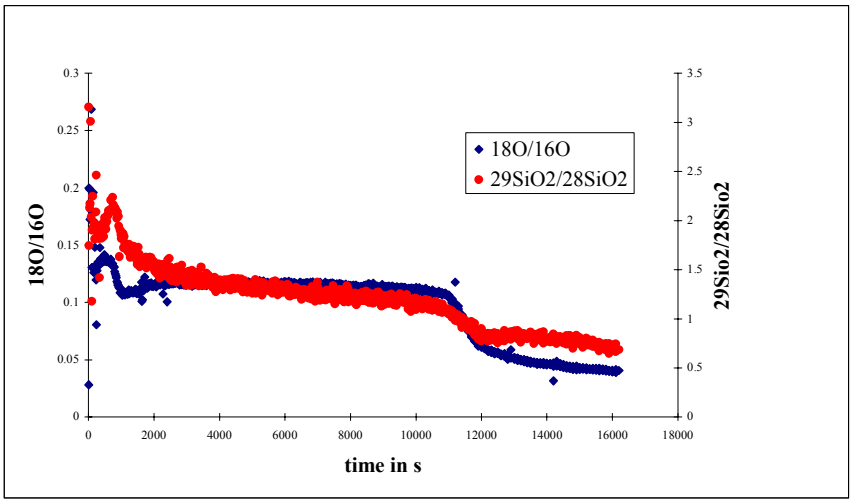

FIG. 4. Evolution of isotopic ratio as a function of depth (time of erosion) of an water altered glass.

The evolution of the isotopic ratios 18O/16O and 29Si/28Si was measured as a function of the erosion depth in a glass with an alteration layer of approximatively 10 µm. The primary beam was Caesium in order to have a correct isotopic ratio for oxygen. Mass resolution was increased to $M/\Delta M = 4000$ in order to avoid mass interference ^{29}Si-^{28}SiH. An electron beam was scanned over the sputtered area in order to avoid sample charging that induces primary beam deflection and can lead to sample chipping.

The obtained profile is presented on figure 4. It evidences three different areas: the first area at the surface of the sample has isotopic ratios equal to those of the solution; the second area, deeper in the solid, has intermediate isotopic ratios between those of the solution and of the glass; the third area should correspond to the bulk glass with natural isotopic ratios [2]. The measured isotopic ratio of the third area were somehow higher than natural ones. This was interpreted as a crater edge effect.

3.3. Oxidised cladding

Once isotopes of interest are detected, the information concerning their location in the sample can be visualised by isotopic cartography. In the case of a water corroded Zircaloy cladding, scanning imaging was used to get the better lateral resolution in order to evidence the protective layer.

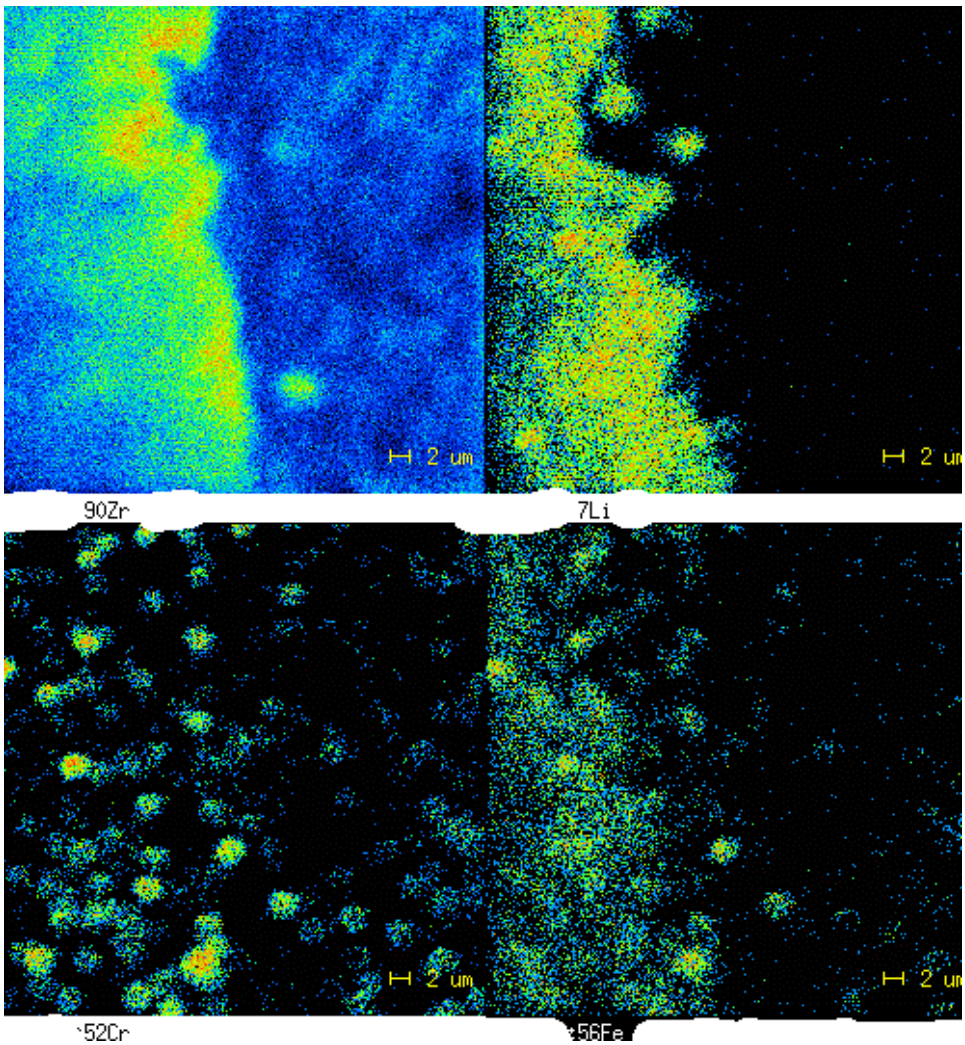

FIG. 5. Cartography of ^{90}Zr, ^{7}Li, ^{52}Cr and ^{56}Fe at the metal-oxide interface in an oxidised cladding.

An unirradiated slice of PWR cladding was oxidised in autoclave with an oxide layer of approximatively ten microns. The slice was settled in a specially designed sample holder and polished parallel to a plane making an angle of 3° with the axis of the slice. This special preparation produced a plane where the thickness of the corrosion layer is artificially increased to allow a better spatial characterisation.

Cartography of Zr, Li, Cr and Fe near the metal-oxide interface was performed by scanning a oxygen micro-beam. Cartography is presented on figure 5. On this figure the metal-oxide interface is evidenced on the Zr mapping by a contrast between the oxide and the metal. The emission yield is indeed higher in the oxide than in the metal as classically observed in SIMS with positive secondary ions. The Li mapping evidenced that the lithium is located in the corrosion layer but does reach the metal-oxide interface. This observation is consistent with the existence of a protective layer of approximately 1 µm as proposed by Pecheur and al. [3]. Iron and Chromium form precipitates in standard Zircaloy 4, during oxidation their behaviour is however different as shown on their mapping. Chromium stays in precipitate while iron tends to dilute in the oxide. This observation is consistent with previous TEM experiment [4].

3.4. Doped UO_2

The use of micro-beams, with low intensity, induces a low erosion speed of the sample. In the case of low abundance isotope, this implies very long acquisition time to get a signal high enough to be detected. Direct imaging provide image with a lower lateral resolution (around 1 µm) but on which isotopes with low abundance can be evidenced in a reasonable acquisition time thanks to a high intensity primary beam. This advantage of direct images is presented with a sulphur doped UO_2 sample.

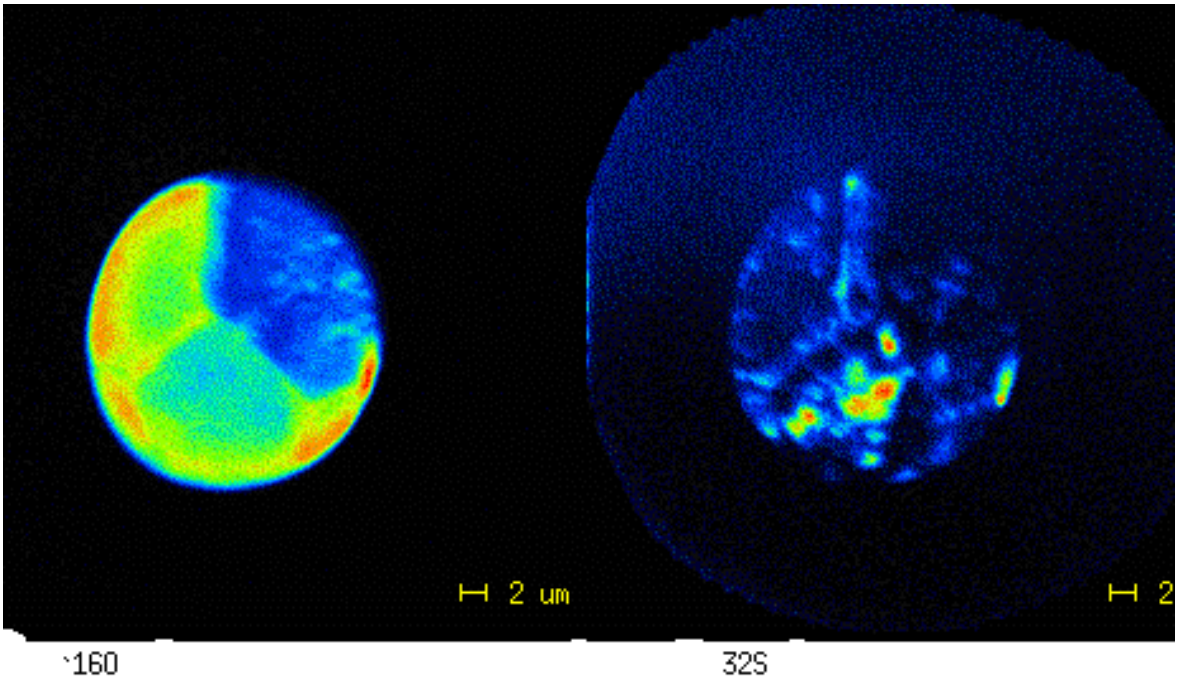

FIG. 6. On a UO_2 sample, direct images of oxygen and sulphur.

In this sample the concentration of sulphur was measured to be of the order of 20 ppm. And we were asked to provide information on the sulphur location. Direct images of sulphur were performed with a oxygen primary beam of 50 nA intensity. High resolution was also needed to resolve the interference between $^{32}S^+$ and $^{16}O_2^+$ ($M/\Delta M$ more than 2000). The sulphur (S^+) cartography is presented on figure 6 were it can be seen that sulphur is mainly located in small aggregates and on grain boundaries. The location of grain boundaries is evidenced on the image obtained with $16O^+$ ions, the emission yield of oxygen indeed depends on the crystallographic orientation of UO_2 and hence on the grain in a polycrystalline sample.

3.5. Rare gases detection

One of the very specific interest in nuclear fuel lays on the behaviour of rare gases in UO_2. They can be released out of the fuel ceramics and increase the internal pressure of the fuel rod. Helium could produce the same effects during storage. SIMS is not currently used for the detection of rare gases, however a specific study on rare gases in UO_2 was performed. UO_2 pellets were fabricated, cut, polished and implanted with Xenon atoms.

First a caesium primary beam was used, because several papers indicate that Xe can be measured using the molecule $XeCs^+$. $XeCs^+$ was indeed detected but the measured profile was too flattened compared to the calculated implantation profile. It was concluded that Xe was recoiled by caesium primary ions which induces some xenon diffusion, and inaccurate measurement.

Oxygen primary beam was used and the obtained profile is presented on Figure 7. This profile is in better agreement with the theoretical one. Principles and problems of depth profiling with SIMS are detailed in [5]. From this experimental data and from the implantation condition, the detection limit of xenon was calculated equal to 10^{18} atom /cm^3 which represent a concentration of approximately 20 ppm.

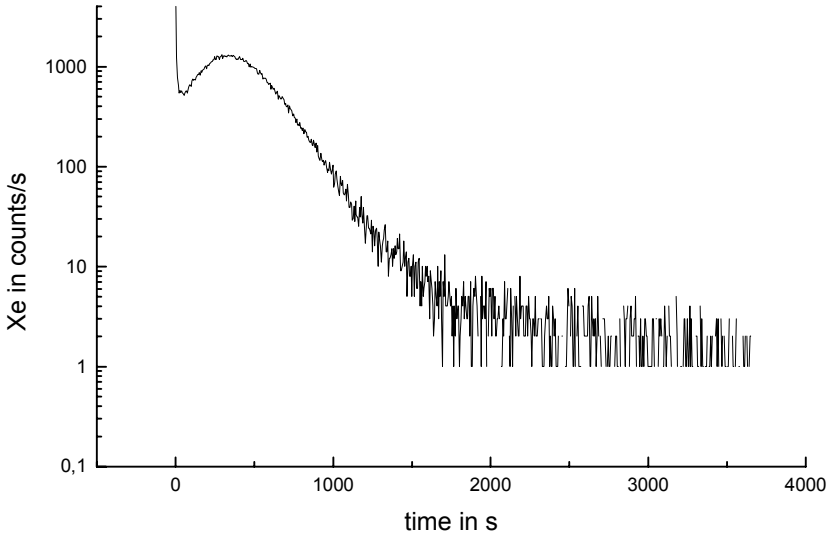

FIG. 7. Depth profile of xenon in a Xe implanted UO_2 sample as a function of the erosion time.

Some other tests were conducted by injecting xenon gas into the sample chamber at a low pressure (10^{-6} bar) on a silicon sample. Xenon isotopes were detected. Using high mass resolution to avoid interference with substrate isotopes, the Xe isotopic composition was measured and founded to be equal to the one reported in literature. From that, it was concluded that xenon could be measured in a gaseous state with our SIMS.

The obtained results with both Xe implanted UO_2 and gaseous xenon make us confident in the ability to detect xenon in nuclear fuel, whether it is implanted or trapped in bubbles. Of course some studies on irradiated fuel are still required, and they will be performed in the beginning of next year. A more detailed description of the results obtained on Xe implanted UO_2 sample will be given in a forthcoming paper [6].

4. CONCLUSION

A shielded SIMS was installed in the LECA facility, CEA Cadarache France. Its design was optimised to handle highly irradiating specimens still keeping the high level of performance of the CAMECA IMS 6f. Its capabilities were tested with unirradiated samples. From the obtained results it is foreseen that SIMS will be an indispensable tool in the following topics:

- determination of local isotopic composition for local burnup estimation or analysis of aerosols
- characterisation of elements with low Z like lithium and boron for the cladding corrosion studies
- characterisation of doping species with low concentration for optimisation of fabrication process
- characterisation of elements important for the environment but with low abundance like iodine etc
- improved characterisation of fission gases in nuclear fuel

After a period of renewal of the facility, the shielded SIMS should be in operation in October 2001.

REFERENCES

[1] B. PASQUET, L. DESGRANGES, B. RASSER, "Technical aspects of shielded SIMS installation in CEA Cadarache", European working group on hot labs and remote handling, Spain, (Sept. 2001) (in press).

[2] N. VALLE, "Traçage isotopique des mécanismes de l'atération du verre de confinement des déchets nucléaires: SON68", Ph. Thesis, Nancy, France, (Déc 1 2000).

[3] D. PECHEUR, J. GODLEWSKI, PH. BILLOT, J. THOMASET, "Microstructure of oxide films formed during the waterside corrosion of the zircaloy-4 cladding in the lithiated environment", Zirconium in the Nuclear Industry Proc. Eleventh international symposium, Garmisch-Partenkirschen, Germany, 11–14 Sept 1995, editors: E.R. BRADLEY and G.P. SABOL, ASTM, PA, USA (1996) 94.

[4] D. PECHEUR, F. LEFEBVRE, A.T. MOTTA, C. LEMAIGNAN, J.F. WADIER, "Precipitate evolution in the zircaloy-4 oxide layer", J. Nucl. Mat. **189** (1992) 318–332.

[5] R.G. WILSON, F.A. STEVIE, C.G. MAGEE, "Secondary ion mass spectrometry". A Practical Handbook for Depth Profiling and Bulk Impurities Analysis, John Wiley & Sons Inc, (1989).

[6] L. DESGRANGES, B. PASQUET, Detection of xenon in UO_2 (to be published).

NON-DESTRUCTIVE AND DESTRUCTIVE FUEL EXAMINATION METHODS — PART 2
(Session 4)

Chairpersons

L. DESGRANGES
France

Y. GOLOVCHENKO
Russian Federation

Measurement of energy introduced into spent fuel under short neutron irradiation

P.A. Privalova, Ju.V. Efremov, I.V. Tzelishchev, A.P. Chetverikov, G.A.Timofeev

State Scientific Center of Russian Federation, Research Institute of Atomic Reactors, Dimitrovgrad, Uljanovsk Region, Russian Federation

Abstract. The fragments of fuel elements that were irradiated in reactors for a certain period of time are exposed to the short-term pulsed irradiation for investigation of nuclear fuel and structural materials behavior under different operating conditions. The energy released during such irradiation is calculated on the basis of the known uranium content and fission products accumulated in fuel.

1. EXPERIMENTAL

^{140}Ba is a suitable indicator for this purpose because of its high accumulation intensity (more than 6% of the fission products quantity), optimum half-life period (Table 1), possibility of its chemical extraction and subsequent selective gamma-spectrometric measurement.

Table 1. Some parameters of the gamma-emitters contained in the measured sources

Radionuclide	^{133}Ba	^{140}Ba	^{140}La
Half-life	10,5 years	12,8 days	40,3 hours
Analytical line, keV	356,0	537,3	1596
Analytical line intensity	0,619	0,244	0,954
Gamma-constant, $(R \cdot cm^2)/(hr/mCu)$	2,94	1,144	11,48

At SSC RF RIAR a technique using isotopic dilution has been developed for determination of the relation of ^{140}Ba activity to the mass of uranium contained in the irradiated oxide fuel samples. The plan of the main procedures is presented in Fig. 1.

A fuel element sample of 2÷5 g is dissolved in 100-200ml of nitric acid of 6-8 mole/liter under weak boiling in the shielded cell conditions. 2 aliquots are sampled from the obtained solution. Both uranium mass and also ^{140}Ba and ^{133}Ba activity are measured in the first aliquot preliminary. These data are used for the estimation of ^{133}Ba and ^{235}U quantities, which are introduced as a complex reference into the second aliquot used for the final analysis by isotopic dilution. The uranium mass is measured by the mass-spectrometric method described in [1], and the ^{140}Ba activity is measured using gamma-spectrometer.

Ba chemical extraction and purification is performed at 3 stages. The first stage is performed in the heavy shielded box. Ba is extracted from the bulk of radioactive and stable elements by its co-precipitation with the carrier in the form of nitrate (Ba or Sr) of concentrated nitric acid (24 mole/l). The precipitate is separated from the aqueous phase by centrifugation. The second stage is performed in the light box. Ba is purified from the daughter ^{140}La and some fission products by their co-precipitation with ferric hydroxide and by separation of the precipitate by centrifugation. At the third stage Ba is purified from Sr by precipitation of Ba bichromate and subsequent separation of the precipitate from the solution where Sr is retained. This stage is performed in the fume hood.

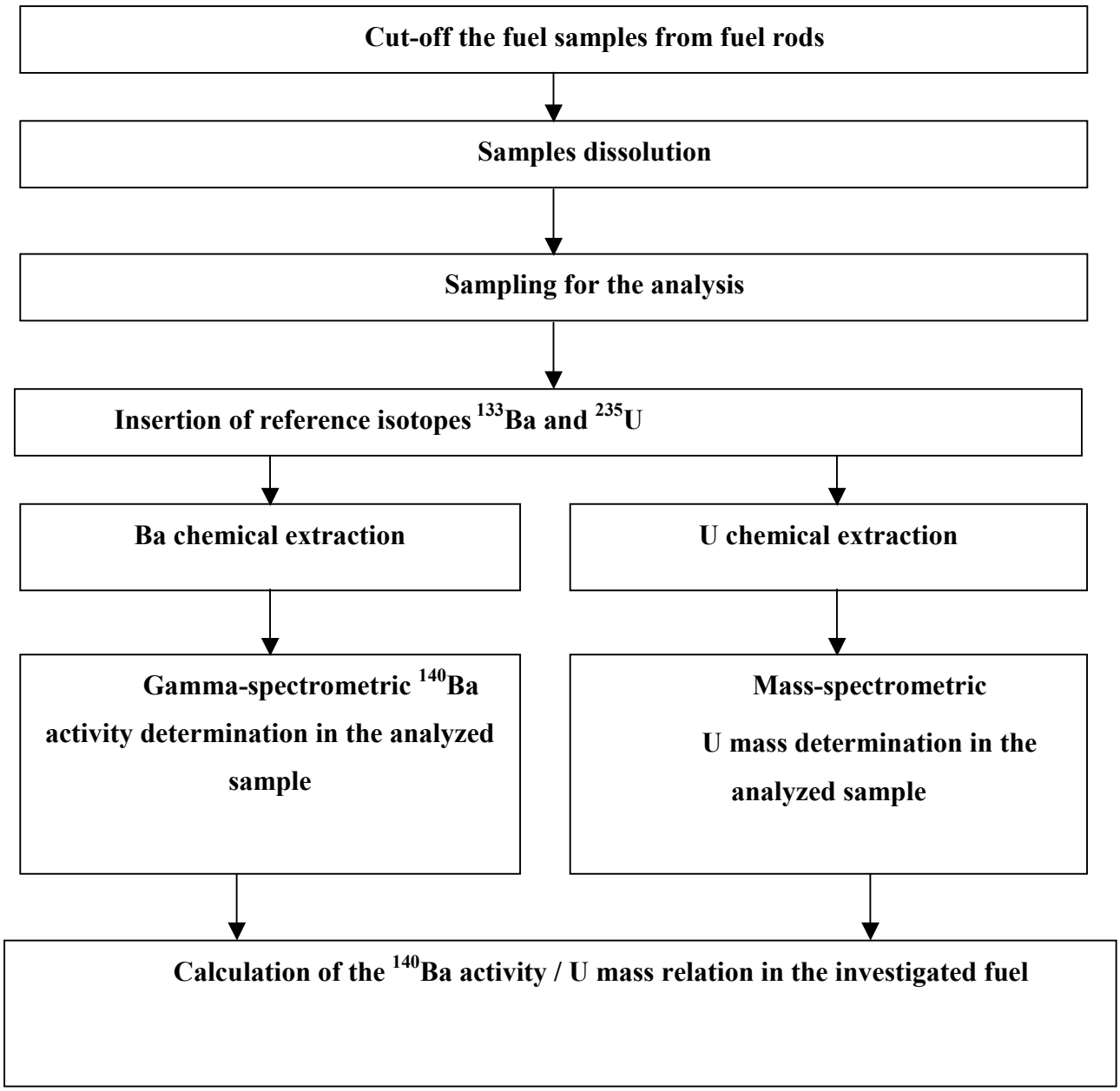

FIG. 1. Procedures during determination of the ^{140}Ba activity/U mass relation.

Ba bichromate precipitate is dissolved in 1,5 – 2ml of nitric acid (2 mole/l). 1 ml aliquot sampled from the obtained solution is placed into the test glass of 14 mm in diameter and represents a source measured using gamma-spectrometer.

The degree of ^{140}Ba purification from other fission products is no less than $1 \cdot 10^6$. That's why only nuclide gamma lines are present (Table 1) in the typical equipment spectrum of gamma-emission (Fig. 2) obtained while measurement of the source with Ba extraction.

The solution volumes required for the analysis and the quantity of the references to be introduced are determined so that the mass-spectrometric samples contain no less than 10mkg of U, and ^{140}Ba activity in the measured source achieves $1{,}0 \cdot 10^3$ - $1{,}0 \cdot 10^4$ Bq and is of the same order with ^{133}Ba activity.

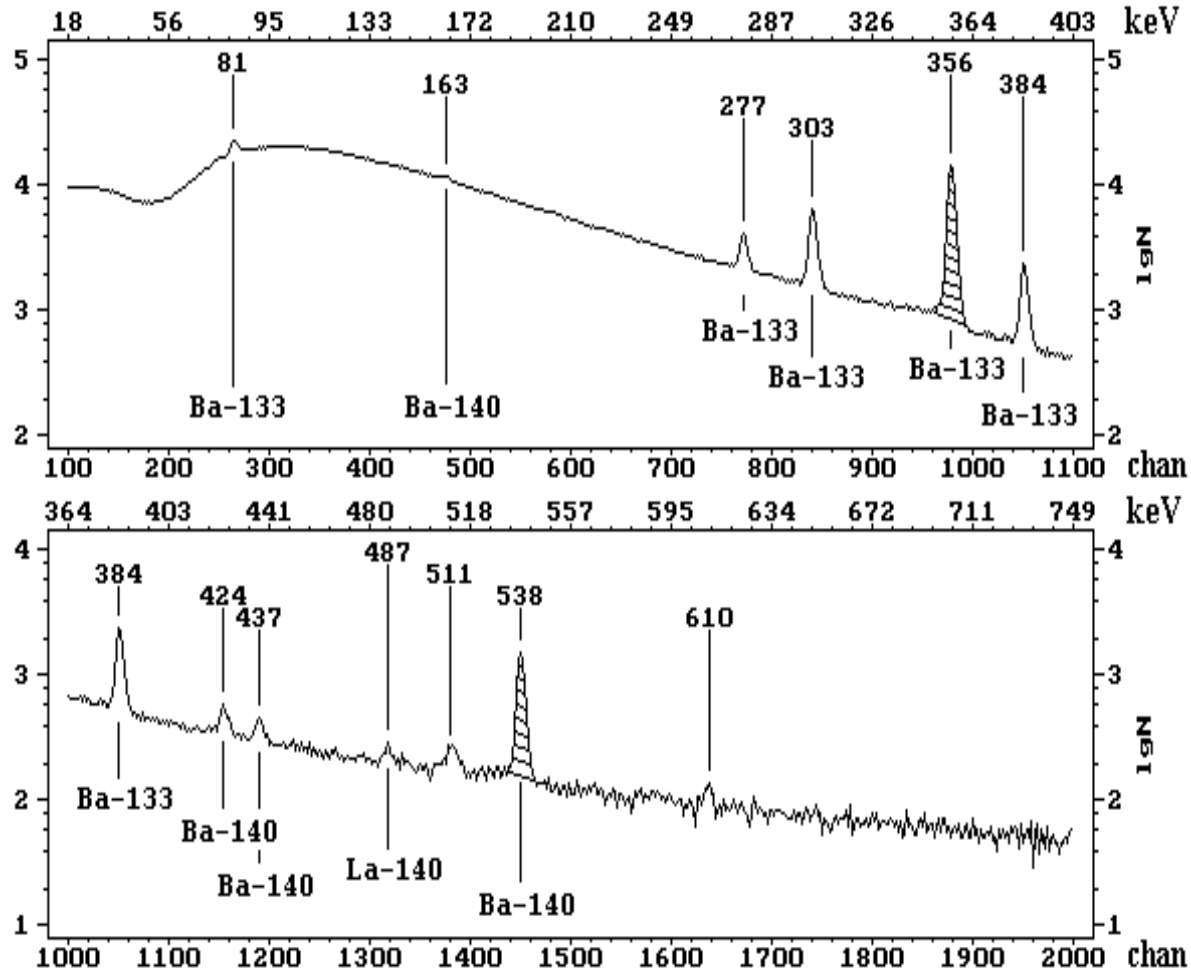

FIG. 2. Typical spectrum of the sample solution with extracted Ba: vertical lines point at the medium energy corresponding to the peaks (keV) and nuclides.

^{140}Ba activity is defined on the basis of the count rate of pulses in the amplitude distribution peaks corresponding to the full photon energy absorption (related to the most intensive analytical lines of ^{140}Ba (537,3keV) and ^{133}Ba (356,keV) introduced into the sample as a reference) in the germanium detector taken account of the photon yield per one fission event and efficiency of their recording for the fixed measurement geometry. Calibration of the spectrometer on the basis of energy and definition of the recording efficiency is performed using ^{133}Ba and ^{152}Eu reference sources.

The duration of the measurement is chosen so that the relative statistical error of the analyzed peak intensities determination for the probability of 95% comprises no more than 2%. The source is measured m times. ^{140}Ba activity in the sampled aliquot (Bq, at the time moment t_o) A_i for every i measurement is calculated by the following formula:

$$A_i = (A_{140,i} \cdot A_{133в} \cdot K_p) / A_{133,i} =$$
$$= (I_{140,i} \cdot \varepsilon_{133} \cdot \gamma_{133} \cdot A_{133в} \cdot \exp((\ln 2 \cdot t)/T_{140}))/(I_{133,i} \cdot \varepsilon_{140} \cdot \gamma_{140}) , \quad (1)$$

where $A_{140,i}$, $A_{133,i}$ - ^{140}Ba and ^{133}Ba activities, calculated on the basis of the i measurement, Bq;
$A_{133в} = A_{133a} \cdot \exp((\ln 2 \cdot t_1)/T_{133})$ – is ^{133}Ba reference activity introduced into the analyzed aliquot, recalculated for the moment of the measurement, Bq (A_{133a} – a reference activity to

the moment of its calibration; t_1 – a time interval between the moment of calibration and the measurement; T_{133} – ^{133}Ba half-life (accepted to be 10,74±0,01 years)). In case when the significant ^{133}Ba content is observed in the initial solution before the reference introduction the appropriate correction is performed;

$K_f = \exp((\ln 2 \cdot t)/T_{140})$ – a correction for the ^{140}Ba fission during the time period t (24 hours) from the time t_o till the measurement;

$I_{140,i}$, ε_{140} , γ_{140} и $I_{133,i}$, ε_{133}, γ_{133} – peak intensity (c^{-1}), detection efficiency, major analytical line intensity is 537,3 kev for ^{140}Ba and correspondingly 356,0 keV for ^{133}Ba (γ_{140} is accepted as 0,244±0,001 and γ_{133} is accepted as 0,619±0,003 [1]);

T_{140} - ^{140}Ba half-life accepted as (12,789±0,006) days.

^{140}Ba activity of the aliquot (A_m, Bq) is calculated on the basis of m measurements using the following formula:

$$A_m = \sum_1^m A_i /m, \qquad (2)$$

where A_i - is ^{140}Ba activity determined by i measurement

The relation D, of ^{140}Ba (A_m) activity Bq/mg) in the analyzed aliquot to the uranium content mass (M_u) is calculated by the following formula:

$$D = A_m / M_u \ . \qquad (6)$$

The formula (1) analysis shows that ^{140}Ba activity, calculated by it, is proportional to the relation of its peak intensity (537,3 keV) to ^{133}Ba reference intensity peak (356,0 keV). It means that when such a calculation is used Ba intensity is considered automatically during its chemical extraction and its dilution during samples preparation. The necessity to correct the miscalculations arising from the high spectrometer loading and the differences in the measurement geometry disappear.

2. SOME EXPERIMENTAL RESULTS

Table 1 presents some data taken from [2] for gamma-emitters incorporated in the analyzed sources. ^{140}La activity accumulated from ^{140}Ba reaches its peak in 5,66 days. In the process their activities become equal. But already 24 hours later ^{140}La 34,7% of ^{140}Ba activity contributes to the spectrometer loading 3 times as much as the parent ^{140}Ba does. It is explained by the fact that ^{140}La gamma-constant is one order higher than ^{140}Ba gamma-constant. Therefore the activity measurement using the gamma-spectrometer should be taken no later than a day after the separation of barium from lanthanum. Otherwise it is necessary purify the measured source from the accumulated daughter ^{140}La, since ^{140}La gamma-emission considerably increases the spectrometer loading and pedestal under the analyzed spectrum peaks. This in its turn leads to the analysis error increase. For example, if in the source spectrum with ^{140}La content of no more than 10% of ^{140}Ba by activity, the peak/pedestal relation achieves 2 and 3 for energies of 356.0 and 537.3 keV respectively, then after coming to equilibrium these values achieve 0.1 and 0.2.

Table 2 presents the results of the determination of ^{140}Ba activity A_m and U mass M_u (A_m and M_u are normalized per source solution volume unit) and their relations D in the samples for 5 fuel rods. The relative error of magnitude D is about 5%. The A_m activity makes the major contribution to it, since the error M_u does not exceed 1 %.

Table 2. The results of ^{140}Ba activity and U mass and their relations determination

Sample	**11**	**65**	**757**	**87**	**79**
Number of measurements	**30**	**14**	**9**	**19**	**13**
^{140} Ba activity in the initial solution (A_m)·10^{-4}, Bq /ml	**1.96**	**2.70**	**2.15**	**3.17**	**239**
^{140} Ba activity error, %	**4.5**	**4.1**	**4.2**	**4.8**	**4.9**
Concentration of U isotopes in the initial solution (M_U), mg/ml	**54.0 ± 0.5**	**55.4 ± 0.5**	**52.4 ± 0.5**	**63.6 ± 0.6**	**47.7 ± 0.5**
A_m / M_U, Bq/mg	**363 ± 17**	**487 ± 19**	**410 ± 18**	**498 ± 24**	**501 ± 25**

3. CONCLUSION

The isotopic dilution method has been developed and successfully tested at examination of several series of experimental fuel rods with the irradiated fuel subjected to a pulse irradiation. The procedural error does not exceed 5 %. Definition of ^{140}Ba activity is a major contributor to this error.

REFERENCES

[1] V.Ja. GABESKIRIYA, Yu.V. EFREMOV, V.V. KALYGIN, at al, Atomnaya Energiya, **55** (3) (1983) 175.

[2] N.G. GUSEV, P.P. DMITRIEV, Quantum emission of radioactive nuclides: Reference book, Atomizdat, Moscow (1977).

Use of "MICROPROFILOMETER-2" in precise measurements of diameters of irradiated rod-type cylindrical specimens

M.V. Kuprienko, V.G. Dvoretsky, E.V. Kubasov, A.D. Rabinovich

State Scientific Center of Russian Federation, Research Institute of Atomic Reactors, Dimitrovgrad, Uljanovsk Region, Russian Federation

Abstract. The paper presents the basic principles of profilometer design, the imposed requirements and some problems emerged in their bringing into practice. Installation designed and made at SSC RF RIAR to precisely measure diameters of rod-type specimens is described. Some results of metrological certification of this installation are given.

1. INTRODUCTION

A remote measurement of current values of outer diameter (profilometry) made for irradiated elements is one of the widely used and universally recognized techniques that has found wide application in the research laboratories. Its importance is supported by the significance of dimensional stability demonstrated by the reactor core elements in the course of normal operation and studies into their deformation in the simulated emergency conditions. . So the quest for safe increase of burnup level and optimization of core structural elements impose more stringent requirements upon profilometry application and reliability of the obtained results.

2. APPLICATION

"MICROPROFILOMETER-2" accumulates all the methodological experience in previous designs and represents the optimized design of contact microprofilometer unit. The following components enter into the baseline model:

- Measuring instrument intended for determination of dimension at the current cross-section of the rod-type specimen;
- Automated mechanism intended for the inductive transducer displacement along the specimen;
- Control and data acquisition systems.

About 70% of the well-known profilometers apply the principle of dimension measurements using the contact method. The mechanisms of sensor displacement along the specimen are based on fine adjustment screws. They move the support with the clamped specimen or measuring instrument having vertical as well as horizontal frame arrangement. Steppers are most commonly used as the controllable electric drives. In modern practice the ball-and-screw pair is most promising base for scanner.

The standard control system meant for modern profilometers is based on PCs. Computerized control system demonstrates the following advantages:

- Flexible and synchronized procedure of scanning and diameter measurement;
- Logging of a large body of measurement data and satellite information in accordance with the experiment objectives;

- Standard mathematical support for the representation and analysis of data obtained in the course of measurements.

As an alternative to the sensing devices from the economical and technical points of view the division shows preference for the contact displacement transducers that are based on the precision slide rule of the "SONY" company production. Taking into consideration a great variety of designs we believe that the measuring instruments in the form of bracket based on plane-parallel motion of clearance gauges in a transverse direction to the rod-type specimen axis are most attractive ones. The analog-to-digital converter (LY51), PC and system designed for remote displacement of the examined piece form the integral part of the methodical profilometry package made for rod-type specimens.

3. MEASUREMENTS OF ROD-TYPE SPECIMEN DIAMETERS AT "MICROPROFILOMETR-2"

3.1. General

The "MICROPROFILOMETER" type devices are designed for studying the radiation-thermal creep of structural materials in normal conditions. They are also intended for studying the form change dynamics of irradiated specimens with the help of electrically heated stand units and irradiation devices using gas-filled tubular specimens. Often it is almost impossible to apply the standard profilometry techniques for fuel elements and fuel assemblies to solve the above-mentioned tasks due to the following reasons:

- The presence of large-sized dead zones that in most cases are comparable with the full length of tubular specimen;
- Modest accuracy of longitudinal positioning;
- Impossibility of bending size defining for the examined piece and hence there is the accumulative error in measurement of the outside specimen diameter;
- Limited operating speed of measurement processes resulting from the universality (a great variety of transducers and hence there is a constant need for their realignment in accordance with a change in dimension-type of the examined specimens).

The accumulated experience in adoption and operation of equipment designed for the outside diameter measurement of full-size, experimental and refabricated fuel elements leads us to development the "MICROPROFILOMETER-2" device that is free of the mentioned -above shortcomings. It incorporates:

- PC/AT-based Computer system (Fig.1);
- Scanner provided with specimen support (Fig.2);
- Servo-driven measuring instrument mounted in spring hangers and provided with two inductive transducers DG-810B (fig.3);
- Analog-to-digital converter LY-51;
- "IXE-T" Stepper control unit ("PHYTRON" company production).

The scanner provided with three steppers, measuring instrument and two inductive transducers are located in the hot cell. The control unit, analog-to-digital converter and PC are in the operator's room. Signal and power cables are ≈10m in length.

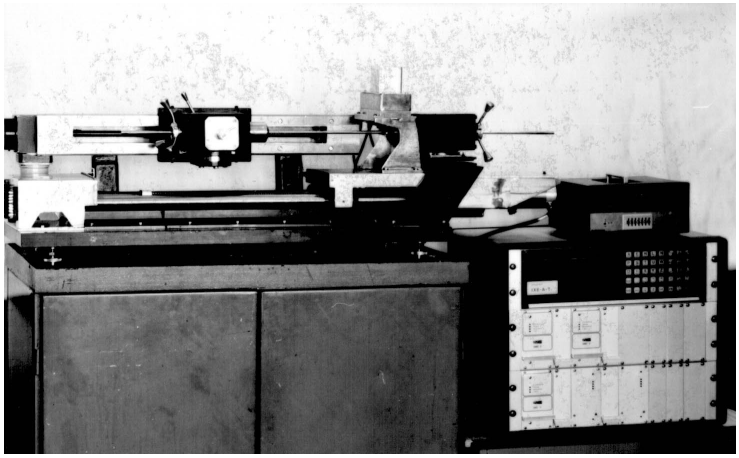

Fig. 1. Scanner (from the left) and PC-based measuring instrument on the instrument desk.

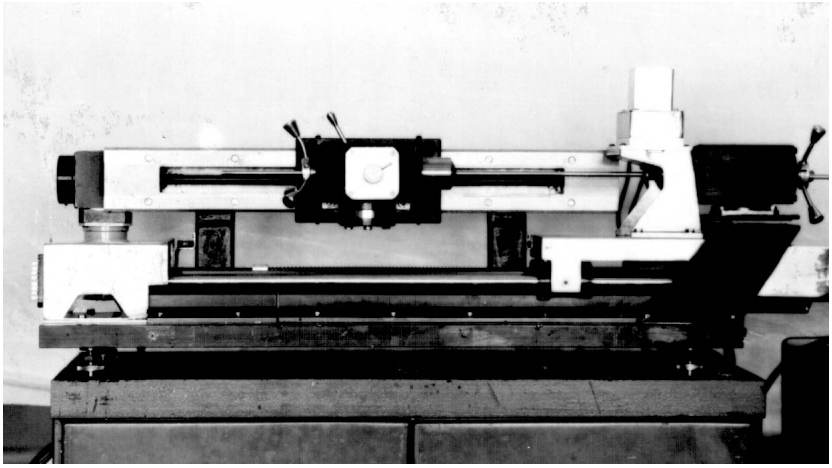

Fig. 2. Scanner.

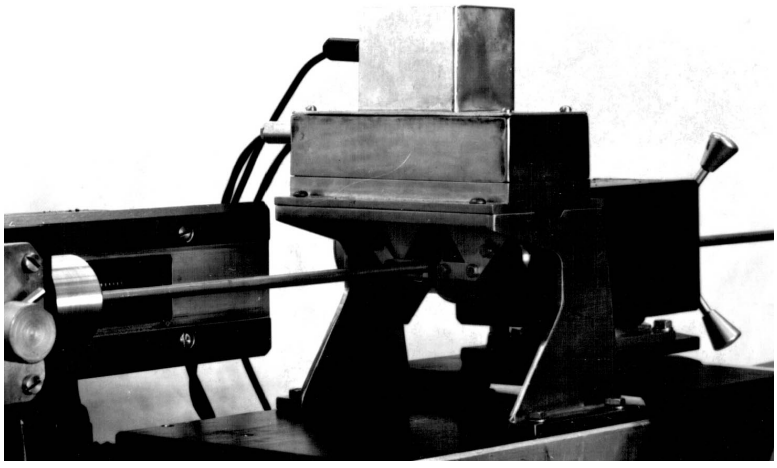

Fig.3. Measuring Instrument Provided with Two Inductive transducers DG-810B.

3.2. Measurement technique

The device implements contact method of the outside diameter measurement using two inductive transducers of DG-810B type and analog-to-digital converter (LY-51). The calibration of linear scale is no more than 0.5μm in error for the inductive transducers over the plunger slipping range 0÷10mm.

The DG-810B inductive transducers are mounted in the movable jaws of the measuring instrument and keep track of distance change between the clearance gauges with the help of plungers. A change in distance between the clearance gauges is equal to the diameter change. The tubular specimen is tightened in the support with the fine adjustment screw that is driven by the stepper and then it is moved past the stationary measuring instrument (clearing gauges).

The measuring instrument together with the DG-810 inductive transducer are calibrated to take the absolute diameter measurements against the outside diameter of the benchmark specimen that has been subjected to certification with the help of instrumentation of high accuracy rating (optimeters, end gages etc.) and supplied with the certified diameter value. The measuring instrument LY-51 outputs the absolute diameter value to PC and its own indicator after calibration.

3.3. "MICROPROFILOMETER-2" technical characteristics

- Measurement concept- performance of contact profilometry over the element of cylindrical surface with the help of slight linear movement pickups;
- Basic range of measured diameters- 0÷20mm, the allowance is made for refastening the gage rods and extending the measurement range up to 20÷40mm;
- Continuous mode of axial specimen movement. There is the allowance for diameter measurement at the point executing 2.5μm –fold step;
- Axial positioning error -±50μm; axial positioning error is ±10μm in case of motion without backlash;
- Remote selection of scan orientation executing a step of 0.5° over the whole range 0° to 360°;
- Inaccuracy of single determination of the current diameter value is ±2.0μm if the confidence coefficient is 0.95;
- Operating mode –semiautomatic;
- Maximum length of the measured specimens is 450mm;
- Overall Dimensions- 1200∗350∗350;
- Horizontal design.

4. RESULTS OF METROLOGICAL CERTIFICATION

"Microprofilometer-2" was subjected to certification that was carried out in the following way. The effective sections of the benchmark specimen (SOP VD 6.9-28) were measured three times at five orientations executing a step of 45° at the beginning, in the middle and at the end of each section. In the course of measurements the deviations from the certified diameter values didn't exceed 1.0μm (Table 1) according to the absolute value.

Table 1. Results of the Outside Diameter Standard Measurement (SOP VD 6.9-28) Made at "MICROPROFILOMETER-2", mm

Specimen Section №	**Orientation-angle of rotation about its own axis, degrees**					**Average diameter value, mm**	**Certified diameter value, mm**
	0	**45**	**90**	**135**	**180**		
First Section Center	7.6510 7.6510 7.6505	7.6505 7.6510 7.6510	7.6510 7.6515 7.6510	7.6515 7.6510 7.6510	7.6515 7.6515 7.6510	7.6511	7.6513±0.0007
Second Section Center	6.9015 6.9010 6.9010	6.9015 6.9015 6.9020	6.9010 6.9010 6.9010	6.9010 6.9010 6.9015	6.9020 6.9015 6.9015	6.9013	6.9015±0.0007
Third Section Center	6.7520 6.7520 6.7515	6.7520 6.7520 6.7520	6.7515 6.7515 6.7520	6.7525 6.7525 6.7520	6.7520 6.7520 6.7515	6.7519	6.7515±0.0007

The Excel 7.0 is used for the obtained data processing and presentation.

5. CONCLUSION

As a result of research and development work, the "MICROPROFILOMETER-2" device designed for diameter measurements (profilometry) of irradiated rod-type cylindrical specimens was tested and put into trial operation. It is distinguished from the previous designs by two inductive transducers, minor uncertainty of the obtained current diameter values. The "MICROPROFILOMETER-2" device makes allowance for measurement of long-length specimens and definition of bending size. The device is in full accord with modern requirements imposed upon the configuration, potentialities of measurements, range of studied parameters and metrological characteristics.

REFERENCES

[1] V.B. IVANOV, B.G. BASOVA, V.G. DVORETSKY, YU.P. KHODYREV, "Automation of Remote Material Science Examinations at the Hot Cell Conditions", Moscow, EnergoAtomizdat, (1986) 152.

[2] B.A. KANASHOV, V.B. IVANOV, "Remote Measurement of Geometrical Parameters of Cylindrical FR Claddings at the Laboratory of Primary Research". Voprocy Atomnoy Nauki i Tekhniki, Series "Material Science and new Materials", **3** (34) (1989) 19-27.

[3] V.G. DVORETSKY, E.V. KUBASOV, M.V. KUPRIENKO, A.D. RABINOVICH, "Profilometry of Small-Size Tubular Specimens, ANS Transactions, **4** (1998) 3-9.

Fission gas release behaviour in MOX fuels

U.K. Viswanathan, S. Anantharaman, K.C. Sahoo

Post Irradiation Examination Division, Bhabha Atomic Research Centre, Mumbai, India

Abstract. As a part of plutonium recycling programme MOX $(U,Pu)O_2$ fuels will be used in Indian boiling water reactors(BWR) and pressurised heavy water reactors(PHWR). Based on successful test irradiation of MOX fuel in CIRUS reactor, 10 MOX fuel assemblies have been loaded in the BWR of Tarapur Atomic Power Station (TAPS). Some of these MOX fuel assemblies have successfully completed the initial target average burnup of ~16,000 MWD/T. Enhancing the burnup target of the MOX fuels and increasing loading of MOX fuels in TAPS core will depend on the feedback information generated from the measurement of released fission gases. Fission gas release behaviour has been studied in the experimental MOX fuel elements (UO_2 - 4% PuO_2) irradiated in pressurised water loop (PWL) of CIRUS. Eight (8) MOX fuel elements irradiated to an average burnup of ~16,000 MWD/T have been examined. Some of these fuel elements contained controlled porosity pellets and chamfered pellets. This paper presents the design details of the experimental set up for studying fission gas release behaviour including measurement of gas pressure, void volume and gas composition. The experimental data generated is compared with the prediction of fuel performance modeling codes of PROFESS and GAPCON THERMAL-3.

1. INTRODUCTION

Approximately 15% of the fission product inventory in irradiated nuclear fuel comprise of noble gases xenon (Xe) and krypton (Kr), in different isotopic states. The behaviour of fission gases plays a dominant role in the fuel performance. The fission gases, if retained in the matrix can cause fuel swelling. If the gases are released it decreases pellet clad gap conductance. The decrease in gap conductance increases the fuel temperature and thereby leading to increased gas release. Enhancing the burnup target of the MOX fuels and loading of more MOX fuels in TAPS core will depend on the feedback information generated from the measurement of released fission gases.

Fission gas release behaviour has been studied in the experimental (UO_2 - 4% PuO_2) MOX fuel element irradiated in Pressurised Water Loop (PWL) of CIRUS. The eight (8) MOX fuel elements examined were irradiated to burnup of ~16,000 MWD/T. These experimental MOX fuel elements contained fuel pellets with a number of design variables to study their effects in fission gas release.

2. MOX FUEL FABRICATION

Mixed oxide (MOX) fuel with UO_2-4% PuO_2 was fabricated for test irradiation in the standardised powder pellet route [1]. UO_2 powder after oxidation-reduction treatment was ball-milled with PuO_2 powder in small batches. For making controlled porosity pellets 0.5wt% of methyl cellulose was mixed with milled powder. MOX powder was pre-compacted at 5 tsi, granulated to 20# sieve size. The final compaction was done at 300 MPa pressure. Sintering was carried out in Ar+5% H_2 mixture at 1680–1700°C for 8 hrs. The sintered pellets were vacuum degassed at 400°C for 8 hrs. Resintering test was carried out at 1700°C for 24 hrs. The pellets of AC-2 cluster were not chamfered whereas all the fuel pellets of AC-3 cluster were chamfered. The Zircaloy-2 clad tubes were of 0.89 mm wall thickness with inside diameter varying from 12.637 to 12.713 mm. Clad tubes and other fuel pin components were out gassed at 220°C for 3hrs before pellet loading. Helium was used as the cover gas. Typical experimental MOX fuel pin is shown in Fig.1.

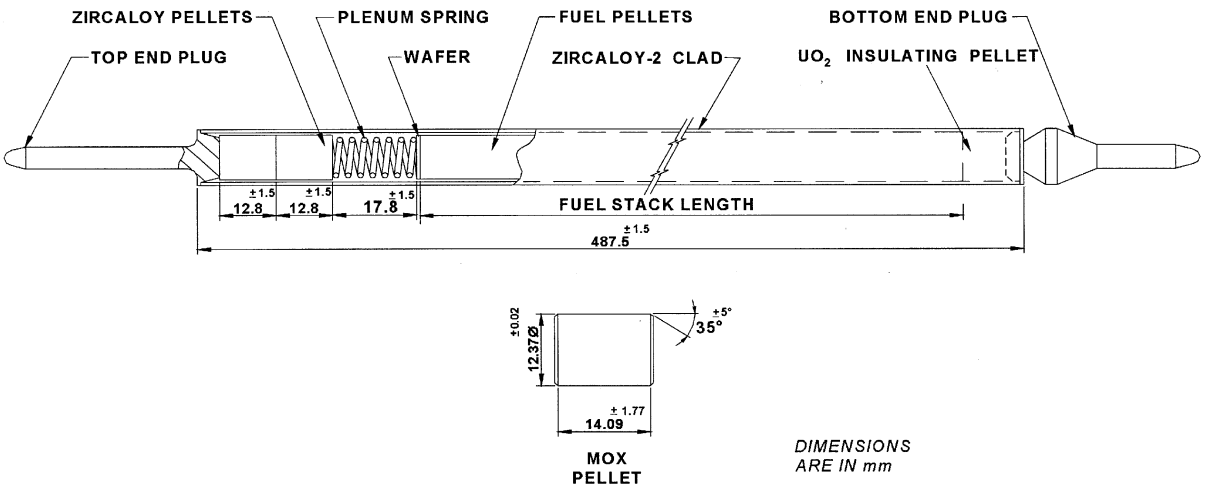

Fig. 1. A typical experimental mox fuel pin.

3. IRRADIATION DETAILS

Experimental MOX fuel pins were test irradiated in the pressurised water loop (PWL) of CIRUS reactor to a target burnup of ~16,000 MWD/T. The irradiation details of AC- 2 and AC-3 clusters are given in Table 1.

4. FISSION GAS RELEASE STUDIES

A new fission gas measuring set up was designed and fabricated to study the behaviour of fuel elements with low void volume and low fission gas releases.

4.1. Fission Gas Collection System Design

The puncture chamber and fission gas collection system was designed with low dead volume for precise determination of void volume of the fuel element. The puncture chamber, which can accommodate both MOX and PHWR type fuel pins, was designed with a very low internal volume. A contoured neoprene pad was provided at the fuel loading port of the chamber to ensure leak tightness. A tungsten carbide-tipped centre drill was used for puncturing the fuel pin. The puncture chamber was connected to the gas collection and analysis system by means of stainless steel tube through a hot cell service plug. The entire gas collection and analysis system was designed using 2 mm bore stainless steel tube to keep the overall system volume low. The vacuum system comprising of a rotary vane pump, capable of pumping down the system to a pressure of $1x10^{-1}$Torr was used.

Table 1. Irradiation Details of MOX Fuel Clusters

Cluster ID	Coolant temperature, °C	Coolant pressure, psi	Neutron flux, n/cm^2/sec		Pin ID	Average burnup, MWD/Te	Relative power Generation	Heat flux, W/cm^2
			Fast flux	Thermal flux				
AC-2	204	1,500	$5*10^{12}$	$5*10^{13}$	TP-1	16,265	1.18	93
					TP-2		1.15	
					TP-3		1.15	
					TP-4		1.15	
					TP-5		1.18	
AC-3	204	1,500	$5*10^{12}$	$5*10^{13}$	TP-6	16,000	1	110
					TP-7			
					TP-8			

A capacitance diaphragm gauge, with a measuring range of 0.1 to 1100 mbar was used to measure the gas pressure. The system was fitted with two calibrated measuring flasks of volumes of 251 cc and 501 cc. A dual column gas chromatograph (GC) with thermal conductivity detector was used for the measurement of released fission gas composition. Helium was used as carrier gas. A quadrupole mass spectrometer (QMS) was used for the estimation of isotopic composition of the gases.

4.2. Experimental

The schematic diagram of the fission gas analysis system is shown in Fig. 2. The surface of the fuel pins was cleaned thoroughly with emery paper and mild organic cleaning aids to get a leak tight contact between Neoprene pad of the puncture chamber and the fuel pin.

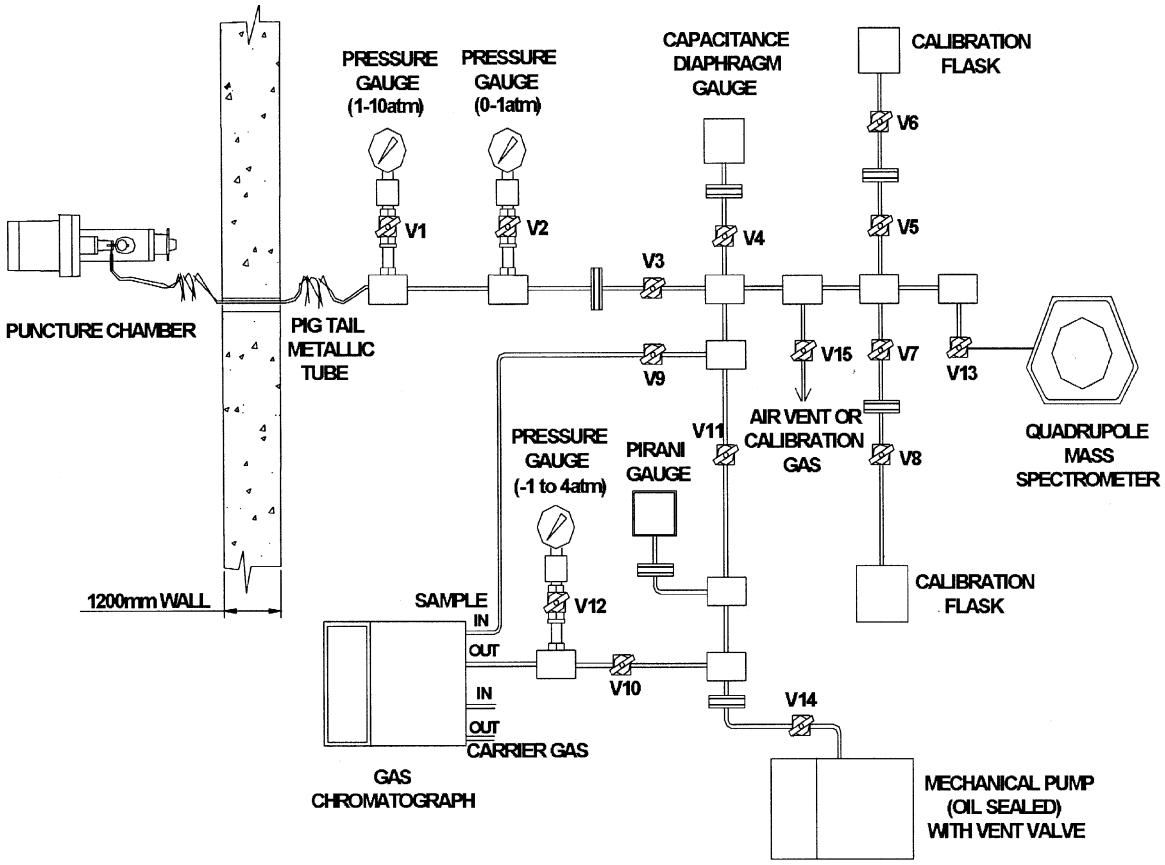

Fig. 2. Schematic diagram of fission gas collection & measuring system.

4.3. Estimation of System Volume

The fuel element was fitted to the puncture chamber and gently tightened against the neoprene pad. The system with the fuel element fixed in the puncture chamber was evacuated to a pressure of ~ 0.1 Torr. The exhaust of the rotary pump was fed to the hot-cell. All the shut-off valves except valves V10, V9 and V13 were kept open during this operation. Closing V5 and V7 valves the calibration flasks were isolated. The pressure (P_1) at which the flasks were isolated was noted from the capacitance diaphragm gauge. The system was isolated from the

rotary pump by shutting off the valve V11. Valve V14 was not used for isolating the system from the pump since the same pump was used to evacuate the injection port of the GC. The system was filled with air to a measured pressure (P_2) and expanded to one of the calibration flasks (volume V_1) at pressure P_1. The resultant system pressure P_3 is noted. Enough time was allowed for the stabilisation of the pressure during above operations. The system volume (V_2) was calculated using the relation:

$$V_2=V_1*(P_1-P_3)/(P_3-P_2) \qquad \text{----------(1)}$$

The experiment was repeated thrice to get concordant values.

4.4. Fission Gas Extraction

The fission gas analysis system including the calibration flasks was re evacuated to 0.1 Torr and isolated. The valve V11 was closed to isolate the system from the rotary pump. The drill on the puncture chamber was activated to puncture the fuel pin. The pressure reading on the capacitance diaphragm gauge was observed during the drilling operation. The puncturing of the fuel pin was indicated by the sudden surge in pressure on the gauge. On occasions when the gas pressure exceeded atmospheric pressure, one of the calibration flasks was connected to the system. The increase in pressure in the system due to the release of fission gas from the fuel pin, P_4, was noted. To minimise undesirable air leak to the system, the puncture chamber was isolated from the measuring system by closing the valve V3.

4.5. Gas Chromatograph

A 3-meter long dual column gas chromatograph packed with molecular sieve in ¼ inch OD stainless steel tube was used to estimate the composition of the released fission gas. Helium was used as the carrier gas. A thermal conductivity detector with tungsten-rhenium filaments was used for detection. The GC and the detector were switched on in advance for system stabilisation. Due to low volume and low pressure of fission gas, the conventional method of purging the GC loop with sample gas was not possible. Since the fission gas pressure on the collection system was sub-ambient, the GC loop had to be evacuated through the sample-loop outlet before admitting the gas through valve V10. The evacuation was ensured by the pressure reading on the gauge connected in the sample out-let path, ahead of valve V12. The valve V10 was closed after evacuation of the loop. The fission gas from the collection system was admitted into the injection loop by opening valve V9 of the sample inlet. The pressure of the gas to be injected to the GC was noted from the capacitance diaphragm gauge before injecting to the GC column. The peak areas were measured from the chromatogram.

4.6. Quadrupole Mass Spectrometer

A quadrupole mass spectrometer with a mass range of 1–300 amu was used for estimating the isotopic ratios of the fission gases. The gases were ionised using a gas tight tungsten ion source and detected using Channeltron/Faraday detector. By opening valve V13, the gas is admitted to the analyzing chamber of the QMS through a non-discriminating gas inlet capillary system. The isotopic ratios of xenon and krypton were estimated from the ionisation currents of the respective isotopes. The spectrometer was calibrated with xenon, krypton and helium gas mixture of known mass ratios.

4.7. Void Volume Estimation of the Punctured Fuel Element

With out disturbing the position of the fuel pin in the puncture chamber, the system volume was estimated as per the procedures described earlier in the section on estimation of system volume. The total system volume included the void volume of the punctured pin. The difference in the volumes in the two cases provides the void volume of the fuel pin.

This procedure of estimating the void volume was checked for repeatability and accuracy by puncturing a few calibration pins of the same geometry. The pins for calibrations had different void volumes and were filled with helium at different pressures. The pressure P_5 of gases inside the fuel pin at ambient temperature is calculated by:

$P_5 = (P_4 - P_0)$* (System volume+ Void volume)/Void volume ----------(2)

where P_0= System pressure before puncturing the fuel pin and
P_4= System pressure after puncturing the fuel pin.

4.8. Methodology used in Processing Gas Release Data

The quantity of fission gases Xe and Kr in the injected volume was estimated using the gas chromatograph output. The quantity of He in the chromatograph-loop was estimated by using ideal gas laws. The corrections to the system leaks were applied by accounting for oxygen and nitrogen peaks, observed in the chromatogram. The methodology of calculation followed for estimating the percentage of fission gas release is given in the Annex.

5. RESULTS

The summary of the results is given in Table 2. Total fission gas produced, percentage of fission gas released and the ratio of released xenon to krypton for each fuel pin are shown in the table. The average fuel pellet density of each pin and change in the void volume of each pin after irradiation are also given in the table.

5.1. Fission Gas Release Code Prediction

Two fuel-modeling codes are in active use at our research centre. The fuel modeling code GAPCON THERMAL-3 [2] is used by Reactor Engineering Division for fuel design and code PROFESS [3] is used by Post Irradiation Examination Division for analysis and interpretation of PIE data. Blind prediction of fission gas release by both the codes based on fuel design and irradiation parameters are given in Table 3 along with experimentally measured values for 5 MOX fuel elements of AC-2 cluster. As can be seen from the predicted values, both the codes over-predicted fission gas release. The codes also over- predict the fuel centre temperature. Since fuel temperature has a strong effect on fission gas release over prediction by the codes is explainable.

6. DISCUSSION

Fission gas release behaviour of standard enriched uranium fuels of Tarapur Atomic Power Station had been studied on 14 fuel elements in the burn up range of 3,200 to 24,000 MWD/Te [4]. The fission gas release ranged from 0.9% to 13.6%. Only one fuel element had fission gas release less than 1%. Nine fuel elements have release fraction ranging from 1 to 5% and the remaining 4 fuel elements had fission gas release in the range of 9 to 13.6%.

Table 2. Released Fission Gas Measured from Experimental MOX Fuel Pins

Cluster ID, burnup& heat flux	Pin No.	Average pellet density, % TD	Post irradiation change in void volume, %	Fission gas produced, cm^3 at STP	Fission gas released, cm^3 at STP	Internal gas pressure, Atmospheres (G)	Xenon to krypton ratio	Fission gas released, %
AC2 16,265 MWD/Te 93 W/cm^2	TU8	94.56	(-) 3.1	47.03	0	0.3	0	0
	TP1	96.27	(-) 20.12	296.18	0.36	0.61	14.44	0.12
	TP2	96.34	(-) 19.53	287.39	0.29	0.56	13.90	0.10
	TP3	94.32	(-) 18.33	282.57	0	0.65	0	0
	TP4	96.26	(-) 19.35	288.16	0.45	0.60	16.38	0.16
	TP5	96.20	(-) 12.47	296.08	1.09	0.58	12.70	0.37
AC3 16,000 MWD/Te 110 W/cm^2	TP6	95.92	(-) 12.1	245.79	20.59	7.37	13.92	8.38
	TP7	95.57	(-) 10.2	245.75	25.88	8.30	13.98	10.53
	TP8	95.81	(-) 17.0	285.84	22.55	7.97	13.93	9.17

(-) Negative sign indicates decrease in void volume

Table 3. Comparispon between Predicted and Released Fission Gas for AC-2

Pin No.	Post irradiation examination		PROFESS FG Model-3		GAPCON-THERMAL-3	
	Estimated centre temperature, °C	Fission gas release, %	Centre temperature, °C	Fission gas release, %	Centre temperature, °C	Fission gas release,%
TP-1	#	0.12	1642	2.1	1440	0.92
TP-2	#	0.10	1606	2.02	1325	1.10
TP-3	#	0	1608	1.77	1380	2.33
TP-4	< 1120	0.16	1586	1.75	1380	0.95
TP-5	< 1120	0.37	1674	2.56	1525	1.14

#Ceramography is awaited

Extension of burnup and additional loading of MOX fuel assemblies to the TAPS core require demonstration of fission gas release in MOX fuel in the same range as that of enriched UO_2 fuels. Fuels in the commercial Power reactors like TAPS showed strong correlation between heat rating and power ramp with the amount of fission gas release. Fuel pins with low heat rating maintained low level of release even at high burnup whereas higher release was observed in high rated fuel pins even at low burnup. Similar behaviour has also been experienced in experimental fuel pins of AC-2 and AC-3 clusters. These observations suggest that fuel centre line temperature is a major parameter in controlling fission gas release. Experiment conducted in Halden Reactor [5] puts 1% release as threshold for which an empirical relationship of centre line temperature and burn up has been derived purely based on experimental data. The correlation is remarkably successful in predicting fission gas release behaviour for a variety of fuel of different design and manufacture including MOX fuel. Using the Halden correlation for a burnup of 16,265 MWD/T, the threshold temperature for 1% release works out to be 1235°C. From the examination of autoradiographs of the fuel

cross section, the estimated centre temperature for AC-2 cluster is <1120°C, which is lower than the threshold and hence <1% fission gas release in the MOX fuel pins in AC-2 cluster is expected. The estimated fuel centre line temperature of AC-3 cluster is 1330°C, which is higher than the threshold temperature calculated from Halden correlation and therefore, higher fission gas release measured in the fuel pins in AC-3 cluster is not surprising.

MOX fuel elements in TAPS core will be operating at an average heat rating of about 90 W/cm^2 under normal operating condition. Hence <1% fission gas release is expected. Peak heat flux experienced by MOX fuel in TAPS will be ~110 W/cm^2 where the fission gas release 8–10% is expected. The fission gas release behaviour of MOX fuel is comparable with the gas release from the standard enriched UO_2 fuel pins in TAPS reactor.

Controlled porosity fuel pin TP-3 in AC-2 cluster, operating at heat rating of 90W/cm^2 has shown no release of fission gas. Further irradiation of fuel elements with pellets of similar characteristics to high burn up and at higher heat rating in the power reactor operating condition is needed to generate more data. Similarly, fuel pins with annular pellets in AC-4 cluster have shown no fission gas release in the exploratory irradiation at heat rating of 110 W/cm^2 to a burnup level of 2000 MWD/T. Irradiation to higher burn up levels in power reactor operating condition is being planned to generate in reactor data.

7. CONCLUSIONS

(1) Less than 1% fission gas release was observed in UO_2-4%PuO_2 MOX fuel irradiated with 93 W/cm^2 heat flux at a burn up of ~16,000 MWD/T.

(2) Fission gas release of the order of 8 –10% was noticed in UO_2-4%PuO_2 MOX fuel elements operated at peak heat flux of 110 W/cm^2 at a burn up of ~16,000 MWD/Te.

(3) Fuel pins with controlled porosity pellets operated at the heat flux 93 W/cm^2 showed no fission gas release up to a burn up of ~16,000 MWD/T.

(4) Annular pellets operating at 110 W/cm^2 showed no fission gas release.

(5) Combination of annular fuel pellet design with controlled porosity appears to provide the best promise of achieving high burn up with low fission gas release.

REFERENCES

[1] P. R. ROY et al, Fabrication of MOX fuel element clusters for irradiation in PWL, CIRUS, BARC, Report-1203, 1983.

[2] V. V. VAZE et al, Fuel Performance Modeling of PWL Pins, Internal Note RED/FES/01/2001.

[3] D. N. SAH et al, Proc. of IAEA Specialists meeting on Water Reactor Fuel Element Performance Computer Modeling, IAEA Report T, IWGFPT/19, IAEA, Vienna, p.237. 1986.

[4] S. CHATTERJEE et al, Fission Gas Release Measurements of TAPS Operated Fuel Elements, Proc. Symposium PIENUP, BARC, Mumbai, p.203–211, 1989.

[5] J. A. TURNBULL et al, Investigations on Radioactive and Stable Fission Gas Release Behaviour at the Halden Reactor, Proc. of International Seminar on Fission Gas Behaviour in Water Reactor Fuels, Cadarache, France, September 2000.

ANNEX

Total no. of moles of gases present in the injection loop **N=PV/RT** ------(1)
where P is the pressure at which the gas is injected in Torr, V is the loop volume in litres, R is the gas constant (62362 lit.atm), T is the temperature of the sample loop in º K.
No. of moles of He in the injection loop $\mathbf{n_{He}=N-(n_{Xe}+n_{Kr}+n_{O2}+n_{N2})}$ -------(2)
where $n_{Xe,}$ n_{Kr}, n_{O2} and n_{N2} are the no. of moles of respective gases which can be estimated from the calibration curves of peak area v/s no. of moles of respective gases which have been already generated at identical detector parameters of the GC.

Since the internal pressure of the fuel pin, $P_5= P_{He}+ P_{Xe}+P_{Kr}$, partial pressure of each component gas can be estimated from the mole fraction of the gases as follows:

$$\mathbf{P_{He}= P_5 * n_{He}/(n_{He}+ n_{Xe}+n_{Kr})} \quad \text{----------(3)}$$

$$\mathbf{P_{Xe}= P_5 * n_{Xe}/(n_{He}+ n_{Xe}+n_{Kr})} \quad \text{----------(4)}$$

$$\mathbf{P_{Kr}= P_5 * n_{Kr}/(n_{He}+ n_{Xe}+n_{Kr})}. \quad \text{----------(5)}$$

Internal pressure due to fission gases Xe and Kr alone can be estimated from:

$$\mathbf{P_{f.g}=P_{Xe}+P_{Kr}} \quad \text{----------(6)}$$

Considering production of 31 cc of fission gas per kg of fuel per MWD burnup[1], the quantity of fission gases generated in the fuel, $V_{f.g}$, was estimated using the equation:

$$\mathbf{V_{f.g} = 31*W*B} \quad \text{----------(8)}$$

where $V_{f.g}$ = volume in cc at STP of fission gases generated in the fuel
W = weight of the fuel in kg and
B = fuel element burn-up in GWD/T of UO_2.

The volume at STP of fission gases released was estimated from:

$$\mathbf{V_r = Void\ volume * P_{f.g} * (273/300)/P_a} \quad \text{----------(9)}$$

Where V_r= volume of fission gases in cc at STP present inside the fuel element
$P_{f.g}$ = internal pressure due to fission gases and
P_a = atmospheric pressure
300= temperature of the hot cells, in K

$$\mathbf{\%\ released\ fission\ gases = V_r * 100 / V_{f.g}} \quad \text{----------(10)}$$

[1] Fission Gas Release and Temperature Data From Instrumented High Burnup LWR Fuel, T. Tverberg et al, Technical Committee Meeting on Economics Limits to Fuel Burnup Extension, San Carlos de Bariloche, Argentina, Nov.15–19, 1999.

Application of scanning electron microscopy and X ray microanalysis for investigating pins of the world's first nuclear power plant

S.N. Ivanov, A.M. Dvoriashin, S.V. Shulepin, S.I. Porollo, V.V. Velichko

SSC RF Institute of Physics & Power Engineering (IPPE),
Obninsk, Kaluga Region, Russian Federation

Abstract. Results of the fuel pin cladding investigation by methods of scanning electron microscopy and X ray microanalysis are presented. Failed pins of the World's First Nuclear Power Plant (Obninsk) as well as tight-leak pins of this reactor after a long term dry storage have been investigated. It was established that the pin failure under irradiation occured due to formation of transgranular brittle cracks and due to corrosion attack at the outer fuel pin cladding surface contacted with gas environment in the reactor. Chlorine was detected on the fuel pin outer surface, the maximum chlorine concentration was observed in defects (cracks and pits) of outer pin cladding. After long term storage of pins for 38 years only an insignificant corrosion damage up to depths of 10 μm on cladding surfaces contacting to air environment have been observed.

1. INTRODUCTION

During more than 46 yr period of the World's First Nuclear Power Plant operation about 1500 subassemblies (S/A) with annular pins with nuclear fuel of the dispersion type have been irradiated in the reactor core. As a whole, the choice of the pin and S/A design and also the selection of fuel and structural materials has allowed to ensure a reliable reactor operation. Nevertheless, in the course of irradiation a number of the leak-tightness losses and pin failures have been occured. In order to determine the mode of pin failure the following methods have been used: the visual examination of outer pin surfaces, measuring the pin diameter, metallography of cladding and fuel materials, and also mechanical tests of cladding materials.

To carry out of a more detailed examination of the pin cladding, to investigate the pin failure mode, and also to determinate the origin of corrosion damage, the methods of scanning electron microscopy and X ray microanalysis have been used in the present work.

2. SUBASSEMBLY DESIGN AND IRRADIATION CONDITIONS

Subassemblies of the World's First Nuclear Power Plant reactor consist of jointed together graphite sleeves of 65 mm in diameter and 150 mm in length having a central cylindrical hole for placement of the steel tube of 15 mm diameter, the latter serves for water supply to the bottom head of S/A /1/. In addition, there are four cylindrical holes located symmetrically at the distance of 20 mm from the sleeve axis for placement of annular pins.

Fuel pins have two cylindrical claddings made from the type 1X18H9T stainless steel between which the dispersion fuel composition is situated. The diameter and wall thickness of the outer pin cladding are equal to 14,0 mm and 0,2 mm, respectively, these values for the inside pin cladding are equal to 9,0 mm and 0,4 mm, respectively. Powders of U-9% Mo alloy or UO_2 dispersed in a magnesium matrix were used as a nuclear fuel in the pins investigated. The fuel column length was equal to 1700 mm, the total pin length equals 1885 mm. Characteristics of the investigated S/A are shown in Table 1.

Table 1. Characteristics of investigated subassemblies

S/A #	Fuel type	Operation period	Operation time, eff. power day	Mean burnup, MW×day/kgU	Neutron fluence, E>0,18 MeV, 10^{24} n/m^2	Number of failured pins
G-42	UO_2	08.84-08.87	197,1	13,74	1,9	1
G-52	UO_2	10.84-08.87	154,7	14,90	1,5	1*
G-72	UO_2	02.86-08.87	56,4	5,39	0,06	1*
010208	UO_2	07.93-04.98	308	28,3	4,5	4
AMK-248	U-9%Mo	05.55-01.58	309	17,6	1,45	0

Note:
* - in the S/A # G-52 and S/A # G-72 was investigated only one pin from four.

Under neutron irradiation the fuel pins were cooled by water under pressure of 10 MPa, flowing into bottom heads of S/A and running through the inner pin cladding. The exterior surface of outside pin claddings was in the nitrogen environment of graphite channels.

The input water coolant temperature was equal to 150–190°C and the outlet coolant temperature reached 210–280°C. The maximum temperature of outside pin claddings was at the core mid-plane and did not exceed 280–310°C.

In order to elucidate the cause of pin failure subassemblies with failed pins were investigated just after irradiation. In addition, pins from the subassembly # AMK-248 have been investigated after 38 year dry storage. After irradiation this subassembly was reassembled, the pins were placed in a metal wrapper and then stored in a leak-tight container in the air environment.

3. EXPERIMENTAL PROCEDURE

3.1 Scanning electronic microscopy

Samples for the scanning electronic microscopy were prepared as follows. On a remote machine fuel pin fragments of 3,5 mm in height were cut. After etching the fuel composition in the 30% solution of nitrogen acid, two rings of both the interior and exterior claddings were obtained. Then the rings were cuts into segments of about 4 mm length.

For cleaning cladding surfaces and removal of deposites all samples were boiled in the 50% water solution of nitrogen acid for one hour. Final cleaning was carried out in ethanol.

The examination of fuel pin cladding surfaces and the study of cladding fracture character were performed using a scanning attachment ASID-4D of the electron microscope JEM-100CX at magnifications ranging from 200 up to 5000.

The local chemical composition of materials was determined using X ray "Kevex" energy dispersion spectrometer

3.2. X ray microanalysis

An examination of the chemical composition and distribution of fission and corrosion products on cladding surfaces was made using a “CAMEBAX – R” electron probe analyzer. The analyzer allows to image pin cladding surfaces under different magnifications from

100 up to 1000 in absorbed, back-scattered and secondary electrons which originate due to interaction between the primary electron beam of 1–2 μm in diameter and sample material. The chemical composition of a material is determined by X ray characteristic emission excited in the sample. The radiation is detected by the "Kevex" energy dispersion spectrometer and a wave dispersion spectrometer with a set of crystals of different lattice parameters. Chemical elements beginning from B and ending Ge are analyzed by K-radiation in the wave length range of 6.76 nm to 0,125 nm. The chemical elements from Cl to U are detected by L- and M-radiation series. The detector angles are chosen in accordance with the Wolf-Brag's law.

Gas flowing proportional counters were used for detecting the X ray radiation. Examinations were carried out at the accelerating voltage of 10–30 kV and at the primary electron beam current ranging from 100 nA to 1 mA. The sensitivity of the analysis depends on a chemical element and in average equals 0.1 %. The accuracy of the quantitative analysis is in limits ± 2–5 %.
Fuel pin cladding samples of ~4 mm×10 mm size were used for the investigation. The samples were cut from damaged parts of claddings. Outer cladding surfaces as well as surfaces of polished cladding cross sections were examined.

4. RESULTS

4.1. Scanning electron microscopy examination of failed fuel pins

Cladding surfaces of failed fuel pins from the subassemblies #G-72 and #010208 and the pin fracture mode were investigated by methods of the scanning electron microscopy.

Strong etching of grain boundaries and pitting corrosion were observed on the outer surface of the outside cladding under examination of a sample from the pin failure zone (at the distance of 250 mm from the pin top) in the S/A #G-72. In addition, several pits of 50 microns in diameter were observed. Inside of the pits the cladding material has undergone a local intergranular cracking. Some pits were filled with crumble deposits (Fig. 1a). By microanalysis it was established that inside these pits together with basic cladding steel components such chemical elements as chlorine, calcium and silicon are present, these elements were not detected on the cladding surface beyond the pits (Fig. 1 b). Far from the pin failure zone (300 mm from the pin bottom) etching of grain boundaries and pitting corrosion were observed in some grains (Fig. 2).

On the outer surface of a sample from the fractured zone in the pin from the subassembly # 010208 (20 mm from the pin bottom) a severe corrosion attack was observed. As a result of this attack etching of grain boundaries, the formation of small pits (up to 10 microns in diameter), large pits (up to 100 microns in diameter) and longitudinal intergranular cracks of more than 100 μm in length occured (Fig. 3). In some large pits aluminum was detected together with steel components.

The fractographic study of a sample from the failure zone in S/A #010208 revealed that the fracture surface of the outside pin cladding consists of two characteristic zones: narrow (of 50 micron in width) and dark zone, located on the exterior cladding side, and wide and light zone, located on the inner cladding side(fig. 4 a). The dark zone is that part of the cladding which has undergone of a severe corrosion. In the light zone of the fracture surface no

corrosion attack was observed. Most probably, this surface was formed during handling the sample (Fig. 4 b). Fractographic examination of the through crack in the cladding of a pin from S/A # G-72 has shown that the fracture surface consists of flat transgranular facets (Fig. 4 c, d). On the inner cladding side the dimple structure of fracture surface is observed that is characteristic of ductile fracture.

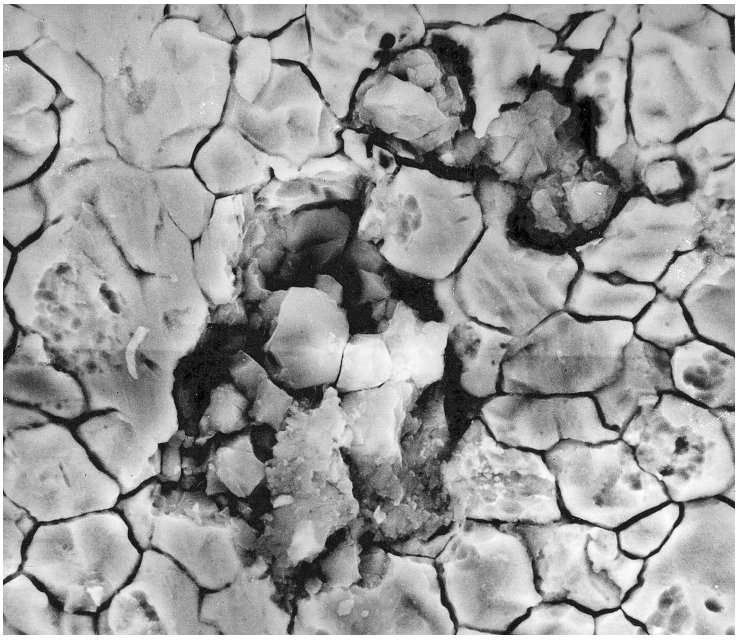

(a) X100

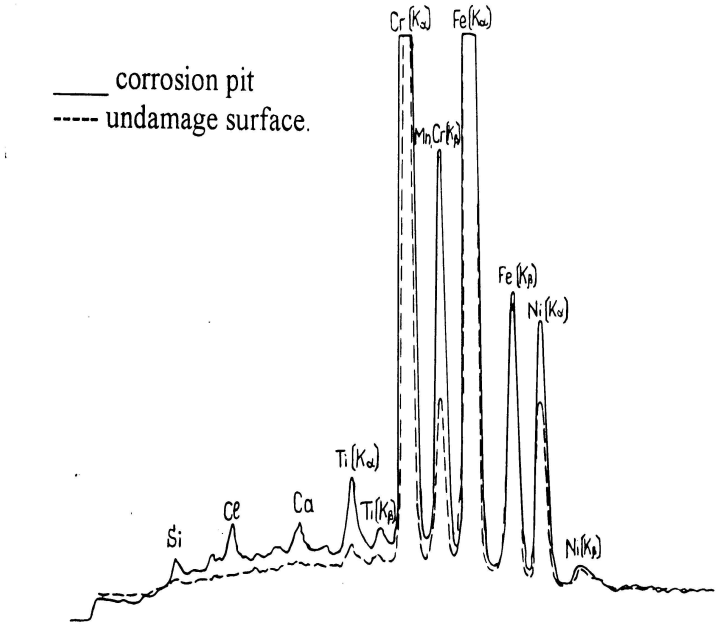

(b)

FIG. 1. Pitting corrosion at the outside surface of outer pin cladding in the fracture zone at the distance of 250 mm from the pin top (a) and X ray spectrum for a corrosion pit and for a neighboring area of the pin cladding surface (b).

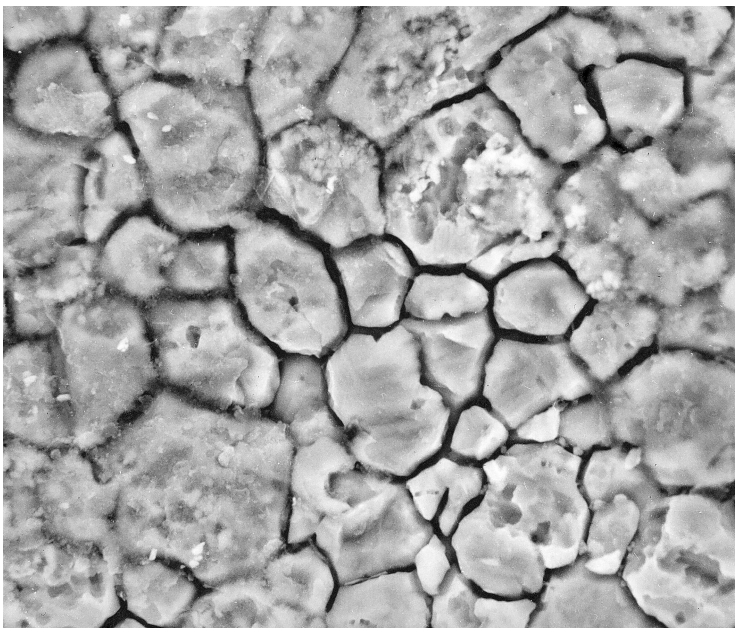

× 1000

FIG. 2. Fragment of the outer surface of the outside pin cladding (S/A # G-72) located at distance of 300 mm from the pin bottom (far from the failure zone).

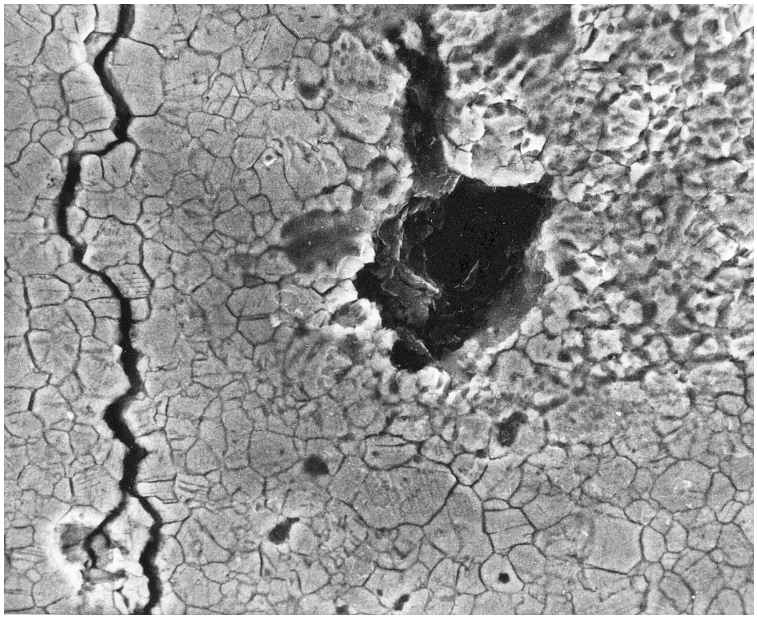

× 500

FIG. 3. Corrosion of the outer surface of outside pin cladding (S/A # 010208) in the fracture zone at the distance of 20 mm from the pin bottom.

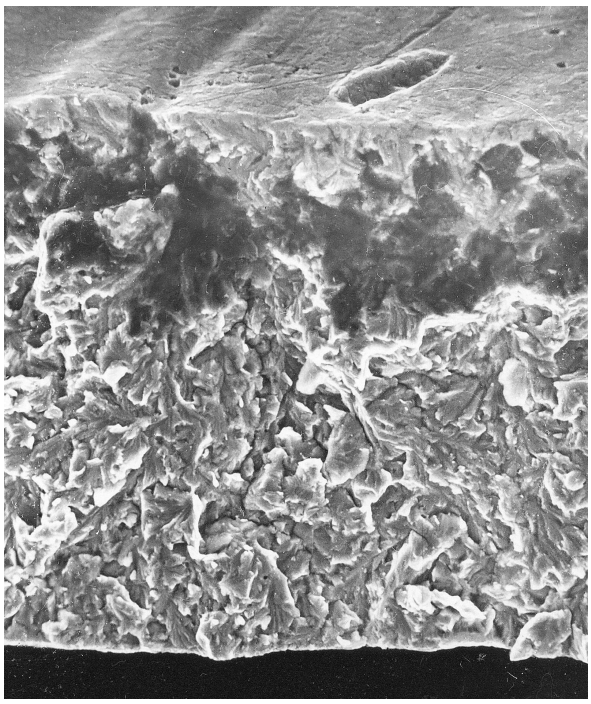

(a) ×500

(b) ×500

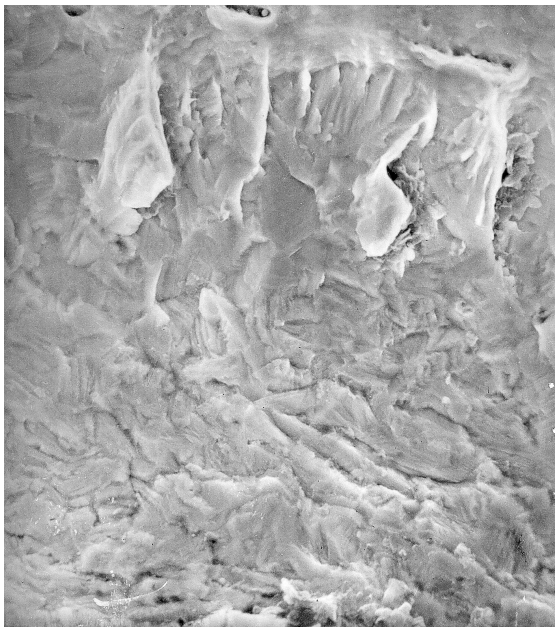

(c) ×500

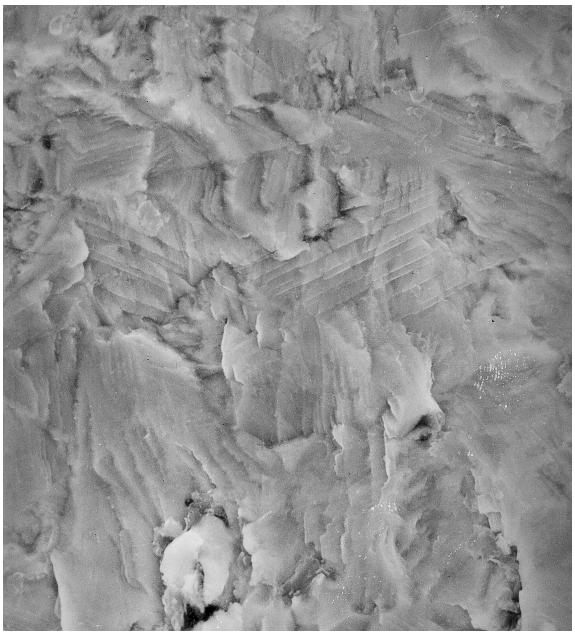

(d) ×1000

FIG. 4. Fracture mode of the outside pin cladding of S/A # 010208 at the distance of 20 mm from the pin bottom (a, b) and the outerside pin cladding of S/A # G-72 at the distance of 250 mm from the pin top (c, d).

4.2. X ray microanalysis of the pin cladding

The X ray microanalysis was conducted for cladding samples from pins of three subassemblies #G-42 (for the cross section at 110 mm from the pin bottom), #G-52 (for the cross section at 310 mm from the pin top) and # 010208 (for the cross section at 30 mm from the pin bottom), cut out from a pin fracture zone. The analysis included a detection of the presence of chemical elements (with atomic numbers above 8) in a given point of samples,

and also measuring the profiles of chemical element concentration over both the sample surfaces and pin cladding cross section surfaces.

The microanalysis of the cladding surface of a pin from the S/A # G-42 has revealed the traces of chlorine, magnesium, calcium and silicon on its exterior surface. Scannogramm obtained for the sample surface gave evidence on a non-uniform distribution of chlorine over the sample surface (Fig. 5a), the maximum chlorine concentration was detected in corrosion pits (Fig. 5b). Also, chlorine was detected on the surfaces of pin cladding cross sections in the corrosion zones (Fig. 5c).

On the cross section cladding surface of the pins from the S/A # G-52 through cracks were observed. On the crack surfaces an elevated chlorine concentration is detected as it can be seen from the curve of chlorine distribution across a crack (Fig. 5 d).

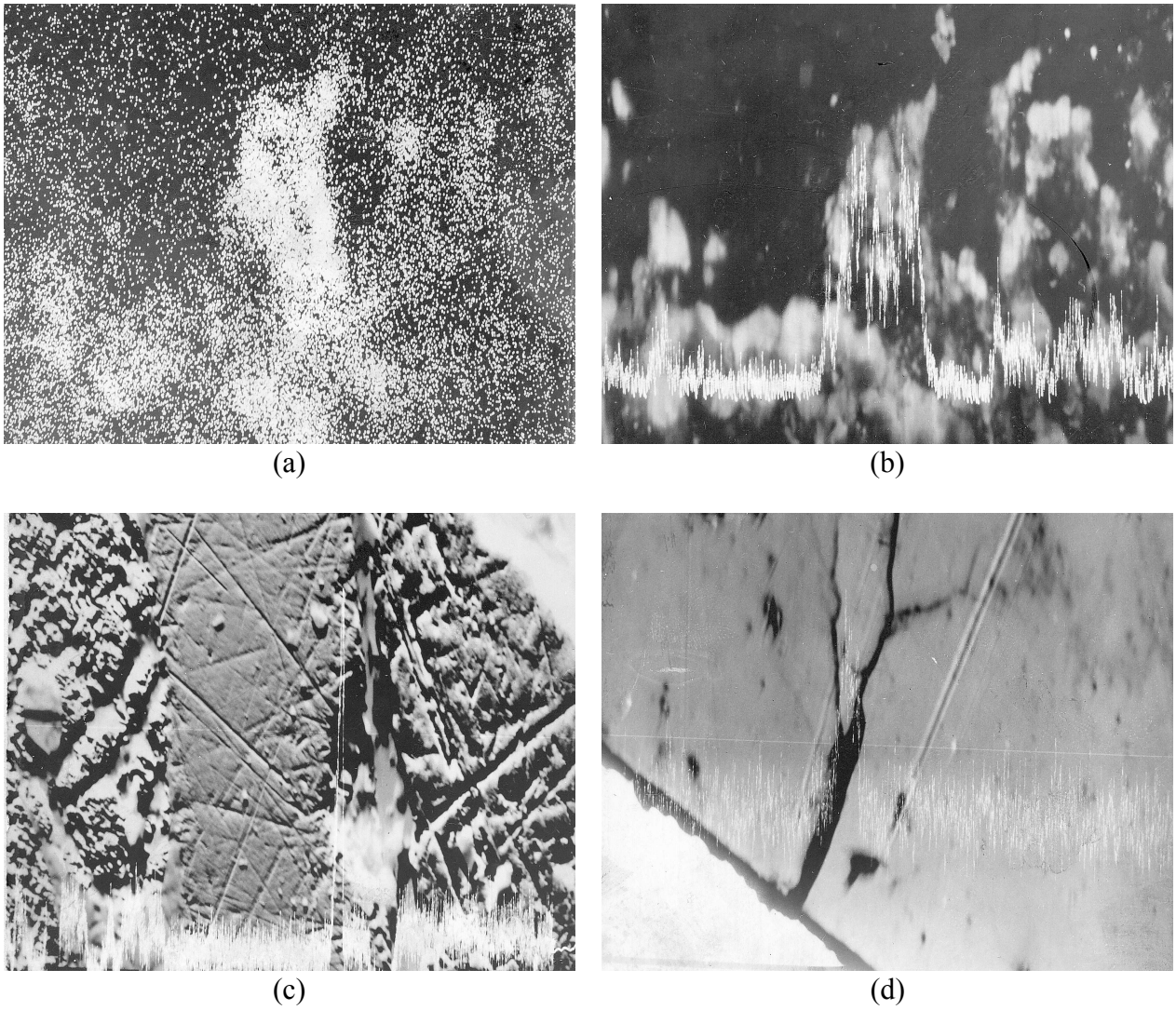

(a) (b)

(c) (d)

FIG. 5. X ray and back-scattering electron images of fuel pin cladding in the fracture zone.
a) X ray (Cl, K_α) outer surface image of the pin from S/A # G-42 at the distance of 110 mm from the pin bottom, ×400;
b) Cl content distribution on the outer surface of the pin from S/A # G-42, ×400;
c) Cl content distribution in the cladding cross-section (S/A # G-42) for a corrosion zone, ×150;
d) Cl content distribution in the cladding cross-section (S/A # G-42) across the crack at the distance of 310 mm from the pin top, ×600.

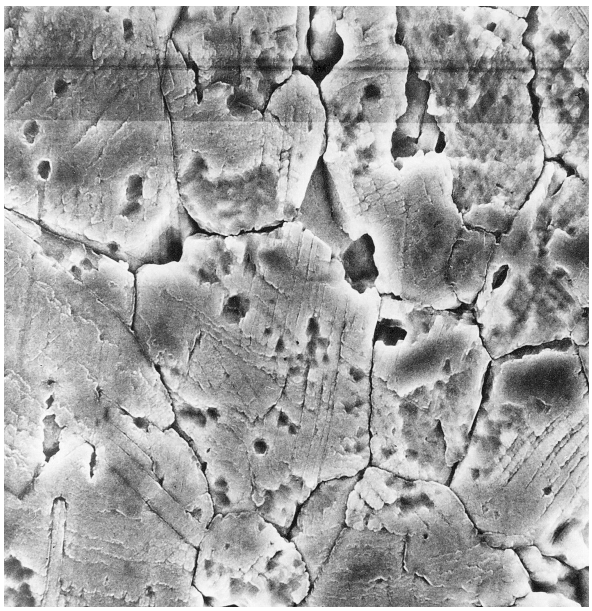

(a) × 5000

(b) × 5000

(c) × 5000

(d) × 5000

FIG. 6. Corrosion damage on surfaces of fuel pins from S/A AMK-248 after a long term storage (at the distance of 700 mm from the pin bottom):
a) general view of the outer surface of an outside pin cladding;
b) typical corrosion damage of the outer surface of the outside pin cladding;
c) typical corrosion damage (crumbled grain and pits) of the inner surface of the inner pin cladding;
d) small pits at the inner surface of outside pin cladding (from the fuel side).

Thus, the examination of samples from failure zones of pin cladding in pits, cracks and other defects on the outer surface of outside cladding revealed an elevated chlorine content as compared with surface area free of such defects. It is known /2 / that chlorine is the most aggressive chemical element in the pitting corrosion of steels. At tension stresses applied this chemical element induces the chlorine stress corrosion cracking, the cracks are of brittle intergranular character.

4.3. Examination of irradiated pin cladding after a long term storage

With the objective to determine an extent of the corrosion damage in steel cladding the interior and exterior surfaces of both outside and inner claddings of fuel pins from the subassembly #AMK-248 have been examined after a long term dry storage using the scanning electron microscopy and X ray microanalysis.

The condition of the surfaces of both outside and inner claddings which were in contact with air during long term storage has appeared to be same. The surfaces have undergone to insignificant corrosion damage (to depths less than 10 μm) in the form of etched grain boundaries, shallow pits of 0,5–2,0 μm in diameter and single crumbled grains (Fig. 6 a–c). It should be noted that the corrosion is more pronounced for the inner cladding in comparison with outside one. Probably, this fact may be related to the contact of the inner cladding with water coolant under neutron irradiation.

On surfaces of pin claddings which were in a contact with fuel only traces of the corrosion damage were detected in the form of etched grain boundaries, twins, a few number of pits with diameter up to 0.5 μm and single shallow pits of up to 15 μm in diameter (Fig. 6 d). The depth of corrosion damage in cladding from the fuel side does not exceed 1μm.

5. CONCLUSIONS

The loss of leak-tightness of fuel pins irradiated in the World's First Nuclear Power Plant occured as a result of the through fracture of outside pin claddings. The fracture happened due to the formation of intergranular brittle cracks and due to the corrosion damage in the form of shallow and deep pits. In the failure zone the presence of chlorine was detected on the outer surface of outside claddings, the maximum chlorine concentration was observed in defects of cladding (in cracks and pits). Chlorine caused the outside pin cladding failure by mechanisms of the chlorine-induced stress corrosion cracking or pitting corrosion.

The long term (38 years) dry storage of irradiated leak-tight pins didn't result in an essential pin cladding corrosion damage. On cladding surfaces which were in contact with air only small corrosion defects of up to 10 μm in depth were observed. The depth of corrosion damage in the cladding from the fuel side does not exceed 1μm. Chemical elements capable to evoke the corrosion of fuel pins during storage were not detected on cladding surfaces.

REFERENCES

[1] USHAKOV G.N. "The First Atomic Power Plant (Experience of Construction and Operation)", Moscow, Saint-Petersburg, Gosudarstvennoe energeticheskoe izdatelstvo, 1959, 17–19.

[2] SOKOL I.YA., ULYANOV E.A., FELDGANDLER E.G. et al. "Structure and Corrosion of Metals and Alloys: Atlas. Reference Book" Moscow, Metallurgy, 1989, 72.

SPECIAL METHODS AND TECHNIQUES FOR FUEL AND CLADDING MATERIAL EXAMINATION
(Session 5)

Chairpersons

H.K. JENSSEN
Norway

A. BYKOV
Russian Federation

In-pile cladding tests at NRI Rez and PIE capabilities and experience

M. Zmítko

Nuclear Research Institute Rez plc, Czech Republic

Abstract. In-pile cladding corrosion test facilities and relevant post-irradiation capabilities at NRI Rez plc are overviewed. Basic information about the research rector LVR-15 and in-pile water loops is given. An experience in the field of Zr-alloy cladding corrosion testing and investigation of cladding corrosion behaviour is demonstrated for two experimental programmes conducted at NRI Rez in the past period. The first example describes results obtained at studying of corrosion behaviour of advanced Zr-alloys under PWR conditions with a special concern to a high lithium content and subcooled surface boiling. The second example informs about completion of the experimental programme supported by the IAEA which is focused on investigation of Zircaloy-4 cladding behaviour under VVER water chemisty, thermal-hydraulic and irradiation conditions with the main to obtain experimental data for an assessment of the Zircaloy-4 cladding compatibility with VVER conditions.

1. INTRODUCTION

In-pile loop experiments and material testing in the research reactor LVR-15 belong to the main activities of Reactor services division in Nuclear Research Institute Rez plc (NRI). An investigation of a simultaneous effect of irradiation, water chemistry and high parameters (pressure, temperature) on behaviour of nuclear power plants structural materials and components is the main goal of the conducted experimental programes. Irradiation projects focused on investigation of fuel rods cladding materials behaviour, water chemistry aspects of radionuclides transport and irradiation effect on structural material corrosion including irradiation assissted stress corrosion cracking (IASCC) are carried out for domestic and foreign customers.

2. EXPERIMENTAL FACILITIES

2.1. Reactor LVR-15

Research reactor LVR-15 operated at NRI Rez is a light water cooled and moderated tank reactor with forced circulation of the coolant. The reactor has combined water-berylium reflector. The reactor core is composed of IRT-2M type fuel assemblies made in Russia with 36% enrichment of ^{235}U which is in a form of UO_2 dispersed in Al matrix. Maximum thermal power of the reactor is 10 MW(th). It operates at atmospheric pressure with maximum coolant core output temperature 45°C. he nominal coolant flow throught the core is 2,100 m^3/hour. The reactor core grid has a pitch of 71.5 mm and 80 cells. In the basic operation configuration, 28–34 cells contain fuel elements, 2–4 of the fuel cells (depends on requirements) are dedicated for channels of experimental irradiation facilities. The reactor core is situated in the reactor vessel (outer diameter 2,300 mm, total height of the vessel 6,235 mm), which is made of stainless steel, the internal parts of the reactor are made of an aluminium alloy. A schematic layout of the LVR-15 reactor is shown in Fig. 1. The reactor

coolant is light demineralised water. Maximum fast (>0.1 MeV) and thermal neutron flux in the core is 3×10^{14} and 1.5×10^{14} n/cm^2.s, respectively. Usual mode of the reactor operation is 3 weeks of operation, 1 week shutdown for refuelling and mantenance. Typically, the reactor is operated for 180–210 EFPD per year.

2.2. Reactor water loops

At present five loops are used to perform a various tests in-core that are focused on study of structure materials behaviour under typical thermal-hydraulic, water chemistry and irradiation conditions of LWRs. Parameters and type of water chemistry are presented in Table 1.

Table 1: High pressure loop parametrs

Loop	Water chemistry	Max. temperature (°C)	Pressure (MPa)	Flow rate (t/h)
RVS-3	VVER/PWR	345	16.5	3-10
BWR-1	BWR	300	10	2
BWR-2	BWR	300	12	8
ZINC	PWR	320	15.5	0.8-1
RVS-4	VVER	322	15.7	2

In general, the reactor water loops are closed stainless steel (SS 321 is used) piping systems with forced circulation of the coolant where one part of the loop — an irradiation channel — is situated in the core of LVR-15 reactor. The loops main components and systems are as follows:

- a main circulation pump,
- an electrical heater and heat exchangers,
- a pressurizer and a volume compensator,
- a make-up water system (chemical additives dosing),
- a purification system (ion-exchange and mechanical filters),
- a coolant sampling system (isokinetic sampling),
- cooling systems,
- auxilliary systems (eg. H_2/O_2 gas injection system, on-line dissolved gases measurement).

A special electrically heated fuel rod immitators has been designed to model heat flux on the cladding surfaces. The heating rod has total length 5100 mm, heated region is 560 mm. Heating wires are made from Ni-Cr alloy, leading wires are from Cu-Cr alloy. Boron nitride is used as an insulation material. Input and output wires are situated at the top of the heating rod. The rod is covered by stainless steel or Inconel sheath and is inserted into the investigated Zr cladding tube.

2.3. Measurement techniques and post-irradiation examination possibilities

NRI Rez has the following measurement techniques and post-irradiation examination (PIE) capabilities in connection with the fuel cladding materials testing:

Non-destructive measurements:
- a visual examination in hot cell; videocamera with recorder,
- a Zr-oxide thickness measurement by eddy current (EC) technique (a Fischerscope device linked with a x-y-z mechanical support; Mylar foils used for calibration),
- a possibility of Zr-oxide intermediate measurement at the reactor or loop shutdowns (test bundle transportation into the hot cell),

Post-irradiation examinations:
- a Zr-oxide thickness and morphology (by optical microscopy — OM and SEM),
- a Zr-oxide microstructure, hydrides distribution and orientation (by SEM and TEM techniques),
- an identification of t-ZrO_2 and m-ZrO_2 fraction in the oxide film (by Raman spectroscopy),
- a hydrogen pick-up measurement (by an extraction method),
- mechanical properties (eg. stress-strain characteristics, cladding ductility)
- an elemental and phase composition of deposited crud (by EDX, Mössbauer spectroscopy - MöS, Infrared spectroscopy - IRS, X ray diffraction - XRD).

In addition, various measurement techniques are employed to idetify and analyse corrosion products (crud) and other impurities in the loop coolant (eg. ion-chromatography, ICP-MS, AAS, microfilters).

3. CLADDING CORROSION TESTS

Till now, the following Zr-cladding corrosion tests were performed at NRI facilities:

I. Testing of new advanced Zr-alloys corrosion behaviour under PWR conditions,
II. Demonstration of Zircaloy-4 cladding compatibility with VVER primary water chemistry conditions.

3.1. Test I: Advanced Zr-alloys under PWR conditions

An experimental programme was conducted at a reactor water loop RVS-3 with the intention to study corrosion behaviour of Zr cladding materials under PWR water chemistry with a high lithium content (5 ppm Li) and subcooled boiling conditions. Technological layout of the RVS-3 loop is shown in Fig. 2.

A test section consisting of four eletrically heated fuel rod immitators was situated in a field tube of the RVS-3 loop active channel located in the core of the reactor. A heated part of the fuel rod immitator matched the reactor core height. The RVS-3 loop was operated at pressure 15 MPa (relevant saturation temperature 342°C). The primary coolant flow rate was 3.85 tons/hr what meant a flow velocity of 2.6 m/s at the test section outlet. Heat flux on the cladding surface was achieved by insertion of a specially designed electrically heated rod into the cladding tube. Total length of the rod was 5,100 mm with a 560 mm long heated part (section) at the rod bottom. Such design allowed to achieve heat flux of 100 W/cm^2 on the outer cladding surface in the heated section. Inlet and outlet coolant temperatures in the heated section were kept 325°C and 335°C, respectively. Thermal-hydraulic parameters of the experiment were chosen so that the upper region of heated section worked at subcooled boiling conditions, ie. cladding surface temperature achieved and slightly exceeded a saturation temperature at a given pressure. Calculated void fraction at the heated section outlet was about 6%. Water chemistry parameters were chosen in aim to study the influence of a

high lithium concentration on Zr cladding behaviour — 5 ppm Li and 650 ppm B was maintained during the experiment. Dissolved hydrogen was kept in concentration range of 20–25 ccSTP/kg. Oxygen concentration was below 5 ppb (by Orbisphere analyser on-line measurement).

An intermediate investigation of the cladding materials — a measurement of Zr oxide thickness by eddy current technique — was foreseen after each irradiation cycle, ie. after 21 days of the reactor operation. After completion of the first irradiation cycle, some deposits were observed on the cladding surface what led to misreading of the eddy current signal (lift-off the signal) at the Zr oxide thickness measurements. The situation was improved and more realistic oxide thickness values were measured after brushing of deposits from the cladding surface. An effect of crud deposits on EC measurement is evident from Fig. 3. A number of analysis and investigations was then performed to identify a nature and characteristics of the deposits on the cladding surface and a quality of the loop primary coolant.
Crud deposits on the Zr cladding surface were observed mainly on the heated part of the fuel rod immitator. Visual inspection showed that in the bottom region of the heated part only a black, easy removable, loose deposit was found. In the upper region, where subcooled boiling area was expected, a black heavy deposit with some "white" spots was found. More detailed investigation showed that the "white" spots are places where the deposits were spalled from the cladding surface. A SEM picture of the spalled oxide is shown in Fig. 4. A "chimney" structure observed on this deposit is related to the boiling phenomena. Another SEM pictures shows that the deposits consist of fine particles with diameter of 1–5 μm. TEM pictures reveal octahedral crystals of magnetite and some amorphous particles.

Elemental composition of the deposits on the cladding surface was analysed by EDAX technique. Summary of the EDAX results and their comparison with the base material composition is given in Table 2. It is clear from the results that the deposits are enriched with chromium and depleted in nickel in comparison with the base material. Elemental composition of the loose and heavy deposits is almost the same taking into account a limited number of analysis and precision of the method. Silica presence was also identified in some samples. MöS identifies non-stoichiometric magnetite Fe_3O_4 with some presence of normal spinel of $Fe_xCr_{3-x}O_4$ or $Fe_xCr_{2-x}(Ni)O_4$ type. IRS reveals non-stoichiometric spinel $Fe_{3-x}Cr_xO_4$ ($x < 1$) with a possible presence of Ni. Some small amount of lithium (only 0.022 mg) was also detected by AAS in the deposits what means that Li/Fe ratio is very low – about 10^{-3}. Three phases were revealed by XRD: a spinel ferrite, the most likely Ni-substituted magnetite, ZrO_2, and chromic hydroxide. Unlike the ferrite and ZrO_2, chromic hydroxide occurs very rarely in "normal" corrosion products.

A reason for the crud deposit formation on Zr cladding surface has not been fully identified and understood, but it is obvious that this process relates to a quality of the loop primary coolant, and local thermal-hydraulic conditions; especially by subcooled boiling. It is also obvious that the presence of corrosion products in the deposits (Fe, Cr, Ni-species) can be affected by a corrosion behaviour of the loop itself.

It was confirmed at this experiment that the EC measurement technique is significantly affected by a presence of corrosion product deposits. The presence of deposits on the cladding surface can influence on electro-magnetic properties of the Zr-oxide layer what means that a calibration procedure performed without presence of deposits is not relevant to such situation. As a consequence of this, the EC measured values are incorrect and do not represent the real picture.

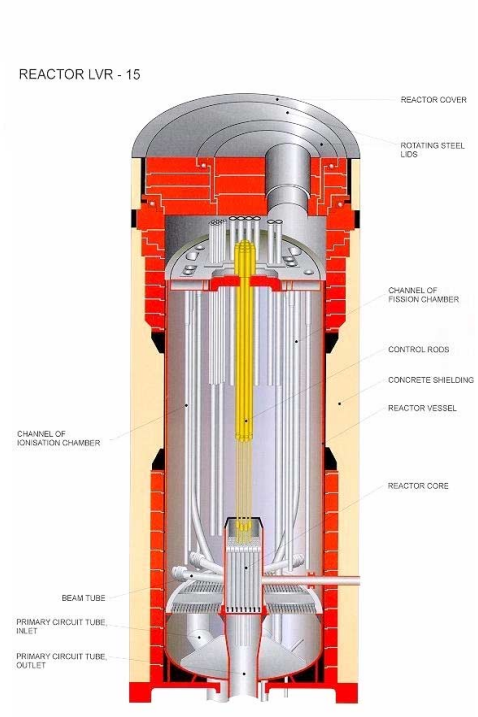

Figure 1: Schematic layout of LVR-15 research reactor

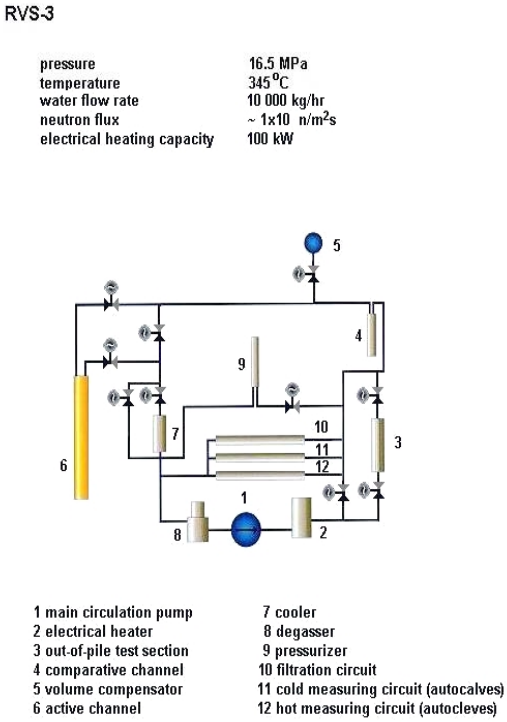

Figure 2: Schematic layout of reactor water loop RVS-3

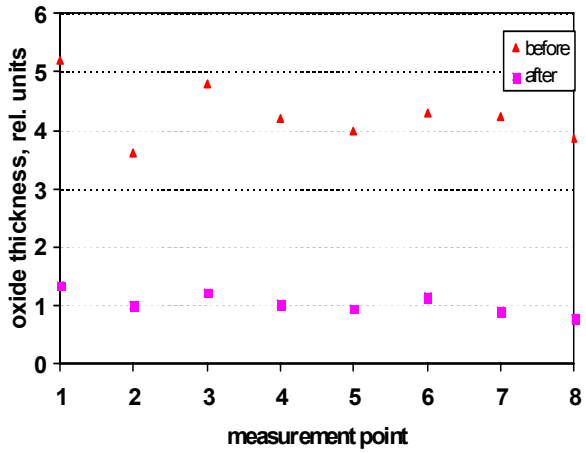

Figure 3: Effect of corrosion product deposits on Zr-oxide thickness measurement (eddy current results before and after brushing)

Table 2: Elemental composition of deposits on cladding surfaces

Sample ID	Elemental composition, wt% (EDAX)				Sample description
	Fe	Cr	Ni	Si	
5900	70.8	24.5	4.5	n.a.	loose deposits
5901	75.6	20.8	3.5	n.a.	loose deposits
5902	81.7	13.7	4.6	n.a.	loose deposits
5903	78.6	16.0	5.4	n.a.	loose deposits
5966	65.3	26.3	8.4	n.a.	heavy deposits
5963	61.4	27.5	11.1	n.a.	heavy deposits
5978	73.3	21.7	5.0	n.a.	heavy deposits
6218	68.2	23.1	8.2	0.5	loose deposits
6219	69.2	21.5	8.2	1.1	loose deposits
6217	68.8	20.7	9.0	1.5	loose deposits
Reference	~ 70	18–19	10–11	-	loop str. material

3.2. Test II: Zircaloy-4 cladding compatibility with VVER chemistry

The main objectives of this project which is performed with a support of the IAEA Technical Co-operation (TC) Project is experimental investigation of Zr cladding materials behaviour under VVER water chemistry, thermal-hydraulic and irradiation conditions. The main tasks of the project is to obtain experimental data (thickness of Zr oxide layer, amount of hydrogen absorbed in the alloy, mechanical properties — cladding ductility) for an assessment of the Zircaloy cladding material compatibility with VVER conditions and for modelling of Zircaloy-4 (Zry-4) corrosion behaviour in VVER units.
The RVS-4 reactor water loop has been built for conducting of the experimental programme. The RVS-4 loop has the following basic design features:

- the RVS-4 is a simple integral loop which a channel situated in the core of the LVR-15 reactor; a schematic layout of the RVS-4 loop is shown in Fig. 5,
- the main loop structure material is an austenitic stainless steel (SS 321 type),
- the in-pile rig consists of pressure channel with field tube for a flow division inside the channel, the in-pile test section consists of four electrically heated fuel rod immitators inserted into an cladding tube made from investigated Zr-alloy,
- the loop make-up water and dosing system provide a continual feed flow of 100 cc/hr to ensure water chemistry specification,
- the loop sampling system ensures continual sampling of the primary coolant with a flow of 100 cc/hr and collects the sampled coolant in a special sampling tank which is kept under N_2 overpressure to avoid dissolved hydrogen desorption,
- the loop consists of an electrical source of DC for the heating rods supply; the heating rods power is controlled by the test section outlet coolant temperature.

As recommended by a group of experts in the frame of the IAEA TC project a preoxidation of Zry-4 specimens was performed. This preoxidation was proposed with an intention to form Zr-oxide on the cladding tube specimens with a thickness simulating two fuel cycle operation in a reactor core, ie. preoxidation f Zry-4 specimens to range of 10–20 μm. To shorten the preoxidation period, it was recommended to preoxidize the Zry-4 specimens in steam at temperature higher than the nominal reactor temperature. To carry out the preoxidation task a special high-pressure, high-temperature autoclave was designed and manufactured in NRI.

The same cladding material supplied by WEC as used in Temelín VVER-1000 units were used for preoxidation, ie. low tin Zry-4 („Improved“) alloy. Four Zry-4 specimens with length of 60 cm each were placed in the autoclave. The preoxidation was performed at temperature of 415±2°C and pressure of 7±0.5 MPa. Each of the four Zry-4 specimens was preoxidized for different duration (from 152 to 381 days) to reach different Zr-oxide thickness on the cladding (in range of 10–25 μm). After each 20–30 days of preoxidation the specimens were removed from the autoclave and Zr-oxide thickness was measured by EC at pre-defined points. Results of the Zr-oxide thickness measurements are plotted in Fig. 6.

A destructive examination of the preoxidized Zry-4 specimens was performed at SKODA-ÚJP a.s., Praha. This destructive examination covered:

- visual examination,
- assessment of Zr-oxide thickness by a metalography method and comparison with results obtained by the EC method (results shown in Fig. 7),
- Zr-oxide morphology including hydrides orientation,
- evaluation of hydrogen amount absorbed by the Zry-4 (results shown in Fig. 8 as a function of Zr-oxide thickness),
- mechanical properties (eg. stress-strain characteristics) on the cladding ring specimens (results for cladding ductility shown in Fig. 9 as a function of Zr-oxide thickness and amount of adsorbed hydrogen).

Results of the destructive examinations showed:

-Thickness of Zr-oxide lies in range of 10–25 μm and is quite uniform on the Zry-4 cladding tube specimens. There is a good agreement between the non-destructive EC method for Zr-oxide thickness measurement and the destructive method. The EC data on the Zr-oxide thickness are systematically slightly higher than the data from destructive examination (approx. 2–3 μm).

- Amount of adsorbed hydrogen depends on thickness of Zr-oxide. Specimen with the longest preoxidation indicates high amount of adsorbed hydrogen (1400–1500 ppm). There is no explanation for such a different behaviour from other specimens. Hydrogen level in some specimens exceeds the operation limit (600 ppm H_2) given for VVER-1000 conditions.

After the preoxidation and characterization stages, the Zry-4 specimens were used for subsequent exposition in the RVS-4 in-pile water loop. Four cladding tubes were prepared to form an in-pile test bundle which is situated in the loop irradiation channel:

- one cladding tube of as received low tin Zry-4 (“improved),
- one cladding tube of as received Zr-1%Nb alloy (original VVER cladding material used in the test as a reference material),
- two cladding tubes of low tin Zry-4 („improved”) formed from preoxidized segments.

The latter cladding tubes consist of four Zry-4 preoxidized segments and were formed by a welding process. A special electrically heated rod is inserted into each cladding tube to simulate heat flux on the cladding surface. A gap between the heating rod and cladding tube contains helium gas to improve its thermal conductivity.

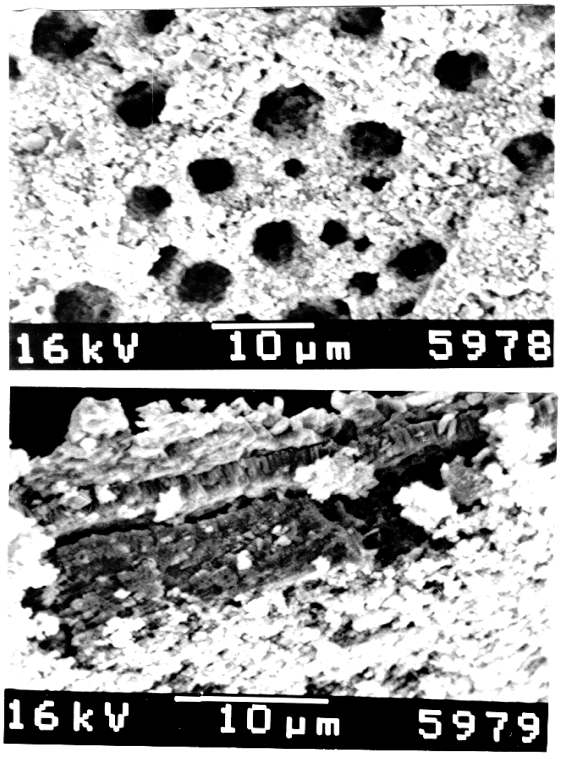

Figure 4: SEM picture of corrosion product deposits on cladding surface in subcooled boiling area (heavy deposits)

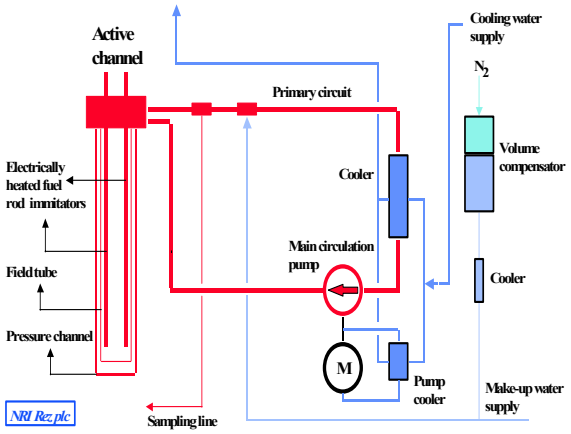

Figure 5: Schematic layout of reactor water loop RVS-4

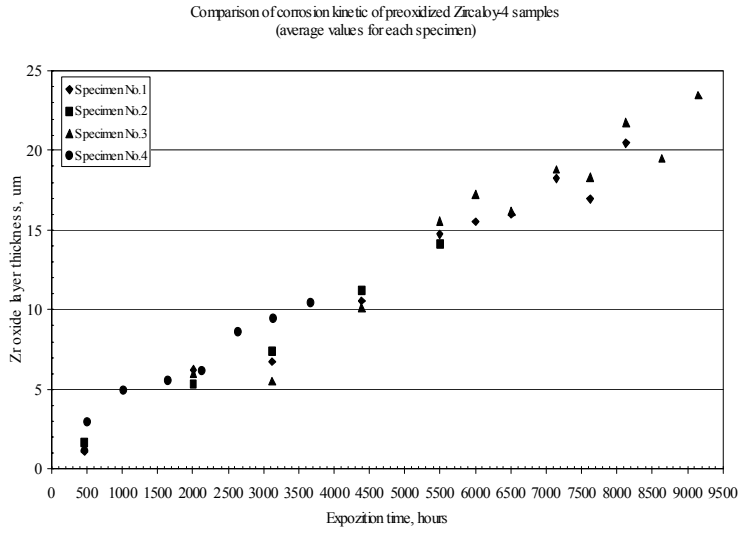

Figure 6: Corrosion kinetic of preoxidized Zry-4 specimens

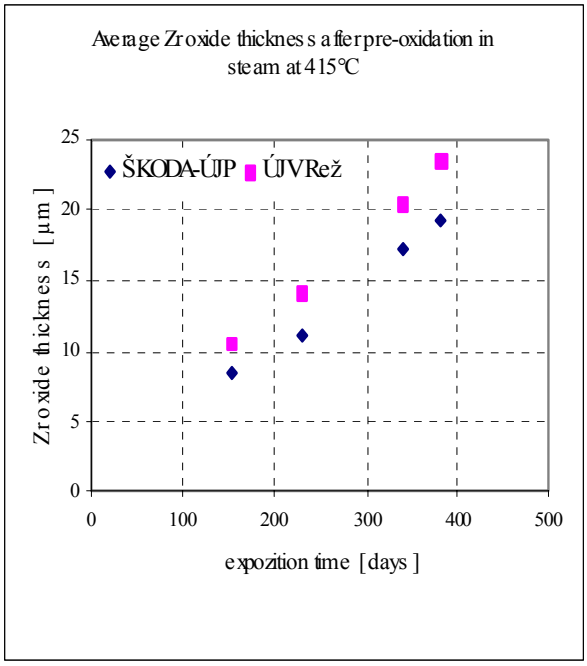

Figure 7: Comparison of Zr-oxide thickness measured by eddy current and metalography methods

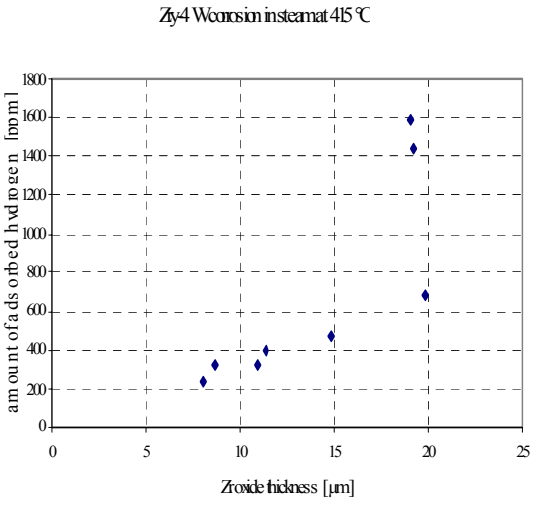

Figure 8: Hydrogen amount adsorbed by Zry-4 specimens (hydrogen pick-up)

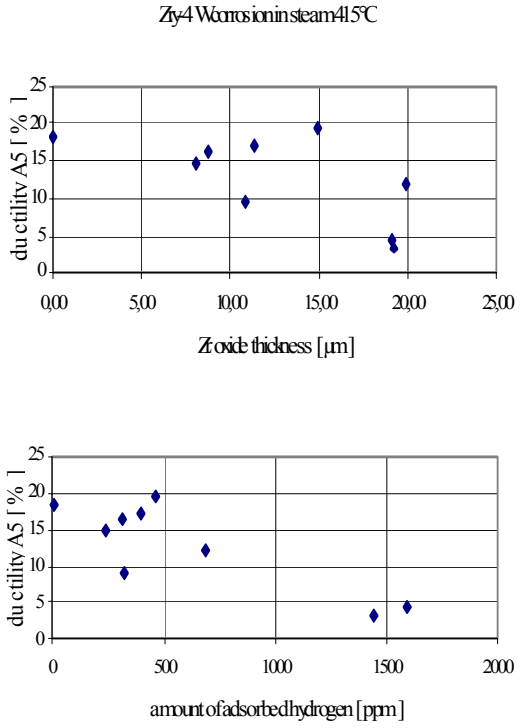

Figure 9: Zry-4 cladding ductility as a function of Zr-oxide thickness and amount of adsorbed hydrogen

After completion of the preparation stage, the in-pile test section was loaded into the loop and an irradiation stage has been started. During this stage the RVS-4 loop is operated at the following thermal-hydraulic and water chemistry parameters:

- loop pressure: 15.7 MPa
- inlet / outlet test section temperature: 311 / 322 °C

- coolant flow rate: 2 tons/hr
- surface heat flux: 60 W/cm^2
- cladding – Zr-oxide temperature: 345–350°C
- boron concentration: 3.5 g H_3BO_3/kg (610 ppm B)
- potassium / lithium concentration: 8 ppm K / 0.5 ppm Li
- ammonia concentration: 15 ppm NH_3
- dissolved hydrogen concentration: 25–35 STPcc H_2/kg
- dissolved oxygen concentration: < 10 ppb O_2

At the moment, the in-pile corrosion test is under progress with a target irradiation time as minimum of 100 irradiation days, ie. five reactor cycles. In the course of irradiation some intermediate non-desctuctive examination is foreseen (eg. visual inspection, Zr-oxide thickness measurement by EC method). After completion of the loop irradiation an extensive post-irradiation examination should be performed. The PIE will include:

- a visual examination,
- an assessment of Zr-oxide thickness by a metalography and electrochemical impedance spectroscopy methods,
- a Zr-oxide microstructure and morphology investigation by OM, SEM and TEM (eg. hydrides distribution, orientation, secondary particles etc.),
- an evaluation of hydrogen amount absorbed by Zry-4 alloy by an extraction method,
- an assessment of mechanical properties (eg. stress-strain characteristics, ductility) on cladding ring specimens.

ACKNOWLEDGEMENT

Reactor Services Division of Nuclear Research Institute Rez plc expresses acknowledgement to the IAEA supporting the experimental project „Assessment of Corrosion of Zircaloy Cladding“ in the frame of the Technical Co-operation Project CZR/4/005, and to the Czech State Office for Nuclear Safety supporting Zircaloy-4 cladding compatibility test.

The repair of irradiated fuel assemblies of RBMK-1500

G. Krivoshein, I. Krivov

Ignalina NPP, Lithuania

Abstract. In 1988 the irradiated fuel assemblies RBMK-1500 examination stand was put into operation at unit 2 of Ignalina NPP. The examination stand was intended to research irradiated fuel assemblies. Some destructive and non-destructive examinations of irradiated fuel assemblies have been developed together with Research Institute of Atomic Reactors. Since 1991 the examination stand has been using for visual examination of irradiated fuel assemblies before loading into the reactor. Visual examination revealed some irradiated fuel assemblies with damaged heat exchange intensifying (HEI) grids. Such defects do not allow loading fuel assemblies into the reactor. In 1996 the examination stand was completed with the module allowed to repair damaged heat exchange intensifying grids. Special fuel rod safety margins were calculated for such fuel assemblies. In 1997 five irradiated fuel assemblies RBMK-1500 were repaired and loaded into the reactor of unit 2. At the moment all repaired fuel assemblies are under control in accordance with the experiment. There have not been any failures.

1. INTRODUCTION

The Ignalina nuclear power plant (INPP) is located in the northeast of Lithuania, closer to the borders with Belarus and Latvia. There are 2 units at INPP, each of which is equipped with RBMK-1500 reactor. The RBMK-1500 is a graphite moderated, channel-type, boiling water reactor. Its design thermal power is 4800 MW. However, for safety reasons, these reactors are currently running at reduced power of maximum 4200 MW. The RBMK-1500 reactor is the most advanced version of RBMK design and the RBMK-1500 fuel assembly has advanced version too.

The fuel assembly contains two fuel bundles. Each bundle has 18 fuel rods arranged within two concentric rings in a central carried rod. The lower bundle of the fuel assembly is provided with an end grid and ten spacing grids. The top bundle has additionally 18 specifically design spacers, which act as turbulence enhances to improve the heat transfer characteristics. The hoop has 12 inclined grooves from which a steam and water mixture gets additional turbulence. This detail is one of distinctive features of RBMK-1500 fuel assembly. The schematic representation of the principal features of the RBMK-1500 fuel assembly is shown in Fig.1. The main parameters of the fuel assembly are presented in Table 1.

Structurally such grids have 6 cells that fix only fuel rods. All grid constructional elements are connected by spot welding (2–3 spots). The skeleton's difference between a heat exchange intensifying (HEI) grid and a spacer grid is shown in Fig.2. Thus heat exchange intensifying grids have a reduced mechanical durability (in comparison with spacer grids) and sometimes that is a reason of their damage during loading (unloading) the fuel assembly into (from) the reactor. Such defect does not allow to load a fuel assembly in reactor again. It is shown in Fig.3.

A note: For realization of the technological control of reactor fuel channels in period preventive maintenance 30–40 fuel assemblies are unloaded from the reactor. After this unloaded fuel assemblies must be passed through examination stand and loading into the reactor.

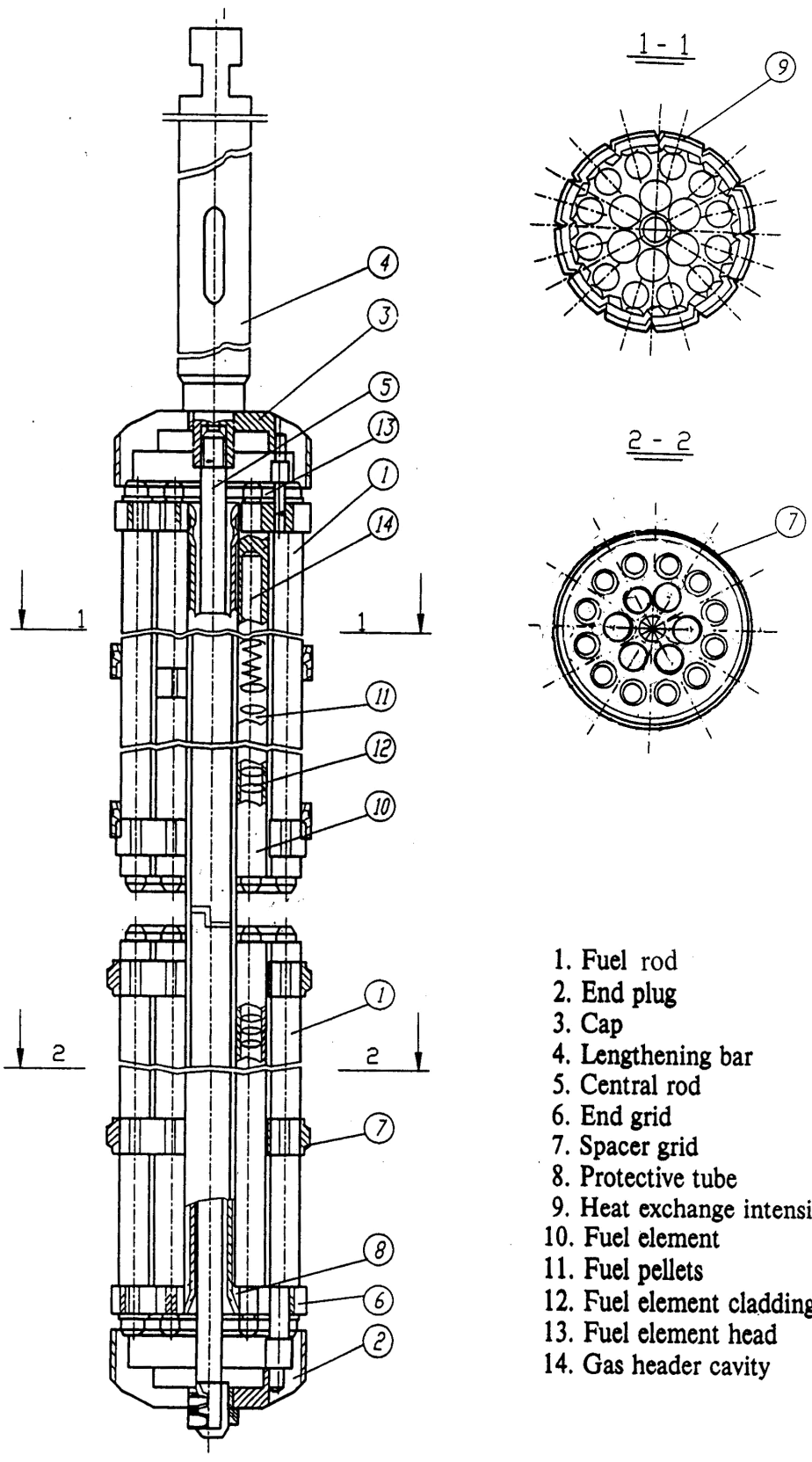

Fig. 1 Fuel assembly RBMK-1500

Table 1. RBMK-1500 fuel assembly parameters

Fuel pellet	
Fuel	Uranium dioxide
Fuel enrichment, % of U^{235}	2, 2.4
Fuel pellet diameter, mm	11.5
Fuel pellet length, mm	15
Pellet central orifice diameter, mm	2
Fuel element	
Cladding material	Zr+1%Nb
Outside diameter, mm	13.6
Length, m	3.64
Cladding thickness, mm	0.825
Pellet/clad gap, mm	0.22-0.38
Helium pressure in the cladding, MPa	0.5
Maximum linear heat generation rate, W/cm	485
Fuel assembly	
Number of bundles	2
Number of fuel rods per bundle	18
Diameter (in the core), mm	79
Mass of uranium within fuel pellet, kg	111.2
Mass of uranium within edge fuel pellet, kg	1.016
Maximum permissible power of fuel channel, MW	4.25

2. EXAMINATION STAND

In 1988 the irradiated fuel assemblies examination stand was put into operation at unit 2 of Ignalina NPP. The stand was intended for researching and getting irradiated fuel assemblies statistical dates which were found to understand RBMK-1500 fuel behaviour. The stand is established in spent fuel pool and it is a rigid underslung steel construction consisting of surface and underwater parts. The schematic obtaining of the examination stand is shown in Fig.4. The surface part includes an operating floor (1) and a frame (4). Two parallel bearing tubes (8) have fasten to operating floor which sinking into the pool water. These tubes are fixed in a lower stand plate (10). The directings are attached to tubes on all length and the movable plate (5) moves vertically on them. The screw (3) passes between bearing tubes. The nut is established rigidly on the movable plate. The motor (11) located on the stand operating floor rotates the screw and so actuates the moveable plate. An immersed video camera (9) and rack for fastening measuring probes are disposed on the movable plate. Fuel assembly has been installed and fixed in the bottom stand support (6) and in the top rotary support (7), which is located on the operating floor. The top part of fuel assembly (2) has been joined to the rotary reducer mechanism equipped by a motor which rotates it. The fixed fuel assembly position limits significant radial movement during its rotation. The stand is equipped with an automated control and a coordinate moving registration systems. The stand height is 13 meters. The part sinking in pit water dimension is 1.5x1.9 meters.

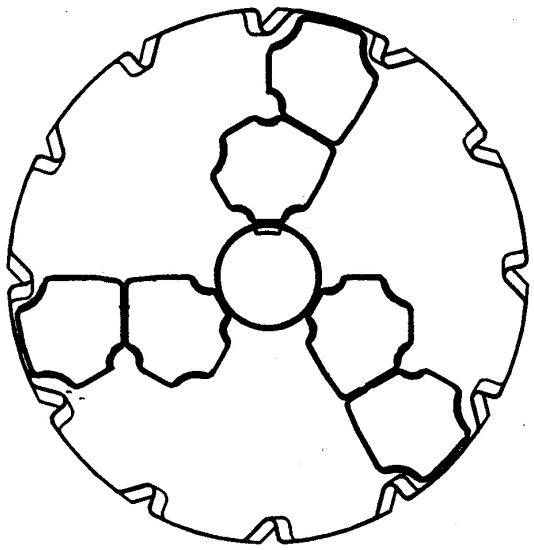

A heat exchange intensifying grid's skeleton

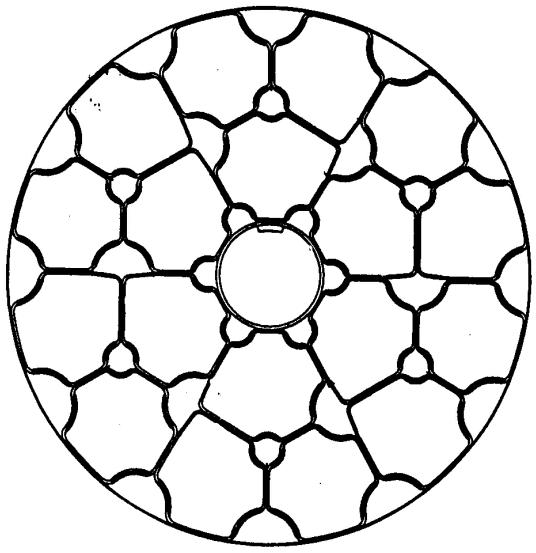

A spaser grid's skeleton

Fig. 2 The skeleton different

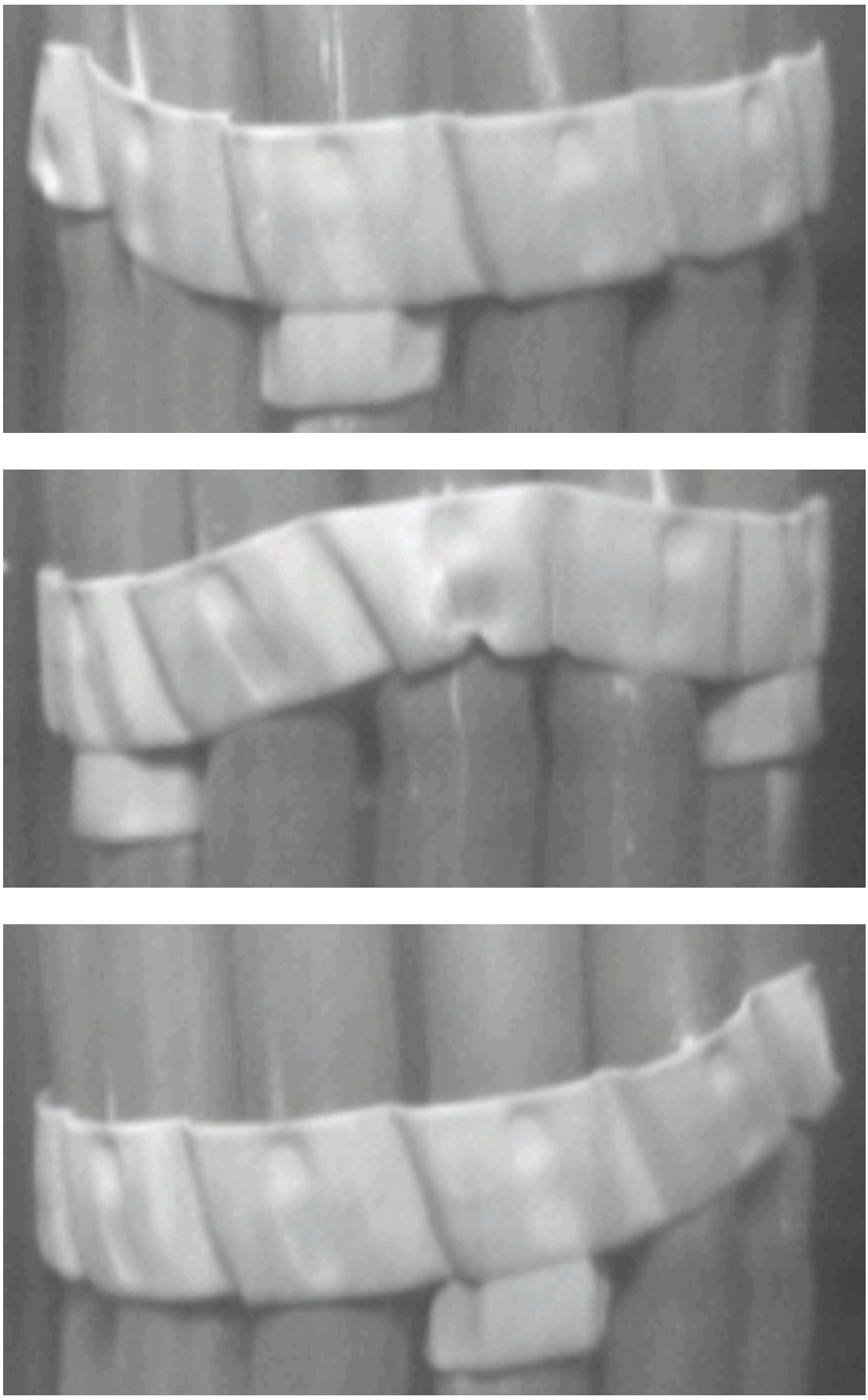

Fig. 3. The damaged HEI grig.

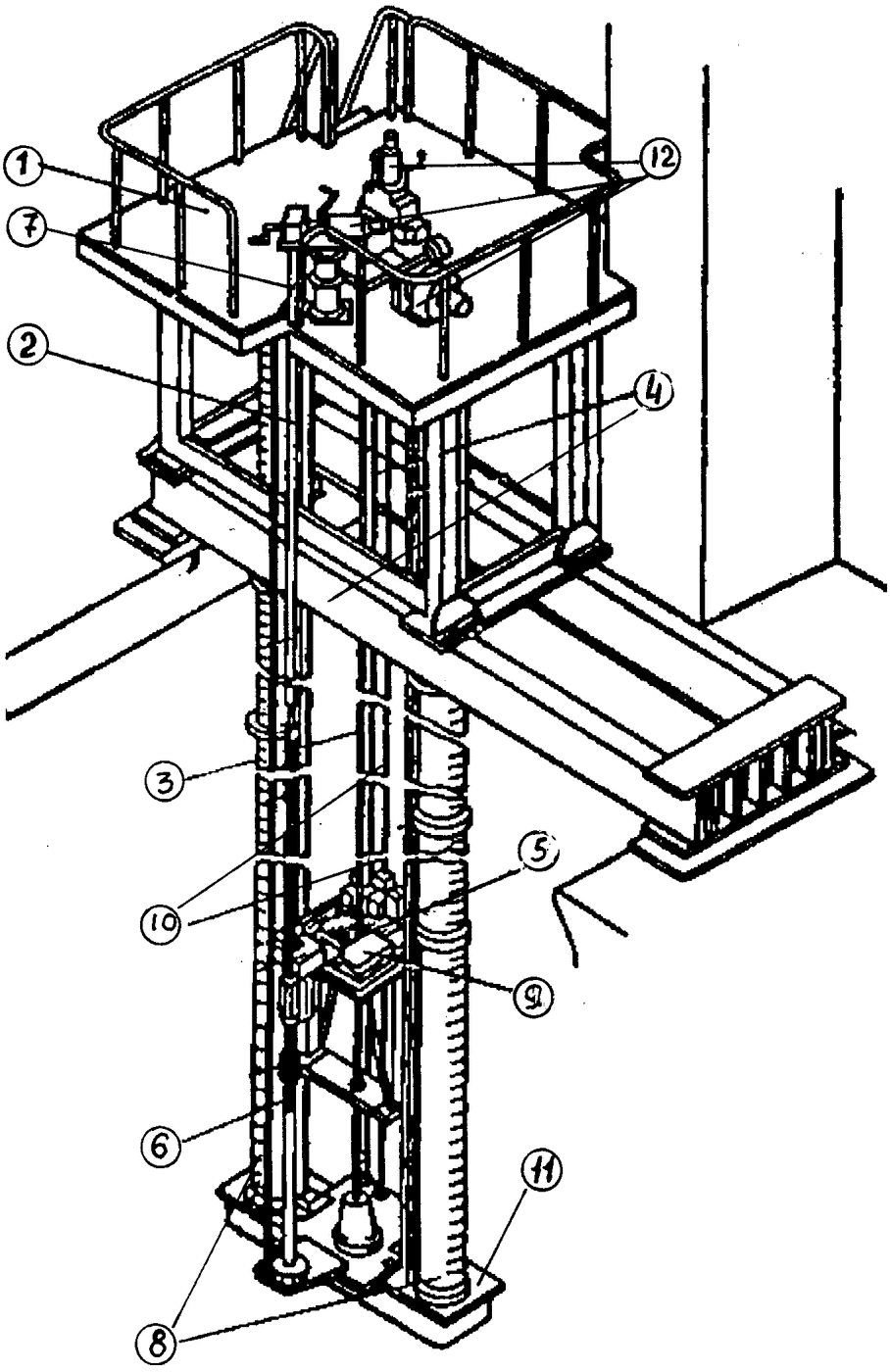

1. Operation floor
2. Fuel assembly
3. Screw
4. Frame
5. Mov-able plate
6. Lower stay
7. Upper stay
8. Bearing tubes
9. Video camera
10. Lover plate
11. Motors

Fig. 4 Examination stand

From 1988 to 1990 some non-destructive methods of irradiated fuel assemblies RBMK–1500 have been developed together with Research Institute of Atomic Reactors [1]. They are:

- visual examination of fuel assembly;
- eddy-current testing of accessible surfaces fuel rod;
- identification of leaking fuel rod;
- fuel rod diameter measurement.

Because since 1991 the financing of this work was stopped, the examination stand has been used for the visual control of irradiated fuel assemblies before loading into reactor only by TV camera "Tellar-32". About 100 irradiated fuel assemblies are passing through the examination stand each year. During visual examination some irradiated fuel assemblies with damaged grids are revealed. It has been offered to carry out the repair of fuel assembly with damaged HIE grid's hoop.

3. REPAIR MODULE

In 1996 together with ENTEK the module was developed, made and fit up on examination stand for the repair of the damaged hoop HEI grids. A module bearing part is a base plate which has been fasten to the stand movable plate. A movable carriage is disposed on the base plate. It provides inputting/outputtig executive mechanisms to the damaged fuel assembly grid. The executive mechanisms have been interchangeably established on the carriage and they serve for the specific repair operation performance. They are "Crocodile shears" mechanism (Fig.5) and "Vice with rotatable grip" mechanism (Fig.6). The fuel assembly has been fixed in holder mechanism. It has 80 mm inner diameter. It limits a fuel assembly radial moving during its repair. The holder has been coaxialy fastened to the stand movable plate. The repair module is equipped with a refuse receptacle for radiactive waste which is located in a lower module part. The receptacle is intended for removing of radioactive hoop parts from the examination stand after a grid repair realization. An executive mechanisms control is handled from the stand operating floor by 3 transmissions rods. The schematic representation of the repair module is shown in Fig.7.

4. REPAIR TECHNOLOGY

A repair technology embraces a total damaged hoop of HEI grid skeleton removal and consists of separated operations. The first operation is carried out by the "Crocodile shears" mechanism. A pullback of damaged hoop is made within 5–7 mm. It is necessary that a shear cutting part would be able to fit behind a hoop surface and to intersect the damaged hoop. The cutting is retrieved in 3 places, approximately through 120° between outside cells of HEI skeleton. Then hoop fragments are bent to fastening point of cell and hoop's fragments. (Fig.8). Then the stand movable plate is risen from water and mechanism is being exchanged. Instead of the "Crocodile shears" mechanism is established the "Vice with ratable grip" mechanism for carrying out next operation. The gripping vice are input to one of bent fragments and the vice compress it as close as possible to a fastening cell and hoop place. A head of the vice has been swing on 20° in one or another direction 7–8 times and a welding fast place has been destroyed. (Fig.9). Further the vice with clutched hoop's fragment is output, the vise is unclamped and a hoop's fragment falls down under its body weight into the refuse receptacle which is located under layer of water. When all three fragments are separated from each cell control operations should be done on the repaired block. They are:

Fig. 5. The "Crocodile shears" mechanism.

Fig. 6. The "Vice with rotatable grip" mechanism.

- A swaging of skeleton cells by a mechanism shown in Fig. 10;
- A checking of a clearance presence between the each skeleton cell and external fuel rod surface where it is fixed.

The control is being carried out by an adaptation "clearance gauge" with thickness 0,5 mm. A criterion is "pass – no pass". (Fig.11). A repaired fuel assembly (without the damaged hoop) is shown in Fig.12.

5. LOADING OF REPAIRED FUEL ASSEMBLIES INTO REACTOR AND THEIR CHECKING

Kurchatov and ENTEK institutes have researched a fuel assembly breadboard with a removed HEI grid hoop which had shown that its removing is a decreasing results of critical thermal power rate in 20–25%. In a regime parameters field of Poutput=7 MPa, Tinput=260°C and Gch = 24 t/h the critical fuel assemblies power rate with removed hoop is about 4500 kW. A maximal channel operate power rate is 4250 kW.

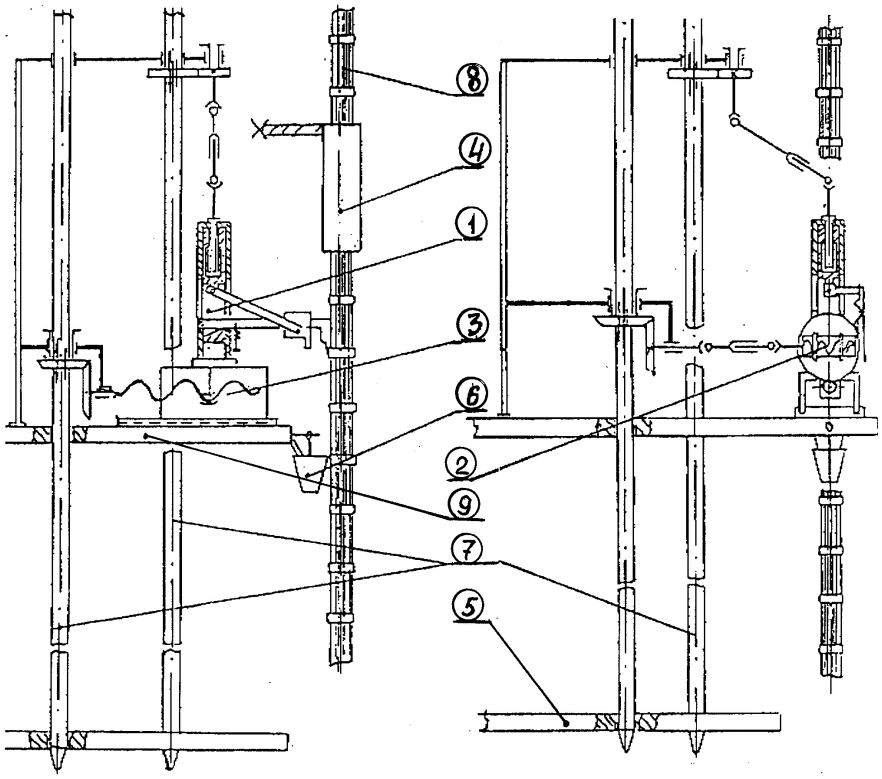

1. Crocodile shears
2. Vice with rotatable grip
3. Carriage
4. Holder
5. Lower plate
6. Refuse receptacle
7. Transmissions rods
8. Fuel assembly
9. Base plate

Fig. 7 Scheme of repair module

From this you can make the conclusion that the critical power rate on repaired fuel assemblies won't arise if the reactor is in a normal operation parametrs. A dry-out safety margin and a safety margin on linear heat rate for the reparied fuel assembly have been calculated and corrected in a operating reactor computer software [2].

In 1997 have been repaired and loaded into reactor 5 fuel assemblies with damaged hoop of HEI grid skeleton at unit 2. Fuel assemblies were loaded by the refueling machine without any problems. Their parameters are shown in Table 2. In accordance with special program a

periodical fixing control has been implementing for repaired fuel assemblies. There have been fixed following parameters:

- Wr – reactor thermal power;
- Wch – channel thermal power;
- Fch – coolant flow rate throught the channel;
- Kd – dry-out safety margin;
- Kl – safety margin on linear heat rate.

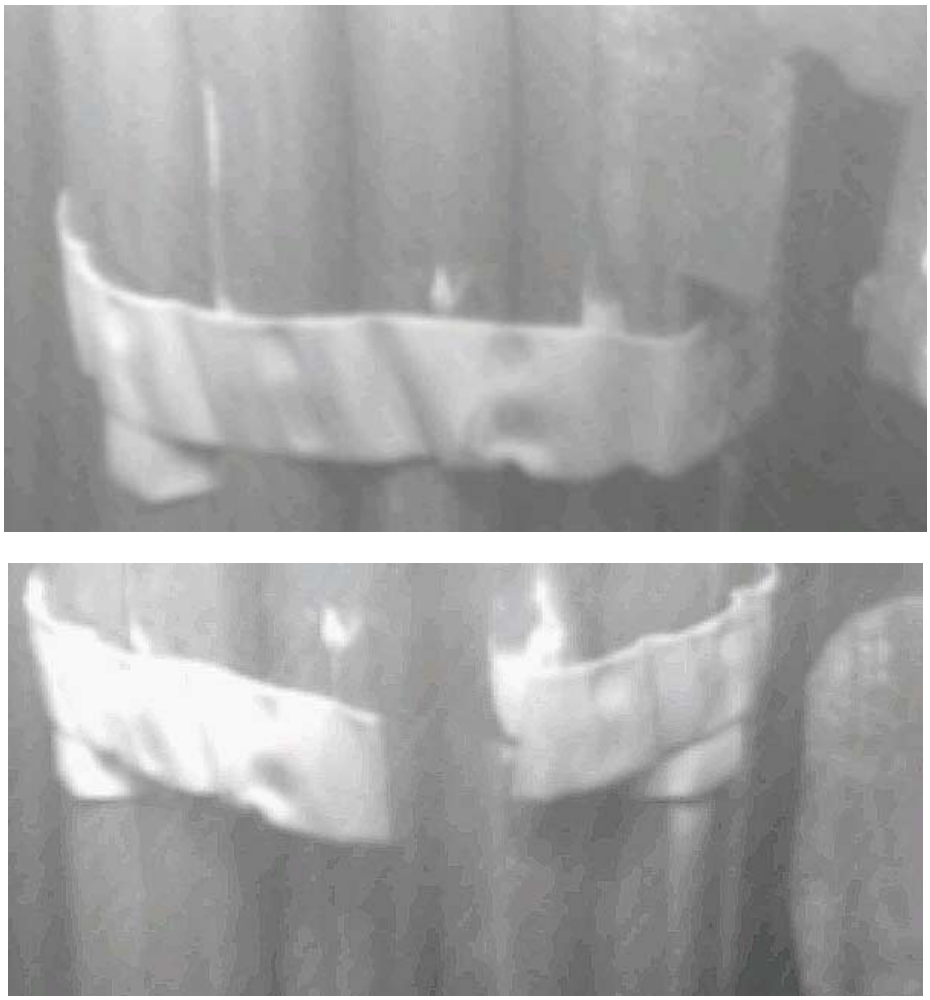

Fig. 8. The cutting of the HEI grid's hoop.

For this period all 5 repaired fuel assemblies are operated in reactor without deviations from established limits. There were fixed minimal values for Kd = 1.44 and Kl = 1.80 in channel number 13-05. In accordance with the experiment some recommendations were worked out for loading of repaired fuel assemblies with various burnup into various reactor zones. A constrain was imposed only on repaired fuel assembly with burnup less than 600 MW day/FA. At the moment all repaired fuel assemblies are under control too. The fuel rods integrity monitoring system confirms that all repaired fuel assemblies are leak-tight. The unloading of the repaired fuel

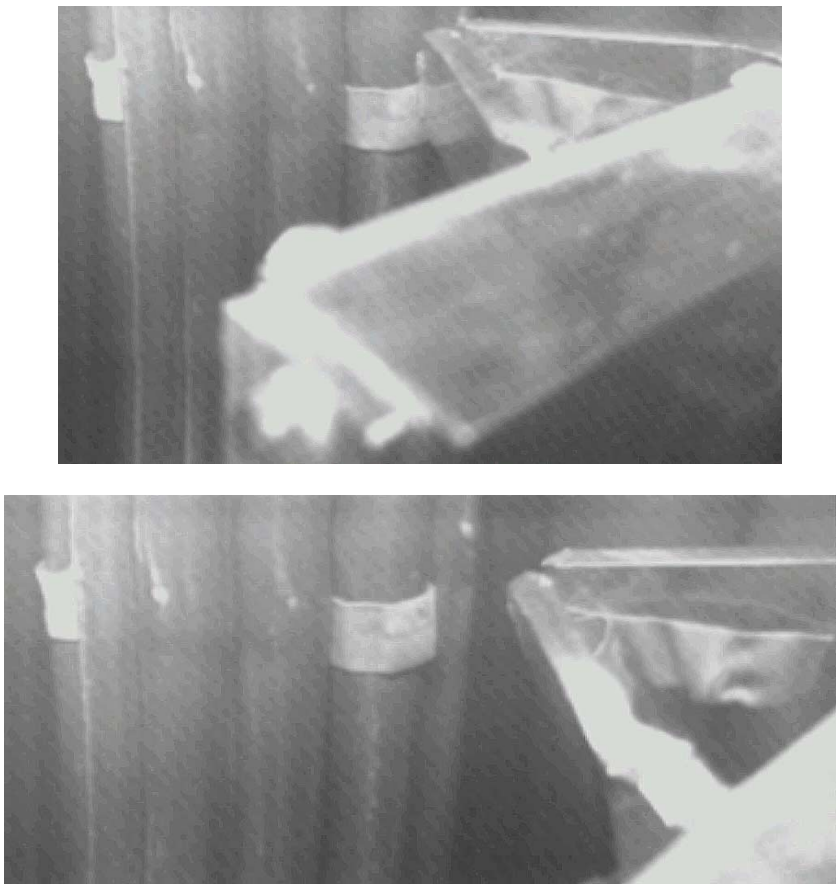

Fig. 9. The isolating of HEI grid's hoop fragments.

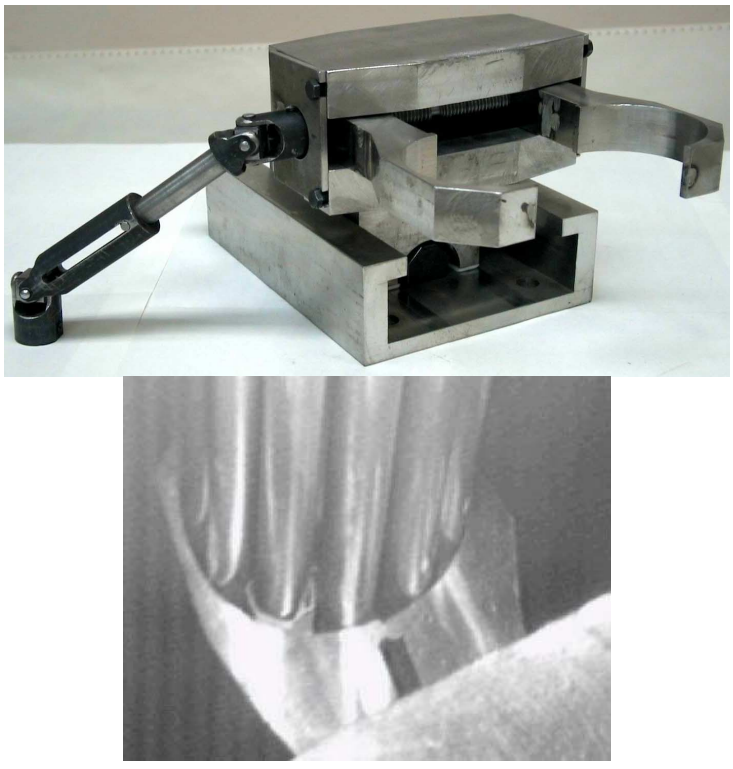

Fig. 10. The "Swaging" mechanism.

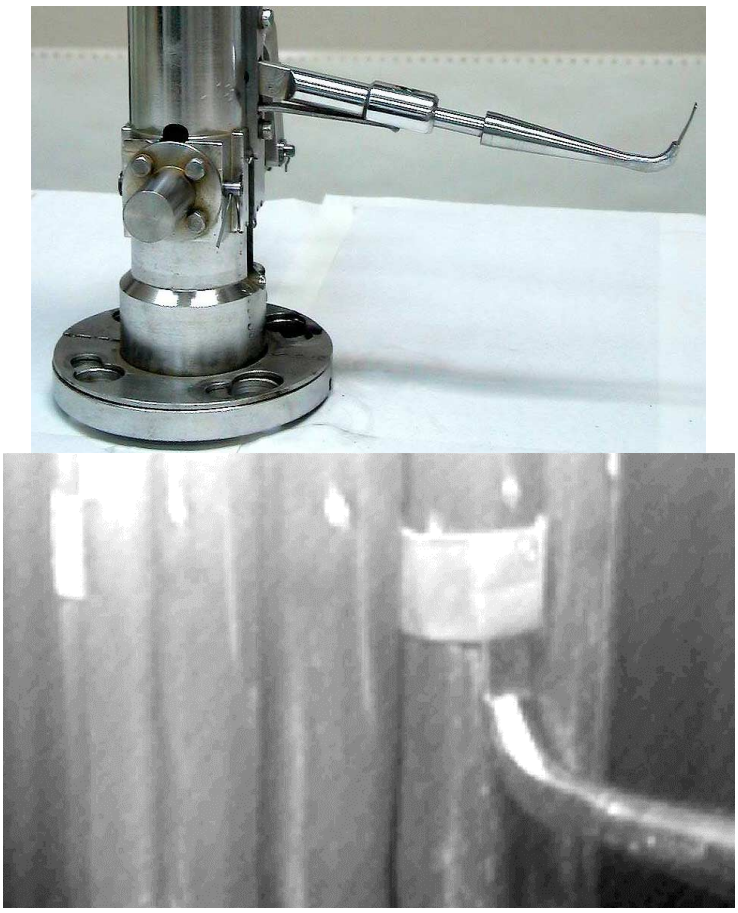

Fig. 11. The checking of a clearance presence by the "Gauge".

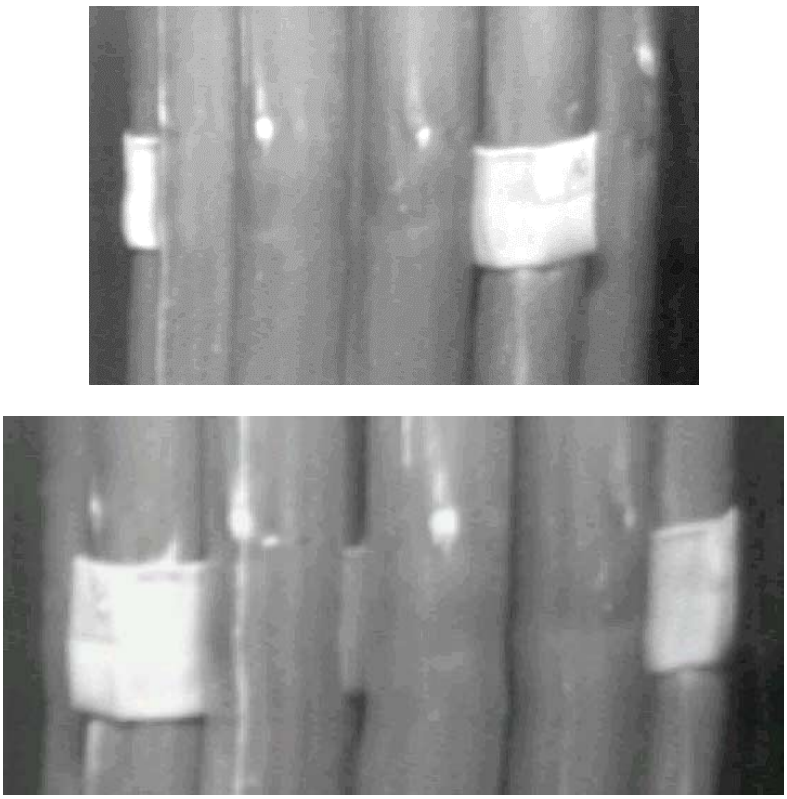

Fig. 12. The repaired HEI grid.

assemblies is being planned when their burn up will reach about 2500 MW d/FA. All unloaded repaired fuel assemblies will take a constructional elements integrity checking on examination stand. This dates will help to develop some recomendations for safety operation of repaired fuel assemblies RBMK-1500 in reactor.

Table 2. Repaired fuel assemblies operation parameters

	Fuel assembly **620-23751-89**	Fuel assembly **620-17580-88**	Fuel assembly **520-1819-86**	Fuel assembly **520-25031-89**	Fuel assembly **520-39833-92**
Loading date	27.06.97	27.06.97	12.07.97	12.07.97	13.07.97
Burn up MW day/FA	0	0	0	0	568
Reactor Coordinate	01-30	05-37	45-35	07-10	13-05
MaxWr, MW(th)	4150	4150	4150	4150	4150
MaxWch, MW(th)	1,56	2,09	2,01	2,25	2,60
Min Fch, m^3/h	33,5	32,3	33,1	29,4	32,1
Min Kd	2,34	1,72	1,82	1,63	1,44
Min Kl	2,88	2,12	2,30	2,05	1,80
Current burn up, MW day/FA	1121	1345	1374	1454	1958

Now about 50 fuel assemblies with damaged HEI grid's hoops are stored at Ignalina NPP spent fuel pools. In 2005 the unit 1 will be shut down for decommissioning and about 1300 fuel assemblies are planned to be removed from unit 1 to unit 2 for loading them into reactor of unit 2. The statistic shows that during the irradiated fuel assemblies handling about 5% of assemblies have got damages of HEI grid's hoop.

A subsequent realization of the repair and loading repaired fuel assemblies into reactor will allow essentially to improve a fuel cycle that will reduce charges on recycling and ultimate storage of high level waste at Ignalina NPP.

6. CONCLUSION

The implementation of the repair of damaged HEI grids at Ignalina NPP shows the following results:

- the repair technology of irradiated fuel assemblies with damaged HEI grid's hoop has been developed;
- the repair module was mantled on the examination stand at unit 2;
- 5 fuel assemblies were repaired;

- all repaired fuel assemblies are being operated in the reactor of unit 2 successfully;
- a results of operation repaired fuel assemblies conditions are received;
- the personnel has got an experience and skills of safe repairing of irradiated fuel assemblies on examination stand.

REFERENCES

[1] ALEXANDROV K., PAVLOV S., PROKUDANOV D. (Research Institute of Atomic Reactors), Krivoshein G., Sladkopevcev A., (Ignalina NPP), Chernobaev V., (ENTEK), Joint report "The Examination stand in spent fuel pool" (1992).

[2] KARTASHEV E., NIKOLAEV V., KOBSAR L., RIABOV A., VINOGRADOV V., (ENTEC) Report "The experimental and settlement research of the dry-out on a fuel assembly RBMK-1500 breadboard with repaired HEI grid" (1990).

In-pile creep test technique for zirconiun alloys examination in BR-10 reactor channels

Yu.M. Pevchikh, A.S. Kruglov, V.M. Troyanov

SSC RF Institute of Physics & Power Engineering (IPPE),
Obninsk, Kaluga Region, Russian Federation

Abstract. The irradiation enhanced creep phenomenon was discovered in stainless steels as a specific physical process accompanying high-intensity neutron flux irradiation in fast reactors. IPPE is also experienced in irradiation creep test activities, studying different types of materials under irradiation in BR-10 fast reactor. Series of in-channel type test facilities were constructed and tested in BR-10 reactor's "dry" channels in order to carry out full-scale instrumented examination regarded to in-pile creep behaviour of different reactor materials. As a result, a specific test technique, named "Tensometric method", has been developed and experimentally proved to be power enough in order to investigate irradiation creep of materials right in situ under neutron irradiation. The main peculiarity of test facility, which is constructed to apply the tensometric method, consists in absence of any special deformation-measurement cell at all. The in-pile creep strain measurement technique developed at IPPE is based on the non-direct measurement of specimen's deformation (either linear tensile strain or angular twisting one), which directly affects the loaded draws' tension parameters. Starting from 1993, in-pile creep experiments to investigate in-reactor creep behaviour of E110 and E635 zirconium alloys were carried out in BR-10. Experimental results and data collected during more than 20-year of BR-10 in-reactor creep test experience can be assumed as a strong evidence that the tensometric technique is a powerful instrument, which can give a chance to study different irradiation effects on reactor materials directly under irradiation.

1. INTRODUCTION

When arising in latest 60-ths, the problem of in-reactor creep study of structural materials was the new and most unusual technical task. The irradiation enhanced creep phenomenon was discovered in stainless steels as a specific physical process accompanying high-intensity neutron flux irradiation in fast reactors. That initiated the most intensive technical effort in many countries to study the new discovered material's behaviour. Since that time IPPE is also experienced in irradiation creep test activities, studying different types of materials under irradiation in BR-10 fast reactor. During this period many design and methodical works were performed to develop the most suitable in-reactor-test technique. Series of in-channel type test facilities were constructed and tested in BR-10 reactor's "dry" channels in order to carry out full-scale instrumented examination regarded to in-pile creep behaviour of different reactor materials. As a result, a specific test technique, named "Tensometric method", has been developed and experimentally proved to be power enough in order to investigate irradiation creep of materials right in situ under neutron irradiation. One of the essential application of tensometric test method is relevant detailed investigation of in-reactor creep behaviour of zirconium alloys used as fuel element cladding materials for water-water power reactors. Description of the method and technical means for its realization, as well as some experimental results to prove tensometric technique capability, are subjects of present report.

2. PRINCIPAL CONSTRUCTION OF TEST FACILITY TO REALIZE TENSOMETRIC TECHNIQUE

The tensometric method to measure the specimen's creep or plastic deformation during in-pile test is rather universal and can be applied to several types of loading scheme: tensile, compression, twisting, bending, mechanical cycling, fatigue. To apply the method it is necessary to use some special construction of test facility. Any in-channel-type test facility, if compared with a standard test device, has some specific peculiarity mostly controlled by channel's geometry. First of all any in-channel machine's construction is affected by a significantly high channel's length/diameter ratio. For example, "M"-type channels of BR-10 have length/diameter ratio about 3000/35 (in millimeters). Load-train system of test facility normally consists of two draws: active and passive one to transfer the load from the load-inducing mechanism, which is usually placed in out-of-irradiation zone, to the specimen, which is located in the active core zone. Because of a large length and of a rather limited cross section of draws, the total elastic strain of draws is also abnormally large if compared with standard test equipment. As usually, a passive unmovable draw simply represents the facility's tubular body "solid-made" by welding or by other means. While the tensile or twisting load is applied to the specimen through the inner active draw or driving shaft the passive tubular body provides stress resistively, which is quite sufficient to prevent any facility's bending, which might be taken in an account.

Schematic diagrams of proper test facilities arranged for tensometric method appliance are shown in Fig.1 and Fig.2. Any test facility schematically consists of four general parts: load inducing mechanism; passive draw, which is facility's body; inner active draw (shaft); load measurement cell. The load inducing mechanism contains an electrical motor, force-increasing gears and, in case of tensile scheme, a motion screw pair to transform the nut's rotation into axial motion of the screw, which at the same time is an upper part of the active draw. The only control device (except thermocouples, of course), which is used in test facility's construction, is a tensometer — a load measurement cell arranged to transform the draws tension into amplitude-modulated electrical signal.

The torsion test facility (Fig.2) schematically is the most simplest construction of all. This circumstance is the grate advantage when the facility is forced to work under in-reactor remote control conditions. The next advantage of the torsion facility, if compared with tensile one, is the low thermal influence on the load measurement cell's signal. That occurs because of any possible draws' axial thermal extension in properly designed torsion type machine cannot affect the twisting strain in such a rate as it takes place in strained draws of the tensile machine. As it has been experimentally proved under BR-10 conditions, temperature dependent error of creep measurement results is about ten times lower for the torsion type facilities than for the tensile ones. Besides, the torsion type of in-channel test facility is one of the suitable machines, which can be used to test thin-walled tubular specimen just being a fragment of a real fuel pin cladding tube.

Both principle in-reactor test constructions described above are quite effective and sensitive instruments to apply the tensometric method of creep-deformation in situ measurement. With this method such natural but rather negative characteristic of in-channel type test facility, like an extremely high elasticity of draws, can be converted into very advanced property, which permits to organize reliable measurement of specimen's creep deformation in the reactor. It should be also mentioned that the real BR-10 in-channel test facilities instead of a single specimen shown schematically in Fig. 1 and 2 are equipped with special rig containing 3÷4

specimens, which can be creep tested one after one without interruption of irradiation. Such multi-specimen approach makes instrumented in-reactor test more informative and less expensive.

3. CREEP-DEFORMATION MEASUREMENT METHOD

The main peculiarity of test facility, which is constructed to apply the tensometric method, consists in absence of any special deformation-measurement cell at all.

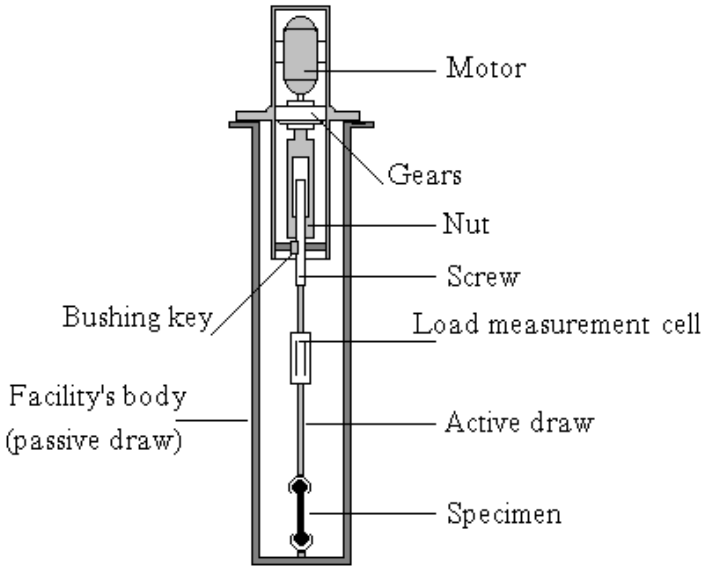

FIG. 1. Schematic diagram of in-channel type tensile test facility.

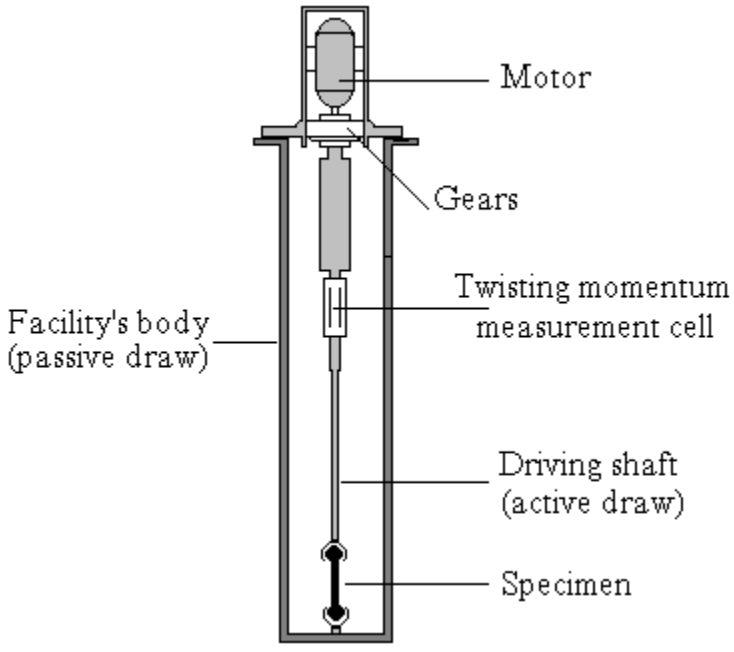

FIG. 2. Schematic diagram of in-channel type torsion test facility.

The in-pile creep strain measurement technique developed at IPPE is based on the non-direct measurement of specimen's deformation (either linear tensile strain or angular twisting one), which directly affects the loaded draws' tension parameters. As it has been experimentally proved this method is the most sensitive beyond the known in-reactor test techniques and is one of the most reliable as far as in situ irradiation creep test is concerned. The physical background of the tensometric method is comparatively simple. As it has been mentioned above, any in-channel-type tensile (or twisting) machine has an abnormally high length/diameter ratio. As a result, a total elastic strain of the load-train draws is also extremely large when compared with standard laboratory equipment. As a result, elastic and creep deformation of specimen during the test is at least in hundredth times lower than total elastic strain of load training draws. For example, the total elastic strain of BR-10 in-cannel tensile machine's draws at 200-kg load applied is about 2 mm. It means that pretending to organize a "strong" mechanical loading scheme, in reality we have nothing but "soft" spring-type loading. In other terms, the constant load being applied to the specimen is controlled by elastic strained draws acting like a "stretched spring".

This "spring", containing also the tested specimen as a part of the "spring's body", is fixed in its "stretched" state at the top side of the active draw when the motor is switched off. If some specimen's creep deformation occurs it affects the "stretched spring" length causing the draws' tension drop. Knowing the total draws' elastic flexibility coefficient and measuring the tension drop it is possible to calculate specimen's inelastic deformation, which was the cause of that drop. Thus, there is the principal technical possibility to measure creep deformation of tested specimen not having any special deformation-measurement device at all. The elastic machine itself, while equipped with some sensitive load control cell, is such a device. Since the load controlling cell can be embedded in an active draw far out of the active core zone, any possible irradiation disturbance of the load controlling system is negligible.

The flexibility of the load-train draws can be easily measured before irradiation as well as periodically measured during irradiation too. Since the only small part of the facility is affected by irradiation or high temperature, the total flexibility of the draws does not practically change during full period of in-reactor test. That was many times experimentally proved for several test facilities by periodic measuring of flexibility coefficient under irradiation in BR-10 for as long as years of facilities' operation time. The most effecting factor, which can really affect creep measurement results, is relative non-stability of a thermal elongation of draws. Any unexpected change of draw's length during tensile test would be translated as creep deformation of the specimen. So, the tensometric method can be successively applied only at stable periods of thermal and power reactor operation. For example, such suitable conditions occur in BR-10 reactor about 20 hours after the reactor is arisen from the shutdown state up to the full power. Afterwards the in-pile-creep measurements could be carried out with no significant troubles.

Creep rate calculation procedure for tensile test is as follows:

k_f - draw-system's flexibility coefficient [mm/kg];
P - average tensile load applied to the specimen during Δt test period;
ΔL - specimen's creep deformation developed during Δt test period;
ΔP - measured draw's tension drop caused by ΔL draw's elastic relaxation;
L, S - specimen initial gage-length and cross section area;
average creep rate = $\Delta\varepsilon / \Delta t = (\Delta L / L) / \Delta t = k_f \cdot (\Delta P / \Delta t) / L$;
average stress = $\sigma = P/S$.

Analogous creep rate calculation procedure in case of torsion test is as follows:

k_f - draw-system's torsion (angular) flexibility coefficient [1/kgmm];
M - average twisting momentum applied to the specimen during Δt test period;
$\Delta\varphi$ - specimen's angular creep deformation during Δt test period;
ΔM - measured draw's tension drop (twisting momentum drop) caused by $\Delta\varphi$ draw's elastic relaxation;
R, δ, L - average radius, wall thickness and gage-length of the tested tubular specimen;
$\Delta\gamma$ - specimen relative angular (share) deformation ($\Delta\gamma = \Delta\varphi/L$);
average share creep rate = $\Delta\gamma / \Delta t = (k_f \cdot R/L) \cdot (\Delta M/\Delta t)$;
average creep rate intensity = $\Delta\varepsilon / \Delta t = (\Delta\gamma / \Delta t) / \sqrt{3}$
average share stress = $\tau = M / (2\pi R^2 \delta)$;
average stress intensity = $\sigma = \tau \cdot \sqrt{3}$.

It is clear that within Δt period specimen creep is caused not by constant load but load ranging from P to P-ΔP. According to standard requirements for a constant-load-mode creep test a load is assumed to be "constant" even if it deviates within some permitted limits (usually about ± 1÷2 %). So, if a creep test could be organized in a way when ΔP (or ΔM) drop would lie inside that permitted limits, the whole experiment can pretended to be classified as a constant-load-mode creep test. To provide all "constant load" requirements, as well as to control and to register whole experiment parameters, the automated computerized control system was developed. The programming support (software) for the "constant load" in-pile-test procedure was prepared too. When the load measuring cell signal indicates that the lower limit of the nominal load level is reached, then the loading mechanism is automatically switched on to restore the load up to upper limit of the nominal level. In fact, any creep deformation curve, which is obtained under the tensometric creep measurement technique described above, consists of continuos series of "partial creep curves" registered within the permitted load-drop "window". These partial curves, following one after one without interruption, being mathematically treated can be converted into a global "constant load" creep deformation curve of the "normal" feature. The illustration of the deformation creep curve formation technique is given in Fig. 3.

BR-10 test facility load control cell, used as deformation measurement cell too, consists of a special elastic element made of "spring-type" steel with several wire-type tensoresistors being fixed on the element's plates and forming DC-bridge electrical scheme. The cell is embedded in the active draw right below the load inducing mechanism. In this position the cell is not effected by neutron or gama irradiation as well as is working at rather low temperature (not higher than 60÷80^{o}C). With such type of tensometer it is possible to register about 0.1 ÷ 0.2-micron specimen elongation or its angular equivalent in a case of torsion test. That is assumed to be upper limit of creep-deformation measurement resolution in case if tensometric technique is applied under "absolutely stable" thermal conditions. In fact the real resolution of method is strongly dependent on amplitude of thermal fluctuations, which can induce the differences in draws' length caused by thermal extension effects. For that very reason the tensometric method is much more resolute and productive with test facilities constructed for torsion load scheme in order to study in-pile creep, which is induced by shear stress application to thin-walled tubular specimens. In fact, all of in-reactor creep results for zirconium alloys were obtained at BR-10 under torsion in-pile tests.

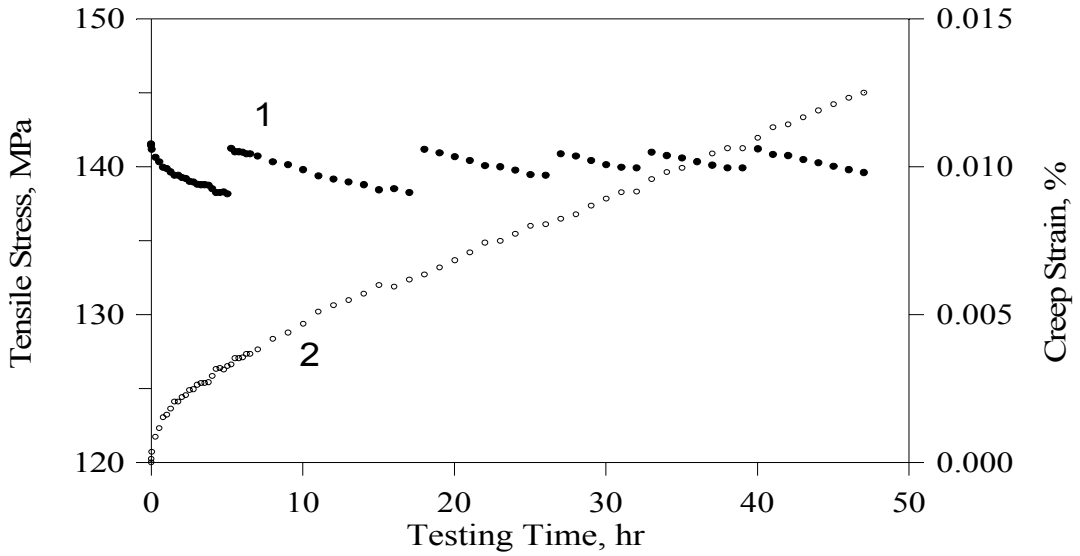

1 - initial tensile stress measurement results registered during the test stress relaxation within the "window"); 2 - creep strain curve calculated out of initial relaxation curve 1.

FIG. 3. Creep data formation technique (Х16Н15М3Б steel, in-pile tensile test).

4. EXPERIMENTAL SUBSTANTIATION OF TENSOMETRIC METHOD

Since tensometric technique is non-direct remote control creep rate measurement method, some technical means and metrology procedures were developed to provide its reliability in order to obtain proper but not false results during creep test. For example, to control stability characteristics of the load cell during in-reactor operation a special standard-like dynamometer was designed to be embedded in the active draw. Another example is related to in situ metrology procedure called "absolutely strong specimen test". An "absolutely strong" specimen (hard enough to be priory not creepable) is included among the normal specimens to be tested. Thus, under the test conditions, which can activate in-reactor creep in normal specimens, creep deformation of the "strong" specimen couldn't be expected at all. In this case any results, which are measured by tensometric method like a creep deformation, simply correspond to thermal deviations in stress resistively of the elastic strained draws. In other words, the use of the "absolutely strong" specimen gives the chance to control thermally dependent characteristics of test facility in situ as well as to evaluate some possible uncertainties, which can effect creep data when real specimen is measured under tensometric technique.

The results of just described in-reactor metrology experiment with the "absolutely strong" specimen are illustrated in Fig. 4. Since any thermally dependent draws' elastic tension change (not caused by specimen's creep) is also calculated by tensometric method like a specimen's strain, this "deformation" is an error of creep measurement results, which is caused by thermal non-stability of the test facility's load training draws. As it is seen out of Fig. 4, thermal deviations realize themselves as a periodic function, which in case of real specimen test is visible superposition around the real creep curve. While calculating steady state creep rate, periodic thermal deviations can be easy filtrated by approximation of the corresponding part of the creep deformation curve by a linear function.

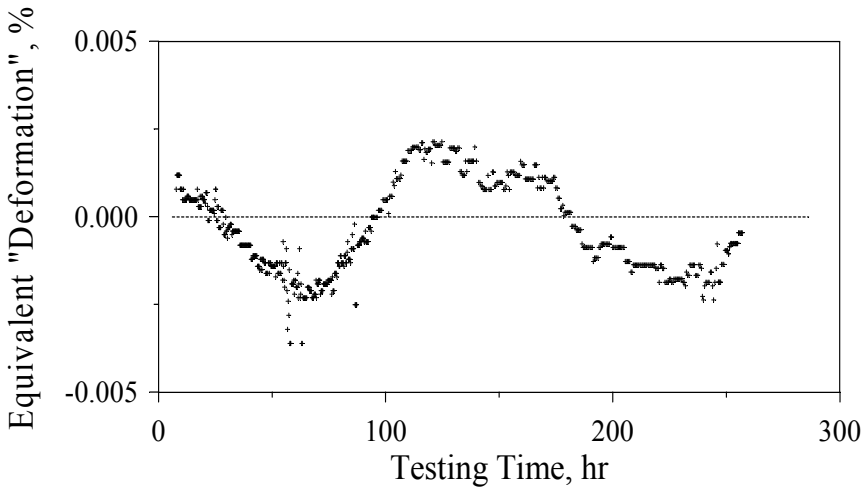

FIG. 4. Deviation of elastic tension of load-train-draws (calculated as equivalent specimen's false deformation) caused by draws' temperature deviation. In-pile torsion test, "absolutely strong" specimen, 325°C.

To obtain direct experimental evidence in substantiation of tensometric method a special experiment was carried out under laboratory out-of-reactor conditions. The test facility was bench-type full-scale functional analogue of the in-pile torsion machine used for BR-10. E110 zirconium alloy, which shows rather significant creep at stresses near the yield point even at room temperature, was chosen as a material to be tested. The creep test was performed under usual "constant" load mode. Using the tensometric method the specimen's creep deformation curve was registered. Then the "tensometric" creep results were compared with analogous results obtained under parallel direct deformation measurement based on specially made optical control system. The extent of conformity of "tensometric" results with those obtained by optical technique can be taken as a criterion of reliability of tensometric method. The results of such comparative creep measuring tests are presented graphically in Fig. 5. E110 zirconium alloy specimens were loaded up to the stress near 90% of the yield point at room temperature. As it can be seen out of fig.5, the "optical" and the "tensometric" creep curves practically coincide along the whole time of loading. This fact can be mentioned as a direct experimental confirmation of the tensometric method reliability.

5. APPLIANCE OF TENSOMETRIC TECHNIQUE FOR ZIRCONIUM ALLOYS IN-REACTOR CREEP STUDY

The best illustration of tensometric creep measurement method ability are experimental results obtained during numerous in-pile tests. For more than 20-year of BR-10 in-reactor creep test experience the tensometric test technique was applied to study irradiation creep of different materials, such as several stainless steels for fast neutron reactors, zirconium hydride, fusion reactor oriented vanadium alloy. Starting from 1993 in-pile creep experiments to investigate in-reactor creep behaviour of E110 and E635 zirconium alloys were carried in BR-10 too. As a result the main irradiation creep characteristics, such as irradiation creep module and creep rate stress dependence were determined for both alloys within rather wide interval of applied stress (Fig. 6).

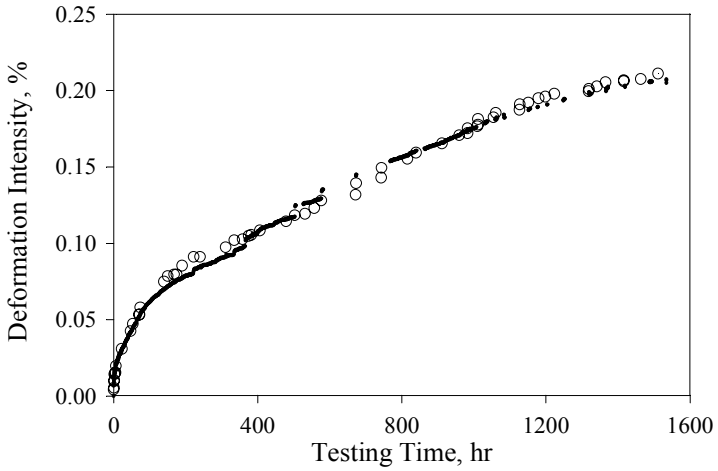

FIG. 5. Results of the parallel creep data measurements obtained with optical system (o) and by tensometric technique (x). E110 zirconium alloy, torsion test at room temperature, no irradiation.

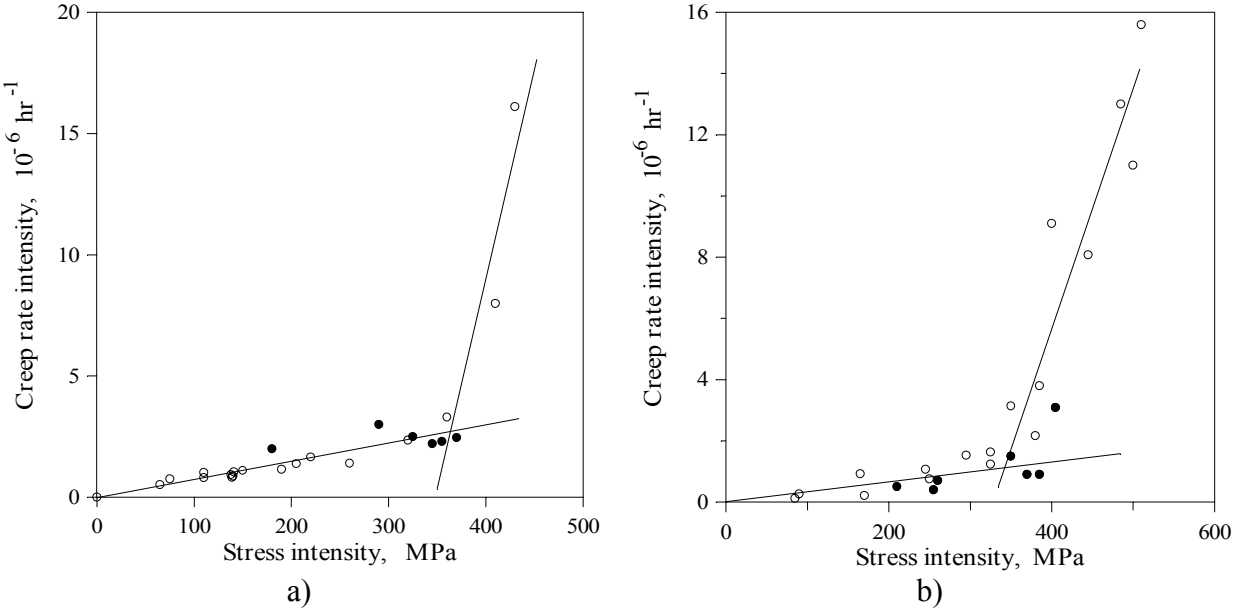

FIG. 6. Stress dependence of zirconium alloys irradiation creep rate. In-pile torsion test. a) - E110 alloy; b) - E635 alloy.

Some advantages of the tensometric in-pile test technique can be illustrated by experiments when irradiation creep was studied under "non-stable" stress conditions. It is significant, that during such tests irradiation creep process dynamics and structure become quite visible (Fig. 7). In respect to study temperature dependence of in-reactor creep, E110 alloy has been tested in reactor at different temperatures including those high enough to initiate thermal creep (Fig. 8).

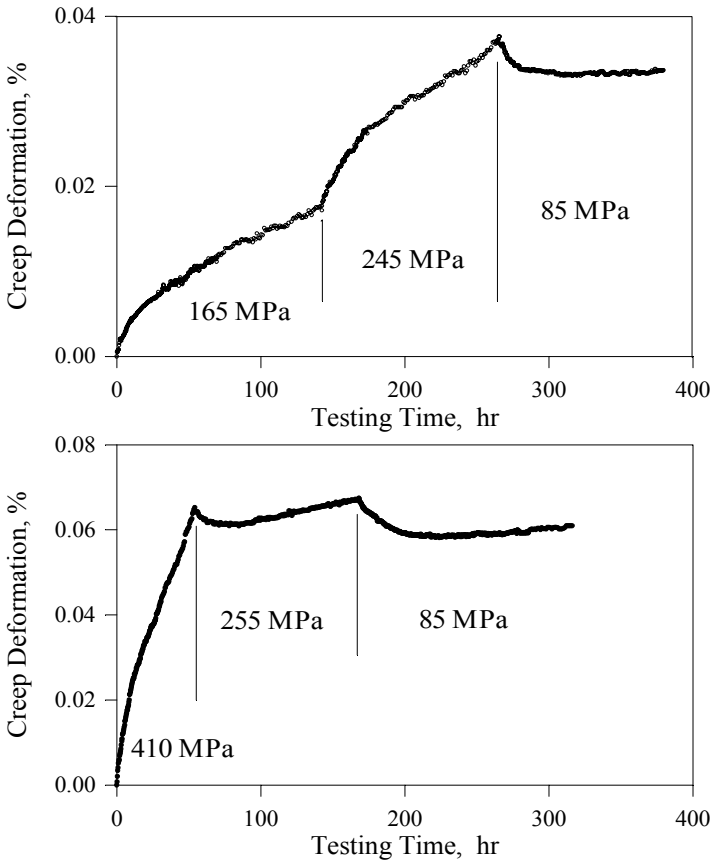

FIG. 7. Irradiation creep under consequent changeable stress application. In-pile torsion test, E635 zirconium alloy.

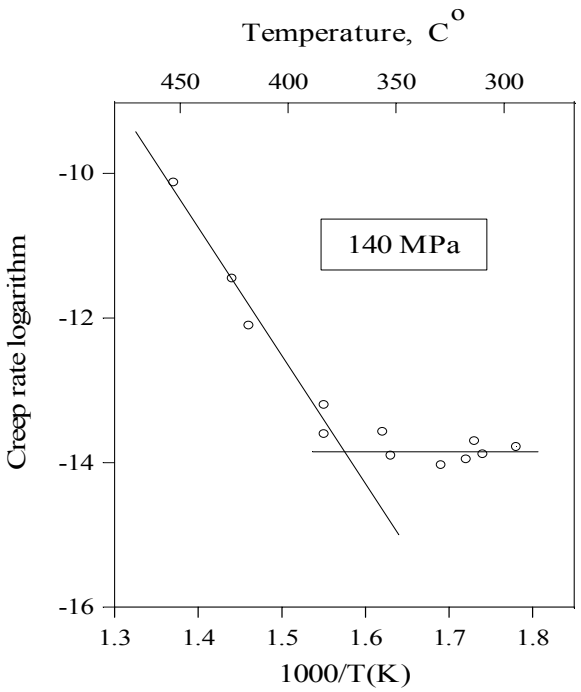

FIG. 8. Temperature dependence of E110 zirconium alloy in-reactor creep rate. In-pile torsion test.

One of the interesting result obtained under tensometric technique application is effect of "plastic deformation jumps" process accompanying irradiation creep in zirconium alloys. It was detected that within some temperature conditions creep deformation of zirconium alloy is developed as an interrupted stepping process (Fig. 9). Using a special fast registration technique it was found that during a "normal smooth creep" some periodic short term plastic deformation "jumps" occur. The inner structure of the "deformation jump", which is shown in fig.10, leaves no doubts that the observed effect is controlled by some local fast plastic deformation process (developed within several seconds) but not by creep.

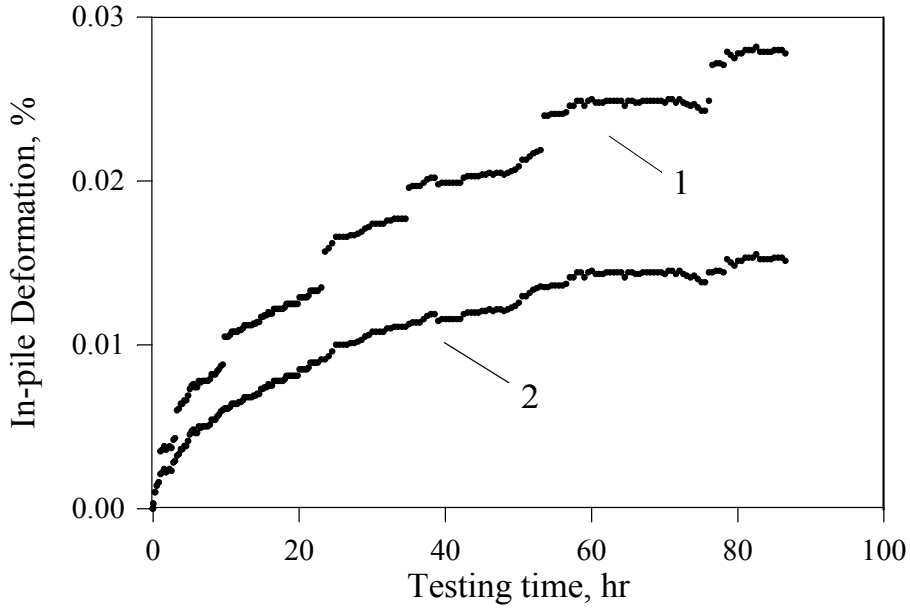

FIG. 9. Plastic deformation "jumps" effect developed during E110 zirconium alloy in-pile torsion creep test at 235°C.
1 - initial deformation curve registered during the test;
2 - "pure creep" curve recalculated by excluding of "jumps".

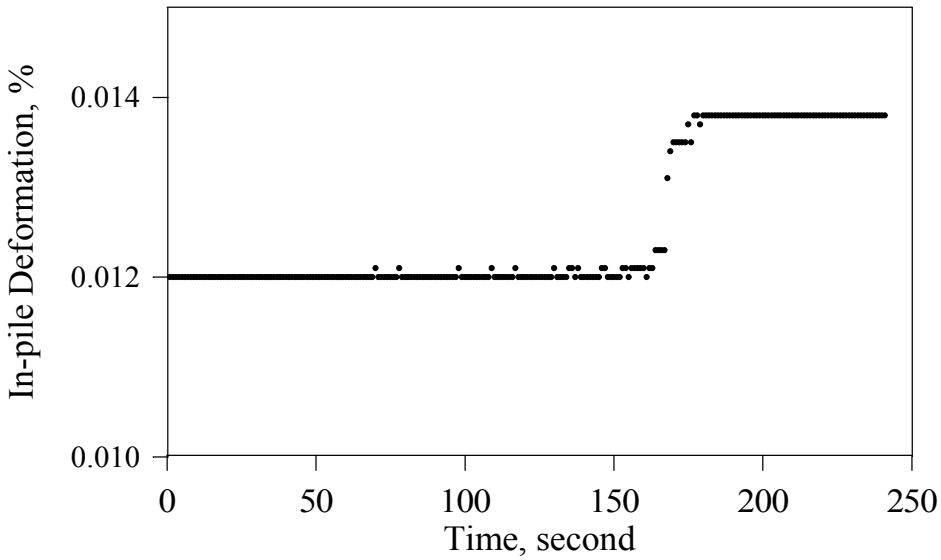

FIG. 10. The structure of plastic deformation "jump" occurred during in-pile creep test illustrated by Fig. 9.

Presented illustrations are only a small part of data collected to confirm tensometric in-pile test technique ability. More detailed description of BR-10 in-pile test results can be found in references given below.

6. CONCLUSION

To summarize the experimental evidence of tensometric technique reliability it should be underlined that this method looks to be one of the most suitable among the known instruments to study irradiation creep dynamics. Another thing to be pointed out is possibility of the tensometric technique effective use for "normal" laboratory test purposes (not under neutron irradiation), including hot laboratories too. On one hand the test facilities, properly designed and fabricated to fit the tensometric method requirements, are cheaper if compared with store-bought standard test equipment. On the other hand the differential sensitivity of the tensometric measurement technique is in many cases and for significant extent higher than that for the standard technique even when applied to laboratory conditions. While being applied to the in-reactor conditions the tensometric technique is one of the most economic and reliable method to get creep data in a relatively short time. Experimental results and data collected during more than 20-year of BR-10 in-reactor creep test experience can be assumed as a strong evidence that the tensometric technique is a powerful instrument, which can give a chance to study different irradiation effects on reactor materials directly under irradiation.

REFERENCES

[1] "Atomic Energy", v.51, 3 (1981), p. 189.
[2] "Atomic Energy", v.54, 1 (1983), p. 57 – 58.
[3] J. Nucl. Mat, 233-237 (1996), p. 381 – 384.
[4] "Atomic Energy", v.80, 5 (1996), p. 386 – 390.

MEASUREMENT OF MECHANICAL PROPERTIES
(Session 6)

Chairpersons

R. MANZEL
Germany

V. RISOVANY
Russian Federation

Advanced techniques for mechanical testing of irradiated cladding materials

V. Grigoriev, R. Jakobsson, B. Josefsson, D. Schrire

Studsvik Nuclear AB, Nyköping, Sweden

Abstract. The justification and licensing of water reactor fuel, which use new materials and designs needed for higher burnup and greater operating flexibility, require further development of different techniques for post-irradiation examination (PIE). Mechanical properties of the cladding are of special importance for the verification and licensing. A number of advanced techniques for mechanical testing of irradiated cladding materials have been recently established at Studsvik Nuclear. The techniques are mainly focused on the characterization of an axial crack in the fuel cladding and on the cladding failure under transient regimes.

1. INTRODUCTION

Further development of post-irradiation examination (PIE) techniques is required for verification and licensing of water reactor fuel using new materials and designs caused by the requirements for higher burnup and greater operating flexibility. A number of advanced techniques for mechanical testing of irradiated cladding materials have been recently established at Studsvik Nuclear. The following properties of the cladding are of main interest:

- mechanical properties in the circumferential direction;
- resistance to low-cycle fatigue failure;
- failure under conditions of a Reactivity Initiated Accident (RIA);
- axial crack growth resistance (*J*-integral);
- subcritical axial crack growth velocity (hydrogen assisted delayed cracking).

To characterize the above-mentioned properties, a number of advanced techniques for mechanical testing have been recently established at Studsvik Nuclear:

- modified ring tension test;
- low-cycle fatigue test;
- "Expansion-Due to-Compression" (EDC) test to simulate RIA conditions under fast loading;
- Pin-Loading Tension (PLT) test (*J*-integral for the cladding);
- PLT delayed cracking test (hydrogen assisted delayed cracking).

A brief description of these techniques is presented in this paper.

2. MODIFIED RING TENSION TEST

In the earlier ring test configurations the tension of a curved gage length created a number of problems. In the modified design the flattening of the ring is prevented by means of a central piece which is inserted into the ring and has almost the same dimension as the ring's internal diameter (Fig. 1) [1]. Three-dimensional FEM has been used to analyse the stress and strain distribution in the specimen, to optimize the specimen-fixture system, to take into account the effect of friction, and to derive a final stress-strain curve [2, 3]. The testing is usually performed at strain rates of 0,003-0,007 min^{-1} in the interval of temperatures from ambient to 385°C. The results show good reproducibility of the final stress-strain curves (Fig. 2) and characterize the effect of test temperature and material conditions (burnup, hydrogen concentration).

3. LOW-CYCLE FATIGUE TEST

Low-cycle fatigue testing is performed using a C-shaped specimen prepared from irradiated cladding. The testing technique is similar to that reported by Nakatsuka, Kubo, and Hayashi [4]. The symmetrical sinusoidal loading at a frequency of 1 Hz is performed in an Ar environment at temperatures of 20-350°C. The strain obtained at the specimen surface (points M and M') is calibrated at room temperature versus the loading rod displacement controlled by means of the LVDT (Fig. 3a). During the calibration test, the strain is measured by means of electric strain gages placed at the specimen surface (Fig. 3b). An example of the calibration plot obtained for an unirradiated specimen with the same nominal dimentions as irradiated cladding is shown in Fig. 3c. Test data obtained for irradiated cladding shows an effect of burnup on the number of cycles to specimen failure (Fig. 4).

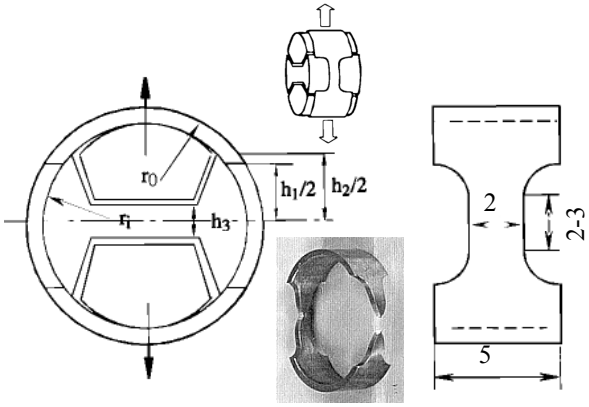

Fig. 1. Schematic of the modified ring tension test. Specimen gage length (2 or 3 mm) depends on specimen diameter (9,6 or 12,25 mm).

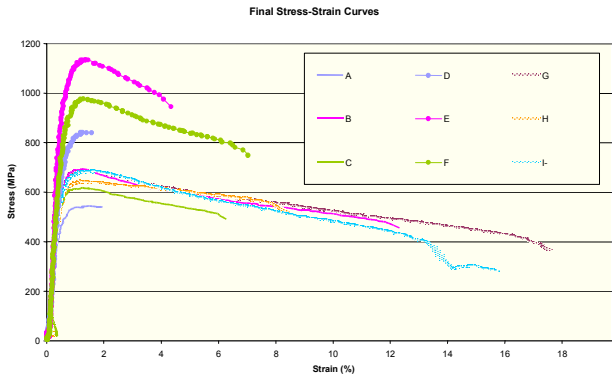

Fig. 2. Stress-strain curves obtained from the modified ring tension tests performed at 25°C and 385°C for irradiated cladding (different burnup and hydrogen concentrations).

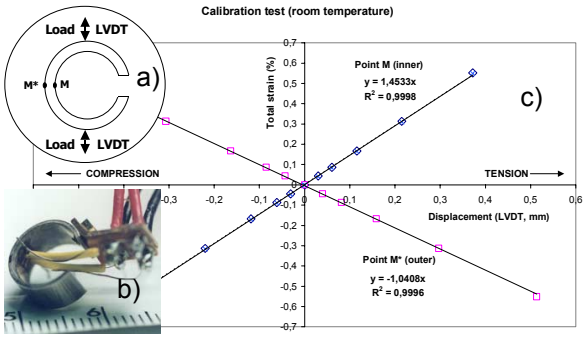

Fig. 3. Calibration data for low-cycle fatigue test of cladding materials.

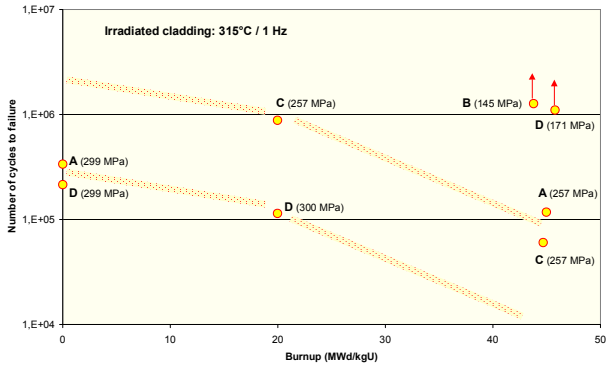

Fig. 4. Low-cycle fatigue test data for irradiated cladding showing effect of burnup on the number of cycles to failure.

4. “EXPANSION-DUE TO-COMPRESSION” (EDC) TEST

A high strain rate mechanical testing technique called the Expansion-Due-to-Compression (EDC) test has been developed at Studsvik to simulate the pellet-clad mechanical interaction (PCMI) loading of the cladding during a Reactivity Initiated Accident (RIA). A piece of irradiated cladding is loaded be means of a polymer pellet compressed axially inside the cladding specimen (Fig. 5). The loading is performed at 25-340°C during 25-100 ms and the main test parameters (axial load, machine crosshead displacement, and specimen outer diameter) are measured with a frequency of 1000 Hz. This testing technique has been used to determine the strain to failure of high burnup PWR cladding at strain rates similar to those in the pulse reactor RIA tests [5]. Specimens A and B failed at 1,5-2,3% of total hoop strain when tested at 25°C (Fig. 6). However, the same material (specimen C) did not fail after 3,7% of hoop strain when tested at 340°C and only failed after 7,3% of strain (specimen D) when tested during 30 ms at 340°C.

Recently, a method for experimental evaluation of the critical strain energy density (CSED) for cladding materials tested by means of the EDC test has been proposed (Fig. 7) [6]. When the data for specimen diameter under the loading are recalculated into the hoop strain and are plotted versus the energy absorbed by the specimen, the data for all specimens follow the same trend (Fig. 8). Based on the specimen diameter measured at the moment of failure, the CSED values obtained for the PWR cladding are in the interval from 15-25 MJ/m^3 for room temperature tests and up to 70-80 MJ/m^3 at 340°C. The derived CSED values are reasonably comparable to the values predicted in the literature for the CABRI REP Na test rods.

5. PIN-LOADING TENSION (PLT) TEST

The Pin-Loading Tension (PLT) technique is used to characterise the properties of an axial crack in irradiated cladding [7-9]. A sharply notched PLT-specimen is manufactured from the cladding tube (Fig. 9a). The specimen is axially notched at both edges. The notches at the front edge of the specimen are sharpened with fatigue cracks.

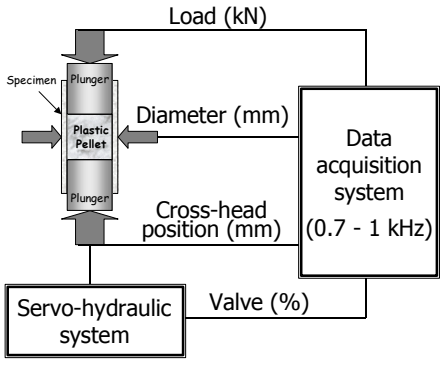

Fig. 5. Schematic of the EDC test for RIA simulation.

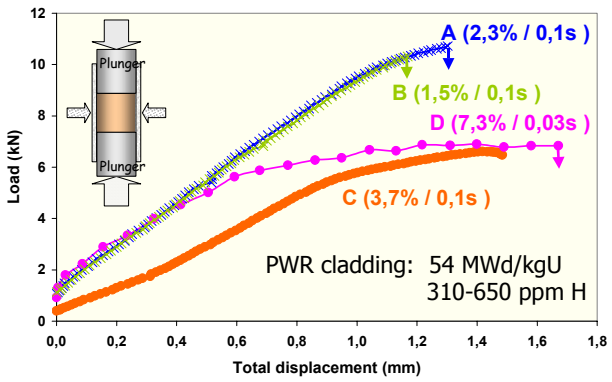

Fig. 6. The record of load versus machine cross-head displacement obtained from the EDC tests for high burnup PWR cladding [5]: test temperature 25°C and 340°C, loading during 0,1s or 0,03s. Specimens A, B, and D failed at different total hoop strain of the specimen. Data for each specimen are shown in brackets.

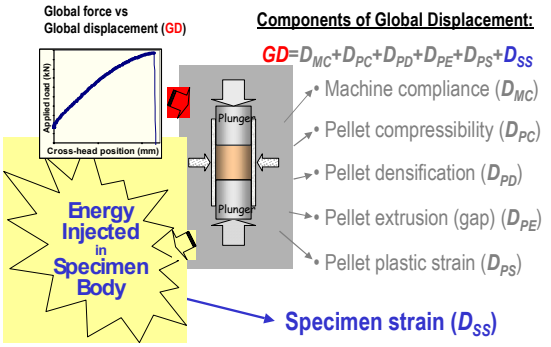

Fig. 7. Schematic of the processes involved in the EDC test (for details read Reference [6]).

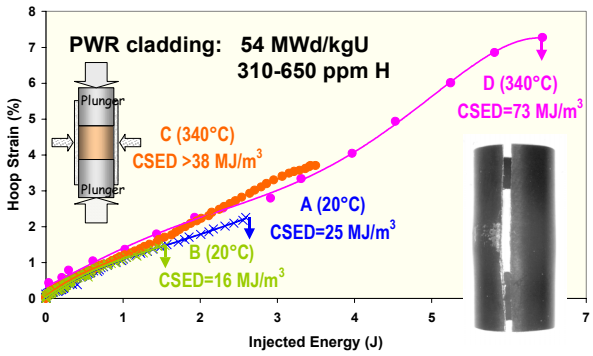

Fig. 8. The data from Fig. 6 re-calculated as the specimen hoop strain versus the injected energy (IE). At specimen failure, the IE being related to the specimen volume is transformed to the CSED.

The PLT-fixture consists of two halves, which when placed together form the cylindrical holder (Fig. 9b). This cylindrical holder has a diameter, which allows it to be inserted into the tubular PLT-specimen, while maintaining a minimal interfacial gap. The fixture halves, being loaded in tension through the pins, have the capability of mutual rotation around the axis determined by a small pin placed between the fixture halves at the end of the cylindrical holder. The rotation of the fixture halves is similar to the rotation of compact specimen (CT) halves under tension, with only one difference: in the PLT-fixture the rotation axis does not change its position when the crack propagates in the specimen.

The specimens are fatigue pre-cracked and then loaded in displacement control to produce about 1 to 2 mm of crack growth. The load and load-point displacement are monitored during the loading to plot the load-displacement record (*LDR*). After unloading, the crack extension area is marked again by short-term fatigue, and the crack extension is measured for two fracture surfaces of the specimen. The average value of the crack extension is used for specimen characterisation. The crack extension during the testing can be monitored by means of DC potential drop measurements (Fig. 10).

The *J*-integral values are calculated from the *LDR* and plotted against the corresponding crack extensions [10]. That plot represents a *J*-resistance curve of the specimen. The *J*-resistance curve obtained for each specimen is used to establish a crack initiation point, $J_{0.2}$, which is the *J*-integral value at the intersection of the 0.2 mm offset line and the *J*-resistance curve. The initial crack growth toughness, dJ/da, is obtained as a linear regression slope of the *J*-resistance curve between the 0.15- and 1.5-mm offset lines (Fig. 11).

6. PLT DELAYED CRACKING TEST

The same experimental set-up as for the PLT fracture toughness testing can be used for the measurements of Delayed Hydride Cracking velocity in Zircaloy cladding [11]. Currently, PLT-specimens with two different lengths, 9 and 13 mm, have been used (see Fig. 9). The pre-cracked hydrided specimen is heated in air and loaded after a specified thermal cycle. To monitor crack growth under the constant load applied to the specimen, the DCPD technique is used. The loading of the specimen is usually accompanied by a step-wise increment of the DCPD reading followed by a gradual increase of the DCPD values (Fig. 12).

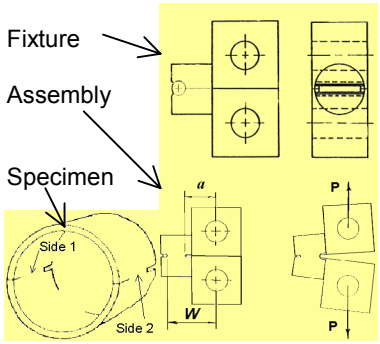

Fig. 9. Schematic of the PLT specimen, fixture, and specimen-fixture assembly.

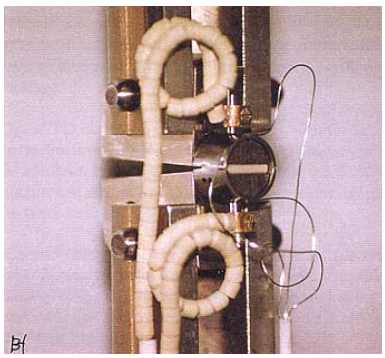

Fig. 10. The PLT specimen with attached DCPD probes mounted in the testing machine.

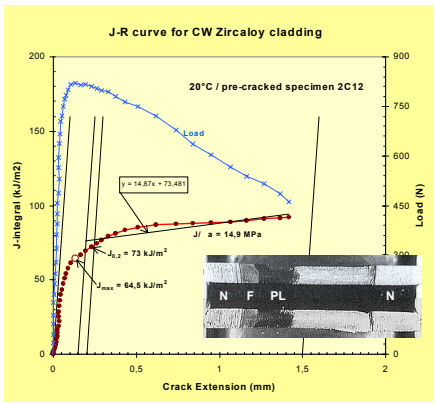

Fig. 11. An example of J-resistance curve and fracture surface of hydrided Zircaloy specimen (200 ppm) tested at 25°C.

Cracking is allowed to continue until the crack has grown about 2 mm. The load is then removed, the furnace is opened and the specimen cooled down to room temperature. The unloading of the specimen is usually accompanied by a step-wise decrease of the DCPD reading (see Fig. 12).

The end of the crack is marked by means of a short-term fatigue. An example of specimen fracture surface obtained after the PLT delayed cracking test is also shown in Fig. 12.

Independently of the specimen length, 9 or 13 mm, good reproducibility of the axial crack velocity, V_{DHC}, is observed. The V_{DHC}-values for 10 identical specimens tested fell within the interval of $2.6 \cdot 10^{-8}$ m/s to $3.0 \cdot 10^{-8}$ m/s. This is slightly below the axial crack velocities earlier obtained for Zr-2.5Nb CANDU pressure tube material tested at the same temperature (315°C / 250°C) and stress intensities (15-25 MPa√m) [12]. Presently, the measurements of delayed cracking velocity for an axial crack in irradiated Zircaloy cladding are in preparation.

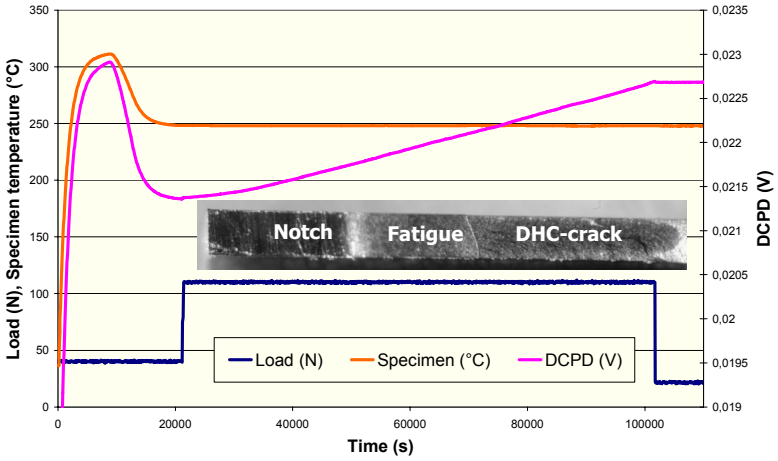

Fig. 12. An example of the data record for entire DHC test performed for hydrided Zircaloy cladding (200 wtppm). The DHC-crack area extended during the time under constant load of 110 N is clearly distinguished at the specimen fracture surface (one side of the specimen is shown).

7. SUMMARY

A number of advanced techniques for mechanical testing of irradiated cladding have been recently established at Studsvik. The experience accumulated at Studsvik in this field can be seen from the table below (up to May 2001): The techniques are shown to be effective for: 1) revealing the effects of burn-up/fast neutron fluence, hydrides, oxide thickness, *etc.* on mechanical properties of the fuel cladding and 2) characterizing the behaviour of an axial crack in the cladding.

	Tested Specimens	
Test Method	Unirradiated	Irradiated
Modified ring tension test	10	> 60
Low-cycle fatigue test	6	18
EDC-test (RIA simulation)	30	24
PLT fracture toughness test	> 90	13
PLT delayed cracking test	10	In preparation

REFERENCES

[1] JOSEFSSON, B. and GRIGORIEV, V., Modified ring tensile testing and a new method for fracture toughness testing of irradiated cladding. Presented at the European Working Group Hot Laboratories and Remote Handling Meeting, May 14-16, 1996, Petten, Netherlands.

[2] ARSENE, S. and BAI, J., A new approach to measuring transverse properties of structural tubing by a ring test. J. of Testing and Eval., Vol. 24, No. 6, Nov. 1996, pp. 386-391.

[3] ARSENE, S. and BAI, J., A new approach to measuring transverse properties of structural tubing by a ring test - Experimental investigation. J. of Testing and Eval., Vol. 26, No. 1, Jan. 1998, pp. 26-30.

[4] NAKATSUKA, M., KUBO, T., and HAYASHI, Y., Fatigue behaviour of neutron irradiated Zircaloy-2 fuel cladding tubes. ASTM STP 1132, American Society for Testing and Materials, PA, 1991, pp. 230-245.

[5] GRIGORIEV, V., SCHRIRE, D., JAKOBSSON, R., JOSEFSSON, B., and JONASSON, A., Mechanical testing of high burnup PWR cladding to simulate RIA. Jahrestagung Kerntechnik 2000, May 23-25, 2000, Bonn, Germany. ISSN 0720-9207, pp. 359-362.

[6] GRIGORIEV, V., JAKOBSSON, R., and SCHRIRE, D., Experimental evaluation of Critical Strain Energy Density for irradiated cladding under simulated RIA conditions. Presented at ENS Topfuel 2001 Conference, May 27-30, 2001, Stockholm, Sweden.

[7] GRIGORIEV, V., JOSEFSSON, B., and ROSBORG, B., Fracture toughness of Zircaloy cladding tubes. ASTM STP 1295, American Society for Testing and Materials, PA, 1996, pp. 431-447.

[8] GRIGORIEV, V., JOSEFSSON, B., ROSBORG, B., and BAI, J., A novel fracture toughness testing method for irradiated tubing - Experimental results and 3D numerical evaluation. Transactions of the 14-th International Conference on Structural Mechanics in Reactor Technology (SMiRT-14), Vol. 2, Division C-4, 1997, pp. 57-64.

[9] LYSELL, G., GRIGORIEV, V., and EFSING, P., Axial splits in failed BWR fuel rods. Presented at ANS International Topical Meeting on Light Water Reactor Fuel, Park City, Utah, USA, April 10-13, 2000.

[10] GRIGORIEV, V., PETTERSSON, K., and ANDERSSON, S., Influence of texture on the fracture toughness of unirradiated Zircaloy cladding. ASTM STP 1354, American Society for Testing and Materials, PA, 2000, pp. 303-315.
[11] GRIGORIEV, V. and JAKOBSSON, R., Application of the Pin-Loading Tension test to measurements of Delayed Hydride Cracking velocity in Zircaloy cladding. Report SKI-00:57 (November 2000).
[12] GRIGORIEV, V. and JAKOBSSON, R., IAEA Co-ordinated Research Program: "Round Robin" on Measuring the Velocity of Delayed Hydride Cracking (DHC). Report SKI-99:39 (September 1999).

Special techniques for tensile tests of irradiated zirconium claddings

V.I. Prokhorov, O.Ju. Makarov, V.P. Smirnov

State Scientific Center of Russian Federation, Research Institute of Atomic Reactors, Dimitrovgrad, Uljanovsk Region, Russian Federation

Abstract. Irradiated zirconium alloy claddings possessing property anisotropy should be tested in transverse and longitudinal directions. Such mechanical tests can be performed in conditions of large variety of geometric peculiarities of specimens, supports or grips. The objective of the work is the development of the unified complex of updated special techniques that allow investigation of mechanical pre- and post-irradiation properties of VVER claddings including radiation effect of property anisotropy changes in the same way.

1. RINGS TESTS

We determine mechanical properties of zirconium claddings in transverse direction by tensile tests of simple ring specimens using special semi-cylindrical support, Fig.1. Loading is carried out up to the specimen rupture at the predetermined temperature and active grip speed (or machine traverse). Tensile load (force) against traverse displacement is recorded (Fig. 2). The strength and plastic characteristics, known out of classical tensile tests, are calculated on the basis of the load-displacement diagram record.

While determining uniform and total elongation from simple ring specimens some methodological difficulties arise because of deformation non-uniformity at different segments of the tensile ring. This problem is solved by choosing a special specimen form with well-defined working length or by performing special tests allowing choosing empirical correlation that might identify elongation parameters correctly. The approximation developed by us is based on the usage of some effective length of a simple ring specimen as a gauge length. It is calculated by the expression:

$$l_g = \frac{\pi \overline{D}}{2} - K \frac{\pi d_m}{2} \quad ,$$

where l_g = gauge length of the ring specimen;
D = average diameter of the cladding tube;
d_m = support diameter;
K = empirical coefficient.

For about 30 years supports with d_m = 4 mm and coefficient K = 0.85 have been used for testing the VVER claddings with the outer diameter of 9.14 – 9.15 mm and the inner diameter of 7.72 ± 0.008 mm.

Analysis and the recent additional investigations made it possible to modify the procedure of testing and processing of primary diagram of simple ring specimens tension and also improved the existing technique in accordance with current requirements and technical capabilities [1,2].

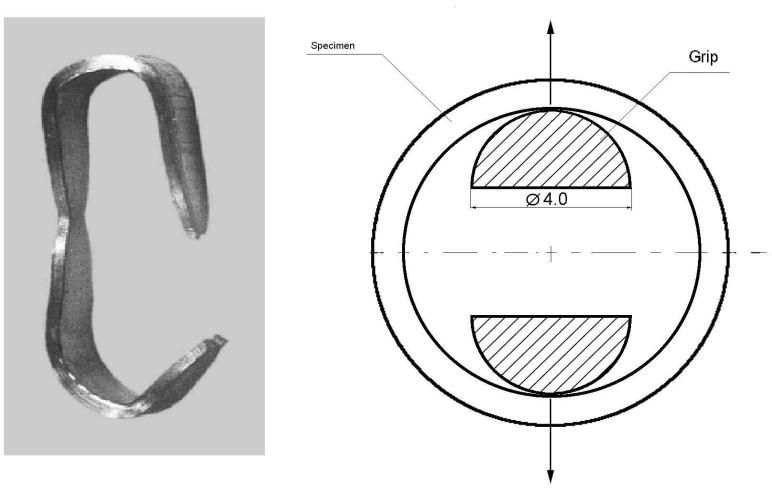

FIG. 1. Cross-section of supports with simple ring specimen and general view of the specimen after testing.

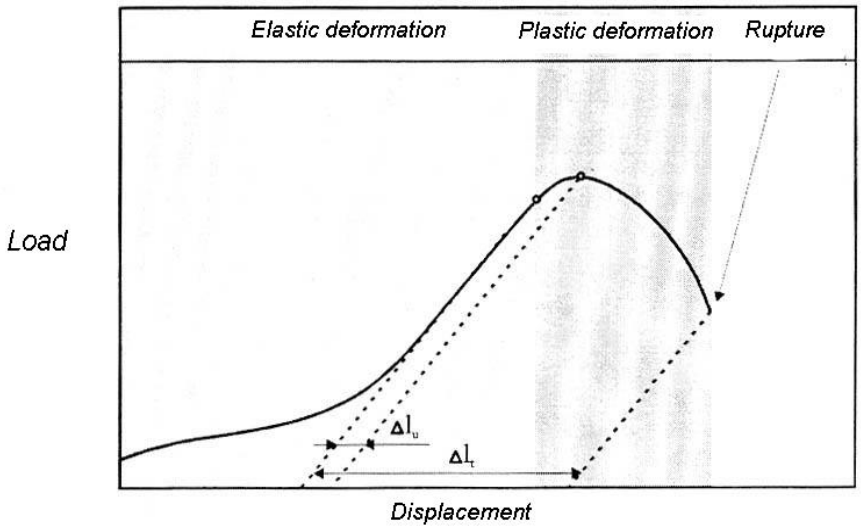

FIG. 2. Plan of the load-displacement diagram.

2. TUBE SAMPLES TESTS

Investigations of mechanical properties of zirconium tubes of small diameter (D≤25mm) in longitudinal direction are performed on sections (tube samples) with full-size cross-sections. Such tests are provided by the standards of a number of countries (ASTM E8M-93, EN10002-5: 1991, GOST 10006-80). Wedges and collet chucks using pipe plugs and basic dimensional proportions (as, for example, at Fig.3, 4) are recommended by these standards. Using this type of the specimens fastening, the tests are performed at 1794U-5 test machine, NIKIMP, (Moscow), equipped with a furnace, in which heating and holding of the sample at the testing temperature are performed at the air (advisable up to the temperature of 500^{o}C). The alternative method of samples fastening was developed in order to use the available machines with vacuum furnaces (1931U-1, 1236R-1/1500 and IR4106), as well as for more effective remote operation using manipulators. This method consists in samples fastening using welding plugs with button heads that are analogous to those made for cylindrical samples.

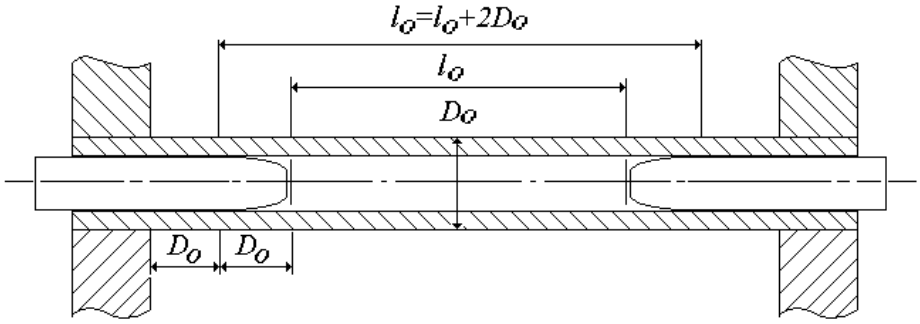

FIG. 3. Dimension proportions of the sample and plug shape according to GOST 10006-80.

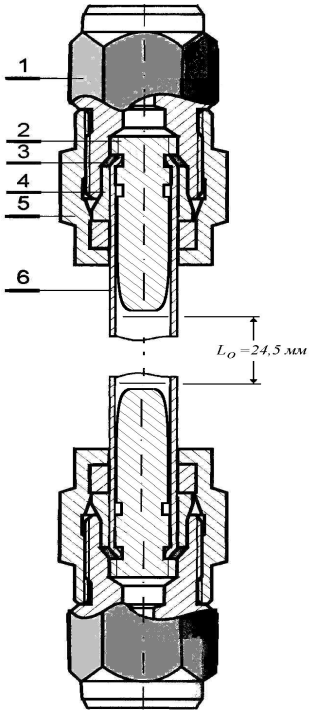

1 – back nut *2 – inner plug*
3 – clamping ring *4 – fit ring*
5 – captive nut *6 – sample*

FIG. 4. Collet chuck for tube sample fastening (Ø9.15x0.7x84 mm).

Shielded-arc welding in argon environment was used for sample manufacturing (drawing 3B.2504.000.00). Mode of girth welding was adjusted for the particular material and provides the use of cooling collet-chuck for the end temperature effects tracing.

The tests of the specimens with marked operating length (by marks at every 1mm at the length of 45mm) were performed for investigation of the behavior during tension of the specimen with welded caps and for evaluation of the accuracy of the chosen dimensions.
The results of the sequential summation of the inter-mark elongations at both sides of the rupture place, and as decreased, are given for different test temperatures in Fig.5. The obtained curves prove that more then 90% of the total elongation are performed on the basis of 25 inter-mark intervals, and in its turn it practically agrees with the standard calculated length, which is accepted as $5{,}65\sqrt{F_0}$.

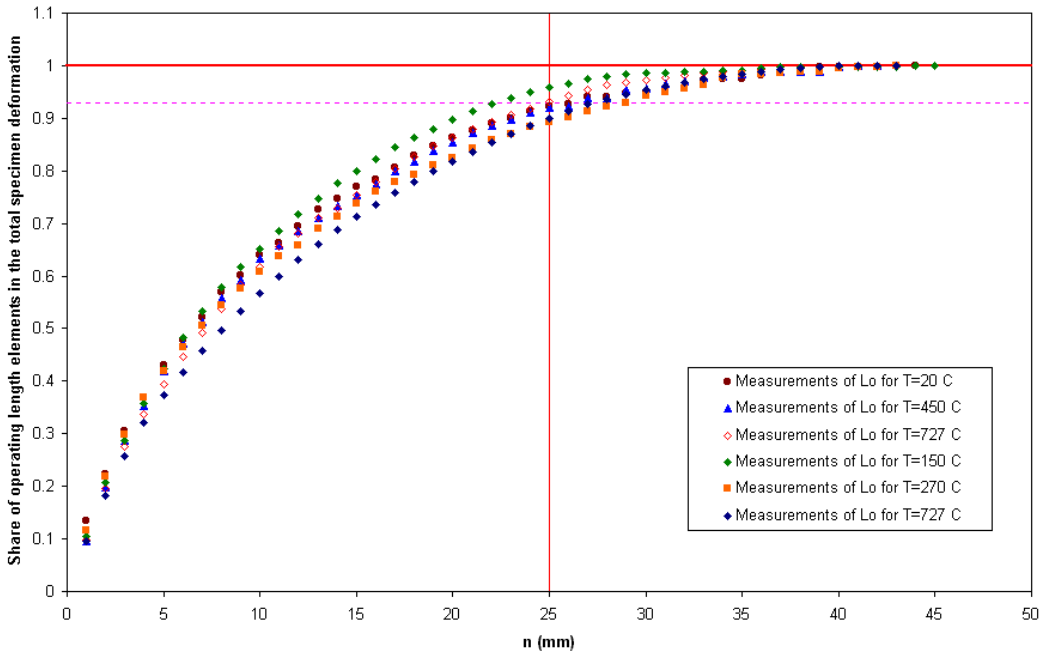

FIG. 5. Operating length of VVER non-irradiated specimens.

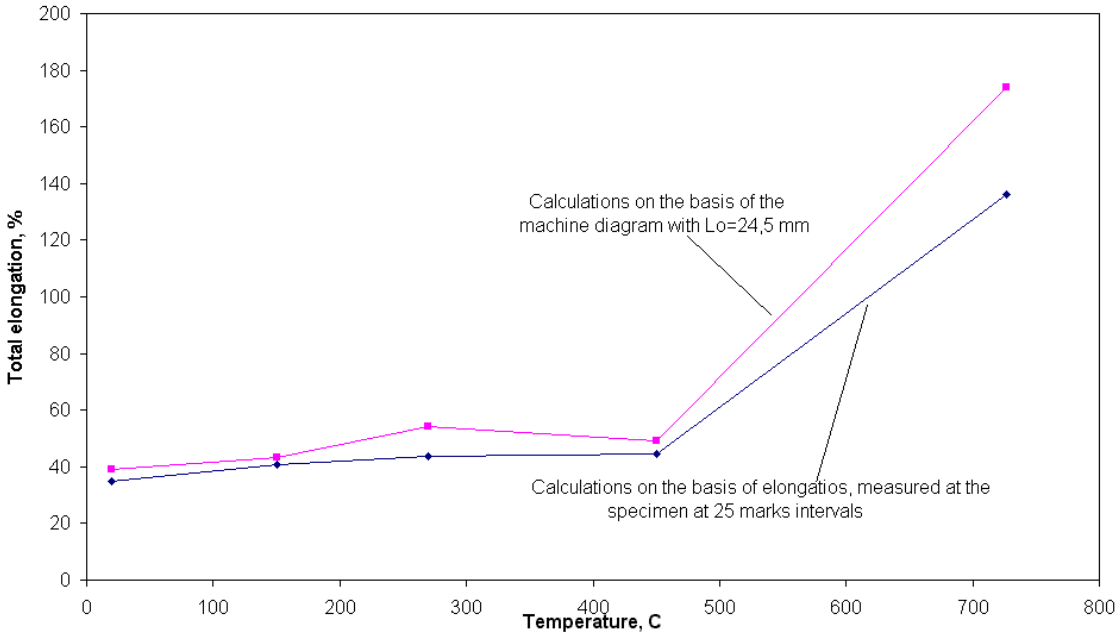

FIG. 6. Dependence of the total elongation upon temperature.

When comparing the total elongation values, calculated on the basis of elongations at 25 inter-mark intervals measured from specimens with values obtained by formal calculation of the machine diagram with l_o=24,5mm the close agreement of all temperatures below 727°C occurs (Fig.6). At the same time no signs of residual deformation in the weld area and at the Ø6mm plug section were observed. For temperature of 727°C the formal calculation highly inflates the elongation (the difference is nearly 40% of elongation). It is connected not only

with considerable elongations beyond the limits of operating length. It is also connected with the peculiarities of the cladding rupture when the complete specimen fragmentation into two parts is not observed, as long as the last fiber exists in the neck which was actually failed long ago and has widely departed fragment edges of the specimen that formally is not yet ruptured. The results obtained at 727^{o}C and at 927^{o}C appear to be very sensitive to any changes of test conditions (such as deformation speed, vacuum depth in the furnace, machine type). Therefore, the data, calculated according to the primary diagrams, should be corrected with consideration of the results obtained from the elongations measurements directly at the specimens.

3. DOUBLED LONGITUDINAL SPECIMENS TESTING

The behavior of the longitudinal specimens of various configuration and dimensions during tension in comparison with tube-samples with full cross-section, provided for GOST 10006-80 was investigated at the end of the last year.

The performed tests and a number of preconditions, connected with the test peculiarities of irradiated materials, allowed to give preference to the doubled longitudinal specimen in which the proportion of operating length and cross-section is adjusted the same as in the simple ring specimen in accordance with СТП 086-373-99 technique.

Thus, the doubled longitudinal specimen should be 2.8mm in width and 8mm in operating length while testing the claddings with diameter of 9.15mm made of E110 alloy that is used for VVER fuel elements. Fig. 7 presents the chosen specimen draft drawing and the insert-plugs, which should be reasonably used for maintenance of the stable shape of heads and of the whole specimen.

Fig. 8 presents the draft drawing of grips and pins, which are the part of fixture while loading of the chosen specimen in the testing machine 1794U-5 for insuring the tests to be performed within the temperature range of 20–500^{o}C.

Fig. 9 presents the view of the specimen in two projections. It is obvious that undesirable geometry affects are practically not observed and that the deformation process mainly occurs on in the limits of the specimen operating length. This result is not random, but it repeats in all cases of the similar investigations of specimens from the given batch (8 pieces). The investigation of the efficiency of the extensometer usage for more precise measurement of longitudinal specimen elongation characteristics from the cladding of Ø 9.15mm was also performed.

Fig.10 (a, b) presents the proved configuration “specimen – fixture – extensometer”. In this configuration the very important thing is matching of initial basic length of the specimen with the extensometer operating range and with the possibility to fix extensometer correctly stably directly on the specimen, including even the choice of the suitable radius of the conjugation of the operating section and specimen head. Meeting all the mentioned requirements allows for excluding unnecessary deformations from the tension diagram, Fig.11. Such types of tests have not been performed before.

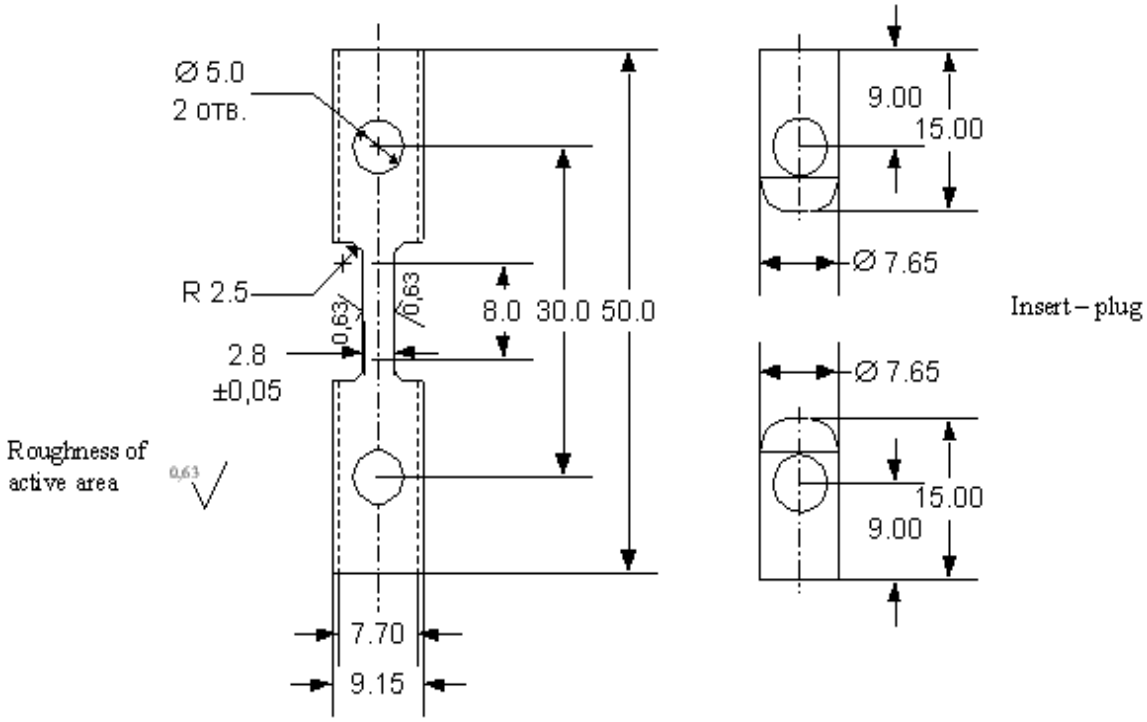

Fig.7. Draft drawing of the longitudinal specimen and insert-plugs

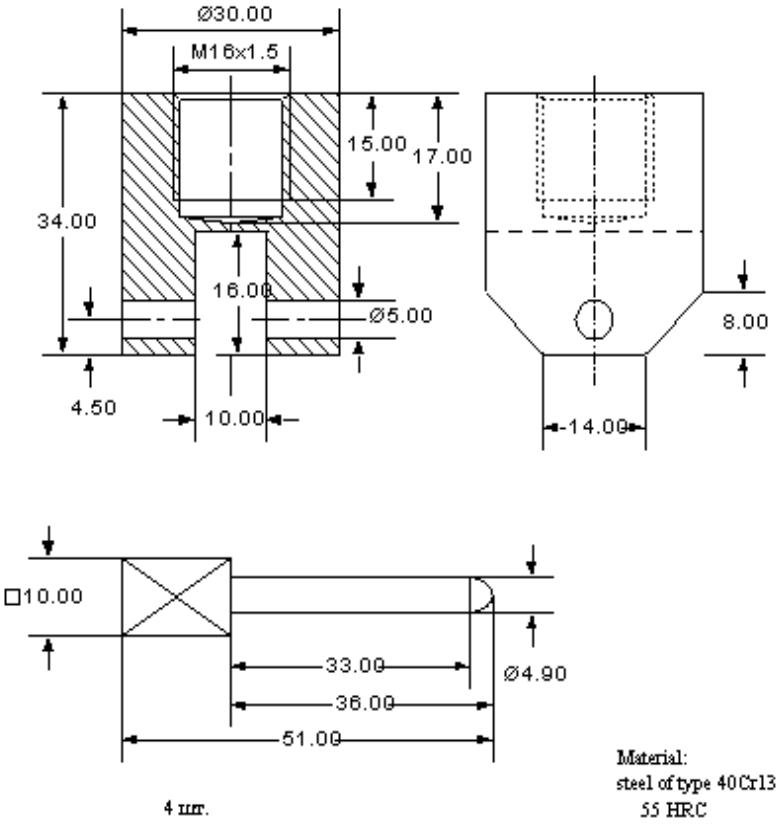

Fig.8. Grips and pins for performing the doubled longitudinal specimen tests

FIG. 9. The view of the tested specimen in two projections.

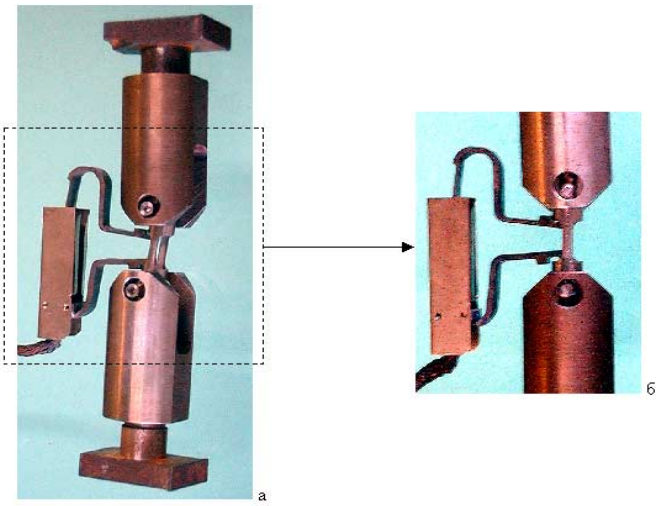

FIG. 10 a.b. Configuration "specimen – fixture – extensometer".

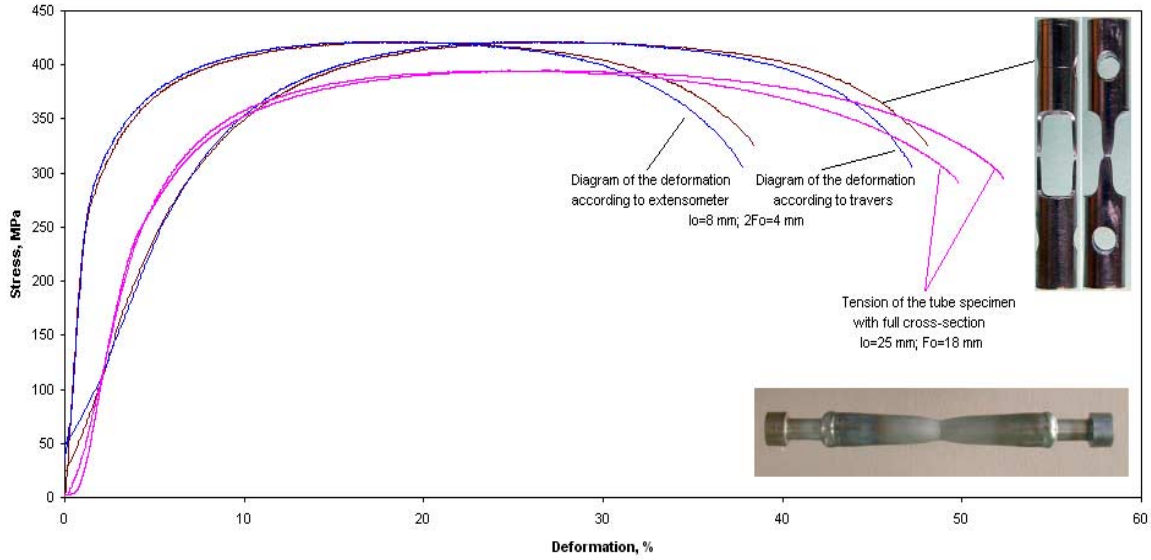

FIG. 11. Deformation diagrams of longitudinal tube samples of Ø 9.15mm made of E110 alloy.

4. CONCLUSION

Thus, all necessary technique elements and the sequence of specimen tests in longitudinal direction were developed, the technique was put into practice and approbated. Its parameters applying to VVER cladding materials allow for obtaining the results that can be compared with the data obtained while simple ring specimens testing in transverse direction. This comprises the basis for unified special techniques that allow for investigating of the claddings pre- and post-irradiation mechanical characteristics including radiation effects of property anisotropy changes.

REFERENCES

[1] O.Ju. MAKAROV, V.I. PROKHOROV, A.V. GORYATCHEV et al, Improved measurement techniques for Zr-1%Nb alloy claddings mechanical properties while simple ring specimens testing, in Abstracts for VI Russian Conference for Reactor Material Science, Dimitrovgrad, September 11–15, 2000.

[2] Plant Standard STP 085-373-99 “Technique for ring specimens of zirconium alloy thin-wall tubes tension measurement”, October 28, 1999.

Sample preparation for special PIE-techniques at ITU

E.H.Toscano[a], R. Manzel[b]

[a]European Commission, Joint Research Centre, Institute for Transuranium Elements, Karlsruhe, Germany
[b]Framatome ANP GmbH, Erlangen, Germany

Abstract. Several sample preparation techniques were developed and installed in hot cells. The techniques were conceived to evaluate the performance of highly burnt fuel rods and include: (a) a device for the removal of the fuel, (b) a method for the preparation of the specimen ends for the welding of new end caps and for the careful cleaning of samples for Transmission Electron Microscopy and Glow Discharge Mass Spectroscopy, (c) a sample pressurisation device for long term creep tests, and (d) a diameter measuring device for creep or burst samples. Examples of the determination of the mechanical properties, the behaviour under transient conditions and for the assessment of the corrosion behaviour of high burnup cladding materials are presented.

INTRODUCTION

In recent years, the extensive application of non-destructive pool techniques has changed the focal point of post-irradiation examinations in the hot cells to more specialised destructive examinations. The steadily increasing fuel assembly discharge burnups and power levels ask for more elaborated techniques aiming to evaluate in great detail the cladding behaviour at high burnup and to better characterise the properties of highly burnt fuel.

To cope with the new requirements and with the support of the European nuclear industry, several remote-handling techniques for sample preparation were installed in the hot cell of ITU.

1. SCOPES OF THE PIE-TECHNIQUES

1.1 Re-fabrication

Transient testing can only be performed in material testing reactors using short rodlets. Whilst in the past ramp testing of pre-irradiated segments was the common practice [1], today the re-fabrication of standard rods became the customary procedure. The advantage of this technique is that any standard fuel rods, irradiated in commercial power reactors, can be selected for re-fabrication and further testing according to in-service criteria (burnup, oxidation level, etc.).

After irradiation in a power reactor to the desired burnup and detailed post-irradiation examination in the hot cell, the original fuel rods are cut and re-fabricated [2] according to the following operation sequence:

- Approximate cutting avoiding spacer positions to ensure uniformity over the segment length
- Adjusting of the length previous to the conditioning of the ends

- Preparation of the upper and lower end
- Welding of the end plugs
- Gas filling and pressurisation
- Conditioning for shipment
-

The main operations to be performed, besides the cuttings, are the cleaning of both ends of the segments from the fuel and the welding of new end caps to the previously prepared ends. To this goal two devices were developed: a lathe for the machining of the extremities of the segments and a Tungsten Inert Gas (TIG) welding system, which will be described below.

1.2 Creep tests

In the last years, the discharge burnup of the light water reactor fuel has been increased continuously, among other things by introducing high corrosion resistant cladding materials. Since dry storage is gaining more and more importance for interim storage, it has become necessary to assess the creep-rupture behaviour of cladding materials used for high burnup fuel rods[3] under these condition.

Creep testing on irradiated cladding has to be performed to demonstrate the strain capability of highly irradiated materials. Two types of test were installed in the hot cells: a short term creep simulation and a long term creep test performed over a realistic time span (≥ 1 year).

In this context, samples from high burnup fuel rods have been prepared for creep testing. The sample preparation and evaluation comprise:

1. Retrieval of the fuel
2. Preparation of the extremities of the sample
3. Pressurisation with gas (He)
4. Measurement of the diameter at the end of each heating period.

Previous to the test, the fuel inside the fuel rod samples has to be retrieved and the extremities prepared for the end cap welding. Before each heating period, the sample diameter has to be measured to establish the permanent strain. In section 2, the fuel removal machines, the gas pressurisation system and the diameter-measuring device will be described.

1.3 Corrosion phenomena

To meet the requirements of the new challenging operating conditions improved zirconium based materials are a prerequisite. Severe fuel duty can lead to local steam formation and might result in new corrosion phenomena such as H-induced accelerated corrosion, Li-corrosion, and O-induced nodular corrosion.

Two techniques were installed in glove boxes at ITU to study such corrosion phenomena: Glow Discharge Mass Spectrometer (GDMS) and Transmission Electron Microscope (TEM).

1.3.1 Transmission Electron Microscopy

Improvements in the process control of heat treatments and optimisation of the chemical composition of zirconium alloys are of essential importance for the amelioration of the

corrosion properties. In particular, alloying elements such as Fe, Ni and Cr, which appear in the form of second-phase particles due to their low solubility in the zirconium matrix, play an important role in determining the corrosion properties of cladding materials.

TEM is used to determine the amount and size of second-phase precipitates.

1.3.2 Glow Discharge Mass Spectrometry

Some chemicals, like B and Li, are added to the reactor cooling water to control reactivity and pH-value. In order to understand the influence of boron and lithium on the mechanism and kinetics of corrosion of zirconium alloys, it is necessary to study the diffusion properties of these elements into the zirconium oxide layer.

For a thickness of the oxide layer of a few tens of micrometers, the GDMS is the appropriated technique to study the concentration profile of the incorporated B and Li in the corrosion layers.

Since, as previously mentioned, the two techniques are installed in ad-hoc glove boxes and not in the hot cells, the samples to be transferred for analysis should be as small as possible and should not include fuel pieces attached to it. A careful cleaning of the cladding is necessary to achieve this requirement. This could be achieved using the device described in Section 2.

2. SAMPLE PREPARATION TECHNIQUES

2.1 Fuel removal machine

Based on a commercial drilling machine with hammer action, a device was developed to remove the fuel from segments of irradiated fuel rods, Fig. 1. The device uses a hard metal drilling tool, fixed during the operation while the rotating fuel rod sample is displaced down onto the fixed drill bit. The system allows a smooth vertical displacement through counterweights, which maintain the sample in quasi-equilibrium during the drilling operation in such a way that the operator has to pressure the sample onto the drilling tool with the manipulator, permitting a careful control of the drilling operation. A special container, provided with sliding sealing, was developed to contain the fuel remnants avoiding the spreading of the fuel particles in the hot cell. After drilling the fuel is sealed in an ad-hoc capsule for the ultimate disposal.

The diameter of the drilling tool was normally around 1 mm smaller than the nominal internal diameter of the sample. Special care was exercised during the drilling operation to avoid damage of the sample wall or to cause the deformation of the sample. Drilling periods were alternated with pauses, to avoid the sample heat-up during the drilling procedure.

2.2 Cladding Machining

As previously described, for several tests cladding with materials, the sample preparation requires an accurate machining of the cladding surface. For instance, it is necessary to weld new end caps (re-fabrication and creep- and burst-test samples) or the carefully cleaning of the internal part of the fuel rod to reduce the sample activity for its handling outside of the hot cells (GDMS and TEM).

Considering that the fuel-cladding interaction at the burnups of interest (more than 50 GWd/tU) can be large, an additional technique was developed to partially remove the interaction layer in the grip zones. To reach this goal, a lathe modified for use under remote controlled conditions and provided with special grinding tools was installed in a hot cell *(Fig. 2)*. The device was used to remove the remaining fuel and, partially, the interaction layer. Calibrated gauges then measure the internal diameter of the sample and the value used to elaborate the end caps to a tolerance of about 20 µm.

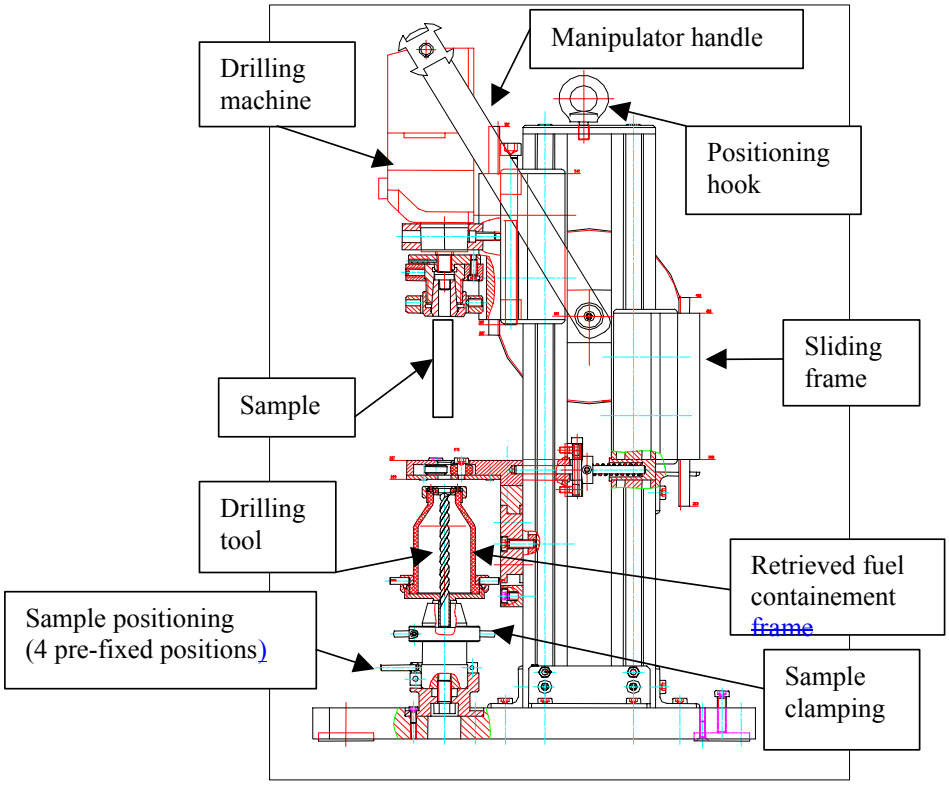

Fig. 1. Fuel removal machine.

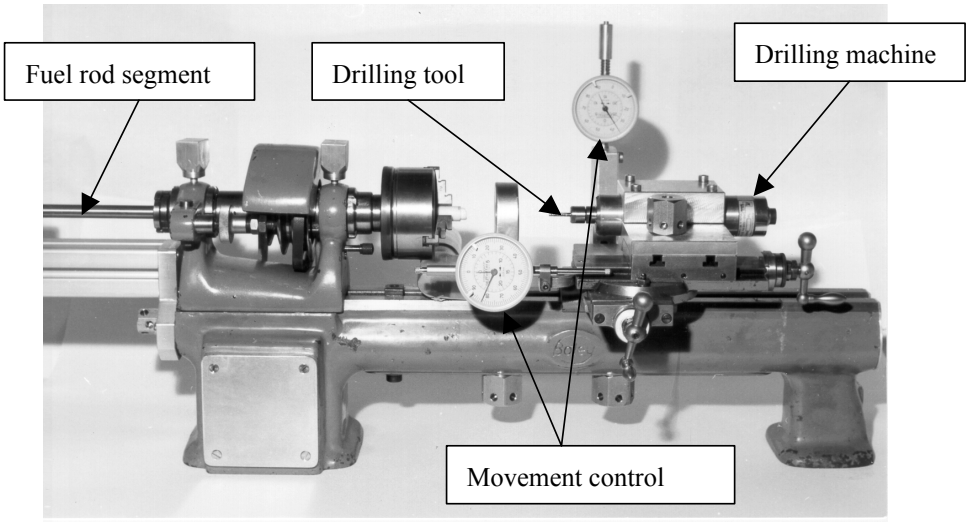

Fig. 2. Lathe and grinding machine.

2.3 Orbital Welding

A commercial device from the company Arc Machines, Model 207-0, provided with a Cassette Weld Head, Model 9-500, was adapted for the use under remote handling conditions. This type of machine is a precision, orbital tungsten inert gas (TIG) welding head, designed for fusion butt welding of tubes with extreme clearance limitations. The machine can weld thin wall tubes of a range of diameters up to 12.7 mm.

The welding system operates in such a way that the sample remains fixed while the electrode rotates during the welding process.

2.4 Sample pressurisation device

To perform the long term creep tests, the samples were internally pressurised. In Fig. 3, a sample with the end cap and the filling valve is shown. Both end caps are welded to the de-fueled sample by means of the TIG orbital welding system. To introduce the filling gas (Ar) a special valve was modified for hot cell applications. The valve consists of a short cylinder, fitting closely to its housing, that can be moved by an advancing screw towards the sealing surface. A spring holds the cylinder in the open position to allow the gas to ingress into the specimen. Once the desired pressure is achieved, the screw can be tightened providing the gas sealing. Finally, to ensure the absolute tightness of the sample, an end cap is welded over the valve.

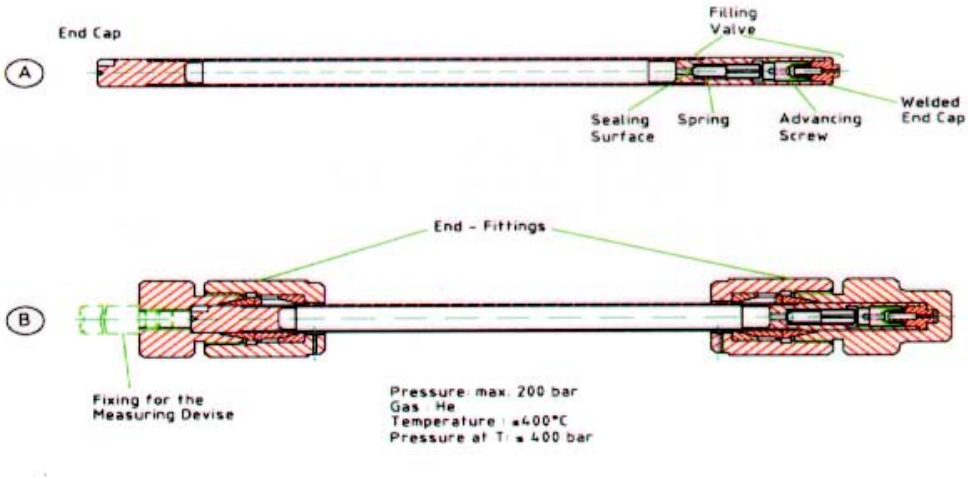

Fig. 3. Creep samples(a) with the end-caps welded and the filling-valve, and (b) with the end-fittings.

After the several welding operations, end-fittings are fixed to the samples as shown in Fig. 3 b. This is performed in order to avoid that the heat-affected zones, free from the radiation damage, can creep with higher creep-rate than the rest of the sample. An special device, described elsewhere[4], was used in order to tighten the end-fittings.

To pressurise the samples with the gas, a device had to be developed. The equipment is shown in Fig. 4. The concept is based on a quick connector and a pressure gage. The massive platform provides the necessary stability to allow the closing of the filling valve. The equipment was designed for a maximum pressure of 250 bar.

2.5 Diameter Measurement

A displacement transducer (LVDT) has been mounted on a floating head to measure the relative movement of two knives, which us calibrated standards as reference (Fig. 5). The device is able to detect variations of ± 0.1 µm in the diameter. The apparatus also performs the measurement of the axial displacement (± 10 µm), allowing the correlation of the diameter measurement with the axial position on the sample.

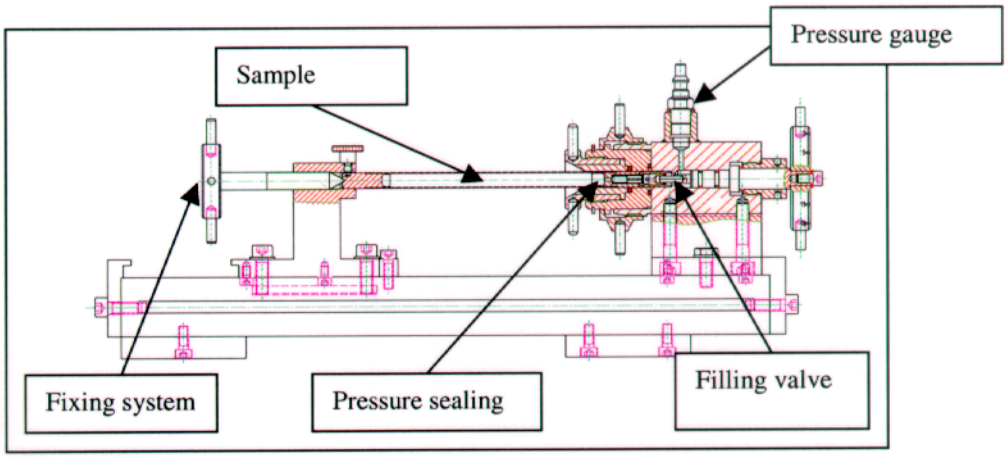

Fig. 4. Sample pressurisation device.

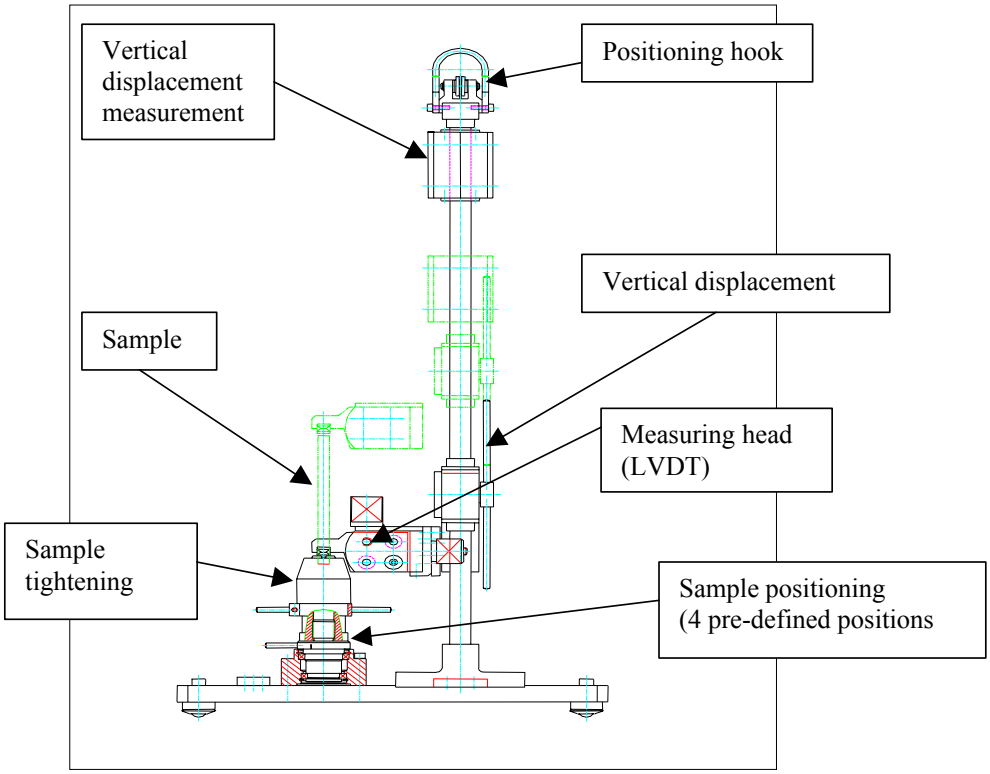

Fig. 5. Diameter measuring device.

3. METHODS EVALUATION

3.1 Re-fabrication

In Fig. 6, a longitudinal cut through a welded end cap is shown. The re-fabrication procedure outlined has so far been used successfully for more than 30 test segments including PWR and BWR fuel rods. A prerequisite for its successful application is that the work in the hot cells has to be performed in the cleanest possible way, avoiding any contamination of the internal part of the segments.

An example of the detrimental effect of impurities is shown in Fig. 7, where hydrogen carbon was introduced during the re-fabrication process causing heavy local hydriding (sunbursts).

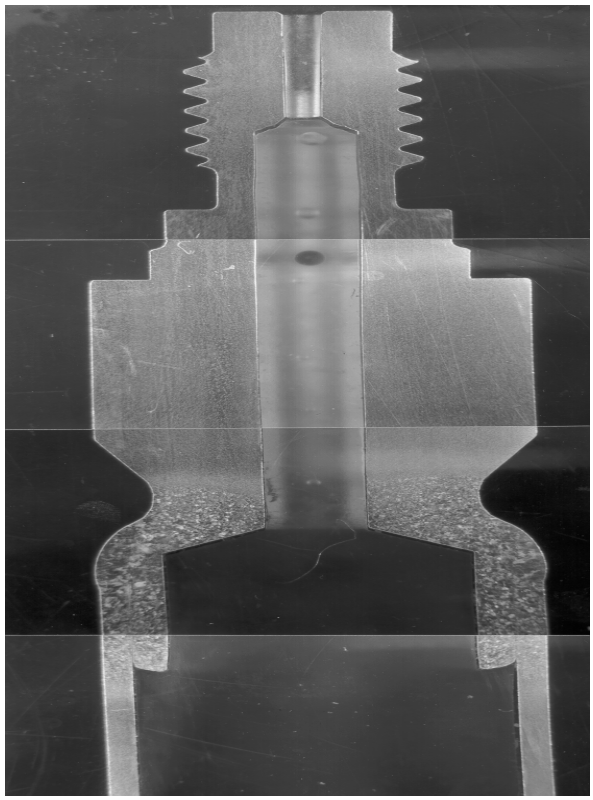

Fig. 6. Metallography of a welded end-cap

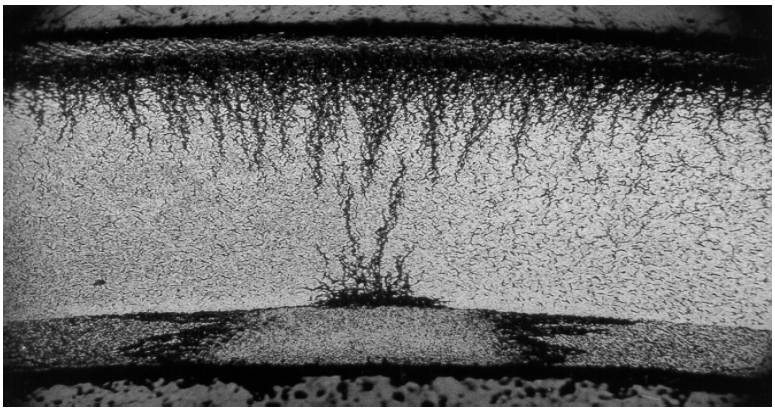

Fig. 7. Hydride distribution in a cladding after hydrogen ingress due to impurities.

3.2 Creep tests

After He-filling the final end-cap is welded. By this operation, care has to be exercise not to overheat the material to avoid the opening valve with the consequent release of the gas. A gas release can cause the blow-up of weld-seam.

For the cold tests a cladding material with high creep strength was chosen to obtain strains comparable to the expected strains of the future irradiated samples. Especially, to test the end-fitting stability under conditions as realistic as possible.

Two samples were filled with He to reach 200 bar at 350 °C and 100 bar at 410 °C. The pressure was measured at room temperature and had to be corrected for the corresponding at the test temperature. The results are presented in Fig 8.

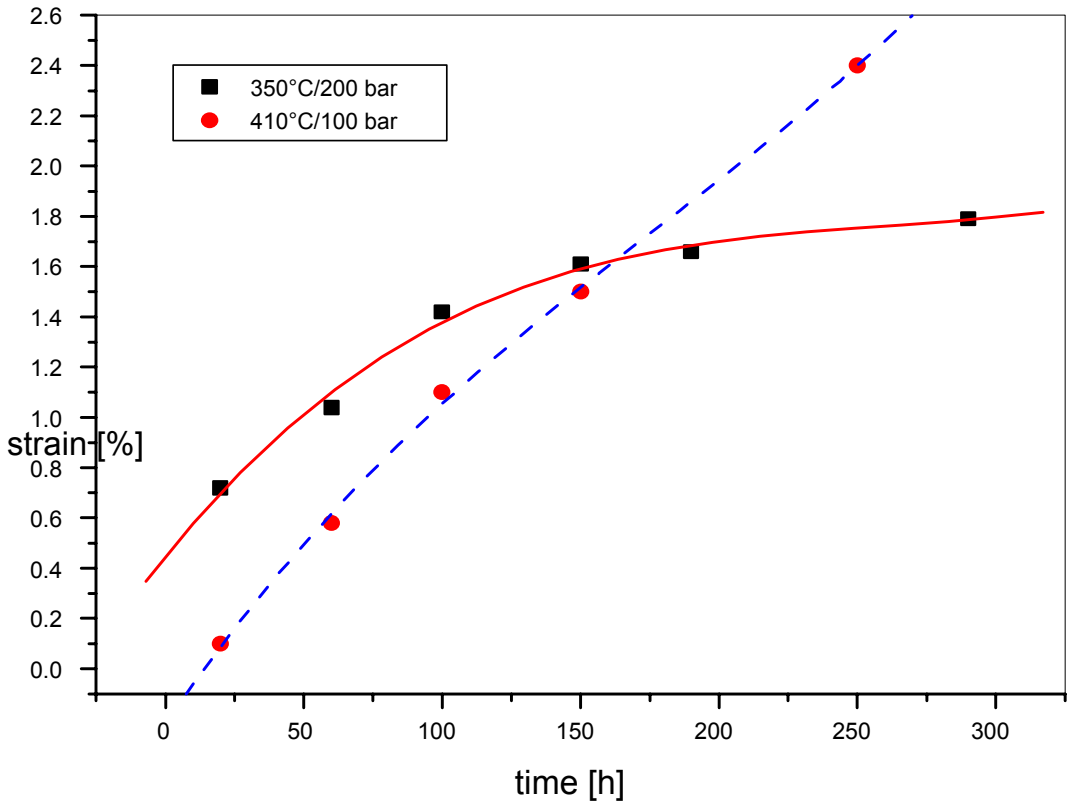

Fig. 8. Creep strain as a function of the testing time.

3.3 TEM

The micrographs in Fig. 9 show the typical appearance of highly irradiated secondary-phase particles (SPPs) in Zry-2. Depicted are $Zr(FrCr)_2$ and $Zr_2(FeNi)$ SPPs, which have been identified by EDX-analysis. These particles tend to dissolve with increasing fluence. The number density distribution as a function of the particle equivalent diameter is determined by geometrical measurements of several hundreds of particles. Comparing number density and chemical composition if irradiated and non-irradiated samples of the same material, the degree of SPP-dissolution can be quantified and correlated to the corrosion behaviour.

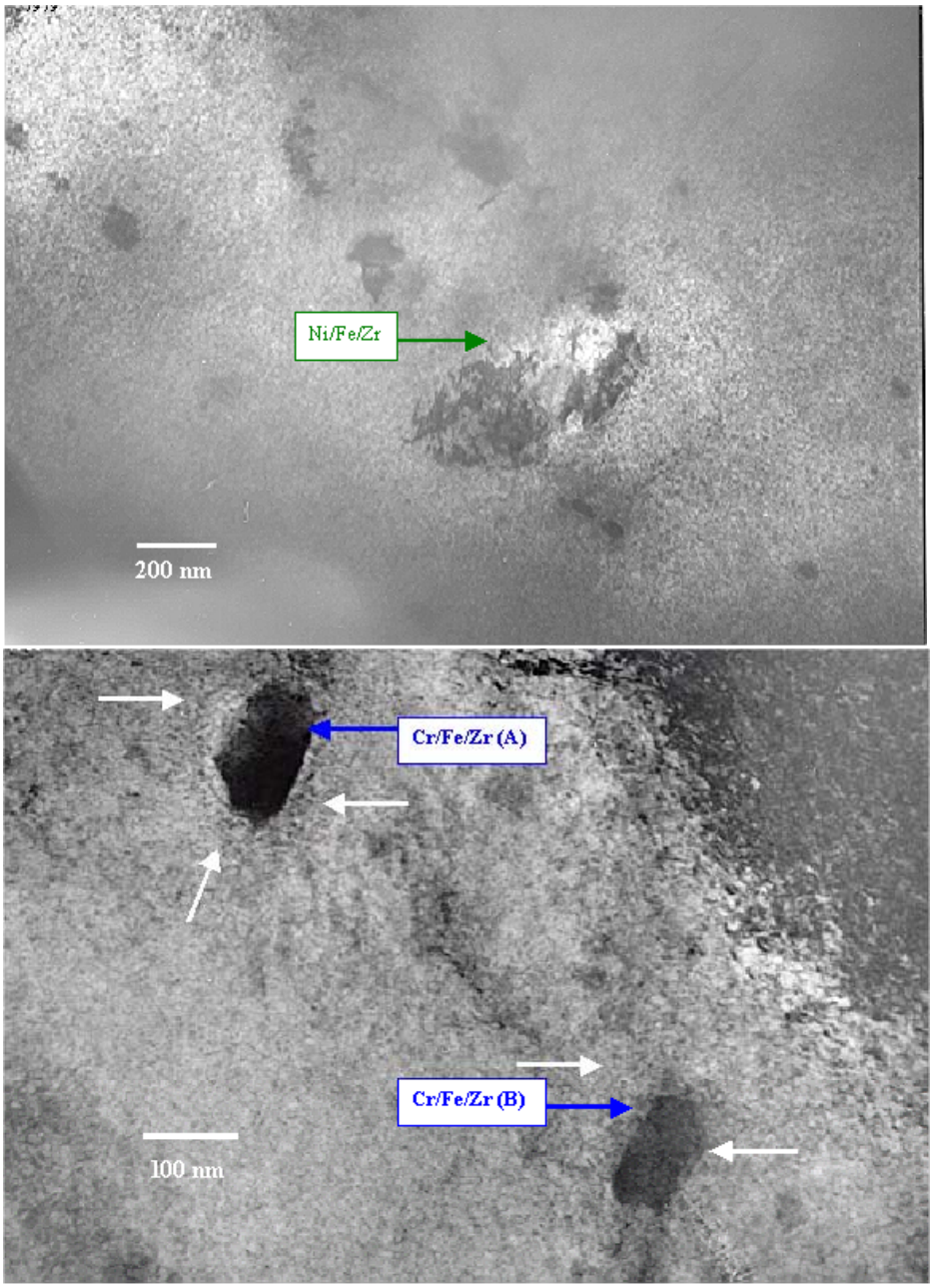

Fig. 9. Typical SPPs in Zry-2.

3.4 GDMS

The technique can be used for the determination of light elements as a function of the depth and can be applied to study their influence on the corrosion behaviour of cladding materials.

As an example, in Fig. 10 a typical concentration profile is shown. The figure depicts the Li-concentration as a function of the depth in a Zircaloy-sample, oxidised in a Li/B-environment (autoclave, 350 °C).

This equipment has been installed in a glove box and can be use for irradiated materials if the sample is clean enough (less than 2 mSv) and may be taken from the hot-cells. This activity level can be achieved by taking the fuel out of the sample with the equipment described in the section 2.2.

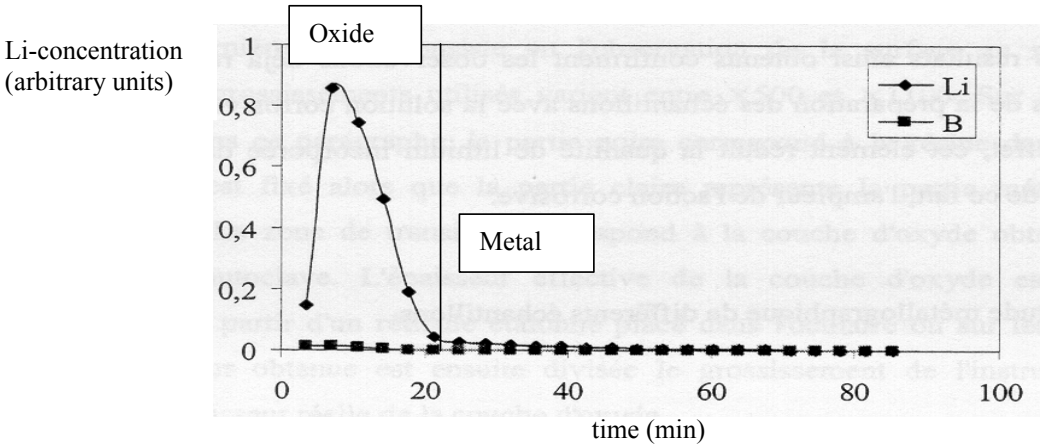

Fig. 10. Typical concentration profile.

CONCLUSIONS

To cope with the new requirements of the nuclear industry for PIE-methods to better characterize the fuel rod behaviour at high burnups, several sample preparation techniques were developed, installed and successfully tested in hot cells. The new techniques permit the preparation of samples to evaluate corrosion phenomena, to test the behaviour under transient conditions, and to examine the mechanical properties of highly burnt fuel rods also in view of dry interim storage.

REFERENCES

[1] W. VOGL et al., Res. Mechanica 14 (1985) 171–195.
[2] A. SEIBOLD, R. MANZEL, K.N. WOODS, N. ITAGAKI, " Fe-Enhanced Zr Liner Cladding", LWR Fuel Performance (Proc. Intern. Topical Meeting, Portland, OR, USA) ANS (1997) 337.
[3] M. Peehs, F. Garzarolli and W. Goll, "Assessment of Dry Storage Performance of Spent LWR Fuel Assemblies with Increasing Burnup", Storage of Spent Fuel From Power Reactors (Proc. Symp. Vienna, 1988), IAEA (1999) 313.
[4] W.GOLL, H. SPILKER and E.H.TOSCANO, J. Nucl. Mater. 289 (2001) 247.

Database "catalogue of techniques applied to materials and products of nuclear engineering"

E.E. Lebedeva, V.N. Golovanov, I.A. Podkopayeva, T.A. Temnoyeva

State Scientific Center of Russian Federation, Research Institute of Atomic Reactors, Dimitrovgrad, Uljanovsk Region, Russian Federation

Abstract. The database "Catalogue of techniques applied to materials and products of nuclear engineering" (IS MERI) was developed to provide informational support for SSC RF RIAR and other enterprises in scientific investigations. This database contains information on the techniques used at RF Minatom enterprises for reactor material properties investigation. The main purpose of this system consists in the assessment of the current status of the reactor material science experimental base for the further planning of experimental activities and methodical support improvement.

1. INTRODUCTION

A comprehensive approach to investigation of the performance of materials and products of nuclear engineering is applied at SSC RF RIAR. This approach includes the following:

- co-ordination of activities at their most expensive stages, i.e. irradiation and PIE with consideration of all operating Industry programs activities;
- discussion of the most significant and large-scope investigations with determination of the necessity of their development or improvement;
- solving problems of methodical support for investigations and development of the reactor material science experimental base.

This problem can be solved only with the complete information on the existing experimental base available, as well as by the provision of its prompt obtaining and usage. The establishment of computerized systems as data banks on methodical support for reactor materials science provides the process of decision making with the necessary and reliable information [1].

The database "Catalogue of techniques applied to materials and products of nuclear engineering" (IS MERI) was developed to provide informational support for SSC RF RIAR and other enterprises in scientific investigations [2]. This database contains information on the techniques used at RF Minatom enterprises for reactor material properties investigation.

The main purpose of this system consists in the assessment of the current status of the reactor material science experimental base for the further planning of experimental activities and methodical support improvement.

2. STAGES OF IS MERI DEVELOPMENT.

The development of IS MERI "Catalogue techniques applied to materials and products of nuclear engineering " consisted of the following stages:

(1) Application domain analysis, information composition determination, data structure development.
(2) Development of IS informational and linguistic support.
(3) Development of the software for input, editing, search and output of the information on the material testing techniques.
(4) Acquisition of the data on the available methodical developments at the Industry enterprises, systematization of the collected information, filling in the input forms.
(5) Input of the information into the database, debugging of edit, view, search, report generation and printout modes.

3. IS MERI DATA STRUCTURE

Fig.1 presents the IS MERI data structure which includes the following:

- The general information on the technique;
- Subject of the investigation;
- Investigated properties;
- Measured and calculated parameters, their ranges and errors;
- Used equipment, and
- Automation devices.

4. IS MERI SOFTWARE

A number of Windows applications were developed to provide the access to the database (DB) and to search for the information. These programs are used as a user's interface. The IS MERI Windows applications were designed in the integrated development environment (IDE) Delphi4, which allows for creation of the dialog operation mode with the database in terms of application domain objects. It also provides convenient, friendly, graphic interface. The applications were designed for Windows 95/98/NT with the usage of visual programming technology. The working language is Object Pascal 7.0.

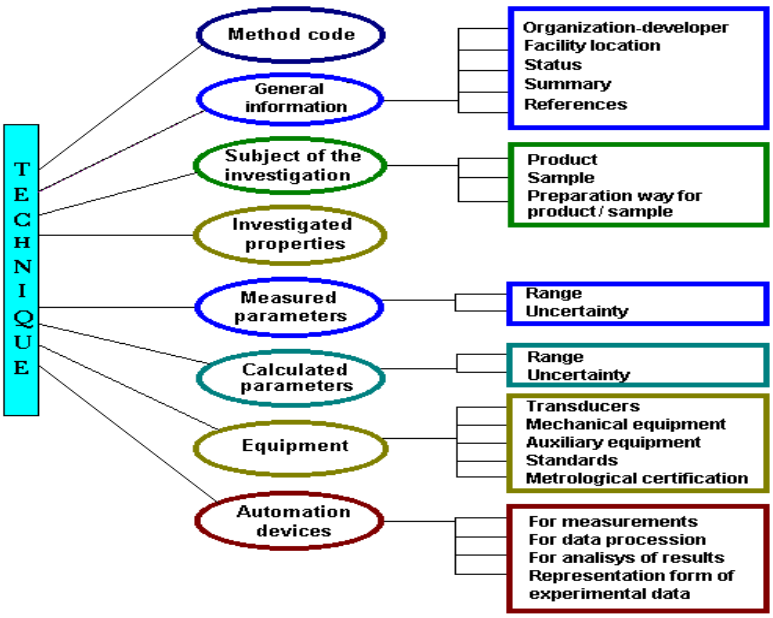

FIG. 1. IS MERI data structure.

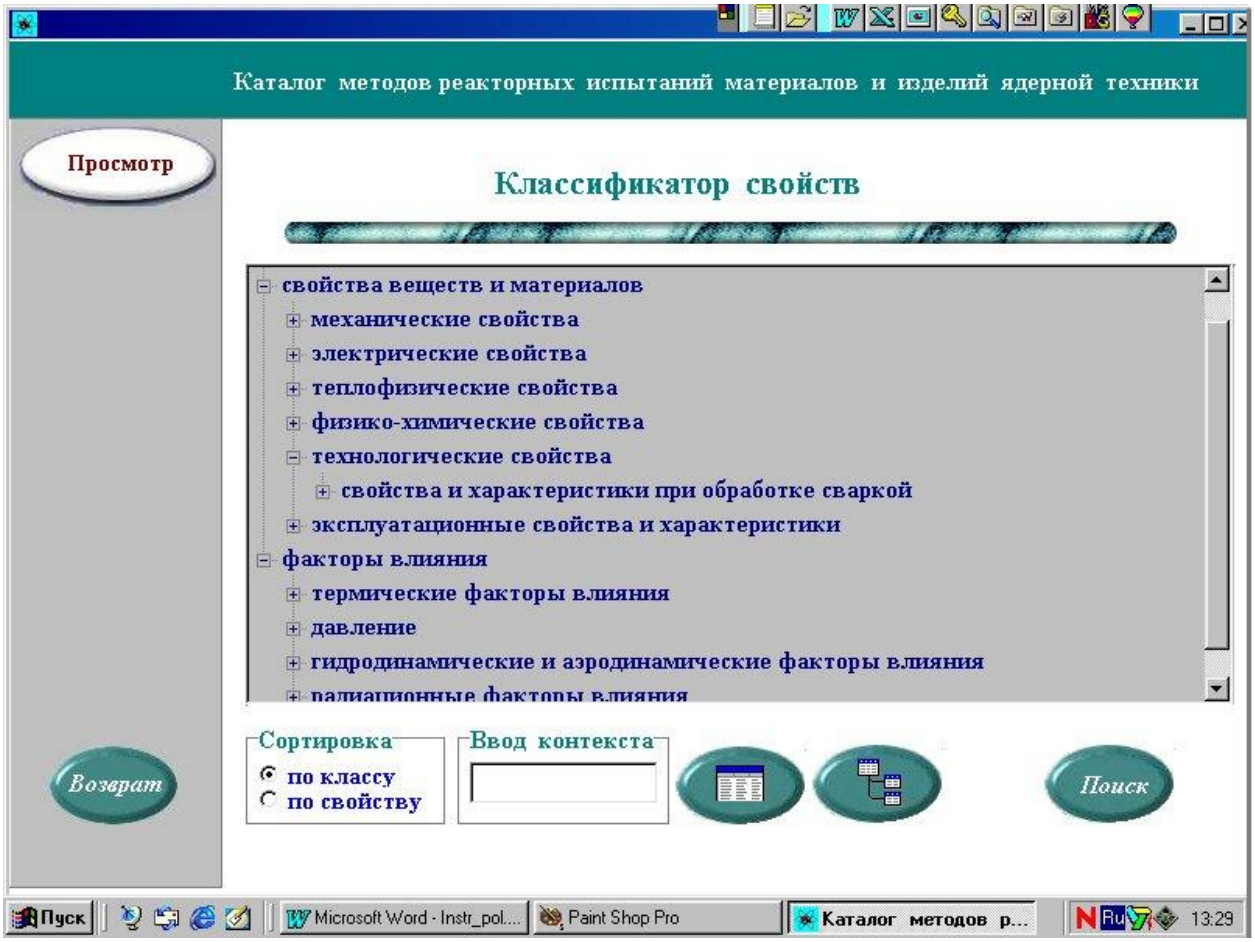

FIG. 2. The classifier of material properties.

5. USER'S INTERFACE

The system main menu gives the possibility to select one of the search directions based on: the number of the technique, organization, examined material, investigated property, and also on the selection of the parameters from the list (fig. 4).

The application composes a query to the DB, selects the information and outputs a list of techniques corresponding to the target search condition.

Depending on the target search condition of the query the user can obtain information on:

- All techniques developed and used at the given enterprise,
- Techniques used for investigation of the material specific property or the property class used at one or all Industry enterprises,
- Techniques used for the specific material examination at one or all Industry enterprises.

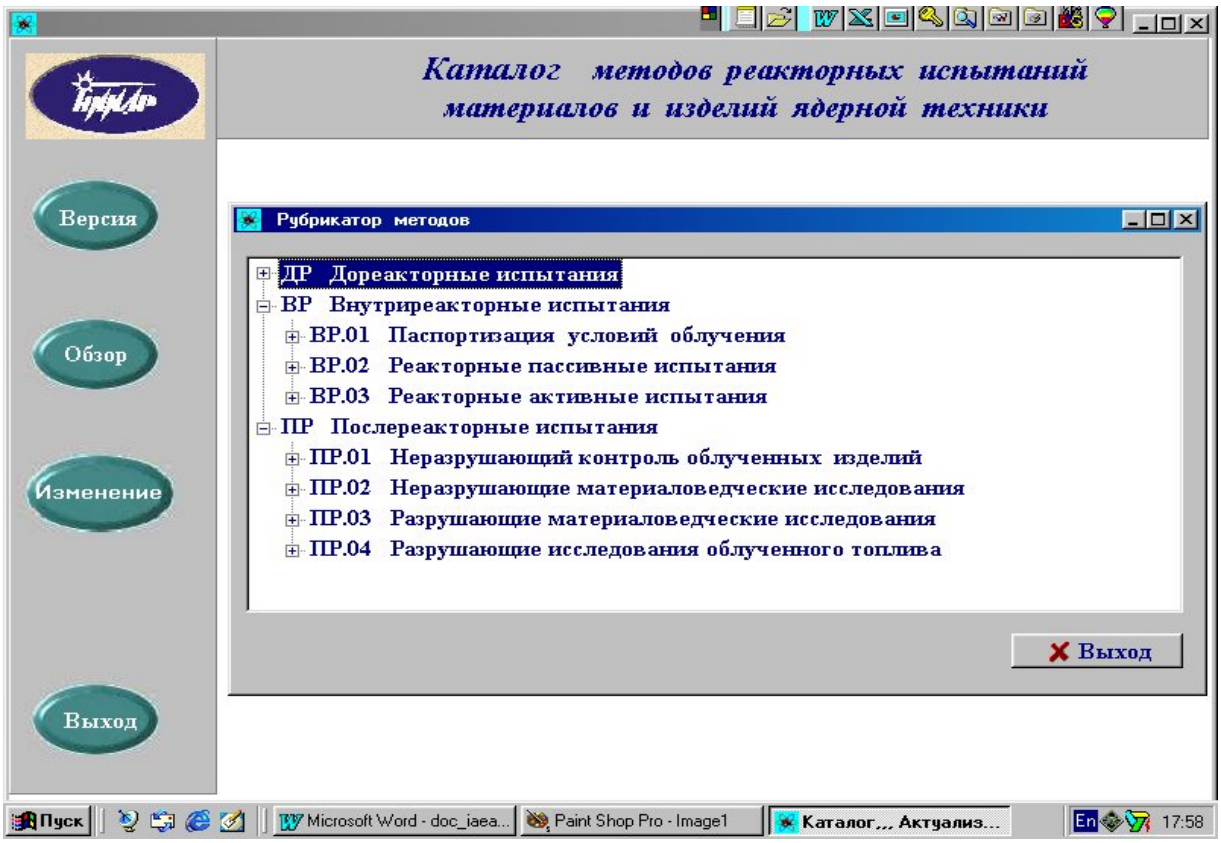

FIG. 3. The methods rubricator.

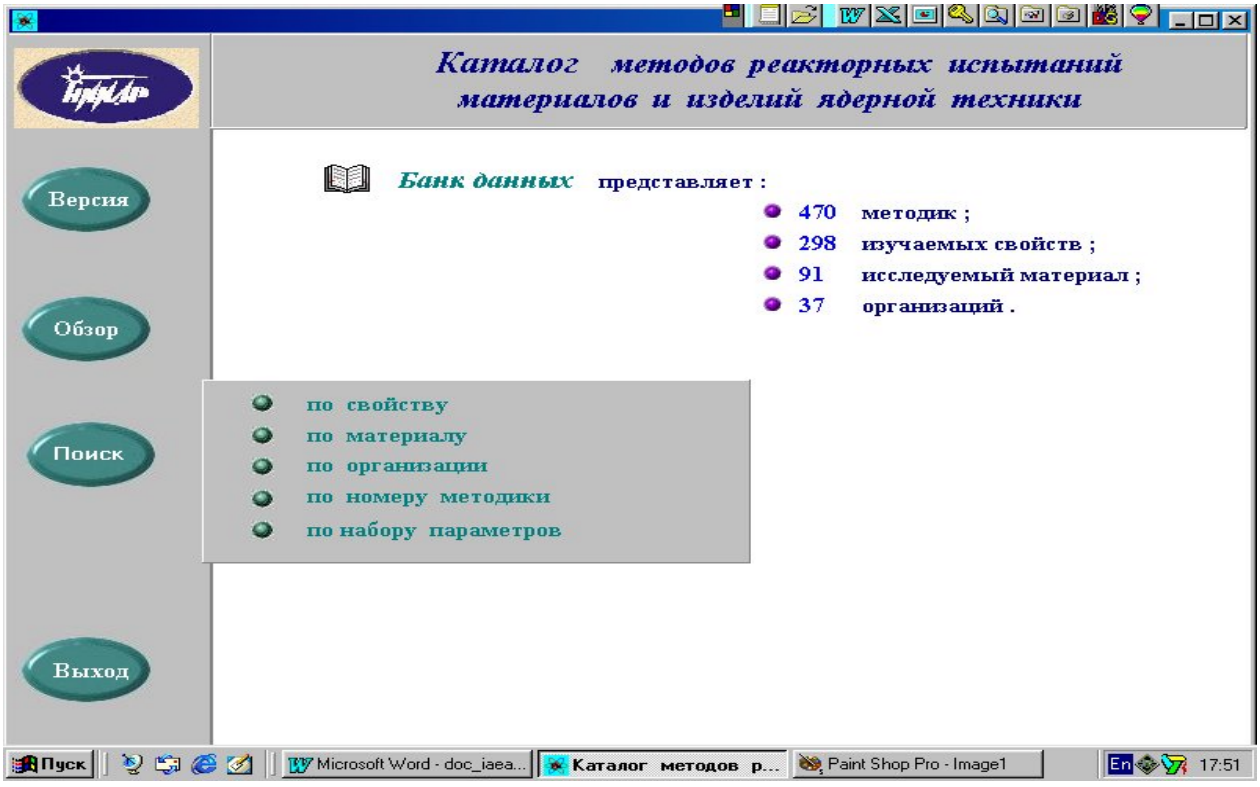

FIG. 4. IS MERI main menu.

Besides, the user is given an opportunity to search according to the arbitrary combination of parameters from the given list. The following technique attributes are presented in the list: the technique code according to the rubricator of the techniques, the organization — developer, the investigated material, the investigated property, reactor, current status, author.

The value of each search parameter is selected from the submitted lists and classifiers. The list/classifier unique for each parameter contains a full list of values of this parameter available in the DB and updated automatically. As a result a list of the technique numbers satisfying the search criterion is generated. Besides, the basic information on each technique and statistical information on the quantity of the techniques satisfying the query is displayed.

6. CONCLUSION

So, the informational system " Catalogue of techniques applied to materials and products of nuclear engineering" (IS MERI) was developed. This system is used for collection, systematisation, search and output of information on reactor examination techniques.

IS MERI allows for prompt obtaining of the information on:

- Materials properties testing techniques;
- Technique equipping and metrological certification;
- Uncertainty of separate testing techniques;
- Characteristics of facilities and devices;
- Used automation devices, etc.

At present IS MERI contains information on 404 reactor testing techniques developed in 17 Industry organizations, the number of investigated properties is about 300, the number of materials is 90. The total volume of the information is 7 Mbytes.

IS MERI was installed at DAE and leading enterprises and repeatedly used for analysis of the current status of the reactor material science experimental base, further experimental activities planning and methodical support improvement.

IS MERI is registered in the State Database Register of CRI ATOMINFORM and assigned No 0229804912.

REFERENCES

[1] V.B. IVANOV, E.E. LEBEDEVA, N.V. MARKINA, V.A. TZYKANOV, Information search system on reactor testing techniques and the role of the methodical information in planning of reactor material science investigations, in Proceedings of International Conference on Radiation Material Science, Alushta, May 22–25, 1990, Kharkov (1990).

[2] N.V. MARKINA, E.E. LEBEDEVA, N.V. ARKHANGELSKY, et al, Informational factographic system "Research base of reactor material science", Atomic Energy, 1994, **76**, 5 (1994) 383–389.

LIST OF PARTICIPANTS

AUSTRIA	Onoufriev, V. International Atomic Energy Agency, Division of Nuclear Fuel Cycle and Waste Technology P.O. Box 100, Wagramer Strasse 5, A-1400 Vienna, Austria
BELGIUM	Sannen, L. SCK/CEN, RMO-LHMA Boeretang 200, B-2400 Mol
BRAZIL	Lopes Claudio, A.E. CTM/SP, Estrada Sorocaba - Iperó 12,5 km Iperó - São Paulo, CEP: 18.560-000
CZECH REPUBLIC	Zmitko, M. Nuclear Research Institute Rez plc, 250 68 Rez near Prague
FRANCE	Bessiron, V. IPSN/SEMAR/LEPAR, Build. 702, Centre de Cadarache, F-13108 Saint-Paul-lez-Durance
	Decroix, G.-M. DEN/DMN/LM2E, CEA Centre de Saclay, F-91191 Gif sur Yvette
	Desgranges, L. DEN/DEC, CEA Centre de Cadarache, Bât 316, F-13108 Saint-Paul-lez-Durance
	Herter, P. DEN/DMN/SEMI, CEA Centre de Saclay, F-91191 Gif sur Yvette
	Segura, J.-C. EDF/SEPTEN, 12-14 avenue Dutrievoz, F-69628 Villeurbanne
GERMANY	Manzel, R. Framatome ANP GmbH, FANP NBTW, P.O. Box 32 20, D-91050 Erlangen

GERMANY (cont.)	Toscano, E.H. European Commission Joint Research Centre, Institute for Transuranium Elements (ITU), Postfach 2340, D-76125 Karlsruhe, Germany
INDIA	Sahoo, K.C. Bhabha Atomic Research Centre (BARC), Radiological Laboratories, Trombay, Mumbai 400 085
JAPAN	Yasuda, R. JAERI, Department of Hot Laboratories, Tokai Research Establishment, Tokai-mura, Ibaraki-ken, 319-1115
LITHUANIA	Krivov, I. Ignalina NPP, Nuclear Fuel Laboratory, Visaginas, 4761
NORWAY	Jenssen, H.K. Institutt for energiteknikk, Instituttveien 18/Postboks 40, N- 2027 Kjeller
RUSSIAN FEDERATION	Golovanov, V.N. State Scientific Centre (SSC), Research Institute of Atomic Reactors (RIAR), 433510 Dimitrovgrad, Ulyanovk Region Egorov, A.A. Ministry of the Russian Federation, for Atomic Energy (MINATOM), Staromonetny per. 26, 109180 Moscow Kadarmetov, I.M. Research Institute of Inorganic Materials, (VNIINM), Nuclear Fuel Department, Rogova Str. 5, 123060 Moscow Krylov, D.V. State Unitary Plant of Polymetalls, Kashirskoe Shosse, 49, 115409 Moscow Sokolov, F. F. Research Institute of Inorganic Materials, (VNIINM), Nuclear Fuel Department, Rogova Str. 5, 123060 Moscow

RUSSIAN FEDERATION (cont.)	State Scientific Centre Institute of Physics and Power Engineering, (SSC-IPPE), Bodarenko Square, 1, 249020 Obninsk, Kaluga Region *Participants:* Birzhevoi, G.A. Ivanov, S.N. Pevchikh, Yu. M. Porollo, S.I. State Scientific Centre Research Institute of Atomic Reactors, (SSC-RIAR), 433510 Dimitrovgrad, Ulyanovk Region *Participants:* Amosov, S.A. Chetverikov, A.P. Dvoretsky, V.G. Golovchenko, Yu.M. Krasnoselov, V.A. Kuprienko, M.V. Lebedeva, E.E. Novoselov, A.E. Prokhorov, V.I. Risovany, V.D. Smirnov, A.V. Smirnov, V.P. Vinogradova, C.N. Zhitelev, V.
SPAIN	Fernandez, J.R. TECNATOM S.A., Avnd. Montes de Oca, 1, E-28709 San Sebastian de los Reyes, Madrid Serna, J.J. ENUSA, Santiago Rusiñol 12, E-28040 Madrid
SWEDEN	Grigoriev, V. Studsvik Nuclear AB, SE-611 82 Nyköping Jakobsson, H.R. Studsvik Nuclear AB, SE-611 82 Nyköping

UKRAINE

Baturevich, D.
National Scientific Centre “Kharkov Institute of Physics & Technology”,
Scientific Technical Complex,
“Nuclear Fuel Cycle”,
Akademicheskaya Str. 1, 61108 Kharkov

Borys, V.
Rovno NPP, Ukrainian Kuznetsovsk,
Kovno Region

Bykov, O.V.
NAEC Energoatom, Arsenalnaya 9/11,
01011 Kiev

Chernukha, V.P.
National Scientific Centre “Kharkov Institute of Physics & Technology”,
Scientific Technical Complex,
“Nuclear Fuel Cycle”,
Akademicheskaya Str. 1,
61108 Kharkov

Grytsyna, V.
National Scientific Centre “Kharkov Institute of Physics & Technology”,
Scientific Technical Complex ,
“Nuclear Fuel Cycle”
Akademicheskaya Str. 1
61108 Kharkov

Piskun, O.
Zaporozhye Nuclear Power Plant,
Zaporozhye Region, 71500 Energodar